2 ELEMENTS OF PHOTOGRAPHIC SYSTEMS

2.1 INTRODUCTION

One of the most common, versatile, and economical forms of remote sensing is aerial photography. The basic advantages aerial photography affords over on-the-ground observation include:

1. **Improved vantage point.** Aerial photography gives a bird's-eye view of large areas, enabling us to see earth surface features in their spatial context. In short, aerial photography permits us to look at the "big picture" in which objects of interest reside. It is often difficult, if not impossible, to obtain this view of the environment through on-the-ground observation. With aerial photography, we also see the "whole picture" in that *all* observable earth surface features are recorded simultaneously. Completely different information might be extracted by different people looking at a photograph. The hydrologist might concentrate on surface water bodies, the geologist on bedrock structure, the agriculturalist on soil or crop type, and so on.
2. **Capability to stop action.** Unlike the human eye, photographs can give us a "stop action" view of dynamic conditions. For example, aerial photographs are very useful in studying dynamic phenomena such

as floods, moving wildlife populations, traffic, oil spills, and forest fires.

3. **Permanent recording.** Aerial photographs are virtually permanent records of existing conditions. As such, these records can be studied at leisure, under office rather than field conditions. A single image can be studied by a large number of users. Airphotos can also be conveniently compared against similar data acquired at previous times, so that changes over time can be monitored easily.
4. **Broadened spectral sensitivity.** Film can "see" and record over a wavelength range about twice as broad as that of the human eye (0.3 to 0.9 μm versus 0.4 to 0.7 μm). With photography, invisible UV and near-IR energy can be detected and subsequently recorded in the form of a visible image; hence film can see certain phenomena the eye cannot.
5. **Increased spatial resolution and geometric fidelity.** With the proper selection of camera, film, and flight parameters, we are able to record more spatial detail on a photograph than we can see with the unaided eye. This detail becomes available to us by viewing photographs under magnification. With proper ground reference data, we can also obtain accurate measurements of positions, distances, directions, areas, heights, volumes, and slopes from airphotos. In fact, most planimetric and topographic maps are currently produced using measurements extracted from airphotos.

This and the following two chapters detail and illustrate the above characteristics of aerial photographs. In this chapter, we describe the various materials and methods used to *acquire* aerial photographs (and digital images) and we deal with the process of *obtaining radiometric measurements* from airphotos. In Chapter 3 we examine various aspects of *measuring* and *mapping* with airphotos (photogrammetry). The topic of *visual image interpretation* of aerial and satellite images is treated in Chapter 4.

2.2 EARLY HISTORY OF AERIAL PHOTOGRAPHY

Photography was born in 1839 with the public disclosure of the pioneering photographic processes of Nicephore Niepce, William Henry Fox Talbot, and Louis Jacques Mande Daguerre. As early as 1840, Argo, Director of the Paris Observatory, advocated the use of photography for topographic surveying. The first known aerial photograph was taken in 1858 by a Parisian photographer named Gaspard-félix Tournachon. Known as "Nadar," he used a tethered balloon to obtain the photograph over Val de Bievre, near Paris. Balloon photography flourished after that. The earliest *existing* aerial photograph was

taken from a balloon over Boston in 1860 by James Wallace Black (Figure 2.1). This photograph was immortalized by Oliver Wendell Holmes, who described it in the *Atlantic Monthly*, July 1863: "Boston, as the eagle and the wild goose see it, is a very different object from the same place as the solid citizen looks up at its eaves and chimneys" (Newhall, 1969).

As an outgrowth of their use in obtaining meteorological data, kites were used to obtain aerial photographs beginning in about 1882. The first aerial photograph taken from a kite is credited to an English meteorologist,

Figure 2.1 Balloon view of Boston photographed by James Wallace Black, October 13, 1860. This was one of the first aerial photographs taken in the United States. It was taken from a captive balloon, Professor Sam King's "Queen of the Air," at an altitude of approximately 365 m. The photograph shows a portion of the Boston business district and the masts of square-rigged ships in the adjacent harbor. (Courtesy J. Robert Quick, Wright Patterson AFB.)

E. D. Archibald. By 1890, A. Batut of Paris had published a textbook on the latest state of the art. In the early 1900s the kite photography of an American, G. R. Lawrence, brought him worldwide attention. On May 28, 1906, he photographed San Francisco shortly after the great earthquake and fire (Baker, 1989).

The airplane, which had been invented in 1903, was not used as a camera platform until 1908, when a photographer accompanied Wilbur Wright and took the first aerial motion pictures (over Le Mans, France). Obtaining aerial photographs became a much more practical matter with the airplane than it had been with kites and balloons. Photography from aircraft received heightened attention in the interest of military reconnaissance during World War I, when over one million aerial reconnaissance photographs were taken. After World War I, former military photographers founded aerial survey companies, and widespread aerial photography of the United States began. In 1934, the American Society of Photogrammetry (now the American Society for Photogrammetry and Remote Sensing) was founded as a scientific and professional organization dedicated to advancing this field.

2.3 BASIC NEGATIVE-TO-POSITIVE PHOTOGRAPHIC SEQUENCE

Many photographic procedures, particularly black and white techniques, employ a two-phase negative-to-positive sequence. In this process, the "negative" and "positive" materials are typically film and paper prints. Each of these materials consists of a light-sensitive photographic *emulsion* coated onto a *base*. The generalized cross sections of black and white film and print paper are shown in Figures 2.2*a* and *b*. In both cases, the emulsion consists of a thin layer of light-sensitive silver halide crystals, or grains, held in place by a solidified gelatin. Paper is the base material for paper prints. Various plastics are used for film bases. When exposed to light, the silver halide crystals within an emulsion undergo a photochemical reaction forming an invisible *latent image*. Upon treatment with suitable agents in the *development process*, these exposed silver salts are reduced to silver grains that appear black, forming a visible image.

The negative-to-positive sequence of black and white photography is depicted in Figure 2.3. In Figure 2.3*a*, the letter *F* is shown to represent a scene that is imaged through a lens system and recorded as a latent image on a film. When processed, the film crystals exposed to light are reduced to silver. The number of crystals reduced at any point on the film is proportional to the exposure at that point. Those areas on the negative that were not exposed are clear after processing because crystals in these areas are dissolved as part of the development process. Those areas of the film that were exposed become various shades of gray, depending on the amount of exposure. Hence a "negative" image of reversed tonal rendition is produced. In Figure 2.3*b* the negative is illuminated and reprojected through an enlarger lens so that it is focused on

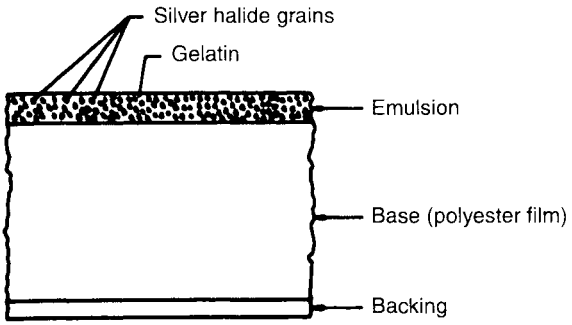

(a)

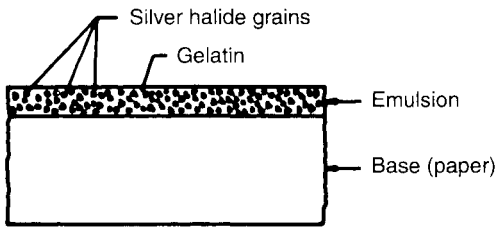

(b)

Figure 2.2 Generalized cross section of black and white photographic materials: (*a*) film and (*b*) print paper. (Adapted from Eastman Kodak Company, 1992.)

print paper, again forming a latent image. When processed, the paper print produces dark areas where light was transmitted through the negative and light areas where the illuminating light was decreased by the negative. The final result is a realistic rendering of the original scene whose size is determined by the enlarger setup. In the two-phase process of creating the final image, the negative provides an image of reversed geometry (left for right and top for bottom) and reversed brightness (light for dark and dark for light). The positive image gives a second reversal and, thus, true relative scene geometry and brightness.

Most aerial photographic paper prints are produced using the negative-to-positive sequence and a *contact printing procedure* (Figure 2.3*c*). Here, the film is exposed and processed as usual, resulting in a negative of reversed scene geometry and brightness. The negative is then placed in emulsion-to-emulsion contact with print paper. Light is passed through the negative, thereby exposing the print paper. When processed, the image on the print is a positive representation of the original ground scene at the size of the negative.

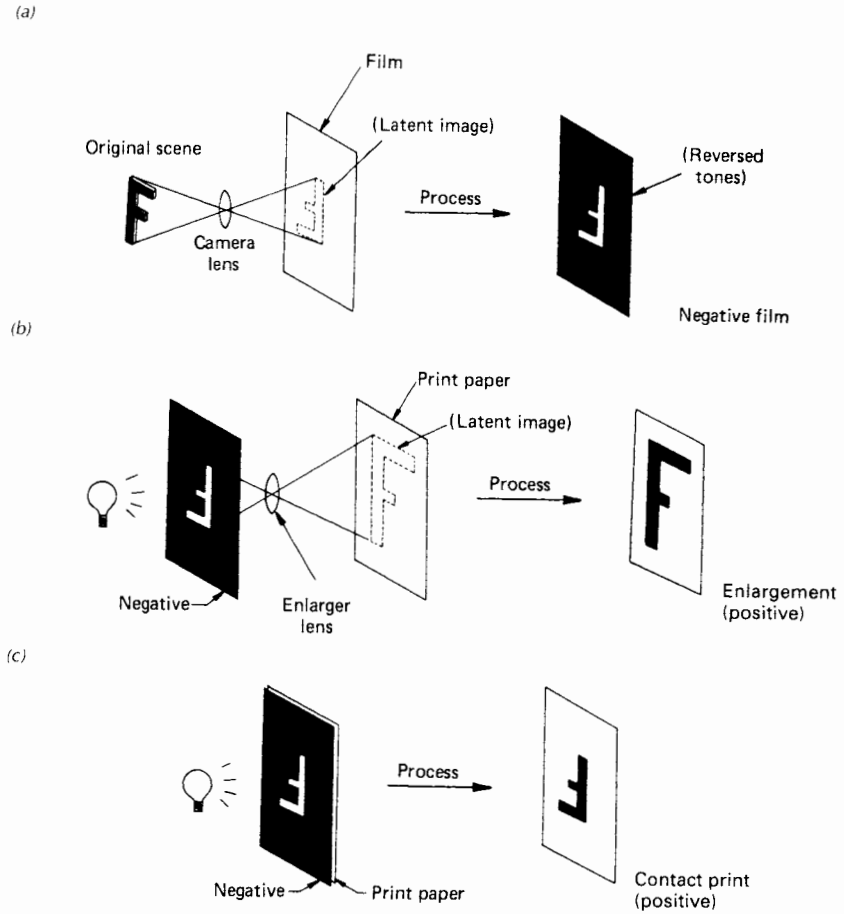

Figure 2.3 Negative-to-positive sequence of photography: (*a*) negative film exposure, (*b*) paper print enlargement, and (*c*) contact printing.

Positive images need not be printed on print paper. For example, transparent positives are often made on plastic-based or glass-based emulsions. These types of images are referred to as *diapositives* or *transparencies*.

2.4 FILM EXPOSURE

The exposure at any point on a photographic film depends on several factors, including the scene brightness, the diameter of the camera lens opening, the exposure time, and the camera lens focal length. In this section, we describe the interrelationships among these factors. We also describe various geometric factors influencing film exposure.

The Simple Camera

The cameras used in the early days of photography were often no more than a light-tight box with a pinhole at one end and the light-sensitive material to be exposed positioned against the opposite end (Figure 2.4*a*). The amount of exposure of the film was controlled by varying the time the pinhole was allowed to pass light. Often, exposure times were in hours because of the low sensitivity of the photographic materials available and the limited light-gathering capability of the pinhole design. In time, the pinhole camera was replaced by the simple lens camera, shown in Figure 2.4*b*. By replacing the pinhole with a lens, it became possible to enlarge the hole through which light rays from an object were collected to form an image, thereby allowing more light to reach the film in a given amount of time. In addition to the lens, an adjustable *diaphragm* and an adjustable *shutter* were introduced. The diaphragm controls the diameter of the lens opening during film exposure, and the shutter controls the duration of exposure. A more detailed illustration of these features can be seen later in Figure 2.28.

The design and function of modern adjustable cameras is conceptually identical to that of the early simple lens camera. To obtain sharp, properly exposed photographs with such systems, they must be focused and the proper exposure settings must be made. We shall describe each of these operations separately.

Focus

Three parameters are involved in focusing a camera: the focal length of the camera lens, f, the distance between the lens and the object to be pho-

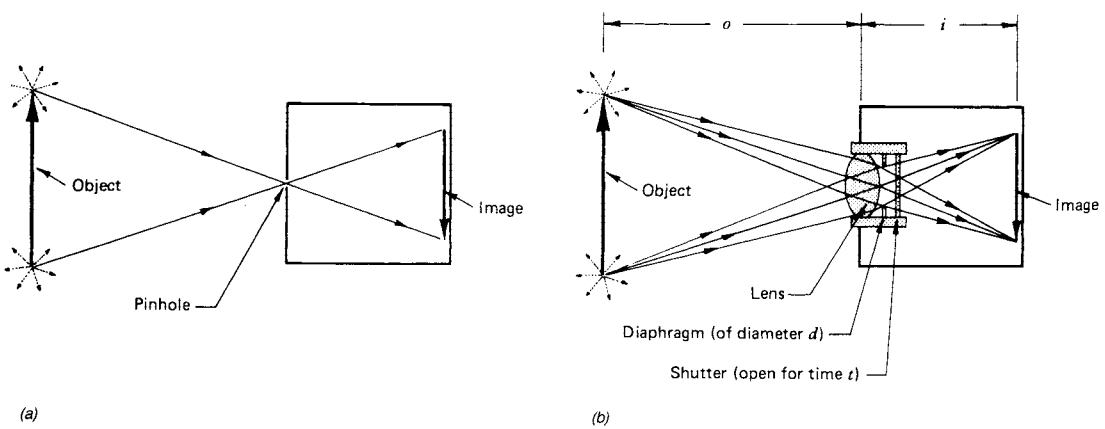

Figure 2.4 Comparison between (*a*) pinhole and (*b*) simple lens cameras.

tographed, o, and the distance between the lens and the image plane, i. The focal length of a lens is the distance from the lens at which parallel light rays are focused to a point. (Light rays coming from an object at an infinite distance are parallel.) Object distance o and image distance i are shown in Figure 2.4*b*. When a camera is properly focused, the relationship among the focal length, object distance, and image distance is

$$\frac{1}{f} = \frac{1}{o} + \frac{1}{i} \tag{2.1}$$

Since f is a constant for any given lens, as object distance o for a scene changes, image distance i must change. This is done by moving the camera lens with respect to the film plane. When focused on an object at a discrete distance, a camera can image over a range just beyond and in front of this distance with acceptable focus. This range is commonly referred to as the *depth of field*.

In aerial photography the object distances involved are effectively infinite. Hence the $1/o$ term in Eq. 2.1 goes to zero and i must equal f. Thus, most aerial cameras are manufactured with their film plane precisely located at a *fixed* distance f from their lens.

Exposure

The exposure[1] at any point in the film focal plane of a camera is determined by the irradiance at that point multiplied by the exposure time, expressed by

$$E = \frac{sd^2t}{4f^2} \tag{2.2}$$

where

E = film exposure, J mm^{-2}
s = scene brightness, J mm^{-2} sec^{-1}
d = diameter of lens opening, mm
t = exposure time, sec
f = lens focal length, mm

It can be seen from Eq. 2.2 that, for a given camera and scene, the exposure reaching a film can be varied by changing the camera shutter speed t and/or the diameter of the lens opening d. Various combinations of d and t will yield equivalent exposures.

[1]The internationally accepted symbol for exposure is H. To avoid confusion with the use of this symbol for flying height, we use E to represent "exposure" in our discussion of photographic systems. Elsewhere, E is used as the internationally accepted symbol for "irradiance."

EXAMPLE 2.1

A film in a camera with a 40-mm-focal-length lens is properly exposed with a lens opening diameter of 5 mm and an exposure time of $\frac{1}{125}$ sec (condition 1). If the lens opening is increased to 10 mm and the scene brightness does not change, what exposure time should be used to maintain proper exposure (condition 2)?

Solution

We wish to maintain the same exposure for conditions 1 and 2. Hence,

$$E_1 = \frac{s_1(d_1)^2 t_1}{4(f_1)^2} = \frac{s_2(d_2)^2 t_2}{4(f_2)^2} = E_2$$

Canceling constants, we obtain

$$(d_1)^2 t_1 = (d_2)^2 t_2$$

or

$$t_2 = \frac{(d_1)^2 t_1}{(d_2)^2} = \frac{5^2}{10^2} \cdot \frac{1}{125} = \frac{1}{500} \text{ sec}$$

The diameter of the lens opening of a camera is determined by adjusting the diaphragm to a particular *aperture setting*, or *f-stop*. This is defined by

$$F = \text{f-stop} = \frac{\text{lens focal length}}{\text{lens opening diameter}} = \frac{f}{d} \tag{2.3}$$

As can be seen in Eq. 2.3, as the f-stop number increases, the diameter of the lens opening decreases and, accordingly, the film exposure decreases. Because the *area* of the lens opening varies as the square of the diameter, the change in exposure with f-stop is proportional to the square root of the f-stop. Shutter speeds are normally established in sequential multiples of 2 ($\frac{1}{125}$ sec, $\frac{1}{250}$ sec, $\frac{1}{500}$ sec, $\frac{1}{1000}$ sec, . . .). Thus, f-stops vary as the square root of 2 (f/1.4, f/2, f/2.8, f/4, . . .). Note that when the value of the f-stop is 2, it is written as f/2.

The interplay between f-stops and shutter speeds is well known to photographers. For constant exposure, an incremental change in shutter speed setting must be accompanied by an incremental change in f-stop setting. For example, the exposure obtained at $\frac{1}{500}$ sec and f/1.4 could also be obtained at $\frac{1}{250}$ sec and f/2. Short exposure times allow one to "stop action" and prevent blurring when photographing moving objects (or when the camera is moving, as in the case of aerial photography). Large lens-opening diameters (small f-stop numbers) allow more light to reach the film and are useful under low light conditions. Small lens-opening diameters (large f-stop numbers) yield

greater depth of field. The f-stop corresponding to the largest lens opening diameter is called the *lens speed*. The larger the lens-opening diameter (smaller f-stop number), the "faster" the lens is.

Using f-stops, Eq. 2.2 can be simplified to

$$E = \frac{st}{4F^2} \tag{2.4}$$

where F = f-stop = f/d.

Equation 2.4 is a convenient means of summarizing the interrelationship among film exposure, scene brightness, exposure time, and f-stop. This relationship may be used in lieu of Eq. 2.2 to determine various f-stop and shutter speed settings that result in identical film exposures.

EXAMPLE 2.2

A film is properly exposed when the lens aperture setting is f/8 and the exposure time is $\frac{1}{125}$ sec (condition 1). If the lens aperture setting is changed to f/4, and the scene brightness does not change, what exposure time should be used to yield a proper film exposure (condition 2)? (Note that this is simply a restatement of the condition of Example 2.1.)

Solution

We wish to maintain the *same exposure* for conditions 1 and 2. With the scene brightness the same in each case,

$$E_1 = \frac{s_1 t_1}{4(F_1)^2} = \frac{s_2 t_2}{4(F_2)^2} = E_2$$

Canceling constants,

$$\frac{t_1}{(F_1)^2} = \frac{t_2}{(F_2)^2}$$

and

$$t_2 = \frac{t_1 (F_2)^2}{(F_1)^2} = \frac{1}{125} \cdot \frac{4^2}{8^2} = \frac{1}{500} \text{ sec}$$

Geometric Factors Influencing Film Exposure

Images are formed on film because of variations in scene brightness values over the area photographed. Ideally, in aerial photography, such variations

would be related solely to variations in ground object type and/or condition. This assumption is a great oversimplification since many factors that have nothing to do with the type or condition of a ground feature can and do influence film exposure measurements. Because these factors influence exposure measurements but have nothing to do with true changes in ground cover type or condition, we term them *extraneous effects*. Extraneous effects are of two general types: geometric and atmospheric. Atmospheric effects were introduced in Section 1.3; here we discuss the major geometric effects that influence film exposure.

Probably the most important geometric effect influencing film exposure is *exposure falloff*. This extraneous effect is a variation in focal plane exposure purely associated with the distance an image point is from the image center. Because of falloff, *a ground scene of spatially uniform reflectance does not produce spatially uniform exposure in the focal plane*. Instead, for a uniform ground scene, exposure in the focal plane is at a maximum at the center of the film format and decreases with radial distance from the center.

The factors causing falloff are depicted in Figure 2.5, which shows a film being exposed to a ground area assumed to be of uniform brightness. For a beam of light coming from a point directly on the optical axis, exposure E_0 is directly proportional to the area, A, of the lens aperture and inversely proportional to the square of the focal length of the lens, f^2. However, for a beam exposing a point at an angle θ off the optical axis, exposure E_θ is reduced from E_0 for three reasons:

1. The effective light-collecting area of the lens aperture, A, decreases in proportion to $\cos\theta$ when imaging off-axis areas ($A_\theta = A\cos\theta$).
2. The distance from the camera lens to the focal plane, f_θ, increases as $1/\cos\theta$ for off-axis points, $f_\theta = f/\cos\theta$. Since exposure varies inversely as the square of this distance, there is an exposure reduction of $\cos^2\theta$.
3. The effective size of a film area element, dA, projected perpendicular to the beam decreases in proportion to $\cos\theta$ when the element is located off-axis, $dA_\theta = dA\cos\theta$.

Combining the above effects, the overall theoretical reduction in film exposure for an off-axis point is

$$E_\theta = E_0\cos^4\theta \tag{2.5}$$

where

θ = angle between the optical axis and the ray to the off-axis point
E_θ = film exposure at the off-axis point
E_0 = exposure that would have resulted if the point had been located at the optical axis

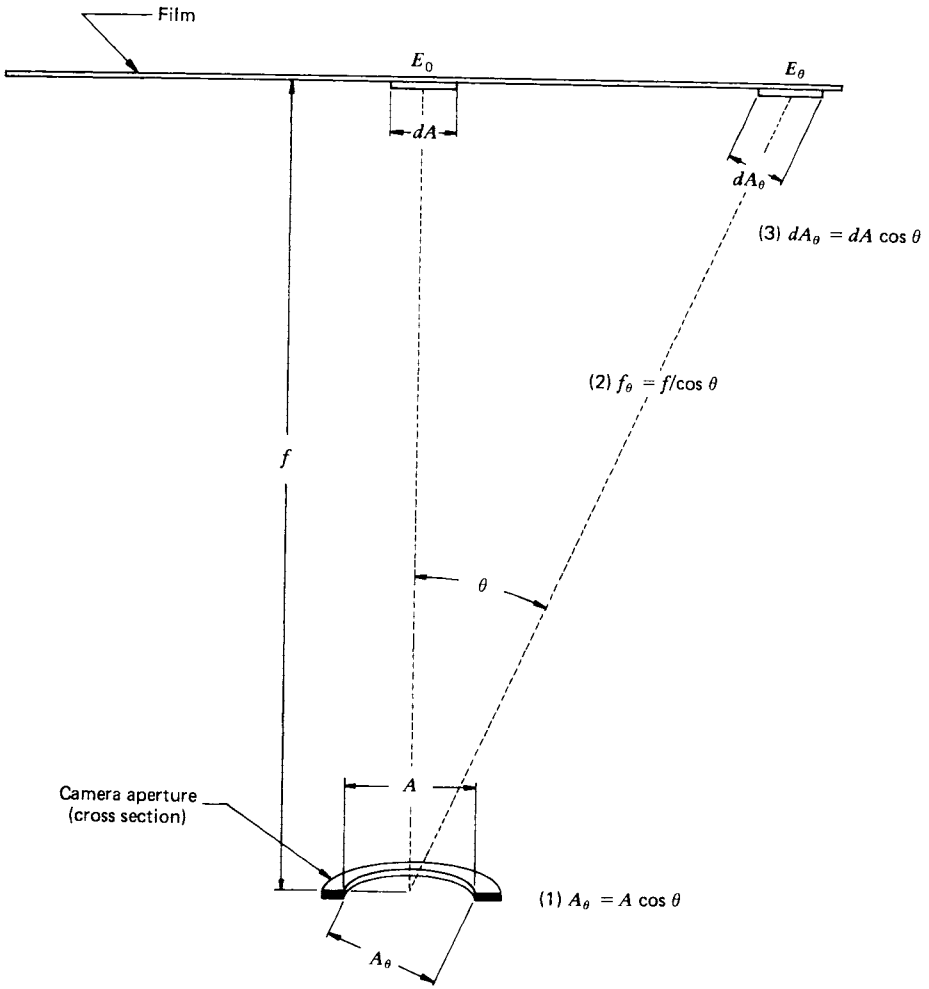

Figure 2.5 Factors causing exposure falloff.

The systematic effect expressed by the above equation is compounded by differential transmittance of the lens and by *vignetting effects* in the camera optics. Vignetting refers to internal shadowing resulting from the lens mounts and other aperture surfaces within the camera. The effect of vignetting varies from camera to camera and varies with aperture setting for any given camera.

Falloff and vignetting are normally mitigated at the time of exposure by using antivignetting filters (see Section 2.9). When such filters are not used, or when they fail to negate the exposure variations completely, it is

appropriate to correct off-axis exposure values by normalizing them to the value they would possess had they been at the center of the photograph. This is done through the application of a correction model that is determined (for a given f-stop) by a radiometric calibration of the camera. This calibration essentially involves photographing a scene of uniform brightness, measuring exposure at various θ locations, and identifying the relationship that best describes the falloff. For most cameras this relationship takes on the form

$$E_\theta = E_0 \cos^n \theta \tag{2.6}$$

Because modern cameras are normally constructed in such a way that their actual falloff characteristics are much less severe than the theoretical $\cos^4$ falloff, n in the above equation is normally in the range 1.5 to 4. All exposure values measured off-axis are then corrected in accordance with the falloff characteristics of the particular camera in use.

The location of an object within a scene can also affect the resulting film exposure, as illustrated in Figures 2.6 and 2.7. Figure 2.6 illustrates the relationships that exist among *solar elevation*, *azimuth angle*, and *camera viewing angle*. Figure 2.7 illustrates geometric effects that can influence the apparent

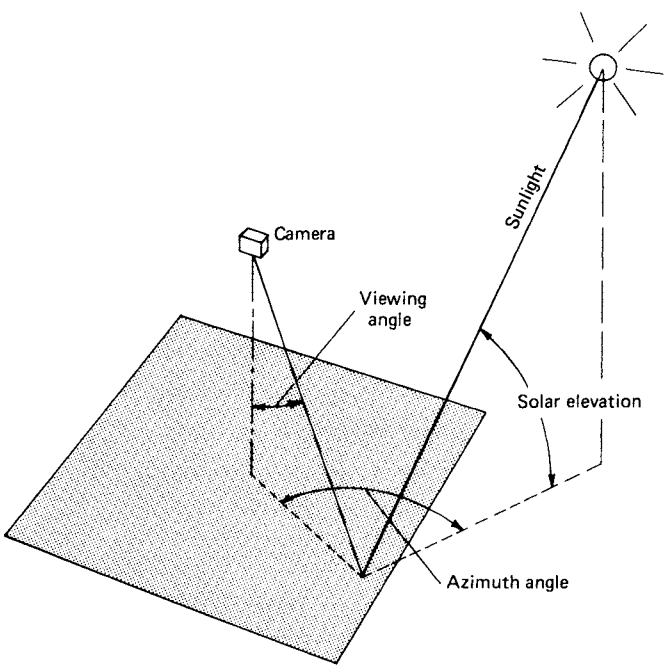

Figure 2.6 Sun–object–image angular relationship.

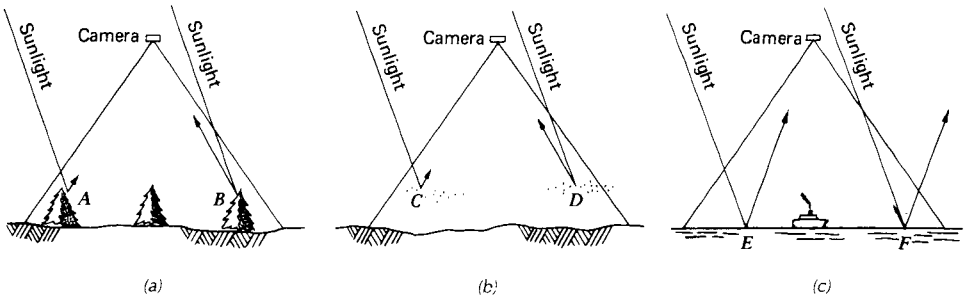

Figure 2.7 Geometric effects that cause variations in focal plane irradiance: (*a*) differential shading, (*b*) differential scattering, and (*c*) specular reflection.

reflectance and exposure. In (*a*), the effect of *differential shading* is illustrated in profile view. Because of relief displacement (Section 3.6), vertical features are imaged in an aerial photograph slightly in side view as well as in top view. Because the sides of features may be either sunlit or shaded, varied exposures can result from identical ground objects at different locations in the image. The film receives more energy from the sunlight side of the tree at *B* than from the shaded side of the tree at *A*. Differential shading is clearly a function of solar elevation and object height, with a stronger effect at low solar angles. The effect is also compounded by differences in slope and aspect (slope orientation) over terrain of varied relief. (Also see BRDF discussion, Section 1.6.)

Figure 2.7*b* illustrates the effect of *differential atmospheric scattering*. Backscatter from atmospheric molecules and particles adds light to that reflected from ground features. The film receives more atmospheric backscatter from area *D* than from area *C* due to geometric relationships. In some analyses, the variation in this "airlight," or path radiance, component is small and can be ignored. However, under hazy conditions, differential quantities of airlight often result in varied exposure across a photograph.

Yet another problem in many analyses is the presence of *specular* reflections in a scene. Photographs taken over water bodies often show areas of specular reflection. They represent the extreme in directional reflectance. Figure 2.7*c* illustrates the geometric nature of this problem. Immediately surrounding point *E* on the image, a considerable increase in exposure would result from specular reflection. This is illustrated in Figure 2.8, which shows areas of specular reflection from the right half of the lake shown in the image. These mirrorlike reflections normally contribute little information about the true character of the objects involved. For example, the small water bodies just below the larger lake take on a tone similar to that of some of the fields in the area. Because of the low information content of specular reflections, they are avoided in most analyses.

.5 FILM DENSITY AND CHARACTERISTIC CURVES

The *radiometric* characteristics of aerial photographs determine how a specific film—exposed and processed under specific conditions—responds to scene energy of varying intensity. Knowledge of these characteristics is often useful, and sometimes essential, to the process of photographic image analysis. This is particularly true when one attempts to establish a quantitative relationship between the tonal values on an image and some ground phenomenon. For example, one might wish to measure the darkness, or optical density, of a transparency at various image points in a corn field and correlate these measurements with a ground-observed parameter such as crop yield. If a correlation exists, the relationship could be used to predict crop yield based on photographic density measurements at other points in the scene. Such an effort can be successful only if the radiometric properties of the particular film under analysis are known. Even then, the analysis must be undertaken with due regard for such extraneous sensing effects as differing levels of illumination across a scene, atmospheric haze, and so on. If these factors can be suffi-

ciently accounted for, considerable information can be extracted from the tonal levels expressed on a photograph. In short, image density measurements may sometimes be used in the process of determining the type, extent, and condition of ground objects. In this section, we discuss the interrelationships between film exposure and film density, and we explain how *characteristic curves* (plots of film density versus log exposure) are analyzed.

A photograph can be thought of as a visual record of the response of many small detectors to energy incident upon them. The energy detectors in a photographic record are the silver halide grains in the film emulsion, and the energy causing the response of these detectors is referred to as a film's *exposure*. During the instant that a photograph is exposed, the different reflected energy levels in the scene irradiate the film for the same length of time. A scene is visible on a processed film only because of the irradiance differences that are caused by the reflectance differences among scene elements. Thus, *film exposure at a point in a photograph is directly related to the reflectance of the object imaged at that point. Theoretically, film exposure varies linearly with object reflectance, with both being a function of wavelength.*

There are many ways of quantifying and expressing film exposure. Most photographic literature uses units of the form *meter-candle-second* (*MCS*) or *ergs/cm*^{2}. The student first "exposed" to this subject might feel hopelessly lost in understanding unit equivalents in photographic radiometry. This comes about since many exposure calibrations are referenced to the sensitivity response of the human eye, through definition of a "standard observer." Such observations are termed *photometric* and result in photometric, rather than radiometric, units. To avoid unnecessary confusion over how exposure is measured and expressed in absolute terms, we will deal with *relative* exposures and not be directly concerned about specifying any absolute units.

The result of exposure at a point on a film, after development, is a silver deposit whose darkening, or light-stopping, qualities are systematically related to the amount of exposure at that point. One measure of the "darkness" or "lightness" at a given point on a film is *opacity O*. Since most quantitative remote sensing image analyses involve the use of negatives or diapositives, opacity is determined through measurement of film *transmittance T*. As shown in Figure 2.9, transmittance T is the ability of a film to pass light. At any given point p, the transmittance is

$$T_p = \frac{\text{light passing through the film at point } p}{\text{total light incident upon the film at point } p} \tag{2.7}$$

Opacity O at point p is

$$O_p = \frac{1}{T_p} \tag{2.8}$$

Although transmittance and opacity adequately describe the "darkness" of a film emulsion, it is often convenient to work with a logarithmic expression,

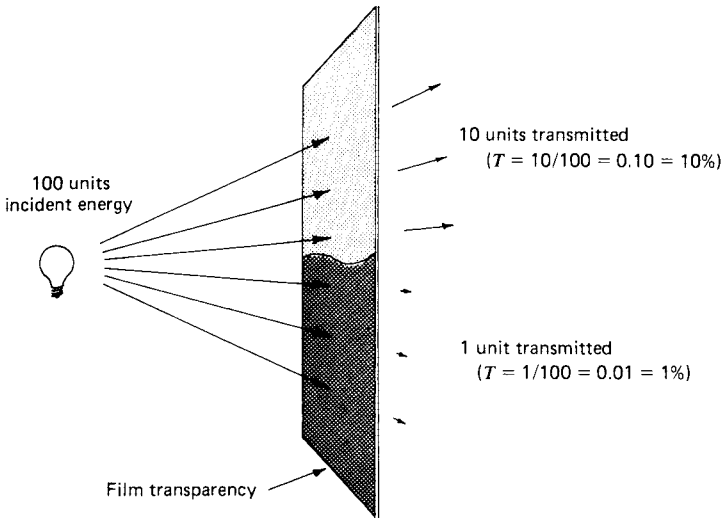

Figure 2.9 Film transmittance. To measure transmittance, a negative or positive transparency is illuminated from one side and the light transmitted through the image is measured on the other. Shown is a section of an image having a transmittance of 0.10 (or 10 percent) at one image point and 0.01 (or 1 percent) at another.

density. This is an appropriate expression, since the human eye responds to light levels nearly logarithmically. Hence, there is a nearly linear relationship between image density and its visual tone. Density D at a point p is defined as the common logarithm of film opacity at that point:

$$D_p = \log(O_p) = \log\left(\frac{1}{T_p}\right) \tag{2.9}$$

Instruments designed to measure density by shining light through film transparencies are called *transmission densitometers*. Density measurements may also be made from paper prints with a *reflectance densitometer*, but more precise measurements can be made on the original film material. When analyzing density on a transparency, the process normally involves placing the film in a beam of light that passes through it. The darker an image is, the smaller the amount of light that is allowed to pass, the lower the transmittance, the higher the opacity, and the higher the density. Some sample values of transmittance, opacity, and density are indicated in Table 2.1.

There are some basic differences between the nature of light absorptance in black and white versus color films. Densities measured on black and white film are controlled by the amount of developed silver in the image areas of measurement. In color photography, the processed image contains no silver and densities are caused by the absorption characteristics of three dye layers

TABLE 2.1 Sample Transmittance, Opacity, and Density Values

Percent Transmittance	T	O	D
100	1.0	1	0.00
50	0.50	2	0.30
25	0.25	4	0.60
10	0.10	10	1.00
1	0.01	100	2.00
0.1	0.001	1000	3.00

in the film: yellow, magenta, and cyan. The image analyst is normally interested in investigating the image density of each of these dye layers separately. Hence, color film densities are normally measured through each of three filters chosen to isolate the spectral regions of maximum absorption of the three film dyes.

An essential task in quantitative film analysis is to relate image density values measured on a photograph to the exposure levels that produced them. This is done to establish the cause (exposure) and effect (density) relationship that characterizes a given photograph.

Since density is a logarithmic parameter, it is convenient to also deal with exposure E in logarithmic form ($\log E$). If one plots density values as a function of the $\log E$ values that produced them, curves similar to those shown in Figure 2.10 will be obtained.

The curves shown in Figure 2.10 are for a typical black and white negative film (*a*) and a color positive film (*b*). Every film has a unique D–$\log E$ *curve*, from which many of the characteristics of the film may be determined. Because of this, these curves are known as *characteristic curves*. (Plotting D versus $\log E$ to express the nature of the photographic response was first suggested in the 1890s by Hurter and Driffield. Consequently, characteristic curves are often referred to as *H and D* as well as D–$\log E$ curves.)

Characteristic curves are different for different film types, for different manufacturing batches within a film type, and even for films of the same batch. Manufacturing, handling, storage, and processing conditions all affect the response of a film (indicated by its D–$\log E$ curve). In the case of color film, characteristic curves also differ between one emulsion layer and another.

Figure 2.11 illustrates the various film response characteristics extractable from a D–$\log E$ curve. The curve shown is typical of a black and white negative film (similar characteristics are found for each layer of a color film). There are three general divisions to the curve. First, as the exposure increases from that of point A to that of point B, the density increases from a minimum,

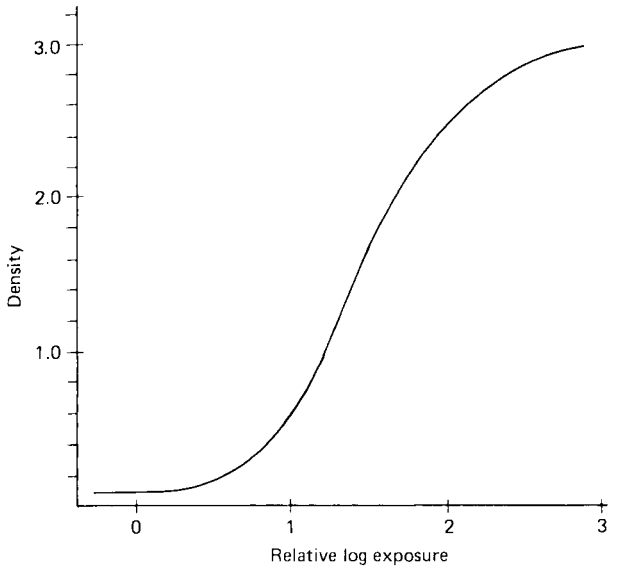

(a)

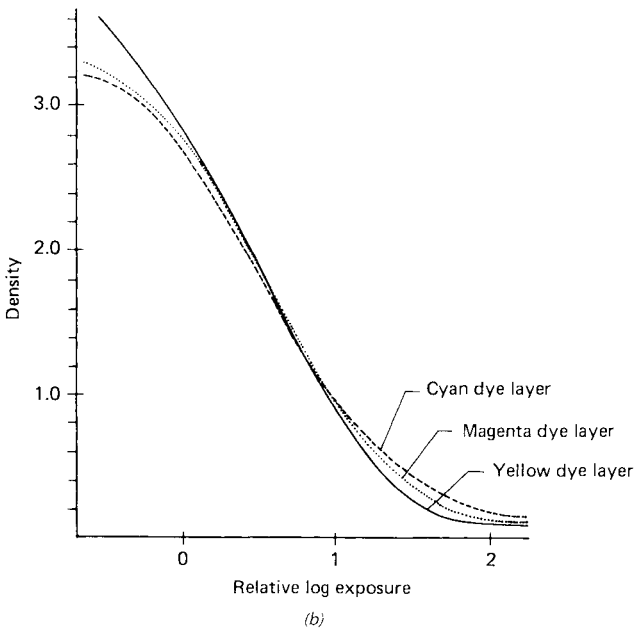

(b)

Figure 2.10 Film density versus log exposure curves: (*a*) black and white negative film; (*b*) color reversal film (positive film). (These curves are referred to as film characteristic curves, *D*–log *E* curves, or H and D curves.)

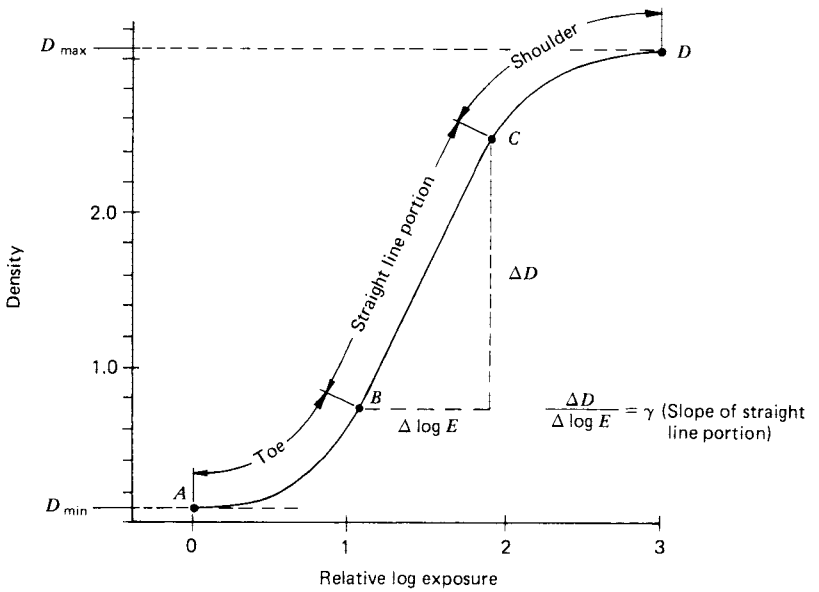

Figure 2.11 Components of a characteristic curve.

D_{min}, at an increasing rate. This portion of the curve is called the *toe*. As exposure increases from point B to point C, changes in density are nearly linearly proportional to changes in log exposure. This region is called the *straight-line portion* of the curve. Finally, as log exposure increases from point C to point D, the density increases at a decreasing rate. This portion is known as the *shoulder* of the curve. The shoulder terminates at a maximum density, D_{max}. Remember that this curve applies to a negative film. For a positive film (Figure 2.10*b*), the relationship is reversed. That is, density decreases with increasing exposure.

It should be noted that even in areas of a film where there is no exposure, a minimum density D_{min} results from two causes: (1) The plastic base of the film has some density D_{base} and (2) some density develops even when an unexposed emulsion is processed. This second type of density is called *fog*, or *net fog*, D_{fog}. Density D_{min} is sometimes called *gross fog* and is expressed as

$$D_{min} = D_{base} + D_{fog} \tag{2.10}$$

The range of densities a film provides is simply the difference between D_{max} and D_{min}.

Another important characteristic of D–log E curves is the slope of the linear portion of the curve. This slope is called *gamma* (γ) and is expressed as

$$\gamma = \frac{\Delta D}{\Delta \log E} \tag{2.11}$$

Gamma is an important determinant of the *contrast* of a film. While the term *contrast* has no rigid definition, in general, the higher the gamma, the higher the contrast of a film. With high contrast film, a given scene exposure range is distributed over a large density range; the reverse is true of low contrast film. For example, consider a photograph taken of a light gray and a dark gray object. On high contrast film, the two gray levels may lie at the extremes of the density scale, resulting in nearly white and nearly black images on the processed photograph. On low contrast film, both gray values would lie at nearly the same point on the density scale, showing the two objects in about the same shade of gray.

Gamma is a function of not only emulsion type but also film development conditions. For example, gamma can be varied by changing developer, development time, and/or development temperature. For any given developer, gamma is usually increased with longer development time or higher development temperature.

An important basic characteristic of a film is its *speed*, which expresses the sensitivity of the film to light. This parameter is graphically represented by the horizontal position of the characteristic curve along the $\log E$ axis. A "fast" film (more light-sensitive film) is one that will accommodate low exposure levels (i.e., it lies farther to the left on the $\log E$ axis). For a given level of scene energy, a fast film will require a shorter exposure time than will a slow film. This is advantageous in aerial photography, since it reduces image blur due to flight motion. However, high speed films are generally characterized by larger film grains, limiting the spatial resolution of images. Thus, no single film speed will be optimum in all cases.

The speed of nonaerial films is typically stated using the International Standardization Organization (ISO) system. This system is generally not used to specify the speed of aerial photographic films. Rather, for panchromatic aerial films, the American National Standard for film responsivity is the *aerial film speed* (*AFS*). By definition,

$$\text{AFS} = \frac{3}{2E_0} \tag{2.12}$$

where E_0 is the exposure (in meter-candle-seconds) at the point on the characteristic curve where the density is 0.3 above $D_{\min}$ under strictly specified processing conditions. For other processing conditions and for color and infrared-sensitive films, *effective aerial film speeds* are used to indicate sensitivity. These values are determined empirically, often by comparison with black and white films in actual flight tests.

In selecting the lens opening and shutter speed combination to give proper exposure for a given film speed, the date of photography, the latitude of the flight area, the time of day, the flight altitude, and the haze conditions must be considered.

Two other useful film characteristics can be determined from the D–$\log E$ curve. These are a film's exposure latitude and its radiometric resolution.

These characteristics are best described with reference to Figure 2.12, where the D–log E curves for two different negative films are shown.

The term *exposure latitude* expresses the range of log E values that will yield an acceptable image on a given film. For most films, good results are obtained when scenes are recorded over the linear portion of the D–log E curves and a fraction of the toe of the curve (Figure 2.12). Features recorded on the extremes of the toe or shoulder of the curve will be underexposed or overexposed. In these areas, different exposure levels will be recorded at essentially the same density, making discrimination difficult. Note in Figure 2.12 that film 2 has a much larger exposure latitude than film 1. (Also note that film 2 is a "slower" film than film 1.)

The term *exposure latitude* is also used to indicate the range of variation from the optimum camera exposure setting that can be tolerated without excessively degrading the image quality. For example, an exposure latitude of $\pm\frac{1}{2}$ stop is generally specified for certain aerial films. This means that the f-stop setting can be $\frac{1}{2}$ stop above or below the optimum setting and still produce an acceptable photograph.

As shown in Figure 2.12, *radiometric resolution* is the smallest difference in exposure that can be detected in a given film analysis. Radiometric resolution

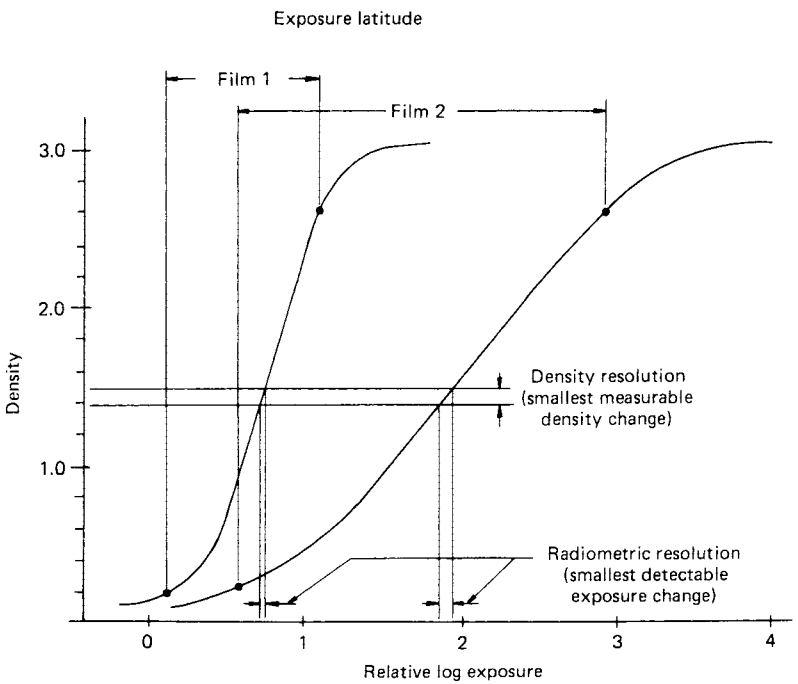

Figure 2.12 Exposure latitude and radiometric resolution of two films. (Film 2 has larger exposure latitude but poorer radiometric resolution than film 1.)

is inversely proportional to contrast, so for a given density resolvability, a higher contrast film (i.e., film 1 in Figure 2.12) is able to resolve smaller differences in exposure.

The trade-offs between contrast, exposure latitude, and radiometric resolution can now be seen. Although exceptions to the rule exist, low contrast films offer greater radiometric range (exposure latitude) at the expense of radiometric resolution. High contrast films offer a smaller exposure range but improved radiometric resolution.

Image density is measured with an instrument called a *densitometer* (or *microdensitometer* when small film areas are measured). While many varieties of densitometers exist, most have the same six basic components, shown in Figure 2.13:

1. **Light source.** Supplies energy to illuminate the image with a beam of incident radiation.
2. **Aperture assembly.** Provides for selectable spot sizes over which density measurements can be made.
3. **Filter assembly.** Allows selection of spectral bands when making density measurements on color film.
4. **Receiver.** A photoelectric device, normally a photomultiplier tube (PMT), that responds electronically to the component of the illuminating beam transmitted through the image.

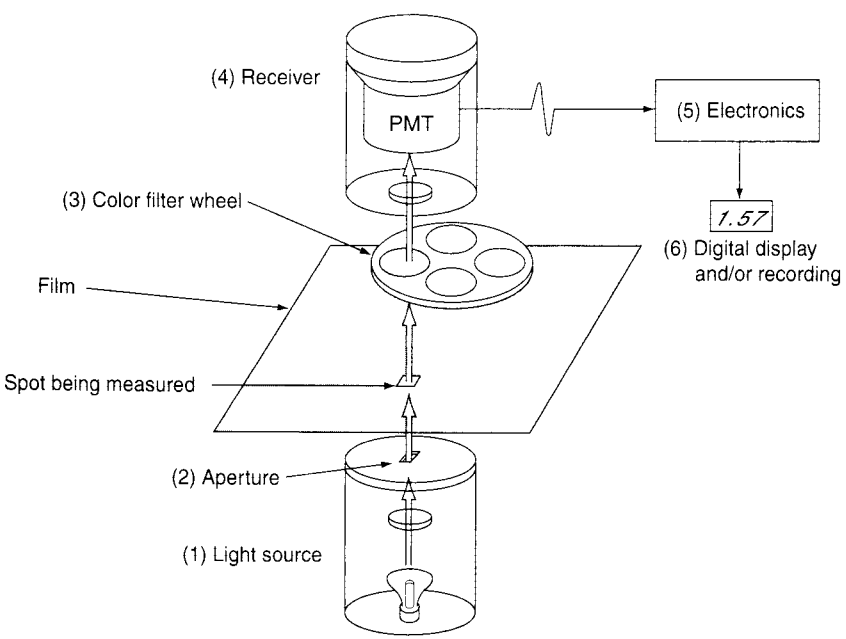

Figure 2.13 Schematic of one configuration of a densitometer.

5. **Electronics.** Amplify the output of the receiver, convert it logarithmically to a density value, and express it in a digital representation. Calibration controls enable the density readings to be referenced to a calibration standard.
6. **Digital display and/or recording.** Indicates the density value. Many densitometers have a provision for recording density values on various computer storage media.

With *spot* densitometers, different reading positions on the image are located by manually translating the image under analysis with respect to the measurement optics. These devices are convenient in applications where conventional visual interpretation is supported by taking a small number of density readings at discrete points of interest in an image. Applications calling for density measurements throughout an entire image dictate the use of *scanning densitometers*.

There are basically two types of film scanning densitometers: *rotating drum* systems and *flatbed* systems. Rotating drum scanners (Figure 2.14) accomplish the scanning task by mounting the film over a square opening in a rotating drum such that it forms a portion of the drum's circumference. The x coordinate scanning motion is provided by the rotation of the drum. The y coordinate motion comes from incremental translation of the source/receiver optics after each drum rotation. Typically, such systems employ a PMT to convert the light energy incident upon the receiver into an electronic signal.

There are several forms of flatbed film scanning systems. The most common form uses a linear array of charge-coupled devices (CCDs; Section 2.12). Optics focus the CCD array on one horizontal line of the subject at a time and step vertically to capture repeated lines.

The output from a scanning film densitometer, whether rotating drum or flatbed, is a digital image composed of pixels whose size is determined by the aperture of the source/receiving optics used during the scanning process. The output is converted to a series of digital numbers. This A-to-D conversion

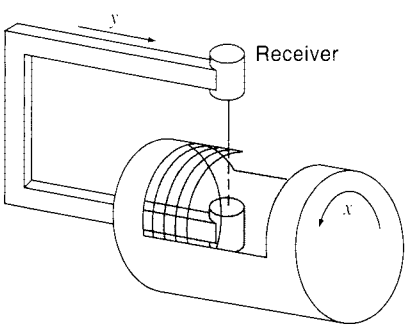

Figure 2.14 Rotating drum scanning densitometer operation.

process normally results in recording the density data on any of several forms of computer storage media.

Scanners with the highest radiometric resolution can record a film density range of 0 to 4, which means that the difference between the lightest and darkest detectable intensities is 10,000 : 1. Typically monochromatic scanning is done with a 12-bit resolution, which results in 4096 levels of gray, although 16-bit resolutions (65,536 levels) are sometimes used. Color scanning is typically 36- to 48-bit scanning (12 to 16 bits per color), resulting in many billions of colors that can be resolved.

Because scanning spot sizes as small as about 6.25 μm can be utilized with drum scanners, the process can result in immense data volumes. For example, assuming a scanning aperture and scan line spacing of 6.25 μm were used, 160 density observations per lineal millimeter in both x and y would result, yielding 25,600 observations for a 1-mm-square film area (more than one billion observations on a 230 $\times$ 230-mm film).

Figure 2.15 illustrates a flatbed scanner that is often employed in soft-copy photogrammetric operations (Section 3.9). This particular scanner permits scanning at resolutions of 7, 14, 21, 28, 56, 112, or 224 μm over formats as large as 250 × 275 mm. Monochromatic scanning at 10-bit resolution, and color scanning at 24-bit resolution (8 bits per color), over a density range of 0.001 to 3.3, are the typical modes of scanning for this system. The geometric accuracy of this scanner is better than 2 μm in each axis of scanning.

2.6 SPECTRAL SENSITIVITY OF BLACK AND WHITE FILMS

Black and white aerial photographs are normally made with either *panchromatic* film or *infrared-sensitive* film. The generalized spectral sensitivities for each of these film types are shown in Figure 2.16. Panchromatic film has long been the "standard" film type for aerial photography. As can be seen from Figure 2.16, the spectral sensitivity of panchromatic film extends over the UV and the visible portions of the spectrum. Infrared-sensitive film is sensitive not only to UV and visible energy but also to near-IR energy.

The use of black and white IR photography to distinguish between deciduous and coniferous trees was illustrated in Figure 1.9. Many other applications of both panchromatic and black and white infrared aerial photography are described in Chapter 4. Here, we simply want the reader to become familiar with the spectral sensitivities of these materials.

It is of interest to note what determines the "boundaries" of the spectral sensitivity of black and white film materials. As indicated in Section 2.1, we

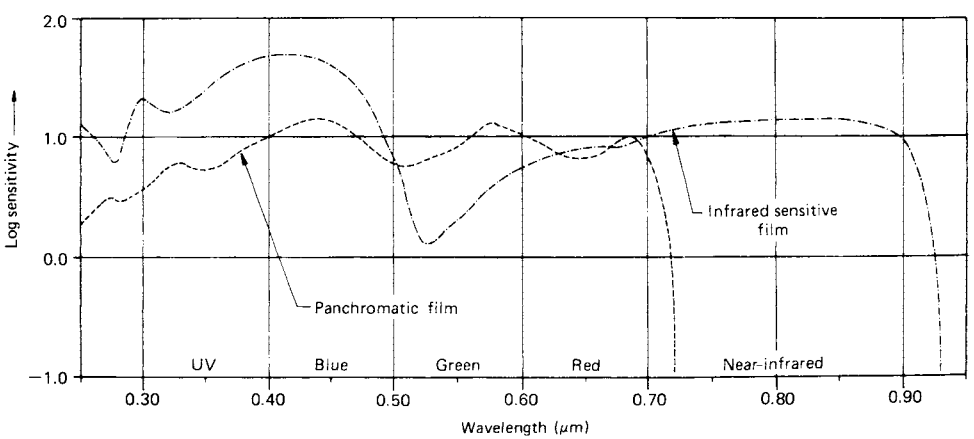

Figure 2.16 Generalized spectral sensitivities for panchromatic and black and white IR-sensitive films. (Adapted from Eastman Kodak Company, 1992.)

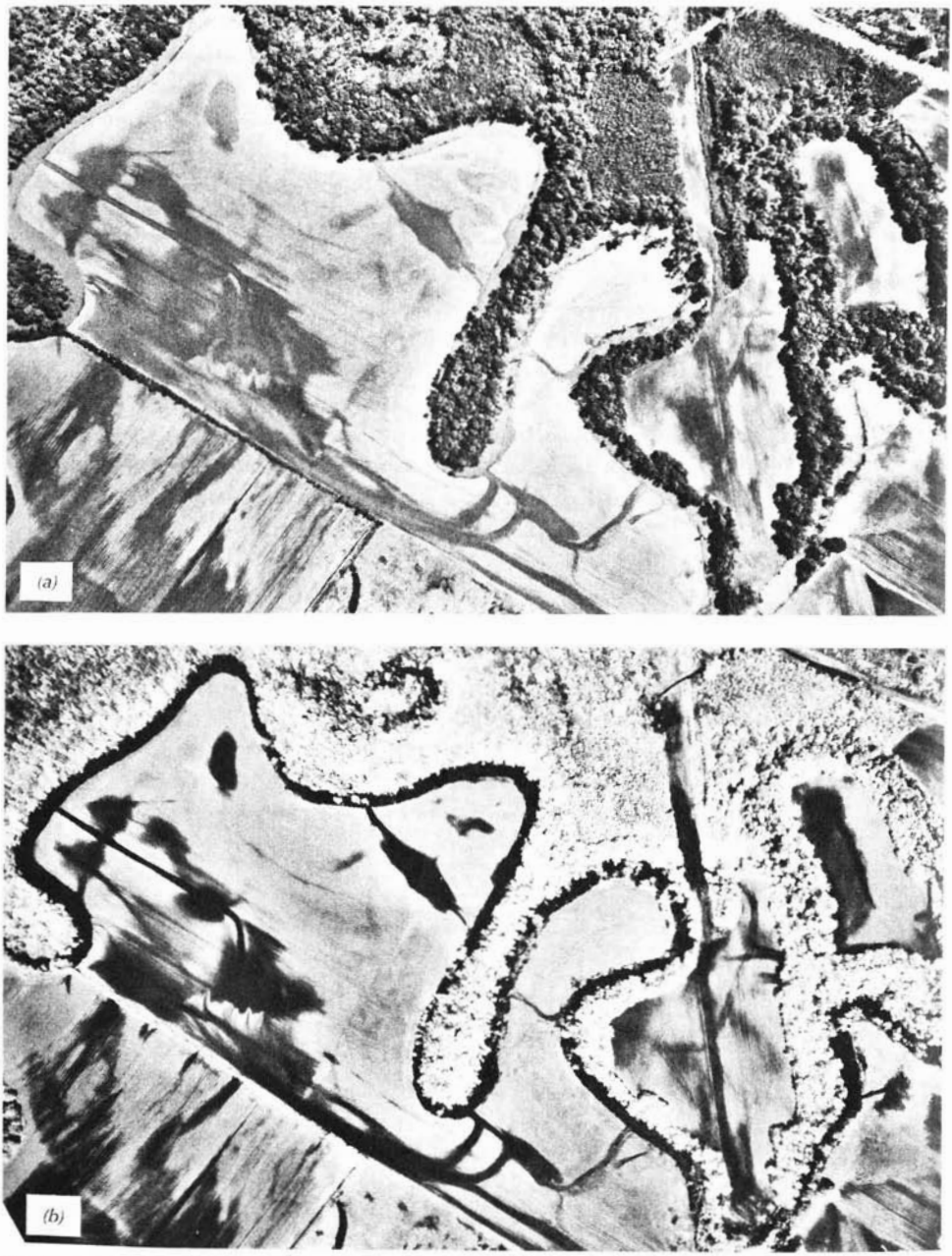

Figure 2.17 Comparison of panchromatic and black and white IR aerial photographs. Flooding of Bear Creek, northwest Alabama (scale 1 : 9000): (*a*) panchromatic film with a Wratten No. 12 (yellow) filter; (*b*) black and white IR film with a Wratten No. 12 filter. (Courtesy Mapping Services Branch, Tennessee Valley Authority.)

can photograph over a range of about 0.3 to 0.9 μm. The 0.9-μm limit stems from the photochemical instability of emulsion materials that are sensitive beyond this wavelength. (Certain films used for scientific experimentation are sensitive out to about 1.2 μm and form the only exception to this rule. These films are not commonly available and typically require long exposure times, making them unsuitable for aerial photography.)

Figure 2.17 shows a comparison between panchromatic and black and white IR aerial photographs. The image tones shown in this figure are very typical. Healthy green vegetation reflects much more sunlight in the near IR than in the visible part of the spectrum; therefore, it appears lighter in tone on black and white infrared photographs than on panchromatic photographs. Note, for example, that in Figure 2.17 the trees are much lighter toned in (*b*) than in (*a*). Note also that the limits of the stream water and the presence of water and wet soils in the fields can be seen more distinctly in the black and white IR photograph (*b*). Water and wet soils typically have a much darker tone in black and white IR photographs than in panchromatic photographs because sunlight reflection from water and wet soils in the near IR is considerably less than in the visible part of the electromagnetic spectrum.

As might be suspected from Figure 2.16, the 0.3-μm limit to photography is determined by something other than film sensitivity. In fact, virtually all photographic emulsions are sensitive in this UV portion of the spectrum. The problem with photographing at wavelengths shorter than about 0.4 μm is twofold: (1) the atmosphere absorbs or scatters much of this energy and (2) glass camera lenses absorb such energy. But photographs can be acquired in the 0.3- to 0.4-μm range if extremes of altitude and unfavorable atmospheric conditions are avoided. Furthermore, some improvement in image quality is realized if quartz camera lenses are used.

To date, the applications of aerial UV photography have been limited in number, due primarily to strong atmospheric scattering of UV energy. A notable exception is the use of UV photography in monitoring oil films on water. Minute traces of floating oil, often invisible on other types of photography, can be detected in UV photography.

2.7 COLOR FILM

Although black and white panchromatic film has long been the standard film type for aerial photography, many remote sensing applications currently involve the use of color film. The major advantage to the use of color is the fact that the human eye can discriminate many more shades of color than it can tones of gray. As we illustrate in subsequent chapters, this capability is essential in many applications of airphoto interpretation. In the remainder of this

section we present the basics of how color film works. To do this, we must first consider the way in which human color vision works.

Color-Mixing Processes

Light falling on the retina of the human eye is sensed by rod and cone cells. There are about 130 million rod cells, and they are 1000 times more light sensitive than the cone cells. When light levels are low, human vision relies on the rod cells to form images. All rod cells have the same wavelength sensitivity, which peaks at about 0.55 μm. Therefore, human vision at low light levels is monochromatic. It is the cone cells that determine the colors the eye sees. There are about 7 million cone cells; some sensitive to blue energy, some to green energy, and some to red energy. The *trichromatic theory of color vision* explains that when the blue-sensitive, green-sensitive, and red-sensitive cone cells are stimulated by different amounts of light, we perceive color. When all three types of cone cells are stimulated equally, we perceive white light. Other theories of color vision have been proposed. The *opponent process of color vision* hypothesizes that color vision involves three mechanisms, each responding to a pair of so-called opposites: white–black, red–green, and blue–yellow. This theory is based on many psychophysical observations and states that colors are formed by a *hue cancellation method*. The hue cancellation method is based on the observation that when certain colors are mixed together, the resulting colors are not what would be intuitively expected. For example, when red and green are mixed together, they produce yellow, not reddish green. (For further information, see Robinson et al., 1995.)

In the remainder of this discussion, we focus on the trichromatic theory of color vision. Again, this theory is based on the concept that we perceive all colors by synthesizing various amounts of just three (blue, green, and red).

Blue, green, and red are termed *additive primaries*. Plate 2*a* shows the effect of projecting blue, green, and red light in partial superimposition. Where all three beams overlap, the visual effect is white because all three of the eyes' receptor systems are stimulated equally. Hence, white light can be thought of as the mixture of blue, green, and red light. Various combinations of the three additive primaries can be used to produce other colors. As illustrated, when red light and green light are mixed, yellow light is produced. Mixture of blue and red light results in the production of magenta light (bluish-red). Mixing blue and green results in cyan light (bluish-green).

Yellow, magenta, and cyan are known as the *complementary colors*, or *complements*, of blue, green, and red light. Note that the complementary color for any given primary color results from mixing the remaining two primaries.

Like the eye, color television and computer monitors operate on the principle of additive color mixing through use of blue, green, and red dots (or ver-

tical lines) on the picture screen. When viewed at a distance, the light from the closely spaced screen elements forms a continuous color image.

Whereas color television simulates different colors through *additive* mixture of blue, green, and red *lights*, color photography is based on the principle of *subtractive* color mixture using superimposed yellow, magenta, and cyan *dyes*. These three dye colors are termed the *subtractive primaries*, and each results from subtracting one of the additive primaries from white light. That is, yellow dye absorbs the blue component of white light. Magenta dye absorbs the green component of white light. Cyan dye absorbs the red component of white light.

The subtractive color-mixing process is illustrated in Plate 2*b*. This plate shows three circular filters being held in front of a source of white light. The filters contain yellow, magenta, and cyan dye. The yellow dye absorbs blue light from the white background and transmits green and red. The magenta dye absorbs green light and transmits blue and red. The cyan dye absorbs red light and transmits blue and green. The superimposition of magenta and cyan dyes results in the passage of only blue light from the background. This comes about since the magenta dye absorbs the green component of the white background and the cyan dye absorbs the red component. Superimposition of the yellow and cyan dyes results in the perception of green. Likewise, superimposition of yellow and magenta dyes results in the perception of red. Where all three dyes overlap, all light from the white background is absorbed and black results.

In color photography, various proportions of yellow, magenta, and cyan dye are superimposed to control the proportionate amount of blue, green, and red light that reaches the eye. Hence, the subtractive mixture of yellow, magenta, and cyan dyes on a photograph is used to control the additive mixture of blue, green, and red light reaching the eye of the observer. To accomplish this, color film is manufactured with three emulsion layers that are sensitive to blue, green, and red light but contain yellow, magenta, and cyan dye after processing.

Structure and Spectral Sensitivity of Color Film

The basic cross-sectional structure and spectral sensitivity of color film are shown in Figure 2.18. As shown in Figure 2.18*a*, the top film layer is sensitive to blue light, the second layer to green and blue light, and the third to red and blue light. Because these bottom two layers have blue sensitivity as well as the desired green and red sensitivities, a blue-absorbing filter layer is introduced between the first and second photosensitive layers. This filter layer blocks the passage of blue light beyond the blue-sensitive layer. This effectively results in selective sensitization of each of the film layers to the blue, green, and red primary colors. The yellow (blue-absorbing) filter layer has no permanent effect on the appearance of the film because it is dissolved during processing.

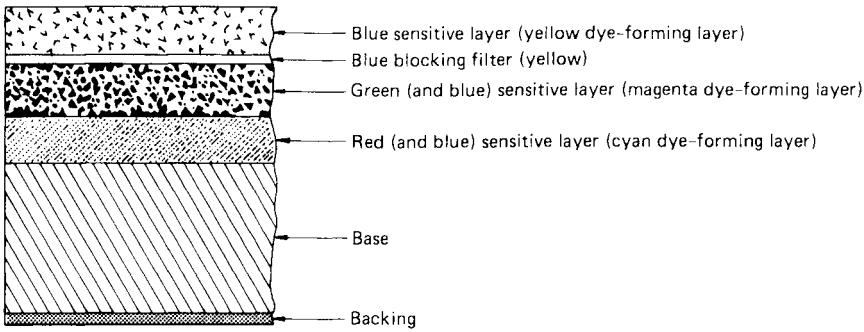

(a)

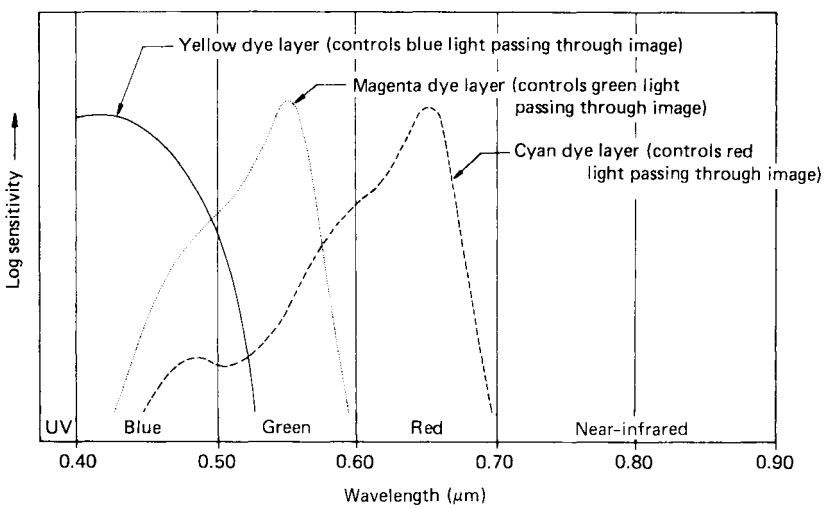

(b)

Figure 2.18 Structure and sensitivity of color film: (*a*) generalized cross section; (*b*) spectral sensitivities of the three dye layers. (Adapted from Eastman Kodak Company, 1992.)

From the standpoint of spectral sensitivity, the three layers of color film can be thought of as three black and white silver halide emulsions (Figure 2.18*b*). Again, the colors physically present in each of these layers after the film is processed are *not* blue, green, and red. Rather, after processing, the blue-sensitive layer contains yellow dye, the green-sensitive layer contains magenta dye, and the red-sensitive layer contains cyan dye (see Figure 2.18*a*). The amount of dye introduced in each layer is inversely related to the inten-

sity of the corresponding primary light present in the scene photographed. When viewed in composite, the dye layers produce the visual sensation of the original scene.

The manner in which the three dye layers of color film operate is shown in Figure 2.19. For purposes of illustration, the original scene is represented schematically in (*a*) by a row of boxes that correspond to scene reflectance in four spectral bands: blue, green, red, and near IR. During exposure, the blue-sensitive layer is activated by the blue light, the green-sensitive layer is activated by the green light, and the red-sensitive layer is activated by the red light, as shown in (*b*). No layer is activated by the near-IR energy since the film is not sensitive to near-IR energy. During processing, dyes are introduced into each sensitivity layer in *inverse* proportion to the intensity of light recorded in each layer. Hence the more intense the exposure of the blue layer to blue light, the less yellow dye is introduced in the image and the more magenta and cyan dyes are introduced. This is shown in (*c*), where, for blue light, the yellow dye layer is clear and the other two layers contain magenta and cyan dyes. Likewise, green exposure results in the introduction of yellow and cyan dyes, and red exposure results in the introduction of yellow and magenta

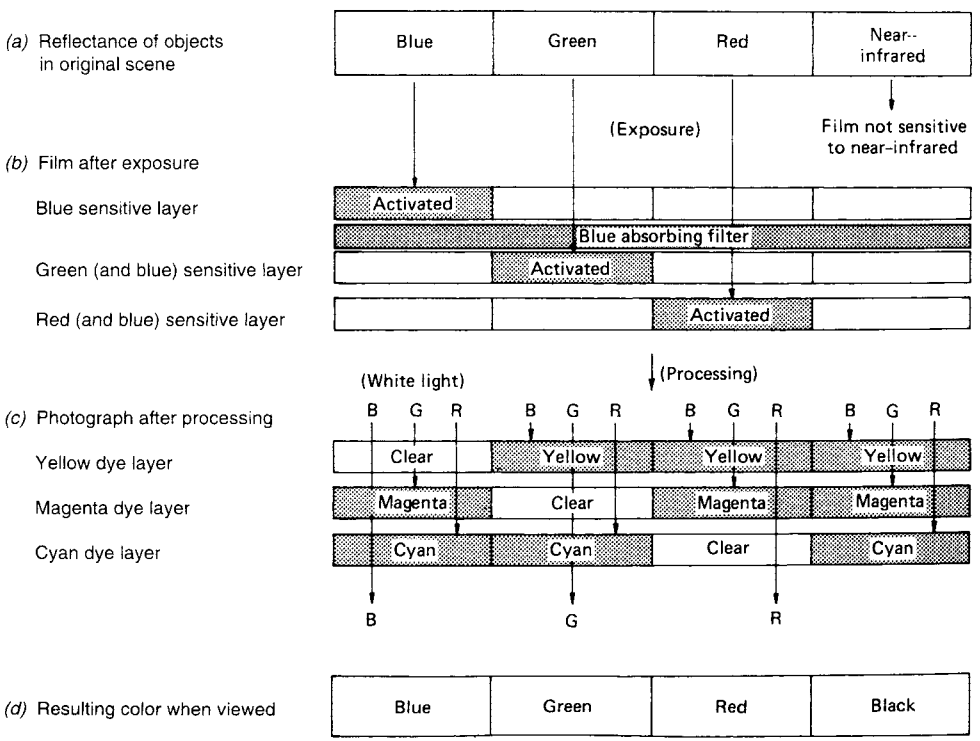

Figure 2.19 Color formation with color film. (Adapted from Eastman Kodak Company, 1992.)

dyes. When the developed image is viewed with a white light source (*d*), we perceive the colors in the original scene through the subtractive process. Where a blue object was present in the scene, the magenta dye subtracts the green component of the white light, the cyan dye subtracts the red component, and the image appears blue. Green and red are produced in an analogous fashion. Other colors are produced in accordance with the proportions of blue, green, and red present in the original scene.

The human eye is more sensitive to green wavelengths than to blue and red wavelengths. For this reason, some films (e.g., Fujicolor Nexia and Superia) employ a fourth, 'cyan-sensitive,' layer in order to improve the color fidelity of the film. This layer is physically located between the green-sensitive and red-sensitive film layers. The sensitivity curve for this layer lies beneath the shorter-wavelength portion of the green-sensitive layer's curve. Magenta dye is used for this 'cyan-sensitive' layer, in addition to the green-sensitive layer.

2.8 COLOR INFRARED FILM

The assignment of a given dye color to a given spectral sensitivity range is a film manufacturing parameter that can be varied arbitrarily. The color of the dye developed in any given emulsion layer need not bear any relationship to the color of light to which the layer is sensitive. Any desired portions of the photographic spectrum, including the near IR, can be recorded on color film with any color assignment.

In contrast to "normal" color film, *color IR* film is manufactured to record green, red, and the photographic portion (0.7 to 0.9 μm) of the near-IR scene energy in its three emulsion layers. The dyes developed in each of these layers are again yellow, magenta, and cyan. The result is a "false color" film in which blue images result from objects reflecting primarily green energy, green images result from objects reflecting primarily red energy, and red images result from objects reflecting primarily in the near-IR portion of the spectrum.

The basic structure and spectral sensitivity of color IR film are shown in Figure 2.20. (Note that there are some overlaps in the sensitivities of the layers.) The process by which the three primary colors are reproduced with such films is shown in Figure 2.21. Various combinations of the primary colors and complementary colors, as well as black and white, can also be reproduced on the film, depending on scene reflectance. For example, an object with a high reflectance in both green and near IR would produce a magenta image (blue plus red). It should be noted that most color IR films are designed to be used with a yellow (blue-absorbing) filter over the camera lens. As further described in Section 2.9, the yellow filter blocks the passage of any light having a wavelength below about 0.5 μm. This means that the blue (and

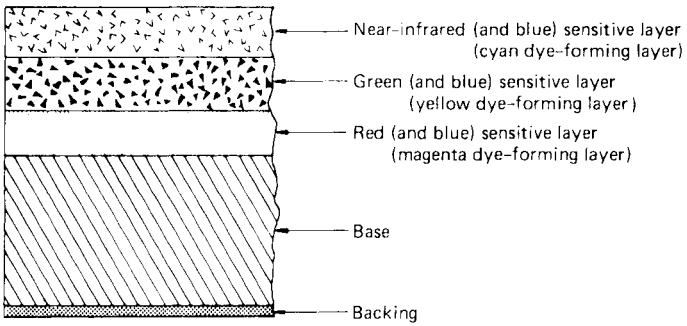

(a)

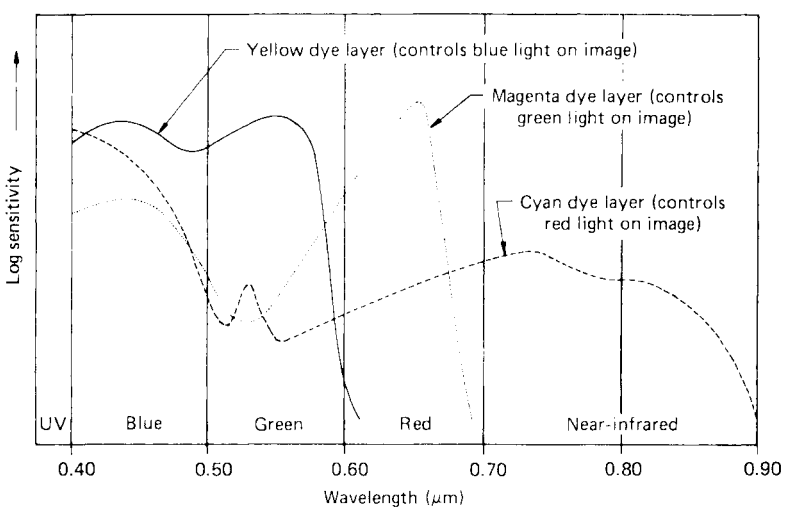

(b)

Figure 2.20 Structure and sensitivity of color IR film: (*a*) generalized cross section; (*b*) spectral sensitivities of the three dye layers. (Adapted from Eastman Kodak Company, 1992.)

UV) scene energy is not permitted to reach the film, a fact that aids in the interpretation of color IR imagery. If a yellow (blue-absorbing) filter were not used, it would be very difficult to ascribe any given image color to a particular ground reflectance because of the nearly equal sensitivity of all layers of the film to blue energy. The use of a blue-absorbing filter has the further advantage of improving haze penetration because the effect of Rayleigh scatter is reduced when the blue light is filtered out.

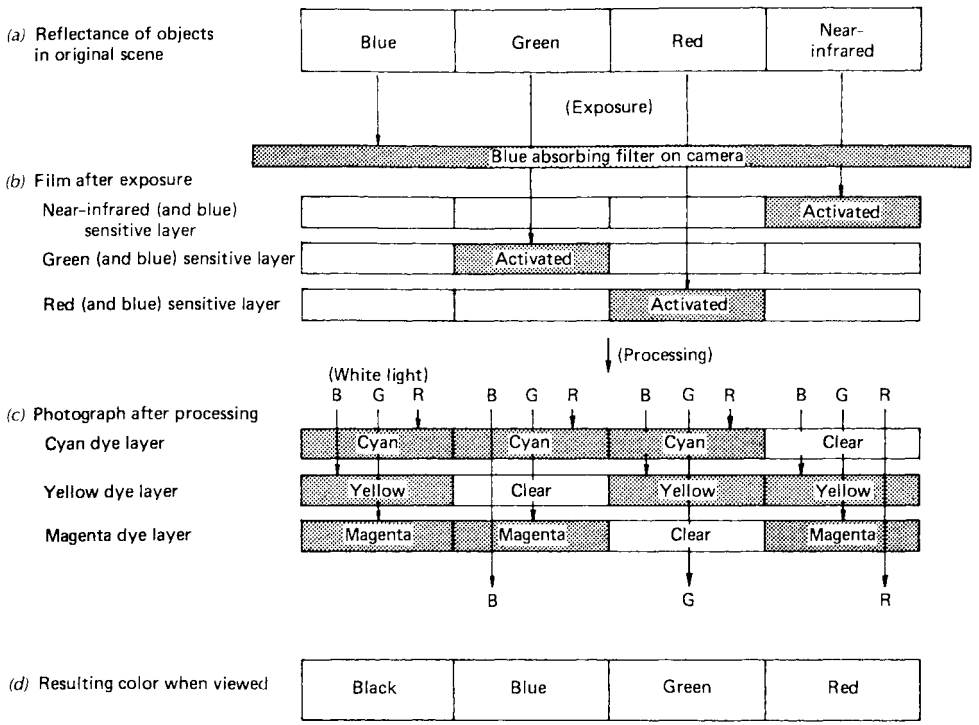

Figure 2.21 Color formation on color IR film. (Adapted from Eastman Kodak Company, 1992.)

Color IR film was developed during World War II to detect painted targets that were camouflaged to look like vegetation. Because healthy vegetation reflects IR energy much more strongly than it does green energy, it generally appears in various tones of red on color IR film. However, objects painted green generally have low IR reflectance. Thus, they appear blue on the film and can be readily discriminated from healthy green vegetation. Because of its genesis, color IR film has often been referred to as "camouflage detection film." With its vivid color portrayal of near-IR energy, color IR film has become an extremely useful film for resource analyses.

Plate 3 illustrates normal color (*a*) and color IR (*b*) aerial photographs of a portion of the University of Wisconsin–Madison campus. The grass, tree leaves, and football field reflect more strongly in the green than in the blue or red and thus appear green in the natural color photograph. The healthy grass and tree leaves reflect much more strongly in the IR than in the green or red and thus appear red in the color IR photograph. The football field has artificial turf that does not reflect well in the IR and thus does not appear red. The large rectangular gravel parking area adjacent to the natural grass practice fields appears a light brown in the normal color photograph and nearly white

in the color IR photograph. This means it has a high reflectance in green, red, and IR. The red-roofed buildings appear a greenish-yellow on the color IR film, which means that they reflect highly in the red and also have some IR reflectance. The fact that the near-IR-sensitive layer of the film also has some sensitivity to red (Figure 2.20) also contributes to the greenish-yellow color of the red roofs when photographed on the color IR film.

Almost every aerial application of color IR photography deals with photographing *reflected sunlight*. The amount of energy *emitted* from the earth at ambient temperature (around 300 K) is insignificant in the range of 0.4 to 0.9 μm and hence cannot be photographed. This means that color IR film cannot, for example, be used to detect the temperature difference between two water bodies or between wet and dry soils. As explained in Chapter 5, electronic sensors (such as radiometers or thermal scanners) operating in the wavelength range 3 to 5 or 8 to 14 μm can be used to distinguish between temperatures of such objects.

The energy *emitted* from extremely hot objects such as flames from burning wood (forest fires or burning buildings) or flowing lava *can* be photographed on color and color IR film. Figure 2.22 shows blackbody radiation curves for earth features at an ambient temperature of 27°C (300 K) and flowing lava at 1100°C (1373 K). As calculated from Wien's displacement law (Eq. 1.5), the peak wavelength of the emitted energy is 9.7 μm for the earth features at 27°C and 2.1 μm for lava at 1100°C. When the spectral distribution of emitted energy is calculated, it is found that the energy emitted from the features

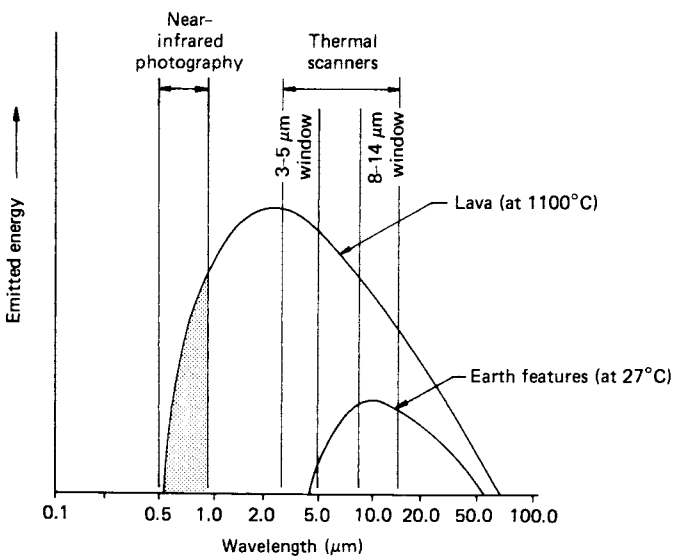

Figure 2.22 Blackbody radiation curves for earth surface features (at 27°C) and flowing lava (at 1100°C).

at 27°C is essentially zero over the range of photographic wavelengths. In the case of flowing lava at 1100°C, the emitted energy in the range of IR photography (0.5 to 0.9 μm) is sufficient to be recorded on photographic films.

Plate 4 shows normal color (*a*) and color IR (*b*) aerial photographs of flowing lava on the flank of Kilauea Volcano on the Island of Hawaii. Although the emitted energy can be seen as a faint orange glow on the normal color photograph, it is more clearly evident on the color IR film. The orange tones on the color IR photograph represent IR energy *emitted* from the flowing lava. The pink tones represent sunlight *reflected* from the living vegetation (principally tree ferns). Keep in mind that it is *only* when the temperature of a feature is extremely high that IR film will record energy emitted by an object. At all other times, the film is responding to *reflected* IR energy that is not directly related to the temperature of the feature.

2.9 FILTERS

Film type is only one variable that determines what information is recorded by a photographic remote sensing system. Equally important is the spectral makeup of the energy exposing the film. Through the use of filters, we can be selective about which wavelengths of energy reflected from a scene we allow to reach the film. Filters are transparent (glass or gelatin) materials that, by absorption or reflection, eliminate or reduce the energy reaching a film in selected portions of the photographic spectrum. They are placed in the optical path of a camera in front of the lens.

Aerial camera filters consist mainly of organic dyes suspended in glass or in a dried gelatin film. Filters are most commonly designated by *Kodak Wratten* filter numbers. They come in a variety of forms having a variety of spectral transmittance properties. The most commonly used spectral filters are *absorption filters*. As their name indicates, these filters absorb and transmit energy of selected wavelengths. A "yellow" filter, for example, absorbs blue energy incident upon it and transmits green and red energy. The green and red energy combine to form yellow—the color we would see when looking through the filter if it is illuminated by white light (see Plate 2*b*).

Absorption filters are often used in film–filter combinations that permit differentiation of objects with nearly identical spectral response patterns in major portions of the photographic spectrum. For example, two objects may appear to reflect the same color when viewed only in the visible portion of the spectrum but may have different reflection characteristics in the UV or near-IR region.

Figure 2.23 illustrates generalized spectral reflectance curves for natural grass and artificial turf, such as those shown in Plate 3. Because the artificial turf is manufactured with a green color to visually resemble natural grass, the reflectance in blue, green, and red is similar for both surfaces. However, the

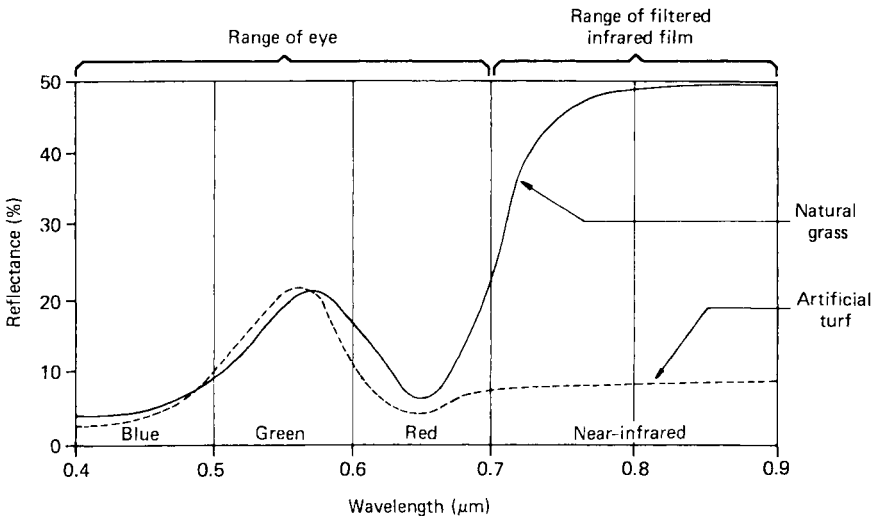

Figure 2.23 Generalized spectral reflectance curves for natural grass and artificial turf.

natural grass reflects very highly in the near IR whereas the artificial turf does not. If we wish to distinguish between natural grass and artificial turf using black and white photography, we can photograph the scene using black and white IR-sensitive film with an absorption filter over the camera lens that blocks all wavelengths shorter than 0.7 μm. Figure 2.24 illustrates the result of such photography. Figure 2.24*a* shows the scene as photographed on panchromatic film in which the natural grass and artificial turf have a similar photographic tone. Figure 2.24*b* shows the scene photographed on black and white IR film using a filter transmitting only wavelengths longer than 0.7 μm. In this case, the natural grass has a very light photographic tone (high IR reflectance) and the artificial turf a very dark photographic tone (low IR reflectance). The filter used in such photography, which selectively absorbs energy below a certain wavelength, is referred to as a *short wavelength blocking* filter or a *high pass* filter.

When one is interested in sensing the energy in only an isolated narrow portion of the spectrum, a *bandpass* filter may be used. Wavelengths above and below a specific range are blocked by such a filter. The spectral transmittance curves for a typical high pass filter and a bandpass filter are illustrated in Figure 2.25. Several high pass and bandpass filters may be used simultaneously to selectively photograph various wavelength bands on separate film images. This results in *multiband imaging*, which we describe in Section 2.14.

There is a large selection of filters from which to choose for any given application. Manufacturers' literature describes the spectral transmittance properties of each available type (e.g., Eastman Kodak Company, 1990). It should be noted that *low pass* absorption filters are not available. *Interference*

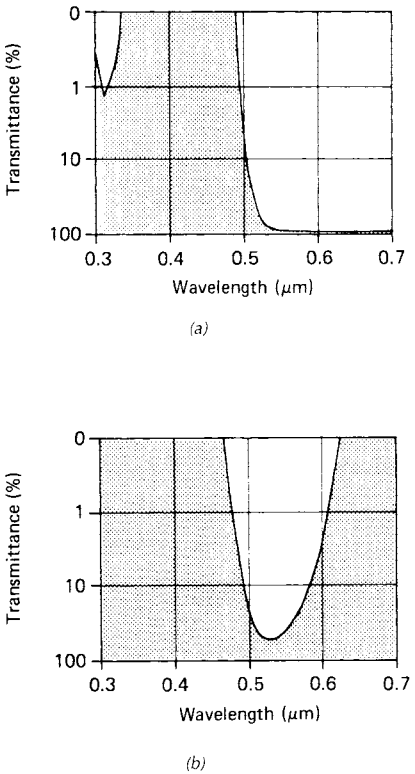

Figure 2.25 Typical transmission curves for filter types commonly used in aerial photography: (*a*) typical high pass filter (Kodak Wratten No. 12); (*b*) typical bandpass filter (Kodak Wratten No. 58). (Adapted from Eastman Kodak Company, 1992.)

filters must be used when short wavelength transmittance is desired. These filters reflect rather than absorb unwanted energy. They are also used when extremely narrow bandpass characteristics are desired.

Panchromatic aerial film is usually exposed through a yellow (blue-absorbing) filter to reduce the effects of atmospheric haze. Black and white IR-sensitive aerial film can be exposed through any of several filters. Typically, a yellow filter (which also transmits IR wavelengths) is used for forestry purposes and a red (which also transmits IR energy) or IR-only filter is used when delineation of water bodies is desired. Normal color film is usually exposed through a UV-absorbing (haze) filter and color IR film through a yellow filter, as shown in Figure 2.26.

Antivignetting filters are often used to improve the uniformity of exposure throughout an image. As described in Section 2.4, there is a geometrically based decrease in illumination with increasing distance from the center of a photograph. To negate the effect of this illumination *falloff*, antivignetting filters are designed to be strongly absorbing in their central area and progressively transparent in their circumferential area. To reduce the number of filters used, and thereby the number of between-filter reflections

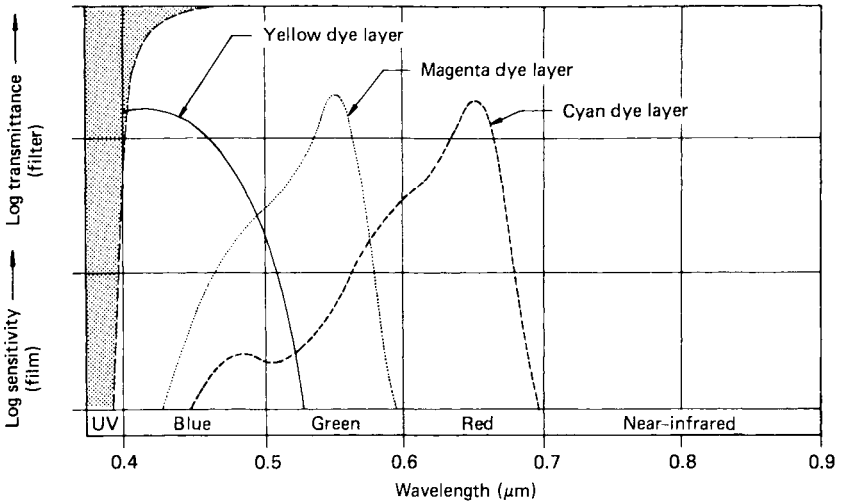

(a)

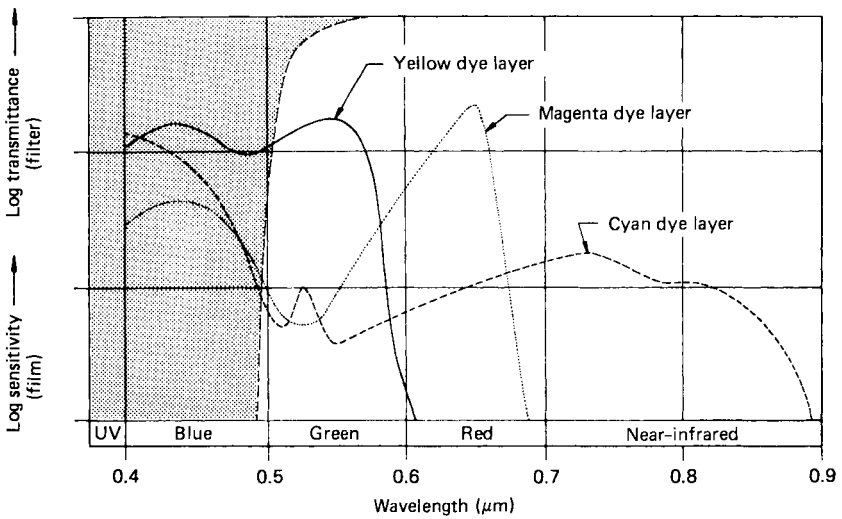

(b)

Figure 2.26 Spectral sensitivities for typical color and color IR film–filter combinations: (*a*) color film with UV-absorbing (haze) filter; (*b*) color IR film with Kodak Wratten™ No. 12 (yellow) filter. (Adapted from Eastman Kodak Company, 1990 and 1992.)

possible, antivignetting features are often built into haze and other absorption filters.

A final note on filtering techniques in aerial photography is that color films (particularly IR-sensitive films) are somewhat sensitive to aging. This causes their color layers to often "go out of balance." For example, the sensitivity of the IR-sensitive layer of a film might decrease with age relative to the other two layers. Such a film might still be exposed with satisfactory results if a *color-compensating* filter is used.

When using filters, it is often necessary to increase exposure to compensate for radiation absorption by the filter. Hence, filter manufacturers publish *filter factors*, or multiplying factors, to express the number of times by which an exposure must be increased for a given filter. Published filter factors are intended only as approximate guidelines, as actual factors vary for different exposure conditions.

2.10 AERIAL FILM CAMERAS

Aerial photographs can be made with virtually any type of camera. Many successful applications have employed aerial photographs made from light aircraft with handheld 35-mm cameras. For example, the photographs in Plates 3, 4, and 9 were made in this manner. The simplicity and low cost of purchase and operation of 35-mm cameras make them ideal sensors for small-area analysis. (The size of images taken with a 35-mm system is 24 × 36 mm; the width of the film is 35 mm.) Seventy-millimeter cameras are also used in many applications. (The size of images made with these systems is 55 × 55 mm.) Most aerial photographic remote sensing endeavors, however, entail the use of aerial photography made with precision-built aerial cameras. These cameras are specifically designed to expose a large number of photographs in rapid succession with the ultimate in geometric fidelity.

There are many different models of aerial film cameras currently in use. Here, we discuss *single-lens frame* cameras and *panoramic* cameras. In Section 2.12, we discuss digital cameras used for aerial photography.

Single-Lens Frame Cameras

Single-lens frame cameras are by far the most common cameras in use today. They are used almost exclusively in obtaining aerial photographs for remote sensing in general and photogrammetric mapping purposes in particular. *Mapping* cameras (often referred to as *metric* or *cartographic* cameras) are single-lens frame cameras designed to provide extremely high geometric image quality. They employ a low distortion lens system held in a fixed position relative to the

plane of the film. The film format size (the nominal size of each image) is commonly a square 230 mm on a side. The total width of the film used is 240 mm, and the film magazine capacity ranges up to film lengths of 120 m. A frame of imagery is acquired with each opening of the camera shutter, which is generally tripped automatically at a set frequency by an electronic device called an *intervalometer*. Figure 2.27 illustrates a typical aerial mapping camera and its associated gyro-stabilized suspension mount.

Although mapping cameras typically use film with a 230 × 230 mm image format, other cameras with different image sizes have been built. For example, a special-purpose camera built for NASA called the *Large Format Camera* (LFC) had a 230 × 460 mm image format. It was used on an experimental basis to photograph the earth from the space shuttle (Doyle, 1985). (See Figures 3.3 and 4.22 for examples of LFC photography.)

Recall that for an aerial camera the distance between the center of the lens system and the film plane is equal to the focal length of the lens. It is at this fixed distance that light rays coming from an effectively infinite distance away from the camera come to focus on the film. (Most mapping cameras cannot be focused for use at close range.) For mapping purposes, 152-mm-focal-length lenses are most widely used. Lenses with 90 and 210 mm focal

lengths are also used for mapping. Longer focal lengths, such as 300 mm, are used for very high altitude applications. Frame camera lenses are somewhat loosely termed as being either (1) *normal angle* (when the angular field of view of the lens system is up to 75°), (2) *wide angle* (when the field of view is 75° to 100°), and (3) *superwide angle* (when the field of view is greater than 100°) (angle measured along image diagonal).

Figure 2.28 illustrates the principal components of a single-lens frame mapping camera. The *lens cone assembly* includes the *lens, filter, shutter,* and *diaphragm*. The lens is generally composed of multiple lens elements that gather the light rays from a scene and bring them to focus in the *focal plane*. The filter serves any of the various functions enumerated in the previous section. The shutter and diaphragm (typically located between lens elements) control film exposure. The shutter controls the duration of exposure (from $\frac{1}{100}$ to $\frac{1}{1000}$ sec) while the diaphragm forms an aperture that can be varied in size. The camera *body* typically houses an electrical film drive

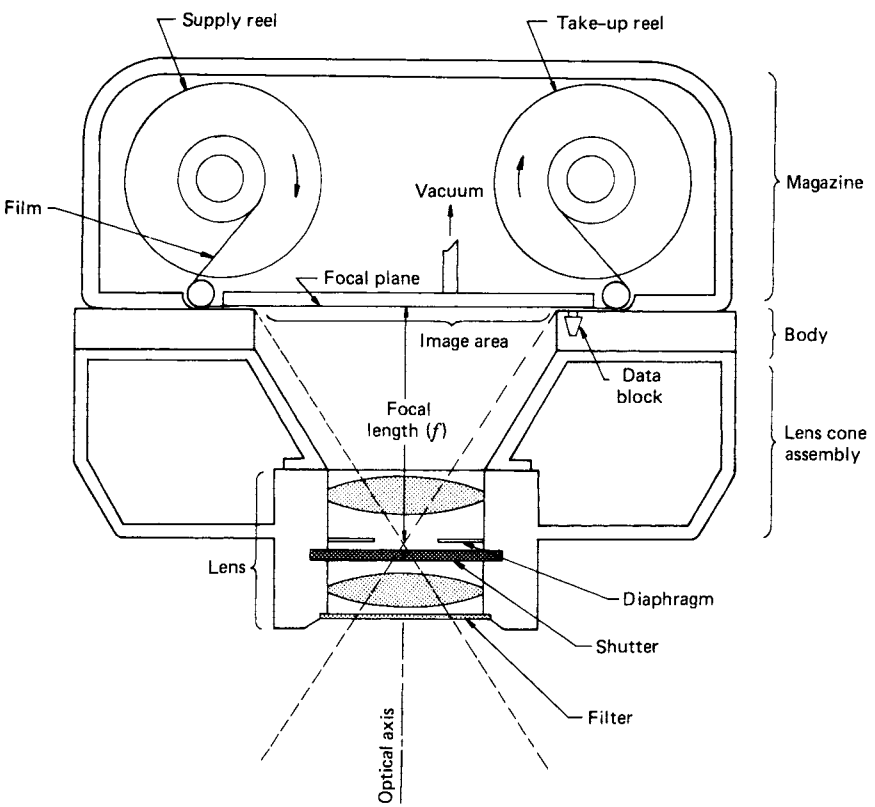

Figure 2.28 Principal components of a single-lens frame mapping camera.

mechanism for advancing the film, flattening the film during exposure, cocking the shutter, and tripping the shutter. The *camera magazine* holds the film supply and takeup reels, the film-advancing mechanism, and the film-flattening mechanism. Film flattening during exposure is often accomplished by drawing the film against a vacuum plate lying behind the focal plane. The focal plane is the plane in which the film is exposed. The *optical axis* of the camera is perpendicular to the film plane and extends through the center of the lens system.

During the time a frame camera shutter is opened for exposure of a photograph, aircraft motion causes the image to blur. To negate this effect, many frame cameras have built-in *image motion compensation*. This works by moving the film across the focal plane at a rate just equal to the rate of image movement. The camera system illustrated in Figure 2.27 incorporates this capability.

Shown in Figure 2.29 is a *vertical photograph* made with a mapping camera whose optical axis was directed as nearly vertical as possible at the instant of exposure. Note the appearance of the four *fiducial marks* at the middle of the image sides. (As illustrated in Figure 3.12, some mapping cameras incorporate corner fiducials.) These marks define the frame of reference for spatial measurements made from such aerial photos (explained in Chapter 3). Lines connecting opposite fiducial marks intersect at a photograph's *principal point*. As part of the manufacturer's calibration of a mapping camera, the camera focal length, the distances between fiducial marks, and the exact location of the principal point are precisely determined.

It should be noted that there are many single-lens frame cameras that are strictly *reconnaissance* cameras, as opposed to mapping cameras. These cameras come in a wide variety of configurations and are not described in any detail here. Most are designed to faithfully record image detail without necessarily providing the geometric fidelity of mapping cameras. However, to acquire high quality color photographs, these cameras must have color-corrected lenses that focus all colors at the same image plane. Many reconnaissance cameras have been designed for optimum focusing when black and white photographs are taken through a minus blue filter. Such cameras are generally not acceptable for color work because the blue image light that they record will be out of focus and degrade image quality.

Panoramic Cameras

Another major type of film camera we consider is the panoramic camera. This camera views only a comparatively narrow angular field at any given instant through a narrow slit. Ground areas are covered by either rotating the camera lens or rotating a prism in front of the lens. Figure 2.30 illustrates the design using lens rotation.

In Figure 2.30, the terrain is scanned from side to side, transverse to the direction of flight. The film is exposed along a curved surface located at the focal distance from the rotating lens assembly, and the angular coverage of the camera can extend from horizon to horizon. The exposure slit moves along the film as the lens rotates, and the film is held fixed during a given exposure. After one scan is completed, the film is advanced for the next exposure.

Panoramic cameras incorporating the rotating prism design contain a fixed lens and a flat film plane. Scanning is accomplished by rotating the

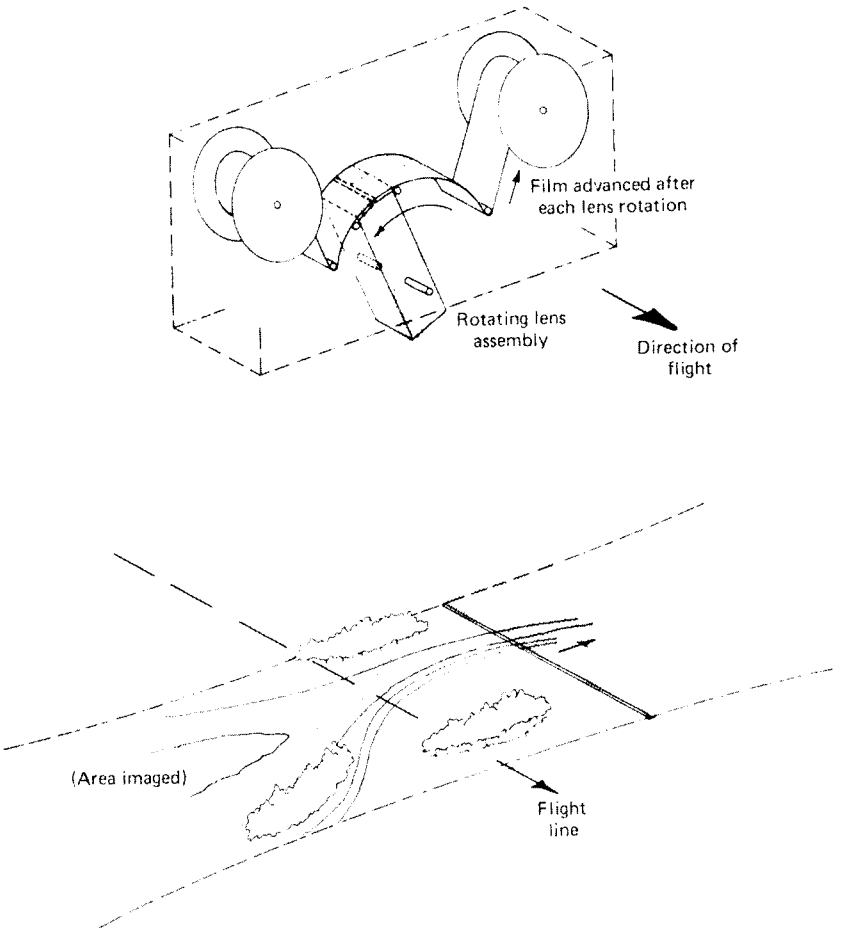

Figure 2.30 Operating principle of a panoramic camera.

prism in front of the lens, yielding imagery geometrically equivalent to that of the rotating lens camera.

Figure 2.31 illustrates the pictorial detail and large area of coverage characteristic of panoramic photography. The distortions inherent in panoramic imaging are also apparent in the figure. Areas near the two ends of the photograph are compressed. This scale variation, called *panoramic distortion*, is a result of the cylindrical shape of the focal plane and the nature of scanning. Also, *scan positional distortion* is introduced in panoramic imaging due to forward motion of the aircraft during the time a scan is made.

Typical of rotating prism panoramic cameras is the *optical bar camera* used by NASA in high altitude flights for reconnaissance purposes. This camera incorporates a 610-mm-focal-length lens, has a total field of view of 120° (60° to each side of the flight line), has a film capacity of 2000 m, and is typi-

cally flown at an altitude of 19,800 m. This yields extremely broad ground coverage, extending 34.3 km to each side of the flight path. As shown in Figure 2.32, the camera can also be used to obtain stereoscopic coverage over the same area. Such cameras have been used extensively for high altitude aerial reconnaissance and were used to photograph more than half the area of the moon during NASA's Apollo missions.

Compared to frame cameras, panoramic cameras cover a much larger ground area. With their narrower lens field of view, panoramic cameras can produce images with greater detail than frame images. Hence, panoramic images yield a broad, yet detailed view of the ground. These factors make panoramic cameras ideal sensors in large-area photographic analyses; *however*, panoramic photographs have the disadvantage that they lack the geometric fidelity of frame camera images. Also, atmospheric effects vary greatly in different portions of the image, because the distance from the camera to the ground in different parts of the scene varies much more with panoramic cameras than with frame cameras, especially when a 180° scan angle is used.

Panoramic photography has been used extensively by the U.S. Forest Service (USFS) and the U.S. Environmental Protection Agency (EPA). The USFS has used panoramic cameras for photographic interpretation purposes such as forest pest damage detection and planning the associated timber salvage operations. The principal advantages of the panoramic camera in such applications are its high image resolution and large area of coverage. The principal disadvantages are its unusual image format of 115 × 1500 mm and the continuously changing photo scale.

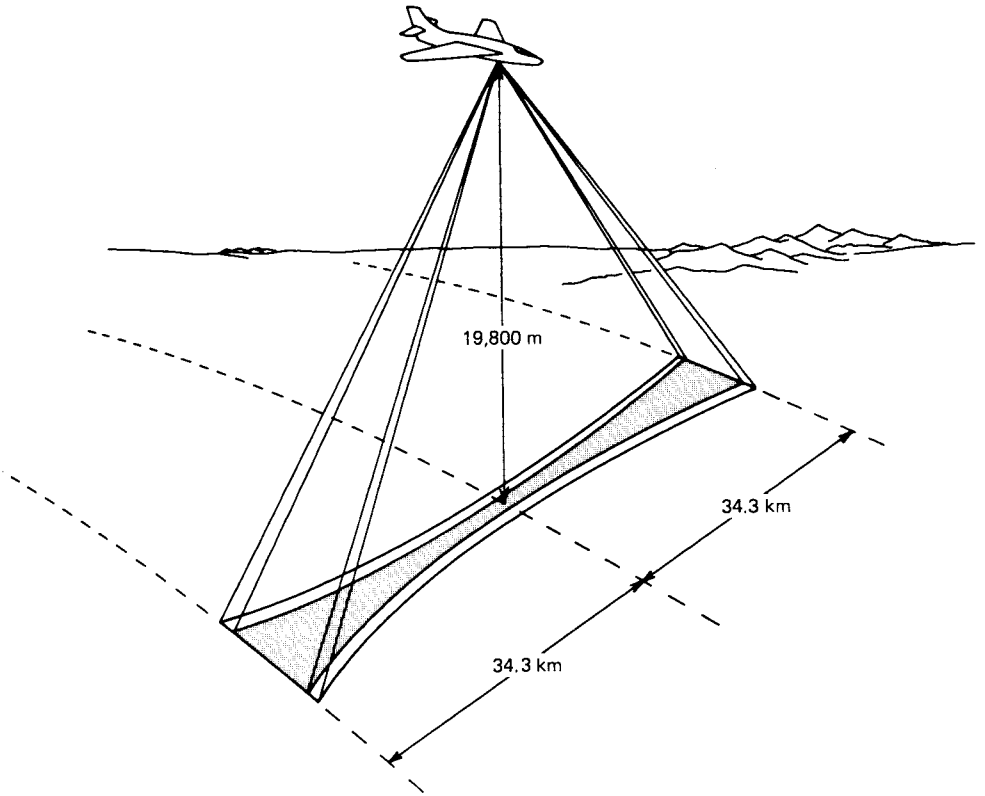

Figure 2.32 Typical ground coverage pattern using the optical bar panoramic camera (shaded area represents area of image overlap). (Adapted from ITEK Optical Systems drawing.)

The EPA has operated panoramic cameras from a device called the *Enviro-Pod*. The device is strapped underneath an aircraft and typically contains two panoramic cameras that record on 70-mm film. One camera is aimed vertically and the other is mounted in a forward-looking orientation. The forward-looking orientation permits the photographing of some objects that are obscured in the vertical photographs (e.g., barrels under a shed roof). The Enviro-Pod was frequently used to obtain high resolution images of industrial pollutants, hazardous waste sites, emergency episodes, and other activities of environmental consequence. The Intelligence Reconnaissance Imagery System III (IRIS III) is another optical imagery system that uses a high-resolution panoramic camera. This system incorporates a 600-mm focal-length lens and is flown in the U-2R aircraft at altitudes above 20,000 m for various surveillance and reconnaissance purposes. Similarly, SPIN-2 satellite photographs (Section 6.16), taken from an altitude of 220 km, are also acquired using a panoramic camera.

2.11 FILM RESOLUTION

Spatial resolution is an expression of the optical quality of an image produce by a particular camera system. Resolution is influenced by a host of param ters, such as the resolving power of the film and camera lens used to obtai an image, any uncompensated image motion during exposure, the atmo pheric conditions present at the time of image exposure, the conditions film processing, and so on. Some of these elements are quantifiable. For e: ample, we can measure the resolving power of a film by photographing standard test chart. Such a chart is shown in Figure 2.33. It consists of grou

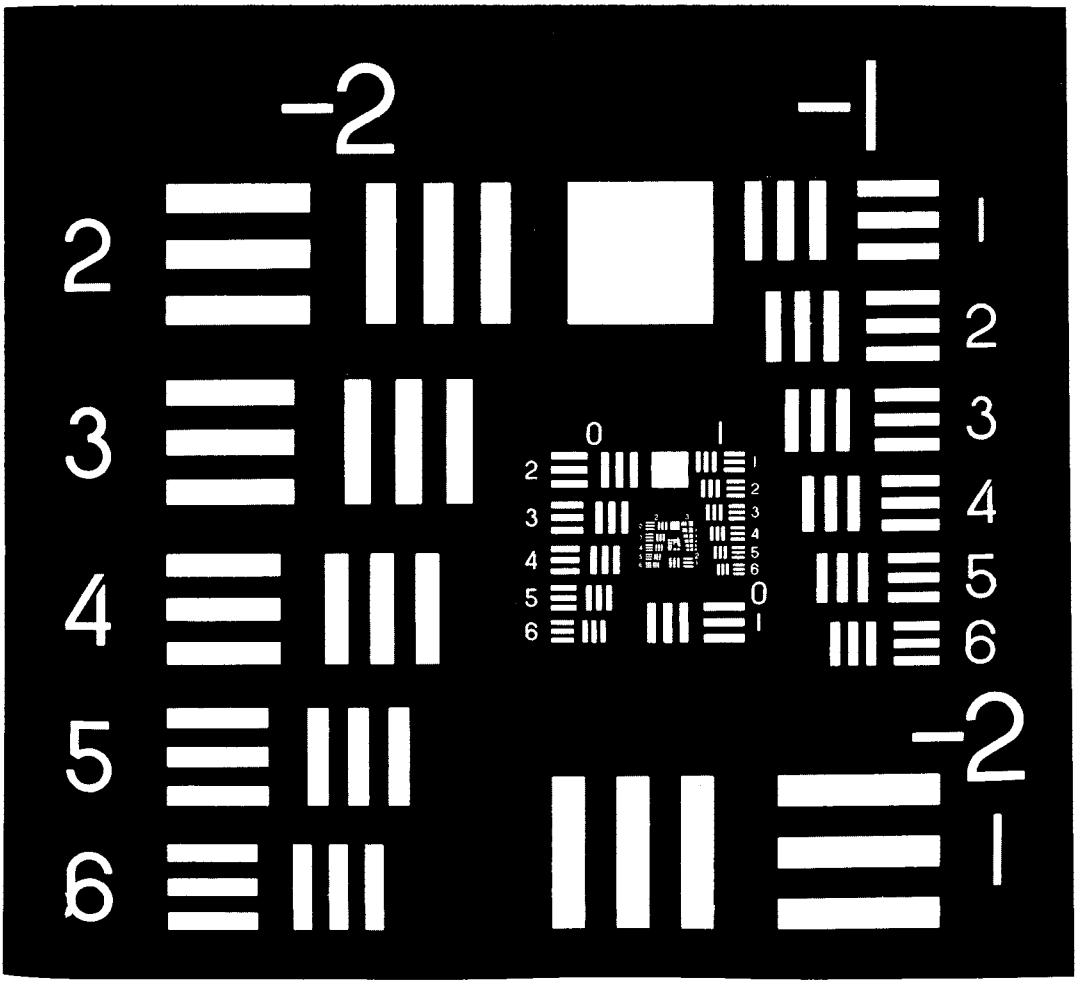

Figure 2.33 Resolving power test chart. (Courtesy Teledyne-Gurley Co.)

of three parallel lines separated by spaces equal to the width of the lines. Successive groups systematically decrease in size within the chart. The resolving power of a film is the reciprocal of the center-to-center distance (in millimeters) of the lines that are just "distinguishable" in the test chart image when viewed under a microscope. Hence, film resolving power is expressed in units of lines per millimeter. Film resolving power is sometimes referred to in units of "line pairs" per millimeter. In this case, the term *line pair* refers to a line (white) and a space (black) of equal width, as shown in Figure 2.33. The terms *lines per millimeter* and *line pairs per millimeter* refer to the same line spacing and can be used interchangeably. Film resolving power is specified at a particular contrast ratio between the lines and their background. This is done because resolution is very strongly influenced by contrast. Typical aerial film resolutions are shown in Table 2.2. Note the significant difference in film resolution between the 1000 : 1 and 1.6 : 1 contrast ratios.

An alternative method of determining film resolution that eliminates the subjectivity of deciding when lines are just "distinguishable" is the construction of a film's *modulation transfer function*. In this method, a scanning microdensitometer (Section 2.5) is used to scan across images of a series of "square-wave" test patterns similar to the one shown in Figure 2.34*a*. An ideal film would exactly record not only the brightness variation (modulation) of the test pattern but also the distinct edges in the pattern. For actual films, the fidelity of the film recording process depends upon the spatial frequency of the pattern. For test patterns with a small number of lines per millimeter, the maximum and minimum brightness values as measured from the film image (Figure 2.34*b*) might correspond exactly with those of the test pattern. At the spatial frequency of this test pattern, the film's modulation transfer is said to be 100 percent. However, note that the test pattern edges are somewhat

TABLE 2.2 Resolution of Selected Kodak Aerial Films

Film Name	Film Number	Film Type	Film Resolution (line pairs/mm)	
			1000 : 1 Contrast Ratio	1.6 : 1 Contrast Ratio
PLUS-X AEROGRAPHIC	2402	Panchromatic (negative)	130	55
AERECON High Altitude	3409	Panchromatic (negative)	630	320
Infrared AEROGRAPHIC	2424	Black and white infrared (negative)	125	50
AEROCOLOR III Negative	2444	Normal color (negative)	125	80
AEROCHROME III MS	2427	Normal color (positive)	100	80
AEROCHROME III Infrared	1443	Color infrared (positive)	100	63

Source: Eastman Kodak Company website (www.kodak.com).

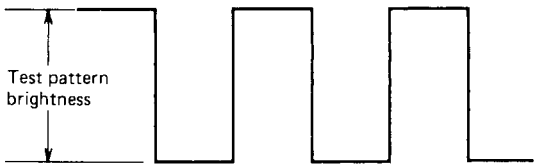

(a)

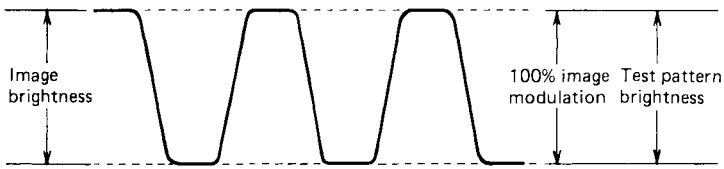

(b)

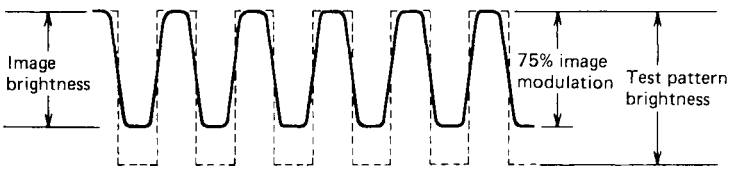

(c)

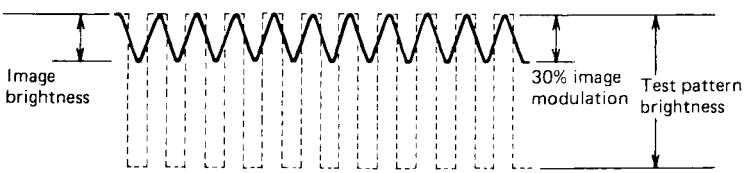

(d)

Figure 2.34 (*a*) Square-wave test pattern. (*b*) Modulation transfer of image of test pattern shown in (*a*). (*c*, *d*) Modulation transfer of images of test patterns having higher spatial frequency. [Note in (*b*) that 100 percent modulation occurs, but the image shows a reduction in edge sharpness as compared with the test pattern.] In (*c*), edge sharpness is further reduced, and, in addition, modulation transfer is reduced to 75 percent of that of the test pattern. In (*d*), further sharpness is lost and modulation transfer is reduced to 30 percent. (Adapted from Wolf and Dewitt, 2000.)

rounded on the film image. As the line width and spacing of the test pattern are reduced, density scans across the film image of the test pattern will produce both reduced modulations and increased edge rounding. This is illustrated in Figures 2.34*c* and *d* (showing 75 and 30 percent modulation transfer, respectively). By measuring film densities across many such patterns of progressively higher spatial frequency, a complete curve for the modulation transfer function can be constructed (Figure 2.35). Again, this curve expresses the fidelity with which images of features over a range of different sizes or spatial frequencies can be recorded by a given film.

The resolution, or modulation transfer, of any given film is primarily a function of the size distribution of the silver halide grains in the emulsion. In general, the higher the granularity of a film, the lower its resolving power. However, films of higher granularity are generally more sensitive to light, or *faster*, than those having lower granularity. Hence, there is often a trade-off between film "speed" and resolution.

The resolving power of any particular camera–film *system* can be measured by flying over and photographing a large bar target array located on the ground. The imagery thus obtained incorporates the image degradation realized in flight resulting from such factors as atmospheric effects and residual image motion during exposure (including that due to camera vibrations). The

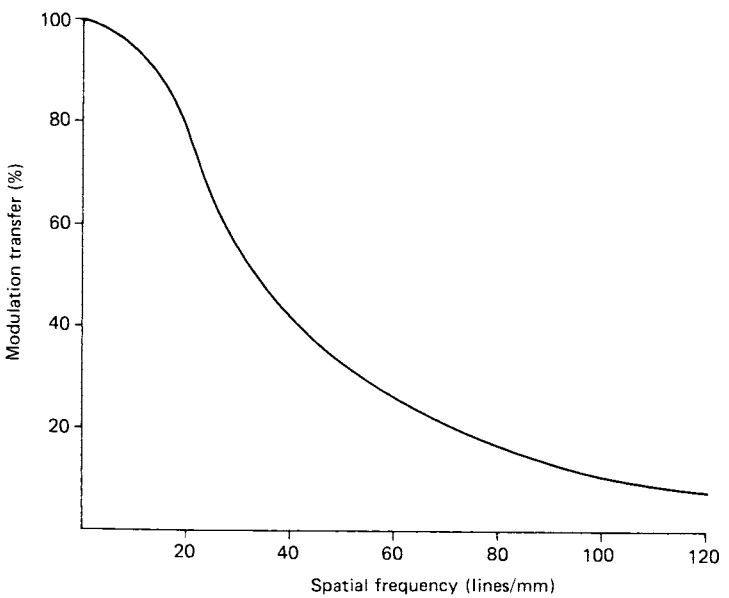

Figure 2.35 Curve of modulation transfer function (MTF). (Adapted from Wolf and Dewitt, 2000).

advantage to this is that we can begin to judge the *dynamic* spatial resolution of the total photographic system instead of the *static* resolution of any one of its components.

We might use the results of such a dynamic resolution test to compare various systems, but the numbers involved are difficult to interpret in a practical sense. Our interest in measuring a system's resolution goes beyond determining the ability of a system to record distinct images of small, nearly contiguous objects of a given shape on a test chart. We are interested not only in object *detection* but also in object *recognition* and *identification*. Hence, "spatial resolution" defies precise definition. At the detection level, the objective is to discern separate objects discretely. At the recognition level, we attempt to determine what objects are—for example, trees versus row crops. At the identification level, we more specifically identify objects—for example, oak trees versus corn.

The effects of scale and resolution can be combined to express image quality in terms of a *ground resolution distance* (GRD). This distance extrapolates the dynamic system resolution on a film to a ground distance. We can express this as

$$\text{GRD} = \frac{\text{reciprocal of image scale}}{\text{system resolution}} \tag{2.13}$$

For example, a photograph at a scale of 1 : 50,000 taken with a system having a dynamic resolution of 40 lines/mm would have a ground resolution distance of

$$\text{GRD} = \frac{50{,}000}{40} = 1250 \text{ mm} = 1.25 \text{ m}$$

This result assumes that we are dealing with an original film at the scale at which it was exposed. Enlargements would show some loss of image definition in the printing and enlarging process.

In summary, the ground resolution distance provides a framework for comparing the expected capabilities of various images to record spatial detail. However, this and any other measure of spatial resolution must be used with caution because many unpredictable variables enter into what can and cannot be detected, recognized, or identified on an aerial photograph.

2.12 ELECTRONIC IMAGING

The previous sections of this chapter have dealt with traditional photography, an imaging process that uses photographic film as the recording and storage medium for images. Here and in the next section we describe electronic image acquisition. Table 2.3 outlines how photographic and electronic

TABLE 2.3 Comparison of Photographic versus Electronic Image Processing

Characteristic	Photographic Processing	Electronic Image Processing
Data capture	Silver halide film in a camera	Photosensitive solid-state devices
Data storage	Photographic film or prints	Magnetic, optical, and solid-state media
Data manipulation	Chemical developing and optical printing	Digital image processing
Data transmission	Mail, delivery service, fax	Telemetry, telephone lines, computer networks
Softcopy display	Projected slides or movies	Computer monitors, television, projection video
Hardcopy display	Silver halide prints	Dye sublimation, inkjet, thermal, and laser printers

Source: Adapted from Khosla, 1992.

imaging differ in their means of image capture, storage, manipulation, transmission, and display.

Electronic imaging instruments typically use one- or two-dimensional detector arrays of light-sensing solid-state devices (photodiodes) for image acquisition, with each *photosite* (position in the array) sensing one pixel in the image field. Most often, there is one photodiode per photosite. Either CCD (charge-coupled device) or CMOS (complementary metal–oxide–semiconductor) image sensors are used. CMOS sensors are less widely used than CCD sensors because they typically have had less light sensitivity, produced data with greater "noise," and required substantially more image processing time. Newer CMOS sensors are overcoming these limitations. When electromagnetic energy strikes the surface of either type of photosite, electronic charges are produced, with the magnitude of the charges being proportional to the scene brightness. Many of the CCD and CMOS image sensors designed for use in remote sensing are capable of differentiating a wider range of scene brightness values than most photographic films.

Charge-coupled device image sensors are monochromatic. To obtain full-color data, each photosite of the CCD is typically covered with a blue, green, or red filter. Usually, photosites are square, with alternating blue-, green-, and red-sensitive sites arranged in a *Bayer pattern* (Figure 2.36). Half of the filters in this pattern are green; the remainder are blue or red, in equal numbers. To assign blue, green, and red values to each photosite, the two missing colors at each photosite are interpolated from surrounding photosites of the same color (see Section 7.2 and Appendix C for a discussion of resampling schemes for such interpolation). The resulting data set is a two-dimensional array of discrete pixels, with each pixel having three DNs representing the scene brightness in each spectral band of sensing. The *color depth*, or *quantization level*, of CCD sensors is typically 8 to 12 bits (256 to 4096 gray levels

G	B	G	B	G	B	G	B	G	B
R	G	R	G	R	G	R	G	R	G
G	B	G	B	G	B	G	B	G	B
R	G	R	G	R	G	R	G	R	G
G	B	G	B	G	B	G	B	G	B
R	G	R	G	R	G	R	G	R	G
G	B	G	B	G	B	G	B	G	B
R	G	R	G	R	G	R	G	R	G
G	B	G	B	G	B	G	B	G	B
R	G	R	G	R	G	R	G	R	G

Figure 2.36 Bayer pattern of blue, green, and red CCD filters. Note that one-half of these filters are green, one-quarter are blue, and one-quarter are red.

per band). A Bayer pattern of yellow, magenta, and cyan filters can also be used (in this case, half the filters are yellow; the remainder are magenta or cyan, in equal numbers). This configuration results in more energy reaching each photosite (providing an increased signal-to-noise ratio), but resampling computations to arrive at red, green, and blue values for each photosite are more complex and time consuming. A combination of yellow, magenta, cyan, and green filters (these filters are present in equal numbers) can also be used. Also, photosites need not be square; some CCDs utilize octagonal-shaped photosites. Under development (as of 2002) are multilayer CCDs where each photosite has three color-sensitive layers (blue, green, and red), akin to color films.

Charge-coupled device photosites need not be limited to a single photodiode sensor; CCDs are available with two photodiodes per photosite, with a larger primary photodiode with high sensitivity and a smaller secondary photodiode with lower sensitivity. It is claimed that this system can capture four times the range of scene brightness values than CCDs with only one photodiode per photosite. This should provide for both the capture of greater detail in highlight (very bright) areas, as well as a greater ability to resolve detail in darker (often shadow) areas.

Also available is a three-layer CMOS sensor that has three photodetectors (blue, green, and red) at every pixel location. This is based on the natural property of silicon to absorb different wavelengths of light at different depths. By placing photodetectors at different depths in the CMOS sensor, blue, green, and red energy can be sensed independently. Conceptually, this should

result in sharper images, better color, and freedom from color artifacts resulting from interpolation (resampling) that are common in Bayer-pattern CCD sensors.

Digital cameras use a camera body and lens but record image data with CCD or CMOS sensors rather than with film. In turn, the electrical signals generated by these detectors are stored digitally, typically using media such as flash memory or CD and DVD media. While this process is not "photography" in the traditional sense (images are not recorded directly onto photographic film), it is often referred to as "digital photography." Two-dimensional array sizes of digital cameras for aerial imaging that use 35-mm camera bodies typically range from about 2000 × 3000 pixels to about 3000 × 4500 pixels. A digital camera's sensitivity to light is measured using the same ISO scale that is used by film cameras. Typical values range from ISO 100 to ISO 1600. The higher sensitivity levels (larger ISO numbers) allow for photographing at shorter exposure times, or in reduced-light conditions, but result in greater noise in the data.

As an example, Figure 2.37 illustrates the Kodak DCS Pro 14n three-band digital camera that uses a Nikon camera body and has a 3048-pixel row by 4560-pixel column CMOS sensor 24 × 36 mm in size (same size as 35-mm film images), with a color depth of 12-bits per band (4096 gray levels per

band). Kodak DCS cameras have been used by astronauts to photograph the earth from several space shuttle missions.

As mentioned above, 35-mm camera format digital cameras typically use a minimum size sensor of around 2000 × 3000 (6,000,000) pixels. No single number can represent the number of pixels photographic film would have—*if it had pixels*. Furthermore, the pixels in the CCD array used in this camera are uniform in size and shape and are arranged in a systematic geometric pattern, whereas the "pixels" in a photographic film (silver halide grain clusters) are irregular in size, shape, and spatial distribution. However, a reasonable equivalent number is around 6 million pixels for a frame of 35-mm film. Thus, the current resolving power of small-format digital imaging systems compares favorably with that of photographic film of similar format and scale.

Digital cameras for aerial photography that use 70-mm-format camera bodies typically have a 4096 × 4096 pixel array. Many of these cameras use "filmback" replacements for 70-mm-format cameras such as the Hasselblad, Mamiya, and Rollei cameras. Because of the array size, data volumes for these cameras are larger than for digital camera systems using 35-mm format camera bodies.

Figure 2.38 is an example of a larger-format digital camera than the 35- and 70-mm-format cameras just described. It shows the Z/I Imaging Digital Mapping Camera (DMC), which consists of eight synchronously operating CCD-based digital cameras. Four of these are panchromatic cameras that have a 7000 × 4000 pixel array and a focal length of 120 mm. In postprocessing of the image data, the four pan images are mosaicked and reprojected through a common virtual perspective center to create a single-frame image having approximately 14,000 × 8000 pixels. The other four cameras are single band (blue, green, red, and near IR) systems, each incorporating a 3000 × 2000 pixel array and a 25-mm-focal-length lens. The ground footprint for these cameras is approximately equivalent to that of the mosaicked pan image. The resulting images can be combined (three at a time) into "normal color" and/or "color infrared" images, as illustrated (with another imaging system) in Figure 2.40 and Plate 7 (Section 2.14). In addition, the color bands can be co-registered with the higher-resolution panchromatic images using techniques explained in Section 7.6.

Very large two-dimensional arrays can be formed by using a one-dimensional linear CCD detector array that records successive lines of data as the aircraft or spacecraft moves along its flight or orbit path (see Section 5.3). An example of this is the 12,000-pixel CCD linear array associated with the ADS40 Airborne Digital Sensor described in Section 5.5.

Plate 5 shows examples of "normal color" and "color infrared" digital camera images, acquired by the Emerge Direct Digital Imagery system. This three-band system has an array size of 4079 × 4092 pixels and can sense in

Figure 2.38 Z/I Imaging Digital Mapping Camera. (Courtesy Z/I Imaging Corporation.)

either blue, green, and red bands (normal color) or green, red, and near IR bands (color infrared). Ground resolution cell sizes for data collection by this system are typically 0.15 to 1.0 m per pixel, depending principally on flying height. This system has provided digital orthorectified mosaic imagery products to a broad range of users for a variety of GIS, mapping, and land management applications.

Digital cameras are typically used for the type of aerial imaging previously done using small-format (35- and 70-mm) film cameras. Relatively inexpensive camera platforms can be used for small-format digital cameras, including ultralight and light aircraft, remote control model aircraft, hot-air blimps, tethered balloons, and kites. At the other extreme, Kodak DCS digital cameras have also been used to obtain images of the earth from the U.S. space shuttle. Figure 2.39 is an astronaut "photograph" from a flying height of 367 km using a Kodak DCS 460 digital camera. It shows several snow-covered volcanoes in the Aleutian Islands. Near the center of the image, smoke can be seen rising from 1730-m-high Mt. Cleveland on Chuginadak Island. Mt. Cleveland is one of the most active volcanoes in the Aleutian Island chain

Figure 2.39 Astronaut "photograph" from a flying height of 367 km using a Kodak DCS 460 digital camera showing several snow-covered volcanoes in the Aleutian Island chain. Note the smoke near the center of the image rising from 1730-m-high Mt. Cleveland, one of the most active volcanoes in the chain. Scale 1 : 270,000. (NASA photograph.)

and produced a major eruption of volcanic ash just 7 weeks after this image was exposed.

The use of small-format digital cameras provides several advantages over the use of 35- and 70-mm film cameras, including rapid turnaround time (images are available for viewing during the flight and immediately afterward) and an inherently computer-compatible format (photographic films need to be scanned to produce computer-compatible data). Image exposures can be optimized in flight—intended targets can be viewed, images acquired, histograms analyzed, and aperture, shutter speed, or ISO adjusted to provide an optimum exposure range. Digital camera data are stored on a reusable medium; the memory devices used for storing digital images can be erased and reused essentially indefinitely. Also, digital images can be copied repeatedly with no loss of image quality unless the data have been excessively compressed. New "wavelet" compression schemes have been shown to produce excellent results with compression ratios of up to 20 : 1 for digital aerial imagery.

The exposure latitude of digital cameras exceeds that of most films, and, as stated earlier, the resolving power of small-format (35- and 70-mm)

digital images is comparable to that of photographic film images of similar format and scale. Another advantage of digital cameras over film cameras is their greater suitability for scientific work, as they can be more easily calibrated radiometrically using targets in the laboratory or field. The CCDs used for digital imaging are linear in response to energy across their entire dynamic range, whereas film response is linear only in the "straight-line portion" of the characteristic curve (Section 2.5). Also, most digital cameras used for aerial imaging have the capability of recording positional data obtained from a GPS receiver along with the image data recorded by the camera.

In their computer-compatible format, digital images can be readily processed and displayed using the digital image processing techniques explained in Chapter 7, including various image enhancement and classification techniques.

The applications in which electronic imaging systems (including both digital frame cameras and aerial video systems) have been successfully operated are numerous. Aerial electronic imaging has been applied in a variety of ways in the resource domains of forestry, range management, agriculture, water resources, geology, and environmental assessment. More specific examples include analysis of hazardous waste sites, detection of soil conditions, land use/land cover mapping, wild rice mapping, wildlife censusing, wildlife habitat studies, trout stream monitoring, right-of-way monitoring, water quality studies, precision agriculture assessments, wetland mapping, crop condition assessment, detection of forest insect and disease problems, irrigation mapping, and detection of frost damage in citrus groves, to mention but a few.

2.13 AERIAL VIDEOGRAPHY

Aerial videography is a form of electronic imaging whereby analog or digital video signals are recorded on magnetic tape or on CD or DVD media. Cameras used for aerial videography can have many configurations, including single-band cameras, multiband cameras, or multiple single-band cameras and can sense in the visible, near-IR, and mid-IR wavelengths (not all cameras have this full range).

Shuttered cameras, with exposure times as short as $\frac{1}{10,000}$ sec, are used for both analog and digital aerial videography. An exposure time of $\frac{1}{1,000}$ sec is typically used, which essentially eliminates image motion.

Analog video recording that follows the NTSC RS-170 standard (used principally in North America and Japan) uses signals conforming to an industry specification of 485 horizontal lines per image frame. The NTSC signals have an aspect ratio (frame width divided by frame height) of 4 : 3.

Image resolution in the vertical direction is set by the number of discrete lines per image frame (485 image lines in the case of NTSC signals). Image resolution in the horizontal direction is defined in terms of "TV lines" (TVLs). Although analog video signals do not have discrete pixels, it is useful to think of horizontal resolution in terms of pixels per line. The number of TVLs is the number of pixels contained in a horizontal distance equal to the frame height. The most widely used analog formats for aerial videography are the Super-VHS and Hi-8 formats, with a resolution of about 400 TVLs. Because of the 4 : 3 aspect ratio, the number of pixels in one frame of a Hi-8 recording would be about 535 × 485, or about 260,000 pixels. This is only about $\frac{1}{50}$ as many pixels per frame as a digital frame camera such as the Kodak DCS Pro 14n.

Digital video recording can follow one of many standards. The primary consumer digital camcorder formats (as of 2002) are Mini-DV, Digital8, MICROMV, and DVD, all with a resolution of about 500 TVLs. There are several DVCPRO formats: DVCPRO, DVCPRO50, DVCPRO P, and DVCPRO HD. They differ in scanning method (interlaced versus progressive), video format (image size), and image data compression. As an example, the DVCPRO format has a resolution of 800 × 485 pixels (388,000 pixels per frame). Other digital video recording formats exist, and more are being developed. This is an improvement over analog video recording, but still only about $\frac{1}{30}$ as many pixels per frame as a high-end 35-mm-format digital frame camera. High definition television (HDTV) has an aspect ratio of 16 : 9. Digital recordings of HDTV signals contain 1920 × 1080 pixels, or about 2.0 million pixels per frame.

Both analog and digital video recordings can be viewed on conventional television equipment through playback of the video tape in a video cassette recorder (VCR). Slow-speed and freeze-frame playback can be used to aid in visual image analysis. Digital video data are in a format that can be readily displayed and processed in a microcomputer. Analog video data can also be viewed and analyzed digitally by using a *video capture card* (digitizer) in a microcomputer.

The use of aerial videography has several advantages when compared with small-format (35- and 70-mm) aerial film photography. As with digital frame cameras, video images can be viewed in the aircraft at the time of data acquisition and are available for analysis immediately after a flight. The resulting imagery is also inexpensive—material costs are typically much lower than for 35-mm photographs for the same area of coverage. Another advantage is that video cassettes have an audio track, which means that verbal comments about specific features or locations can be recorded in synchronization with the imagery. In addition, GPS equipment can be used to record the latitude, longitude, and elevation of the aircraft directly onto the video image at the time of data acquisition.

Ground objects sensed by aerial videography are viewed from multiple vantage points as they pass under the aircraft. Thus, there are multiple view angle–sun angle combinations that can be analyzed.

Aerial video recording has the capability of recording more than 200,000 frames on a single tape (2 hours of flying time), which makes it especially well suited to imaging linear features such as roads, power lines, and rivers.

The principal disadvantage of video recording is the lower spatial resolution in comparison with 35- and 70-mm aerial film cameras and digital frame cameras. Also, aerial video imagery cannot be easily used for stereoscopic viewing, and video tapes can be somewhat cumbersome to index and handle when subsequent viewing of discrete image segments (or single frames) is desired (this is especially true of analog video recordings). Aerial video data recorded on CD or DVD media are much less cumbersome to index and retrieve.

Plate 6 shows two examples of color IR video composite images compared with color IR photographs. In this plate, (*a*) and (*b*) are images of a cotton field infested with harvester ants. Although the spatial resolution of the video image (*a*) is lower than the photograph (*b*), most of the ant mounds (white spots) can easily be detected in the video image. Shown in (*c*) and (*d*) are images of a cotton field with saline soils. The barren to sparsely vegetated saline areas can generally be distinguished as readily in the video as in the photographic image. The color tones of the video composite images are comparable to the color IR film tones in both scenes.

2.14 MULTIBAND IMAGING

Earlier in this chapter, we saw that both normal color and color IR films were three-layer systems. Normal color film has layers individually sensitive to blue, green, and red energy, and color IR film (used with an appropriate filter) has layers individually sensitive to green, red, and near-IR energy. Upon processing, these three-layer films produce color images because of the dye layers that control the amount of blue, green, and red energy that form the final photographic image.

Three individual bands from many types of sensing systems (e.g., digital cameras, video cameras, and various airborne and satellite multispectral scanners) can be displayed simultaneously to produce color images.

Multiband images are images sensed simultaneously from essentially the same geometric vantage point but in different bands of the electromagnetic energy spectrum. In the case of *multiband photography*, different parts of the spectrum are sensed with different film–filter combinations. Multiband digital camera images and video images are also typically exposed onto the camera's CCD or CMOS sensor(s) through different filters. Electro-optical sensors such as the Landsat Thematic Mapper (discussed in Chapter 6) typically

sense in at least several bands of the electromagnetic spectrum. Hyperspectral sensors (Chapter 5) may sense in hundreds of very narrow portions of the spectrum.

The "best" combination of multiband images for discriminating a given scene varies with the spectral response patterns for the objects of interest within that scene. The "taking apart" of object reflectances (and/or emittances) through multiband imaging normally yields enhanced contrast between different terrain feature types and between different conditions of the same feature type. To optimize this contrast, band–color combinations are chosen for the specific features of interest in spectral regions where the maximum spectral reflectance differences are known, or are anticipated, to exist.

Multiband images are typically viewed by selecting three of the available bands and displaying one band as blue, one band as green, and one band as red through the use of some additive color device, typically a computer monitor. (Computer monitors, like color televisions, have three separate graphic planes that control independently the intensity of blue, green, and red light at each position on the screen.)

Figure 2.40 shows the images of four individual bands acquired by the ADAR System 5500, a multispectral digital aerial camera system. The standard configuration for this system is to employ four CCD sensors, capturing data in the blue, green, red, and near-IR spectral regions. Ground resolution cell sizes used for ADAR applications are typically 0.5 to 3 m per pixel, depending on the flying height. In addition to storing digital image data, this system continually monitors a GPS receiver, recording latitude, longitude, and elevation data to provide the location of the aircraft at the time each image is acquired. ADAR data have been used in a variety of applications, including natural resource management, forestry, wetland monitoring, precision agriculture, and urban planning.

Plate 7 shows "normal color" and "color IR" images that were prepared from the individual band images shown in Figure 2.40 by combining these image bands, as shown in Table 2.4. Note that, as is typical of multiband data in this spectral range, there is a great deal of correlation among the reflections in the blue, green, and red spectral bands and a large difference in reflections between the three visible-wavelength bands and the near-IR band. For example, the water is much darker toned in the near-IR band, and the trees are much lighter toned in the near-IR band. There are, however, sufficient differences among reflections in the blue, green, and red bands to produce a color composite image with colors that resemble a normal color photograph.

Multiband viewing is not restricted to visible and near-IR bands. Multiband viewing may also include mid-IR and thermal-IR bands, as illustrated later. Regardless of the number and wavelength bands of the images, only three bands are selected for viewing at one time, with one band displayed as blue, one band as green, and one band as red.

Figure 2.40 Multiband digital camera images, Chesapeake Bay, MD, early October. (*a*) Blue band, (*b*) green band, (*c*) red band, and (*d*) near IR band. Scale 1 : 9000. (Courtesy Positive Systems, Inc.)

Figure 2.40 *(Continued)*

TABLE 2.4 Band–Color Combinations Used to Produce Normal Color and Color Infrared Images

To Simulate a Normal Color Image		To Simulate a Color Infrared Image	
EM Band	Display Color	EM Band	Display Color
Blue	Blue	Green	Blue
Green	Green	Red	Green
Red	Red	Near IR	Red

2.15 CONCLUSION

As we indicated earlier in this chapter, aerial photography has historically been the most widely used form of remote sensing due to its general availability, geometric integrity, versatility, and economy. However, as with any other sensing system, aerial photography has certain limitations and requirements. Airphotos are often difficult to obtain, handle, store, calibrate, and interpret. Current technological trends seem to indicate that more and more inherently digital recording systems will be used in many applications where aerial photographs have traditionally been employed.

SELECTED BIBLIOGRAPHY

Ahmad, A., and J.H. Chandler, "Photogrammetric Capabilities of the Kodak DC40, DCS420 and DCS460 Digital Cameras," *Photogrammetric Record*, vol. 16, no. 94, 1999, pp. 601–615.

American Society for Photogrammetry and Remote Sensing (ASPRS), *15th Biennial Workshop on Videography & Color Photography in Resource Assessment*, ASPRS, Bethesda, MD, 1995.

American Society for Photogrammetry and Remote Sensing (ASPRS), "The First North American Symposium on Small Format Aerial Photography," *Technical Papers*, ASPRS, Bethesda, MD, 1997a.

American Society for Photogrammetry and Remote Sensing (ASPRS), *16th Biennial Workshop on Videography & Color Photography in Resource Assessment*, ASPRS, Bethesda, MD, 1997b.

American Society for Photogrammetry and Remote Sensing (ASPRS), *Corona Between the Sun and the Earth: The First NRO Reconnaissance Eye in Space*, ASPRS, Bethesda, MD, 1997c.

American Society of Photogrammetry (ASP), *Manual of Color Aerial Photography*, ASP, Falls Church, VA, 1968.

American Society of Photogrammetry (ASP), *Manual of Photogrammetry*, 4th ed., ASP, Falls Church, VA, 1980.

American Society of Photogrammetry (ASP), *Manual of Remote Sensing*, 2nd ed., ASP, Falls Church, VA, 1983.

Baker, S., "San Francisco in Ruins: The 1906 Aerial Photographs of George R. Lawrence," *Landscape*, vol. 30, no. 2, 1989, pp. 9–14.

Canadian Journal of Remote Sensing, Special Issue on Aerial Optical Remote Sensing, vol. 21, no. 3, 1995.

Doyle, F.J., "The Large Format Camera on Shuttle Mission 41-G," *Photogrammetric Engineering and Remote Sensing*, vol. 51, no. 2, 1985, pp. 200–203.

Drake, S., "Visual Interpretation of Vegetation Classes from Airborne Videography: An Evaluation of Observer Proficiency with Minimal Training," *Photogrammetric Engineering and Remote Sensing*, vol. 62, no. 8, 1996, pp. 969–978.

Eastman Kodak Company, *Aerial Imaging—Online Publications*, Available over the Internet at http://www.kodak.com/US/en/government/aerial/technicalPubs/.

Eastman Kodak Company, *Applied Infrared Photography*, Eastman Kodak Company, Rochester, NY, 1981.

Eastman Kodak Company, *Kodak Photographic Filters Handbook*, Eastman Kodak Company, Rochester, NY, 1990.

Eastman Kodak Company, *Kodak Data for Aerial Photography*, 6th ed., Eastman Kodak Company, Rochester, NY, 1992.

Edirisinghe, A., G.E. Chapman, and J.P. Louis, "Radiometric Corrections for Multispectral Airborne Video Imagery," *Photogrammetric Engineering and Remote Sensing*, vol. 67, no. 8, 2001, pp. 915–922.

Escobar, D.E., et al., "A Twelve-Band Airborne Digital Video Imaging System (ADVIS)," *Remote Sensing of Environment*, vol. 66, 1998, pp. 122–128.

Fritz, N.L., "Optimum Methods for Using Infrared-Sensitive Color Films," *Photogrammetric Engineering*, vol. 33, no. 10, 1967, pp. 1128–1138.

Fritz, N.L., "Filters: An Aid in Color-Infrared Photography," *Photogrammetric Engineering and Remote Sensing*, vol. 43, no. 1, 1977, pp. 61–72.

Gao, J., and S.M. O'Leary, "The Role of Spatial Resolution in Quantifying SSC from Airborne Remotely Sensed Data," *Photogrammetric Engineering and Remote Sensing*, vol. 63, no. 3, 1997, pp. 267–271.

Graham, R., *Digital Imaging*, Whittles Publishing, Caithness, Scotland, 1998.

Hess, L.L., et al., "Geocoded Digital Videography for Validation of Land Cover Mapping in the Amazon Basin," *International Journal of Remote Sensing*, vol. 23, no. 7, 2002, pp. 1527–1555.

Holopainen, M., and G. Wang, "The Calibration of Digitized Aerial Photographs for Forest Stratification," *International Journal of Remote Sensing*, vol. 19, no. 4, 1998, pp. 677–696.

Jacobson, R.E., *The Manual of Photography—Photographic and Digital Imaging*, 9th ed., Focal Press, Oxford, UK, 2000.

Khosla, R.P., "From Photons to Bits," *Physics Today*, vol. 45, no. 12, 1992, pp. 42–49.

King, D.J., "Airborne Multispectral Digital Camera and Video Sensors: A Critical Review of System Designs and Applications," *Canadian Journal of Remote Sensing*, vol. 21, no. 3, August 1995, pp. 245–273.

King, D., P. Walsh, and F. Ciuffreda, "Airborne Digital Frame Camera Imaging for Elevation Determination," *Photogrammetric Engineering and Remote Sensing*, vol. 60, no. 11, 1994, pp. 1321–1326.

Light, D.L., "Film Cameras or Digital Sensors? The Challenge Ahead for Aerial Imaging," *Photogrammetric Engineering and Remote Sensing*, vol. 62, no. 3, 1996, pp. 285–291.

Luman, D.E., C. Stohr, and L. Hunt, "Digital Reproduction of Historical Aerial Photographic Prints for Preserving a Deteriorating Archive," *Photogrammetric Engineering and Remote Sensing*, vol. 63, no. 10, 1997, pp. 1171–1179.

Luther, A.C., *Video Camera Technology*, Artech House, Boston, MA, 1998.

Luther, A.C., *Video Recording Technology*, Artech House, Boston, MA, 1999.

Milton, E.J., "Low-Cost Ground-Based Digital Infra-Red Photography," *International Journal of Remote Sensing*, vol. 23, no. 5, 2002, pp. 1001–1007.

Photogrammetric Engineering and Remote Sensing, Special Issue on Panoramic Photography and Forest Remote Sensing, vol. 48, no. 5, 1982.

Newhall, B., *Airborne Camera*, Hastings House, NY, 1969.

Ramsey, E.W., et al., "Mapping Chinese Tallow with Color-Infrared Photography," *Photogrammetric Engineering and Remote Sensing*, vol. 68, no. 3, 2002, pp. 251–255.

Robinson, A.H., et al., *Elements of Cartography*, 6th ed., Wiley, New York, 1995.

Slater, P.N., *Remote Sensing and Optical Systems*, Addison-Wesley, Reading, MA, 1980.

Tomer, M.D., J.L. Anderson, and J.A. Lamb, "Assessing Corn Yield and Nitrogen Uptake Variability with Digitized Aerial Infrared Photographs," *Photogrammetric Engineering and Remote Sensing*, vol. 63, no. 3, 1997, pp. 299–306.

Warner, W.S., R.W. Graham, and R.E. Read, *Small Format Aerial Photography*, American Society for Photogrammetry and Remote Sensing, Bethesda, MD, 1996.

Weigand, C.L., J.H. Everitt, and A.J. Richardson, "Comparison of Multispectral Video and SPOT-1 HRV Observations for Cotton Affected by Soil Salinity," *International Journal of Remote Sensing*, vol. 13, no. 8, 1992, pp. 1511–1525.

Wolf, P.R., and B. Dewitt, *Elements of Photogrammetry with Applications in GIS*, 3rd ed., McGraw-Hill Higher Education, New York, NY, 2000.

3 BASIC PRINCIPLES OF PHOTOGRAMMETRY

3.1 INTRODUCTION

Photogrammetry is the science and technology of obtaining spatial measurements and other geometrically reliable derived products from photographs. Photogrammetric analysis procedures can range from obtaining approximate distances, areas, and elevations using hardcopy photographic products, unsophisticated equipment, and simple geometric concepts to generating precise digital elevation models (DEMs), orthophotos, thematic GIS data, and other derived products through the use of digital raster images and relatively sophisticated analytical techniques.

We use the terms *digital* and *softcopy* photogrammetry interchangeably to refer to any photogrammetric operation involving the use of digital raster photographic image data rather than hardcopy images. Digital photogrammetry is changing rapidly and forms the basis for most current photogrammetric operations. However, the same basic geometric principles apply to traditional hardcopy (analog) and softcopy (digital) procedures. In fact, it is often easier to visualize and understand these principles in a hardcopy context and then extend them to the softcopy environment. This is the approach we adopt in this discussion. We also stress *aerial* photogrammetric techniques and procedures, but the same general principles hold for *space*-based operations.

Historically, the most common use of photogrammetry has been to produce hardcopy topographic maps. Today, photogrammetric procedures are used extensively to produce a range of GIS data products such as precise raster image backdrops for vector data and digital elevation models. Thematic data (in three dimensions) can also be extracted directly from photographs for inclusion in a GIS.

In this chapter, we introduce only the most basic aspects of the broad subject of photogrammetry. Our objective is to provide the reader with a fundamental understanding of how hardcopy photographs can be used to measure and map earth surface features and how softcopy systems work conceptually. We discuss the following photogrammetric activities.

1. **Determining the scale of a vertical photograph and estimating horizontal ground distances from measurements made on a vertical photograph.** The scale of a photograph expresses the mathematical relationship between a distance measured on the photo and the corresponding horizontal distance measured in a ground coordinate system. Unlike maps, which have a single constant scale, aerial photographs have a range of scales that vary in proportion to the elevation of the terrain involved. Once the scale of a photograph is known at any particular elevation, ground distances at that elevation can be readily estimated from corresponding photo distance measurements.
2. **Using area measurements made on a vertical photograph to determine the equivalent areas in a ground coordinate system.** Computing ground areas from corresponding photo area measurement is simply an extension of the above concept of scale. The only difference is that whereas ground distances and photo distances vary linearly, ground areas and photo areas vary as the square of the scale.
3. **Quantifying the effects of relief displacement on vertical aerial photographs.** Again unlike maps, aerial photographs in general do not show the true plan or top view of objects. The images of the tops of objects appearing in a photograph are displaced from the images of their bases. This is known as *relief displacement* and causes any object standing above the terrain to "lean away" from the principal point of a photograph radially. Relief displacement, like scale variation, precludes the use of aerial photographs directly as maps. However, reliable ground measurements and maps can be obtained from vertical photographs if photo measurements are analyzed with due regard for scale variations and relief displacement.
4. **Determination of object heights from relief displacement measurements.** While relief displacement is usually thought of as an image distortion that must be dealt with, it can also be used to estimate the heights of objects appearing on a photograph. As we later

illustrate, the magnitude of relief displacement depends on the flying height, the distance from the photo principal point to the feature, and the height of the feature. Because these factors are geometrically related, we can measure an object's relief displacement and radial position on a photograph and thereby determine the height of the object. This technique provides limited accuracy but is useful in applications where only approximate object heights are needed.

5. **Determination of object heights and terrain elevations by measurement of image parallax.** The previous operations are performed using vertical photos individually. Many photogrammetric operations involve analyzing images in the area of overlap of a stereopair. Within this area, we have two views of the same terrain, taken from different vantage points. Between these two views, the relative positions of features lying closer to the camera (at higher elevation) will change more from photo to photo than the positions of features farther from the camera (at lower elevation). This change in relative position is called *parallax*. It can be measured on overlapping photographs and used to determine object heights and terrain elevations.
6. **Use of ground control points.** The accuracy of photogrammetric measurements is usually premised on the use of *ground control points*. These are points that can be accurately located on the photograph and for which we have information on their ground coordinates and/or elevations (often through GPS observations). This information is used as "geometric ground truth" to calibrate photo measurements. For example, we commonly use ground control to determine the true (slightly tilted) angular orientation of a photograph, the flying height of a photograph, and the airbase of a pair of overlapping photographs (the distance between successive photo centers). This information is critical in a host of photogrammetric operations.
7. **Mapping with aerial photographs.** As mentioned previously, "mapping" from aerial photographs can take on numerous forms and can employ either hardcopy or softcopy approaches. Traditionally, topographic maps have been produced from hardcopy stereopairs in a device called a *stereoplotter*. With this type of instrument, the photographs are mounted in special projectors that can be mutually oriented to precisely correspond to the angular tilts present when the photographs were taken. Once oriented properly, the projectors recreate an accurate model of the terrain that, when viewed stereoscopically, can be used to plot a planimetric map having no relief distortions. In addition, topographic contours can be plotted on the map and the height of vertical features appearing in the model can be determined.

   Whereas a stereoplotter is designed to transfer *map* information, without distortions, from stereo photographs, a similar device can be

used to transfer *image* information, with distortions removed. The resulting undistorted image is called an *orthophotograph* (or *orthophoto*). Orthophotos combine the geometric utility of a map with the extra "real-world image" information provided by a photograph. The process of creating an orthophoto depends on the existence of a reliable DEM for the area being mapped. The DEMs are usually prepared photogrammetrically as well. In fact, *photogrammetric workstations* generally provide the integrated functionality for such tasks as generating DEMs, digital orthophotos, topographic maps, perspective views, and "fly-throughs," as well as the extraction of spatially referenced GIS data in two or three dimensions.

8. **Preparation of a flight plan to acquire aerial photography.** Whenever new photographic coverage of an area is to be obtained, a photographic flight mission must be planned. This process begins with selecting an image scale, camera lens and format size, and desired image overlap. The flight planner can then determine such geometric factors as the appropriate flying height, the distance between image centers, the direction and spacing of flight lines, and the number of images required to cover the study area. Based on these factors, a flight map and a list of specifications are prepared for the firm providing the photographic services.

Each of these photogrammetric operations is covered in separate sections in this chapter. We first discuss some general geometric concepts that are basic to these techniques.

3.2 BASIC GEOMETRIC CHARACTERISTICS OF AERIAL PHOTOGRAPHS

Geometric Types of Aerial Photographs

Aerial photographs are generally classified as either vertical or oblique. *Vertical photographs* are those made with the camera axis directed as vertically as possible. Vertical photography made with a single-lens frame camera is by far the most common type of aerial photography used in remote sensing applications. However, a "truly" vertical aerial photograph is rarely obtainable because of unavoidable angular rotations, or tilts, caused by the angular attitude of the aircraft at the instant of exposure. These unavoidable tilts cause slight (1° to 3°) unintentional inclination of the camera optical axis, resulting in the acquisition of *tilted photographs*.

Virtually all photographs are tilted. When tilted unintentionally and slightly, tilted photographs are usually referred to as being "vertical." For most elementary measurement applications, these photographs are treated as being vertical without introduction of serious error.

When aerial photographs are taken with an intentional inclination of the camera axis, *oblique photographs* result. *High oblique photographs* include an image of the horizon, and *low oblique photographs* do not. We limit our discussion in this chapter to the subject of vertical aerial photographs.

Taking Vertical Aerial Photographs

Most vertical aerial photographs are taken with frame cameras along *flight lines*, or *flight strips*. The line traced on the ground directly beneath the aircraft during acquisition of photography is called the *nadir line*. This line connects the image centers of the vertical photographs. Figure 3.1 illustrates the typical character of the photographic coverage along a flight line. Successive photographs are generally taken with some degree of *endlap*. Not only does this lapping ensure total coverage along a flight line, but an endlap of at least 50 percent is essential for total *stereoscopic coverage* of a project area. Stereoscopic coverage consists of adjacent pairs of overlapping vertical photographs called *stereopairs*. Stereopairs provide two different perspectives of the ground area in their region of endlap. When images forming a stereopair are viewed through a stereoscope, each eye psychologically occupies the vantage

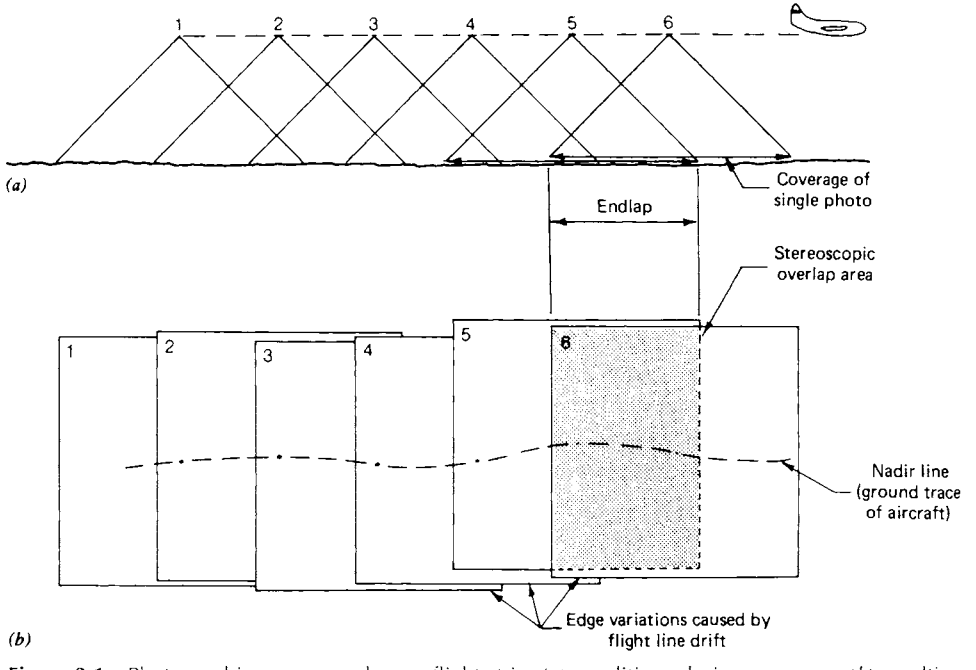

Figure 3.1 Photographic coverage along a flight strip: (*a*) conditions during exposure; (*b*) resulting photography.

Figure 3.2 Acquisition of successive photographs yielding a stereopair. (Courtesy Wild Heerbrugg, Inc.)

point from which the respective image of the stereopair was taken in flight. The result is the perception of a three-dimensional *stereomodel*. As pointed out in Chapter 4, most applications of aerial photographic interpretation entail the use of stereoscopic coverage and stereoviewing.

Successive photographs along a flight strip are taken at intervals that are controlled by the camera *intervalometer*, a device that automatically trips the camera shutter at desired times. The area included in the overlap of successive photographs is called the *stereoscopic overlap area*. Typically, successive photographs contain 55 to 65 percent overlap to ensure at least 50 percent endlap over varying terrain, in spite of unintentional tilt. Figure 3.2 illustrates the ground coverage relationship of successive photographs forming a stereopair having approximately a 60 percent stereoscopic overlap area.

The ground distance between the photo centers at the times of exposure is called the *air base*. The ratio between the air base and the flying height above ground determines the *vertical exaggeration* perceived by photo interpreters. The larger the *base–height ratio*, the greater the vertical exaggeration.

Figure 3.3 shows Large Format Camera photographs of Mt. Washington and vicinity, New Hampshire. These stereopairs illustrate the effect of varying the percentage of photo overlap and thus the base–height ratio of the photographs. These photographs were taken from a flying height of 364 km. The

stereopair in (*a*) has a base–height ratio of 0.30. The stereopair in (*b*) has a base–height ratio of 1.2 and shows much greater apparent relief (greater vertical exaggeration) than (*a*).

Most project sites are large enough for multiple-flight-line passes to be made over the area to obtain complete stereoscopic coverage. Figure 3.4 illustrates how adjacent strips are photographed. On successive flights over the area, adjacent strips have a *sidelap* of approximately 30 percent. Multiple strips comprise what is called a *block* of photographs. Modern aerial surveys usually employ data from the aircraft's precise GPS navigation system to control flight line direction, flight line spacing, and photo exposure intervals.

Geometric Elements of a Vertical Photograph

The basic geometric elements of a vertical aerial photograph are depicted in Figure 3.6. Light rays from terrain objects are imaged in the plane of the film negative after intersecting at the camera lens exposure station, L. The negative is located behind the lens at a distance equal to the lens focal length, f.

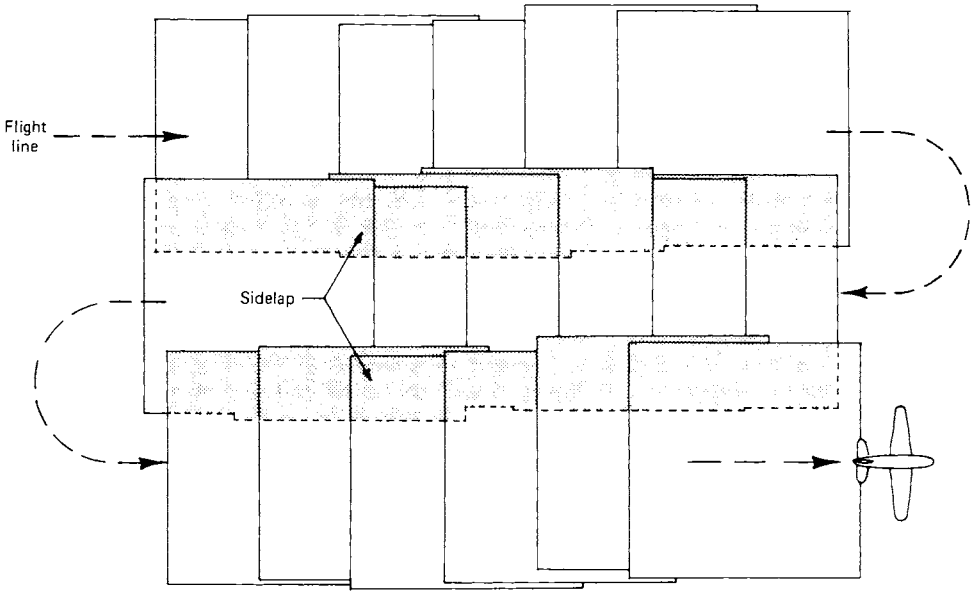

Figure 3.4 Adjacent flight lines over a project area.

Assuming the size of a paper print positive (or film positive) is equal to that of the negative, positive image positions can be depicted diagrammatically in front of the lens in a plane located at a distance f. This rendition is appropriate in that most photo positives used for measurement purposes are contact printed, resulting in the geometric relationships shown.

The x and y coordinate positions of image points are referenced with respect to axes formed by straight lines joining the opposite fiducial marks (see Figure 2.29) recorded on the positive. The x axis is arbitrarily assigned to the fiducial axis most nearly coincident with the line of flight and is taken as positive in the forward direction of flight. The positive y axis is located 90° counterclockwise from the positive x axis. Because of the precision with which the fiducial marks and the lens are placed in a metric camera, the photocoordinate origin, o, can be assumed to coincide exactly with the *principal point*, the intersection of the lens optical axis and the film plane. The point where the prolongation of the optical axis of the camera intersects the terrain is referred to as the *ground principal point*, O. Images for terrain points A, B, C, D, and E appear geometrically reversed on the negative at a', b', c', d', and e' and in proper geometric relationship on the positive at a, b, c, d, and e. (Throughout this chapter we refer to points on the image with lowercase letters and corresponding points on the terrain with uppercase letters.)

The xy photocoordinates of a point are the perpendicular distances from the xy coordinate axes. Points to the right of the y axis have positive x coordi-

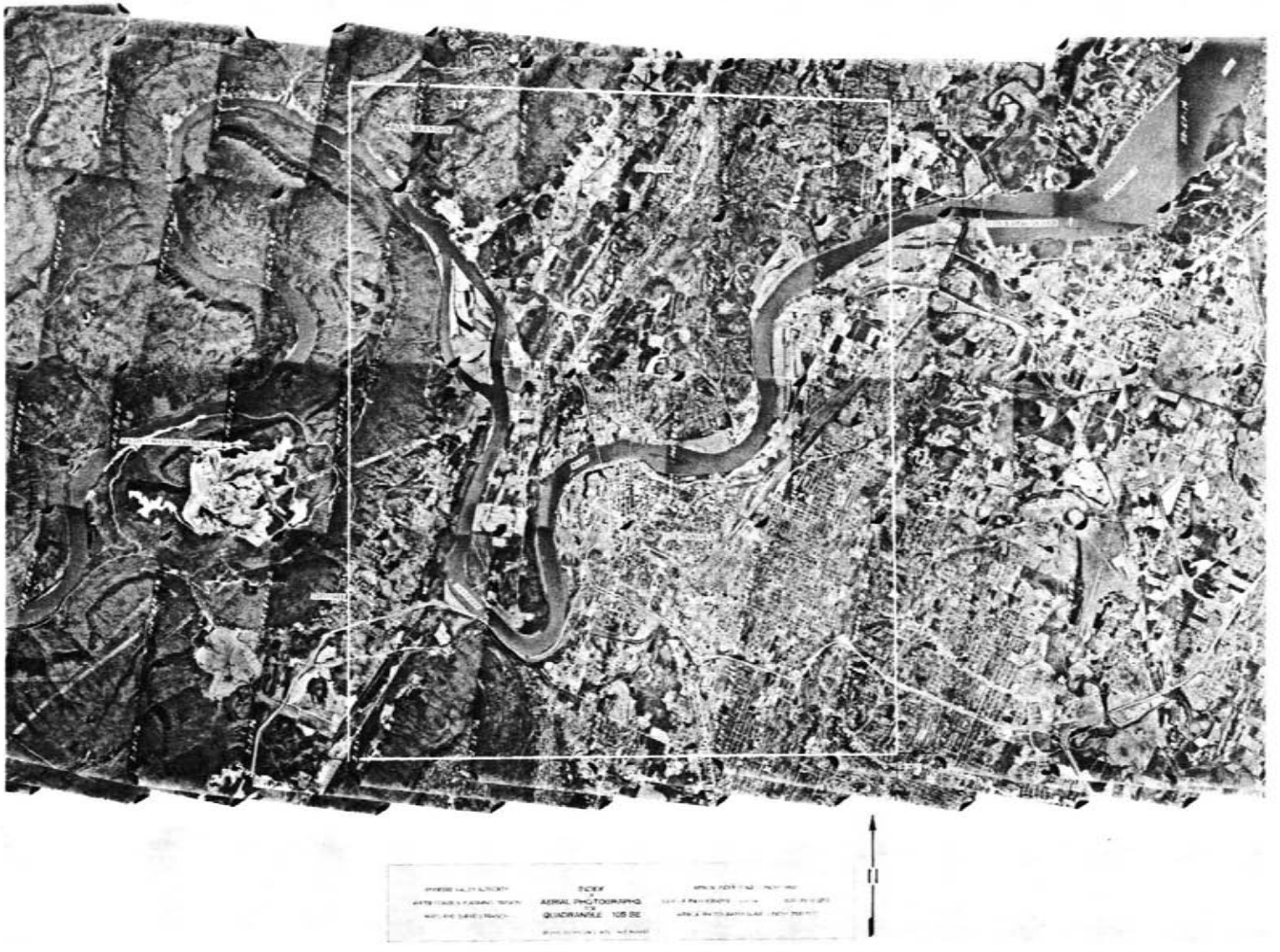

Figure 3.5 Flight index mosaic showing four east–west flight lines of aerial photography over Chattanooga, TN. Area outlined in white indicates coverage area of a single 1 : 24,000 quadrangle map. (Courtesy Mapping Services Branch, Tennessee Valley Authority.)

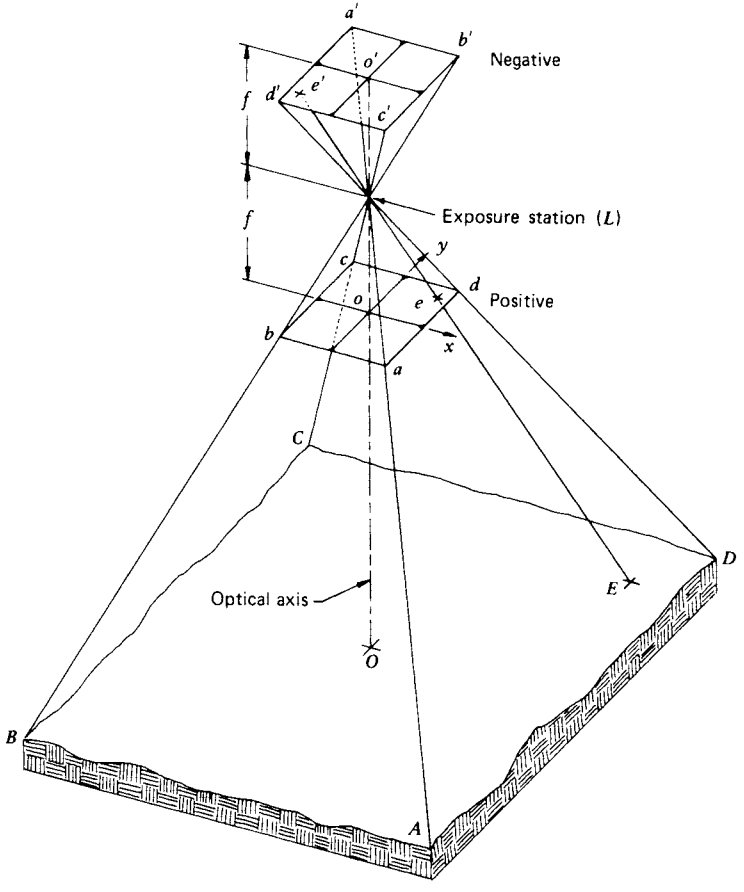

Figure 3.6 Basic geometric elements of a vertical photograph.

nates and points to the left have negative x coordinates. Similarly, points above the x axis have positive y coordinates and those below have negative y coordinates.

Photocoordinate Measurement

Measurements of photocoordinates may be obtained using any one of many measurement devices. These devices vary in their accuracy, cost, and availability. For rudimentary photogrammetric problems—where low orders of measurement accuracy are acceptable—a triangular *engineer's scale* or *metric scale* may be used. When using these scales, measurement accuracy is generally improved by taking the average of several repeated measurements. Mea-

surements are also generally more accurate when made with the aid of a magnifying lens.

Photocoordinates can also be measured using a *coordinate digitizer* (see Figure 3.11). Such devices continuously display the *xy* positions of a spatial reference mark as it is positioned anywhere on the photograph. Another option for photocoordinate measurement is the use of a precision instrument called a *comparator*. A *monocomparator* can be used to measure very accurate coordinates on one photograph at a time; a *stereocomparator* can be used for making measurements on stereopairs.

In softcopy photogrammetric operations, individual points in a photograph are referenced by their row and column coordinates in the digital raster representation of the image. The relationship between the row and column coordinate system and the camera's fiducial axis coordinate system is determined through the development of a mathematical *coordinate transformation* between the two systems. This process requires that some points have their coordinates known in both systems. The fiducial marks are used for this purpose in that their positions in the focal plane are determined during the calibration of the camera, and they can be readily measured in the row and column coordinate system. (Appendix C contains a description of the mathematical form of the *affine coordinate transformation*, which is often used to interrelate the fiducial and row and column coordinate systems.)

Irrespective of what approach is used to measure photocoordinates, these measurements contain errors of varying sources and magnitudes. These errors stem from sources such as camera lens distortions, atmospheric refraction, earth curvature, failure of the fiducial axes to intersect at the principal point, and shrinkage or expansion of the photographic material on which measurements are made. Sophisticated photogrammetric analyses include corrections for all these errors. For simple measurements made on paper prints, such corrections are usually not employed because errors introduced by slight tilt in the photography will outweigh the effect of the other distortions.

3.3 PHOTOGRAPHIC SCALE

One of the most fundamental and frequently used geometric characteristics of aerial photographs is that of *photographic scale*. A photograph "scale," like a map scale, is an expression that states that one unit (any unit) of distance on a photograph represents a specific number of units of actual ground distance. Scales may be expressed as *unit equivalents*, *representative fractions*, or *ratios*. For example, if 1 mm on a photograph represents 25 m on the ground, the scale of the photograph can be expressed as 1 mm = 25 m (unit equivalents), or $\frac{1}{25{,}000}$ (representative fraction), or 1:25,000 (ratio).

Quite often the terms "large scale" and "small scale" are confused by those not working with expressions of scale on a routine basis. For example, which photograph would have the "larger" scale—a 1:10,000 scale photo covering several city blocks or a 1:50,000 photo that covers an entire city? The intuitive answer is often that the photo covering the larger "area" (the entire city) is the larger scale product. This is not the case. The larger scale product is the 1:10,000 image because it shows ground features at a larger, more detailed, size. The 1:50,000 scale photo of the entire city would render ground features at a much smaller, less detailed size. Hence, in spite of its larger ground coverage, the 1:50,000 photo would be termed the smaller scale product.

A convenient way to make scale comparisons is to remember that the same objects are smaller on a "smaller" scale photograph than on a "larger" scale photo. Scale comparisons can also be made by comparing the magnitudes of the representative fractions involved. (That is, $\frac{1}{50,000}$ is smaller than $\frac{1}{10,000}$.)

The most straightforward method for determining photo scale is to measure the corresponding photo and ground distances between any two points. This requires that the points be mutually identifiable on both the photo and a map. The scale S is then computed as the ratio of the photo distance d to the ground distance D,

$$S = \text{photo scale} = \frac{\text{photo distance}}{\text{ground distance}} = \frac{d}{D} \tag{3.1}$$

EXAMPLE 3.1

Assume that two road intersections shown on a photograph can be located on a 1:25,000 scale topographic map. The measured distance between the intersections is 47.2 mm on the map and 94.3 mm on the photograph. (a) What is the scale of the photograph? (b) At that scale, what is the length of a fence line that measures 42.9 mm on the photograph?

Solution

(a) The ground distance between the intersections is determined from the map scale as

$$0.0472 \text{ m} \times \frac{25,000}{1} = 1180 \text{ m}$$

By direct ratio, the photo scale is

$$S = \frac{0.0943 \text{ m}}{1180 \text{ m}} = \frac{1}{12,513} \quad \textit{or} \quad 1:12,500$$

(Note that because only three significant, or meaningful, figures were present in the original measurements, only three significant figures are indicated in the final result.)

(b) The ground length of the 42.9-mm fence line is

$$D = \frac{d}{S} = 0.0429 \text{ m} \div \frac{1}{12{,}500} = 536.25 \text{ m} \quad \text{or} \quad 536 \text{ m}$$

For a vertical photograph taken over flat terrain, scale is a function of the focal length f of the camera used to acquire the image and the flying height above the ground, H', from which the image was taken. In general,

$$\text{Scale} = \frac{\text{camera focal length}}{\text{flying height above terrain}} = \frac{f}{H'} \tag{3.2}$$

Figure 3.7 illustrates how we arrive at Eq. 3.2. Shown in this figure is the side view of a vertical photograph taken over flat terrain. Exposure station L is at

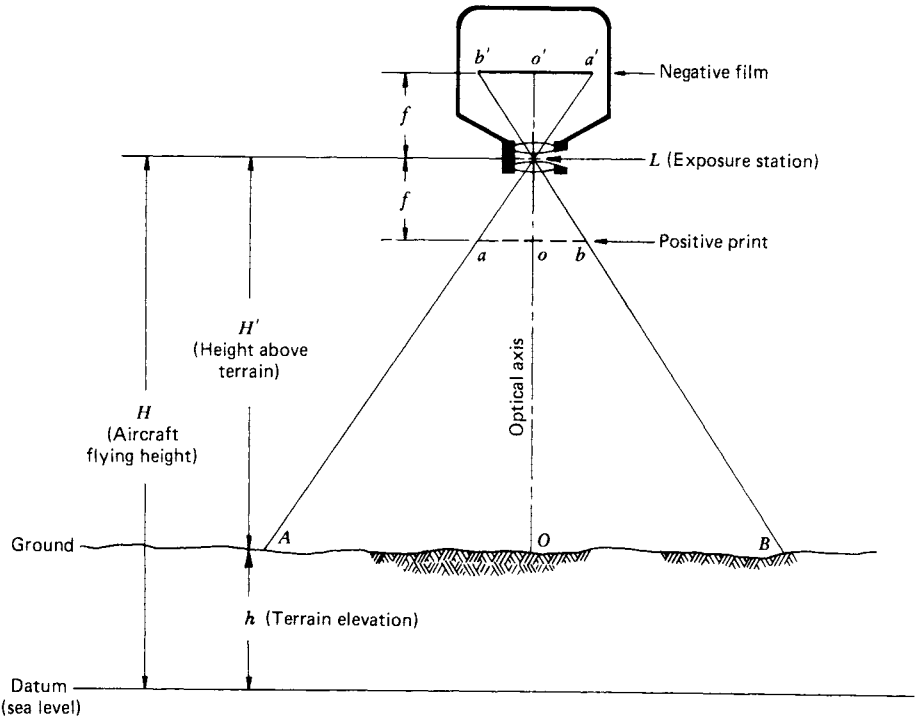

Figure 3.7 Scale of a vertical photograph taken over flat terrain.

an aircraft *flying height* H above some *datum*, or arbitrary base elevation. The datum most frequently used is mean sea level. If flying height H and the elevation of the terrain h are known, we can determine H' by subtraction ($H' = H - h$). If we now consider terrain points A, O, and B, they are imaged at points a', o', and b' on the negative film and at a, o, and b on the positive print. We can derive an expression for photo scale by observing similar triangles Lao and LAO, which are corresponding photo and ground distances. That is,

$$S = \frac{\overline{ao}}{\overline{AO}} = \frac{f}{H'} \tag{3.3}$$

Equation 3.3 is identical to our scale expression of Eq. 3.2. Yet another way of expressing these equations is

$$S = \frac{f}{H - h} \tag{3.4}$$

Equation 3.4 is the most commonly used form of the scale equation.

EXAMPLE 3.2

A camera equipped with a 152-mm-focal-length lens is used to take a vertical photograph from a flying height of 2780 m above mean sea level. If the terrain is flat and located at an elevation of 500 m, what is the scale of the photograph?

Solution

$$\text{Scale} = \frac{f}{H - h} = \frac{0.152 \text{ m}}{2780 \text{ m} - 500 \text{ m}} = \frac{1}{15{,}000} \quad \text{or} \quad 1:15{,}000$$

The most important principle expressed by Eq. 3.4 is that photo scale is a function of terrain elevation h. Because of the level terrain, the photograph depicted in Figure 3.7 has a constant scale. However, *photographs taken over terrain of varying elevation will exhibit a continuous range of scales associated with the variations in terrain elevation.* Likewise, tilted and oblique photographs have nonuniform scales.

EXAMPLE 3.3

Assume a vertical photograph was taken at a flying height of 5000 m above sea level using a camera with a 152-mm-focal-length lens. (a) Determine the photo scale at

points A and B, which lie at elevations of 1200 and 1960 m. (b) What ground distance corresponds to a 20.1-mm photo distance measured at each of these elevations?

Solution

(a) By Eq. 3.4,

$$S_A = \frac{f}{H - h_A} = \frac{0.152 \text{ m}}{5000 \text{ m} - 1200 \text{ m}} = \frac{1}{25{,}000} \quad \text{or} \quad 1{:}25{,}000$$

$$S_B = \frac{f}{H - h_B} = \frac{0.152 \text{ m}}{5000 \text{ m} - 1960 \text{ m}} = \frac{1}{20{,}000} \quad \text{or} \quad 1{:}20{,}000$$

(b) The ground distance corresponding to a 20.1-mm photo distance is

$$D_A = \frac{d}{S_A} = 0.0201 \text{ m} \div \frac{1}{25{,}000} = 502.5 \text{ m} \quad \text{or} \quad 502 \text{ m}$$

$$D_B = \frac{d}{S_B} = 0.0201 \text{ m} \div \frac{1}{20{,}000} = 402 \text{ m}$$

Often it is convenient to compute an *average scale* for an entire photograph. This scale is calculated using the average terrain elevation for the area imaged. Consequently, it is exact for distances occurring at the average elevation and is approximate at all other elevations. Average scale may be expressed as

$$S_{\text{avg}} = \frac{f}{H - h_{\text{avg}}} \tag{3.5}$$

where h_{avg} is the average elevation of the terrain shown in the photograph.

The result of photo scale variation is geometric distortion. All points on a *map* are depicted in their true relative horizontal (planimetric) positions, but points on a *photo* taken over varying terrain are displaced from their true "map positions." This difference results because a map is a scaled *orthographic* projection of the ground surface, whereas a vertical photograph yields a *perspective* projection. The differing nature of these two forms of projection is illustrated in Figure 3.8. As shown, a map results from projecting vertical rays from ground points to the map sheet (at a particular scale). A photograph results from projecting converging rays through a common point within the camera lens. Because of the nature of this projection, any variations in terrain elevation will result in scale variation *and* displaced image positions.

On a map we see a top view of objects in their true relative horizontal positions. On a photograph, areas of terrain at the higher elevations lie

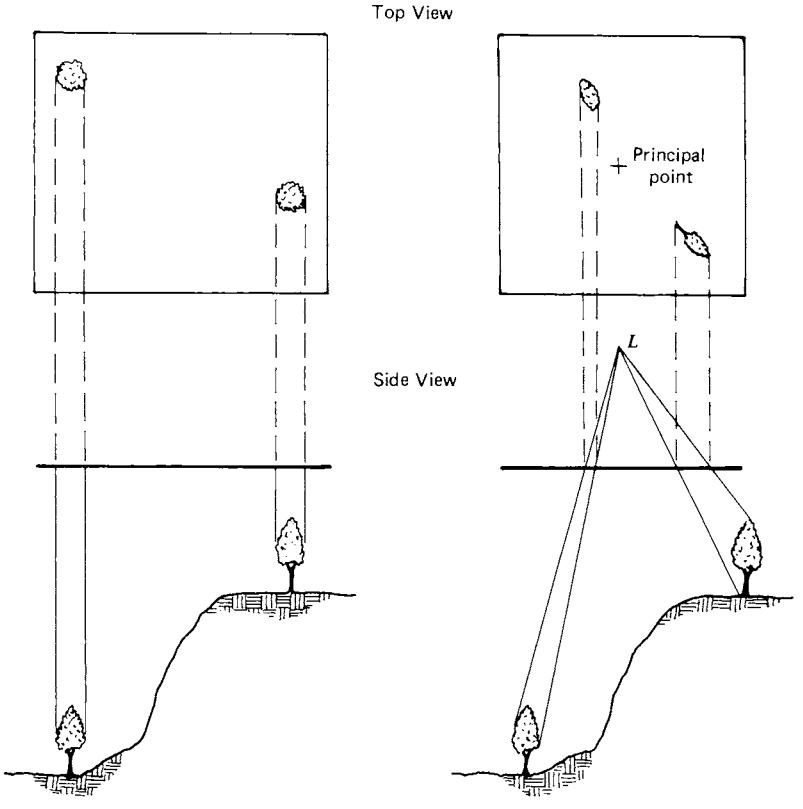

Figure 3.8 Comparative geometry of (*a*) a map and (*b*) a vertical aerial photograph. Note differences in size, shape, and location of the two trees.

closer to the camera at the time of exposure and therefore appear larger than corresponding areas lying at lower elevations. Furthermore, the tops of objects are always displaced from their bases (Figure 3.8). This distortion is called *relief displacement* and causes any object standing above the terrain to "lean" away from the principal point of a photograph radially. We treat the subject of relief displacement in Section 3.6.

By now the reader should see that the only circumstance wherein an aerial photograph can be treated as if it were a map directly is in the case of a vertical photograph imaging uniformly flat terrain. This is rarely the case in practice and the image analyst must always be aware of the potential geometric distortions introduced by such influences as tilt, scale variation, and relief

displacement. Failure to deal with these distortions will often lead, among other things, to a lack of geometric "fit" among image-derived and nonimage data sources in a GIS. However, if these factors are properly addressed photogrammetrically, extremely reliable measurements and map products can be derived from aerial photography.

3.4 GROUND COVERAGE OF AERIAL PHOTOGRAPHS

The ground coverage of a photograph is, among other things, a function of camera format size. For example, an image taken with a camera having a 230 × 230-mm format (on 240-mm film) has about 17.5 times the ground area coverage of an image of equal scale taken with a camera having a 55 × 55-mm format (on 70-mm film) and about 61 times the ground area coverage of an image of equal scale taken with a camera having a 24 × 36-mm format (on 35-mm film). As with photo scale, the ground coverage of photography obtained with any given format is a function of focal length and flying height above ground, H'. For a constant flying height, the width of the ground area covered by a photo varies inversely with focal length. Consequently, photos taken with shorter focal length lenses have larger areas of coverage (and smaller scales) than do those taken with longer focal length lenses. For any given focal length lens, the width of the ground area covered by a photo varies directly with flying height above terrain, with image scale varying inversely with flying height.

The effect that flying height has on ground coverage and image scale is illustrated in Figures 3.9*a*, *b*, and *c*. These images were all taken over Chattanooga, Tennessee, with the same camera type equipped with the same focal length lens but from three different altitudes. Figure 3.9*a* is a high altitude, small-scale image showing virtually the entire Chattanooga metropolitan area. Figure 3.9*b* is a lower altitude, larger scale image showing the ground area outlined in Figure 3.9*a*. Figure 3.9*c* is a yet lower altitude, larger scale image of the area outlined in Figure 3.9*b*. Note the trade-offs between the ground area covered by an image and the object detail available in each of the photographs.

3.5 AREA MEASUREMENT

The process of measuring areas using aerial photographs can take on many forms. The accuracy of area measurement is a function of not only the measuring device used, but also the degree of image scale variation due to relief in the terrain and tilt in the photography. Although large errors in

area determinations can result even with vertical photographs in regions of moderate to high relief, accurate measurements may be made on vertical photos of areas of low relief.

Simple scales may be used to measure the area of simply shaped features. For example, the area of a rectangular field can be determined by simply measuring its length and width. Similarly, the area of a circular feature can be computed after measuring its radius or diameter.

EXAMPLE 3.4

A rectangular agricultural field measures 8.65 cm long and 5.13 cm wide on a vertical photograph having a scale of 1:20,000. Find the area of the field at ground level.

Solution

$$\text{Ground length} = \text{photo length} \times \frac{1}{S} = 0.0865 \text{ m} \times 20{,}000 = 1730 \text{ m}$$

$$\text{Ground width} = \text{photo width} \times \frac{1}{S} = 0.0513 \times 20{,}000 = 1026 \text{ m}$$

$$\text{Ground area} = 1730 \text{ m} \times 1026 \text{ m} = 1{,}774{,}980 \text{ m}^2 = 177 \text{ ha}$$

The ground area of an irregularly shaped feature is usually determined by measuring the area of the feature on the photograph. The photo area is then converted to a ground area from the following relationship:

$$\text{Ground area} = \text{photo area} \times \frac{1}{S^2}$$

EXAMPLE 3.5

The area of a lake is 52.2 cm^2 on a 1:7500 vertical photograph. Find the ground area of the lake.

Solution

$$\text{Ground area} = \text{photo area} \times \frac{1}{S^2} = 0.00522 \text{ m}^2 \times 7500^2 = 293{,}625 \text{ m}^2 = 29.4 \text{ ha}$$

Numerous methods can be used to measure the area of irregularly shaped features on a photograph. One of the simplest techniques employs a transparent grid overlay consisting of lines forming rectangles or squares of known area. The grid is placed over the photograph and the area of a ground unit is estimated by counting grid units that fall within the unit to be measured. Perhaps the most widely used grid overlay is a *dot grid* (Figure 3.10). This grid, composed of uniformly spaced dots, is superimposed over the photo, and the dots falling within the region to be measured are counted. From knowledge of the dot density of the grid, the photo area of the region can be computed.

$$\text{Dot density} = \frac{1 \text{ cm}^2}{25 \text{ dots}} \times 20{,}000^2 = 16{,}000{,}000 \text{ cm}^2/\text{dot} = 0.16 \text{ ha/dot}$$

$$\text{Ground area} = 129 \text{ dots} \times 0.16 \text{ ha/dot} = 20.6 \text{ ha}$$

The dot grid is an inexpensive tool and its use requires little training. When numerous regions are to be measured, however, the counting proce-

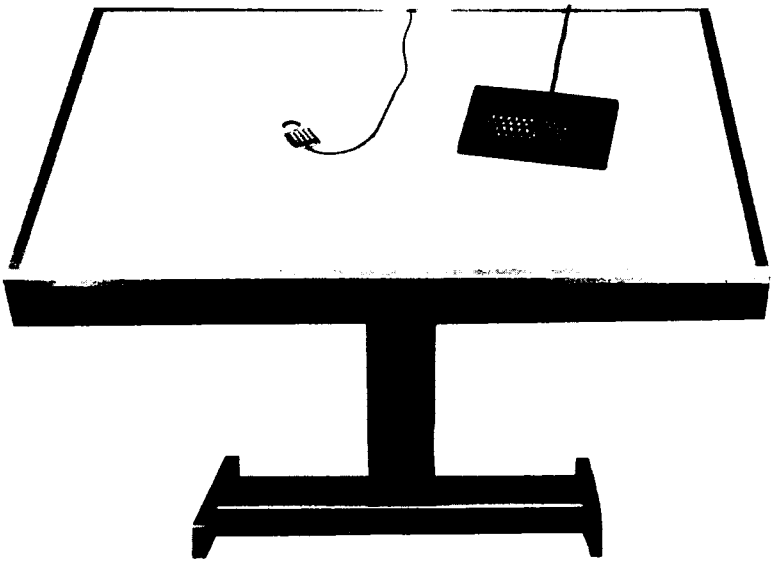

Figure 3.11 Precision coordinate digitizer. (Courtesy Altek Corp.)

dure becomes quite tedious. An alternative technique is to use either a coordinate digitizer or digitizing tablet (Figure 3.11). These devices are typically interfaced with a computer such that area determination simply involves tracing around the boundary of the region of interest and the area can be read out directly. When photographs are available in softcopy format, area measurement often involves digitizing from a computer monitor using a mouse or other form of cursor control.

3.6 RELIEF DISPLACEMENT OF VERTICAL FEATURES

Characteristics of Relief Displacement

In Figure 3.8, we illustrated the effect of relief displacement on a photograph taken over varied terrain. In essence, an increase in the elevation of a feature causes its position on the photograph to be displaced radially outward from the principal point. Hence, when a vertical feature is photographed, relief displacement causes the top of the feature to lie farther from the photo center than its base. As a result, vertical features appear to lean away from the center of the photograph.

The pictorial effect of relief displacement is illustrated by the aerial photographs shown in Figure 3.12. These photographs depict the construction site of the Watts Bar Nuclear Plant adjacent to the Tennessee River. An operating coal-fired steam plant with its fan-shaped coal stockyard is shown in the


N

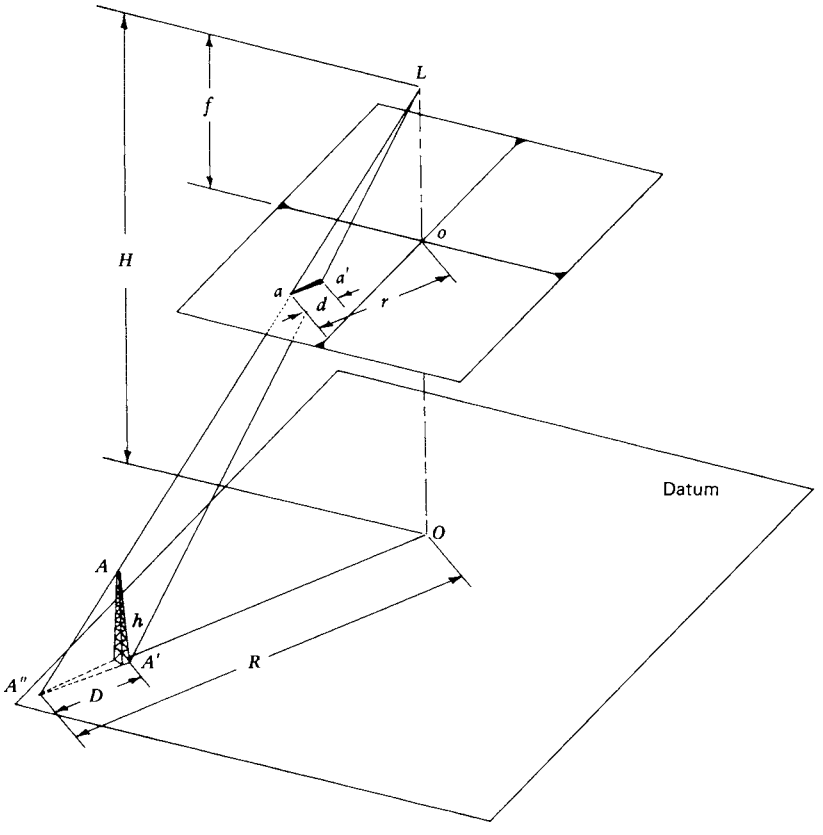

Figure 3.13 Geometric components of relief displacement.

taken from flying height H above datum. When considering the relief displacement of a vertical feature, it is convenient to arbitrarily assume a datum plane placed at the base of the feature. If this is done, the flying height H must be correctly referenced to this same datum, *not* mean sea level. Thus, in Figure 3.13 the height of the tower (whose base is at datum) is h. Note that the top of the tower, A, is imaged at a in the photograph whereas the base of the tower, A', is imaged at a'. That is, the image of the top of the tower is radially displaced by the distance d from that of the bottom. The distance d is the relief displacement of the tower. The equivalent distance projected to datum is D. The distance from the photo principal point to the top of the tower is r. The equivalent distance projected to datum is R.

We can express d as a function of the dimensions shown in Figure 3.13. From similar triangles $AA'A''$ and LOA'',

$$\frac{D}{h} = \frac{R}{H}$$

Expressing distances D and R at the scale of the photograph, we obtain

$$\frac{d}{h} = \frac{r}{H}$$

Rearranging the above equation yields

$$d = \frac{rh}{H} \tag{3.6}$$

where

d = relief displacement
r = radial distance on the photograph from the principal point to the displaced image point
h = height above datum of the object point
H = flying height above the same datum chosen to reference h

An analysis of Eq. 3.6 indicates mathematically the nature of relief displacement seen pictorially. That is, relief displacement of any given point increases as the distance from the principal point increases (this can be seen in Figure 3.12), and it increases as the elevation of the point increases. Other things being equal, it decreases with an increase in flying height. Hence, under similar conditions high altitude photography of an area manifests less relief displacement than low altitude photography. Also, there is no relief displacement at the principal point (since $r = 0$).

Object Height Determination from Relief Displacement Measurement

Equation 3.6 also indicates that relief displacement increases with the feature height h. This relationship makes it possible to indirectly measure heights of objects appearing on aerial photographs. By rearranging Eq. 3.6, we obtain

$$h = \frac{dH}{r} \tag{3.7}$$

To use Eq. 3.7, both the top and base of the object to be measured must be clearly identifiable on the photograph and the flying height H must be known. If this is the case, d and r can be measured on the photograph and used to calculate the object height h. (When using Eq. 3.7, it is important to remember that H must be referenced to the elevation of the base of the feature, not to mean sea level.)

EXAMPLE 3.7

For the photo shown in Figure 3.13, assume that the relief displacement for the tower at A is 2.01 mm, and the radial distance from the center of the photo to the top of the

tower is 56.43 mm. If the flying height is 1220 m above the base of the tower, find the height of the tower.

Solution
By Eq. 3.7

$$h = \frac{dH}{r} = \frac{2.01 \text{ mm } (1220 \text{ m})}{56.43 \text{ mm}} = 43.4 \text{ m}$$

While measuring relief displacement is a very convenient means of calculating heights of objects from aerial photographs, the reader is reminded of the assumptions implicit in the use of the method. We have assumed use of truly vertical photography, accurate knowledge of the flying height, clearly visible objects, precise location of the principal point, and a measurement technique whose accuracy is consistent with the degree of relief displacement involved. If these assumptions are reasonably met, quite reliable height determinations may be made using single prints and relatively unsophisticated measuring equipment.

Correcting for Relief Displacement

In addition to calculating object heights, quantification of relief displacement can be used to correct the image positions of terrain points appearing in a photograph. Keep in mind that terrain points in areas of varied relief exhibit relief displacements as do vertical objects. This is illustrated in Figure 3.14. In this figure, the datum plane has been set at the average terrain elevation (not at mean sea level). If all terrain points were to lie at this common elevation, terrain points A and B would be located at A' and B' and would be imaged at points a' and b' on the photograph. Due to the varied relief, however, the position of point A is shifted radially outward on the photograph (to a), and the position of point B is shifted radially inward (to b). These changes in image position are the relief displacements of points A and B. Figure 3.14*b* illustrates the effect they have on the geometry of the photo. Because A' and B' lie at the same terrain elevation, the image line $a'b'$ accurately represents the scaled horizontal length and directional orientation of the ground line AB. When the relief displacements are introduced, the resulting line ab has a considerably altered length and orientation.

Angles are also distorted by relief displacements. In Figure 3.14*b*, the horizontal ground angle ACB is accurately expressed by $a'cb'$ on the photo. Due to the displacements, the distorted angle acb will appear on the photograph. Note that, because of the radial nature of relief displacements, angles about the origin of the photo (such as aob) will not be distorted.

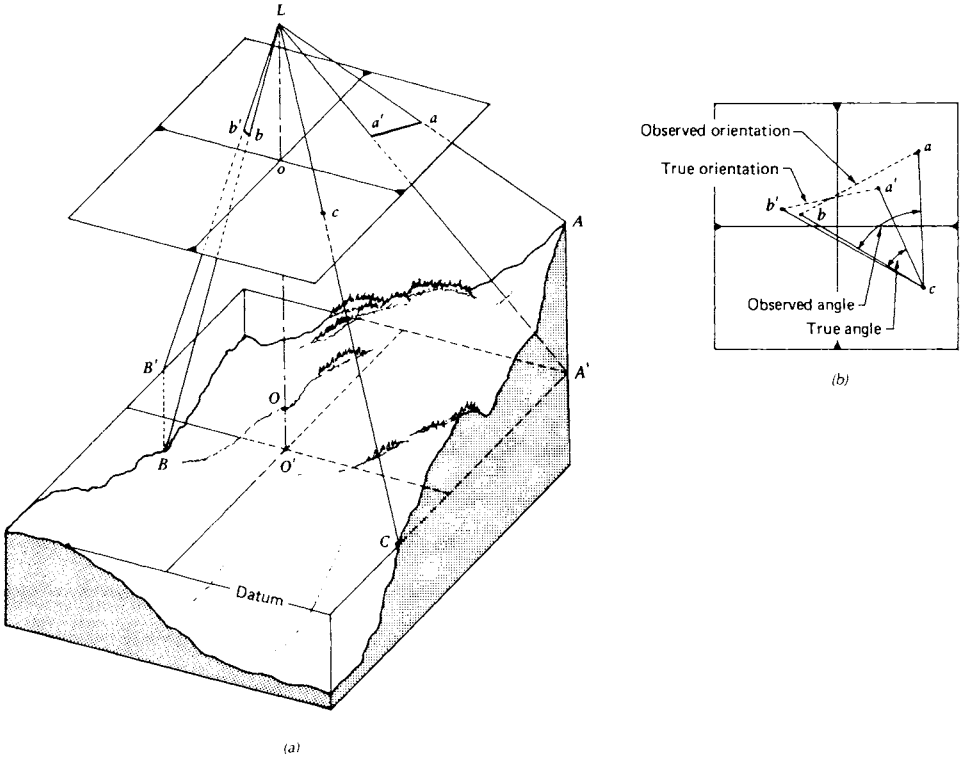

Figure 3.14 Relief displacement on a photograph taken over varied terrain: (*a*) displacement of terrain points; (*b*) distortion of horizontal angles measured on photograph.

Relief displacement can be corrected for by using Eq. 3.6 to compute its magnitude on a point-by-point basis and then laying off the computed displacement distances radially (in reverse) on the photograph. This procedure establishes the datum-level image positions of the points and removes the relief distortions, resulting in planimetrically correct image positions at datum scale. This scale can be determined from the flying height above datum ($S = f/H$). Ground lengths, directions, angles, and areas may then be directly determined from these corrected image positions.

EXAMPLE 3.8

Referring to the vertical photograph depicted in Figure 3.14, assume that the radial distance r_a to point A is 63.84 mm and the radial distance r_b to point B is 62.65 mm. Flying height H is 1220 m above datum, point A is 152 m above datum, and point B is 168 m below datum. Find the radial distance and direction one must lay off from points a and b to plot a' and b'.

Solution
By Eq. 3.6

$$d_a = \frac{r_a h_a}{H} = \frac{63.84 \text{ mm} \times 152 \text{ m}}{1220 \text{ m}} = 7.95 \text{ mm} \qquad \text{(plot inward)}$$

$$d_b = \frac{r_b h_b}{H} = \frac{62.65 \text{ mm} \times (-168 \text{ m})}{1220 \text{ m}} = -8.63 \text{ mm} \qquad \text{(plot outward)}$$

3.7 IMAGE PARALLAX

Characteristics of Image Parallax

Thus far we have limited our discussion to photogrammetric operations involving only single vertical photographs. Numerous applications of photogrammetry incorporate the analysis of stereopairs and use of the principle of *parallax*. The term *parallax* refers to the apparent change in relative positions of stationary objects caused by a change in viewing position. This phenomenon is observable when one looks at objects through a side window of a moving vehicle. With the moving window as a frame of reference, objects such as mountains at a relatively great distance from the window appear to move very little within the frame of reference. In contrast, objects close to the window, such as roadside trees, appear to move through a much greater distance.

In the same way that the close trees move relative to the distant mountains, terrain features close to an aircraft (i.e., at higher elevation) will appear to move relative to the lower elevation features when the point of view changes between successive exposures. These relative displacements form the basis for three-dimensional viewing of overlapping photographs. In addition, they can be measured and used to compute the elevations of terrain points.

Figure 3.15 illustrates the nature of parallax on overlapping vertical photographs taken over varied terrain. Note that the relative positions of points *A* and *B* change with the change in viewing position (in this case, the exposure station). Note also that the *parallax displacements occur only parallel to the line of flight*. In theory, the direction of flight should correspond precisely to the fiducial *x* axis. In reality, however, unavoidable changes in the aircraft orientation will usually slightly offset the fiducial axis from the flight axis. The true flight line axis may be found by first locating on a photograph the points that correspond to the image centers of the preceding and succeeding photographs. These points are called the *conjugate principal points*. A line drawn through the principal points and the conjugate principal points defines the

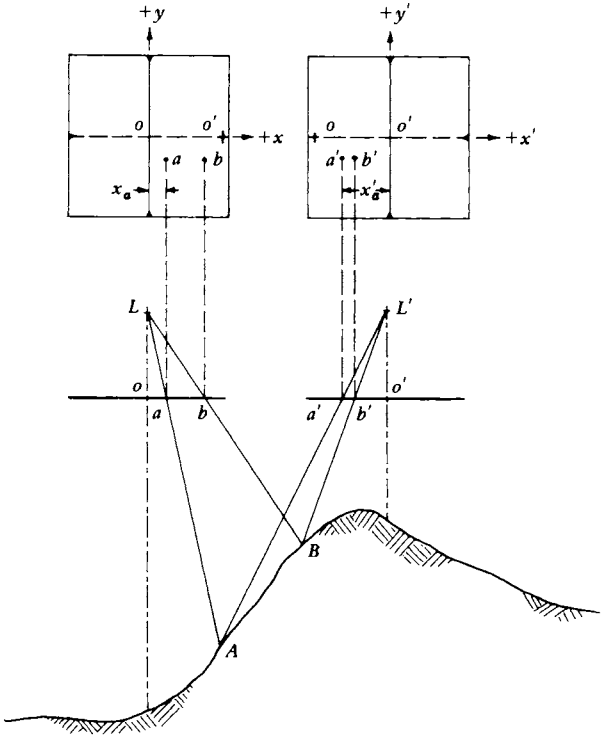

Figure 3.15 Parallax displacements on overlapping vertical photographs.

flight axis. As shown in Figure 3.16, all photographs except those on the ends of a flight strip normally have two sets of flight axes. This happens because the aircraft's path between exposures is usually slightly curved. In Figure 3.16, the flight axis for the stereopair formed by photos 1 and 2 is flight axis 12. The flight axis for the stereopair formed by photos 2 and 3 is flight axis 23.

The line of flight for any given stereopair defines a photocoordinate x axis for use in parallax measurement. Lines drawn perpendicular to the flight line and passing through the principal point of each photo form the photographic y axes for parallax measurement. The parallax of any point, such as A in Figure 3.15, is expressed in terms of the flight line coordinate system as

$$p_a = x_a - x'_a \tag{3.8}$$

where

p_a = parallax of point A

x_a = measured x coordinate of image a on the left photograph of the stereopair

x'_a = x coordinate of image a' on the right photograph

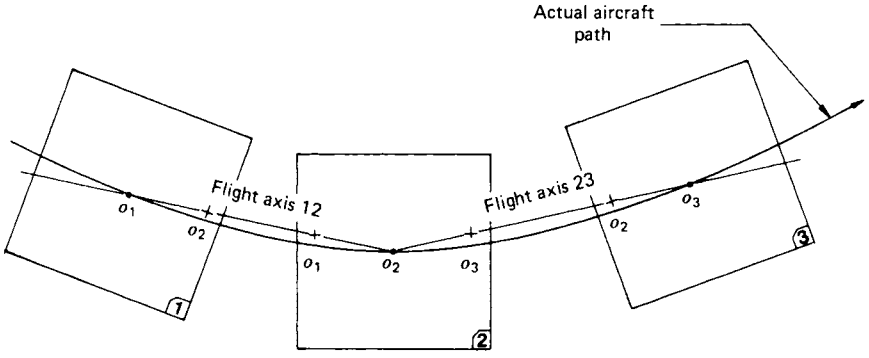

Figure 3.16 Flight line axes for successive stereopairs along a flight strip. (Curvature of aircraft path is exaggerated.)

The x axis for each photo is considered positive to the right of each photo principal point. This makes x_a' a negative quantity in Figure 3.15.

Object Height and Ground Coordinate Location from Parallax Measurement

Figure 3.17 shows overlapping vertical photographs of a terrain point, A. Using parallax measurements, we may determine the elevation at A and its ground coordinate location. Referring to Figure 3.17*a*, the horizontal distance between exposure stations L and L' is called B, the *air base*. The triangle in Figure 3.17*b* results from superimposition of the triangles at L and L' in order to graphically depict the nature of parallax p_a as computed from Eq. 3.8 algebraically. From similar triangles $La_x'a_x$ (Figure 3.17*b*) and LA_xL' (Figure 3.17*a*)

$$\frac{p_a}{f} = \frac{B}{H - h_A}$$

from which

$$H - h_A = \frac{Bf}{p_a} \tag{3.9}$$

Rearranging yields

$$h_A = H - \frac{Bf}{p_a} \tag{3.10}$$

Also, from similar triangles LO_AA_x and Loa_x,

$$\frac{X_A}{H - h_A} = \frac{x_a}{f}$$

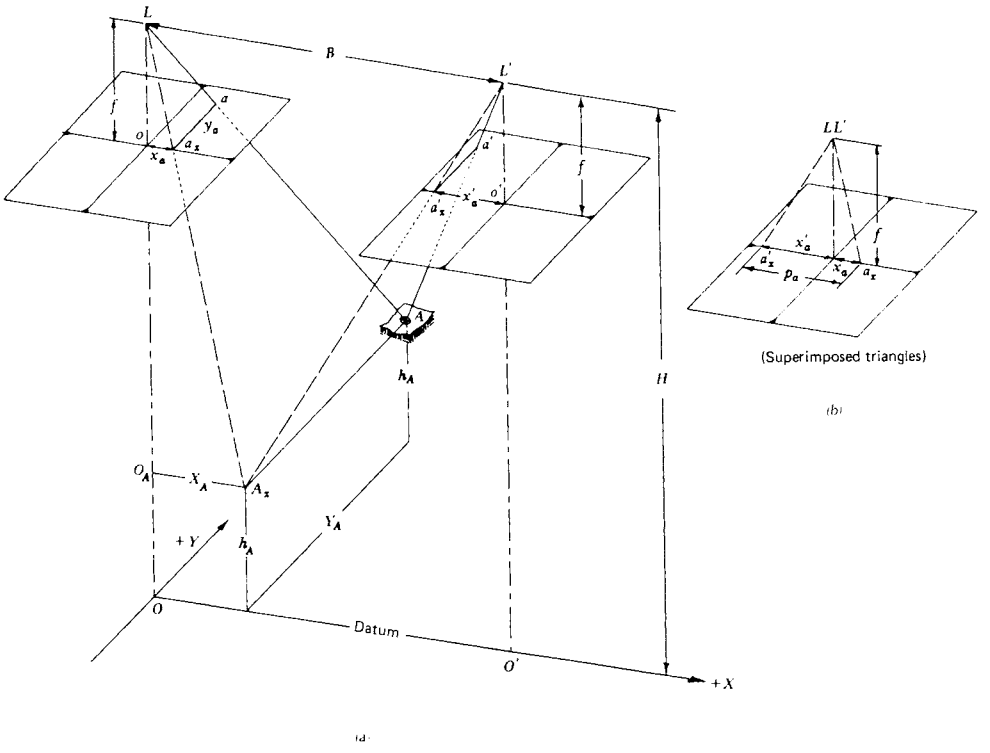

Figure 3.17 Parallax relationships on overlapping vertical photographs: (*a*) adjacent photographs forming a stereopair; (*b*) superimposition of right photograph onto left.

from which

$$X_A = \frac{x_a(H - h_A)}{f}$$

and substituting Eq. 3.9 into the above equation yields

$$X_A = B\frac{x_a}{p_a} \tag{3.11}$$

A similar derivation using y coordinates yields

$$Y_A = B\frac{y_a}{p_a} \tag{3.12}$$

Equations 3.10 to 3.12 are commonly known as the *parallax equations*. In these equations, X and Y are ground coordinates of a point with respect to an arbitrary coordinate system whose origin is vertically below the left exposure station and with positive X in the direction of flight; p is the parallax of the point in question; and x and y are the photocoordinates of the point on the left-hand

photo. The major assumptions made in the derivation of these equations are that the photos are truly vertical and that they are taken from the same flying height. If these assumptions are sufficiently met, a complete survey of the ground region contained in the photo overlap area of a stereopair can be made.

EXAMPLE 3.9

The length of line AB and the elevation of its endpoints, A and B, are to be determined from a stereopair containing images a and b. The camera used to take the photographs has a 152.4-mm lens. The flying height was 1200 m (average for the two photos) and the air base was 600 m. The measured photographic coordinates of points A and B in the "flight line" coordinate system are $x_a = 54.61$ mm, $x_b = 98.67$ mm, $y_a = 50.80$ mm, $y_b = -25.40$ mm, $x_a' = -59.45$ mm, and $x_b' = -27.39$ mm. Find the length of line AB and the elevations of A and B.

Solution

From Eq. 3.8

$$p_a = x_a - x_a' = 54.61 - (-59.45) = 114.06 \text{ mm}$$

$$p_b = x_b - x_b' = 98.67 - (-27.39) = 126.06 \text{ mm}$$

From Eqs. 3.11 and 3.12

$$X_A = B\frac{x_a}{p_a} = \frac{600 \times 54.61}{114.06} = 287.27 \text{ m}$$

$$X_B = B\frac{x_b}{p_b} = \frac{600 \times 98.67}{126.06} = 469.63 \text{ m}$$

$$Y_A = B\frac{y_a}{p_a} = \frac{600 \times 50.80}{114.06} = 267.23 \text{ m}$$

$$Y_B = B\frac{y_b}{p_b} = \frac{600 \times (-25.40)}{126.06} = -120.89 \text{ m}$$

Applying the Pythagorean theorem yields

$$AB = [(469.63 - 287.27)^2 + (-120.89 - 267.23)^2]^{1/2} = 428.8 \text{ m}$$

From Eq. 3.10, the elevations of A and B are

$$h_A = H - \frac{Bf}{p_a} = 1200 - \frac{600 \times 152.4}{114.06} = 398 \text{ m}$$

$$h_B = H - \frac{Bf}{p_b} = 1200 - \frac{600 \times 152.4}{126.06} = 475 \text{ m}$$

In many applications, the *difference* in elevation between two points is of more immediate interest than is the actual value of the elevation of either point. In such cases, the change in elevation between two points can be found from

$$\Delta h = \frac{\Delta p\, H'}{p_a} \tag{3.13}$$

where

Δh = difference in elevation between two points whose parallax *difference* is Δp
H' = flying height above the lower point
p_a = parallax of the higher point

Using this approach in our previous example yields

$$\Delta h = \frac{12.00 \times 802}{126.06} = 77 \text{ m}$$

Note this answer agrees with the value computed above.

Parallax Measurement

To this point in our discussion, we have said little about how parallax measurements are made. In Example 3.9 we assumed that x and x' for points of interest were measured directly on the left and right photos, respectively. Parallaxes were then calculated from the algebraic differences of x and x', in accordance with Eq. 3.8. This procedure becomes cumbersome when many points are analyzed, since two measurements are required for each point.

Figure 3.18 illustrates the principle behind methods of parallax measurement that require only a single measurement for each point of interest. If the two photographs constituting a stereopair are fastened to a base with their flight lines aligned, the distance D remains constant for the setup, and the parallax of a point can be derived from measurement of the single distance d. That is, $p = D - d$. Distance d can be measured with a simple scale, *assuming a and a' are identifiable*. In areas of uniform photo tone, individual features may not be identifiable, making the measurement of d very difficult.

Employing the principle illustrated in Figure 3.18, a number of devices have been developed to increase the speed and accuracy of parallax measurement. These devices also permit parallax to be easily measured in areas

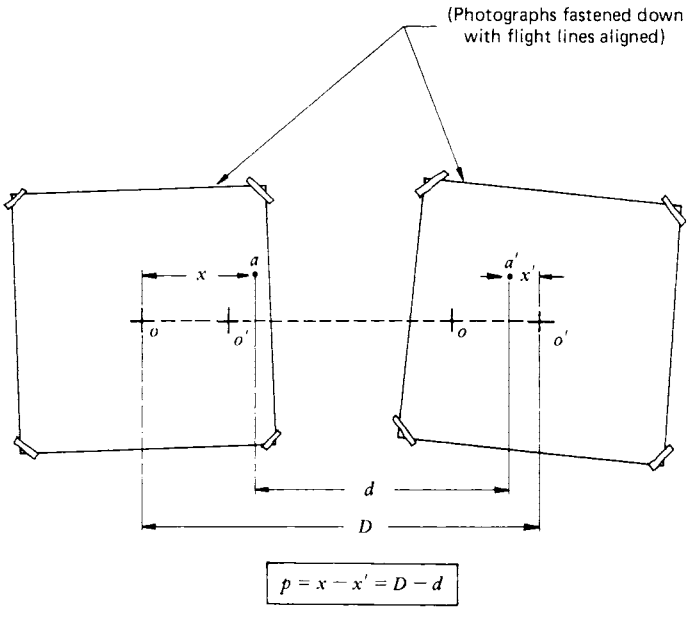

Figure 3.18 Alignment of a stereopair for parallax measurement.

of uniform photo tone. All employ stereoscopic viewing and the principle of the *floating mark*. This principle is illustrated in Figure 3.19. While viewing through a stereoscope, the image analyst uses a device that places small identical marks over each photograph. These marks are normally dots or crosses etched on transparent material. The marks—called *half marks*—are positioned over similar areas on the left-hand photo and the right-hand photo. The left mark is seen only by the left eye of the analyst and the right mark is seen only by the right eye. The relative positions of the half marks can be shifted along the direction of flight until they visually fuse together, forming a single mark that appears to "float" at a specific level in the stereomodel. The apparent elevation of the floating mark varies with the spacing between the half marks. Figure 3.19 illustrates how the fused marks can be made to float and can actually be set on the terrain at particular points in the stereomodel. Half-mark positions (a, b), (a, c), and (a, d) result in floating-mark positions in the model at B, C, and D.

A very simple device for measuring parallax is the *parallax wedge*. It consists of a transparent sheet of plastic on which are printed two converging lines or rows of dots (or graduated lines). Next to one of the converging lines is a scale that shows the horizontal distance between the two lines at each

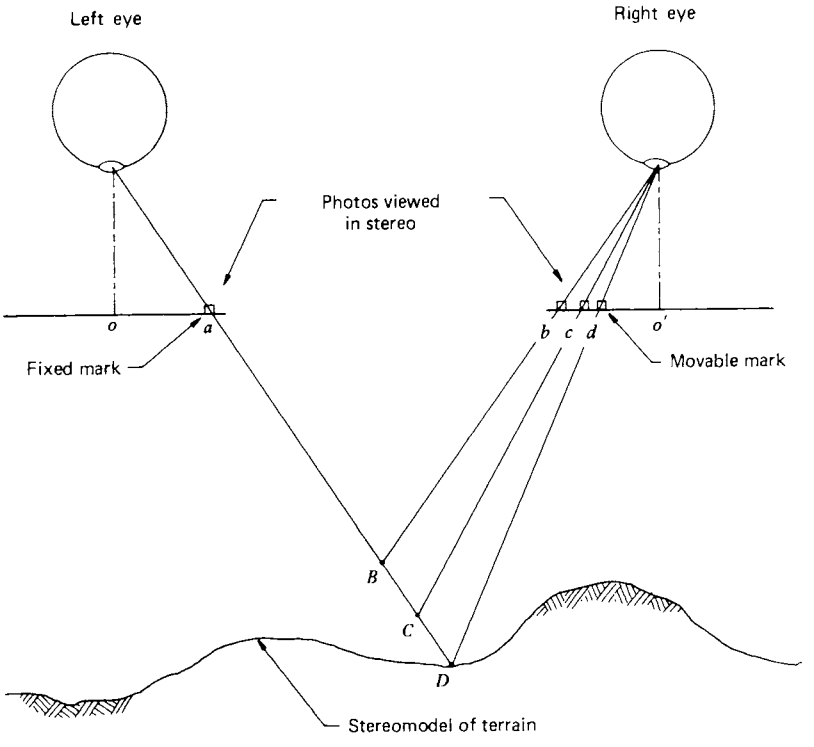

Figure 3.19 Floating-mark principle. (Note that only the right half mark is moved to change the apparent height of the floating mark in the stereomodel.)

point. Consequently, these graduations can be thought of as a series of distance d measurements as shown in Figure 3.18.

Figure 3.20 shows a parallax wedge set up for use. The wedge is positioned so that one of the converging lines lies over the left photo in a stereopair and one over the right photo. When viewed in stereo, the two lines fuse together over a portion of their length, forming a single line that appears to float in the stereomodel. Because the lines on the wedge converge, the floating line appears to slope through the stereoscopic image.

Figure 3.21 illustrates how a parallax wedge might be used to determine the height of a tree. In Figure 3.21*a*, the position of the wedge has been adjusted until the sloping line appears to intersect the top of the tree. A reading is taken from the scale at this point (58.55 mm). The wedge is then positioned such that the line intersects the base of the tree, and a reading is taken (59.75 mm). The difference between the readings (1.20 mm) is used to determine the tree height.

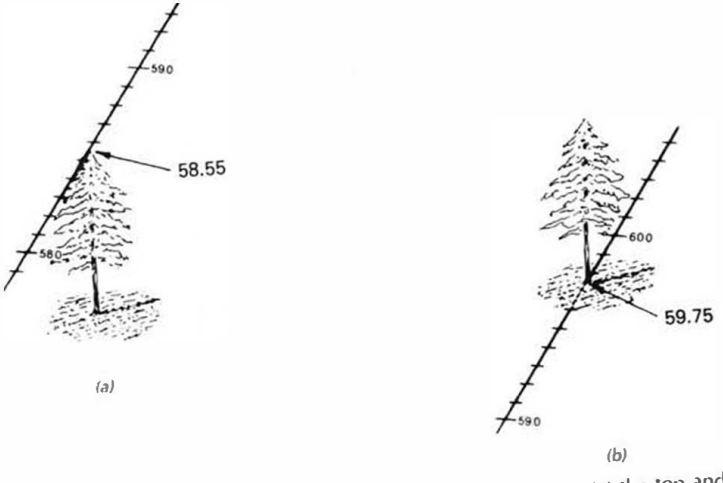

Figure 3.21 Parallax wedge oriented for taking a reading on (*a*) the top and (*b*) the base of a tree.

EXAMPLE 3.10

The flying height for an overlapping pair of photos is 1600 m above the ground and p_a is 75.60 mm. Find the height of the tree illustrated in Figure 3.21.

Solution
From Eq. 3.13

$$\Delta h = \frac{\Delta p\, H'}{p_a}$$

$$= \frac{1.20 \times 1600}{75.60} = 25 \text{ m}$$

Parallax measurement in softcopy photogrammetric systems usually involves some form of numerical *image correlation* to match points on the left photo of a stereopair to their conjugate images on the right photo. Figure 3.22

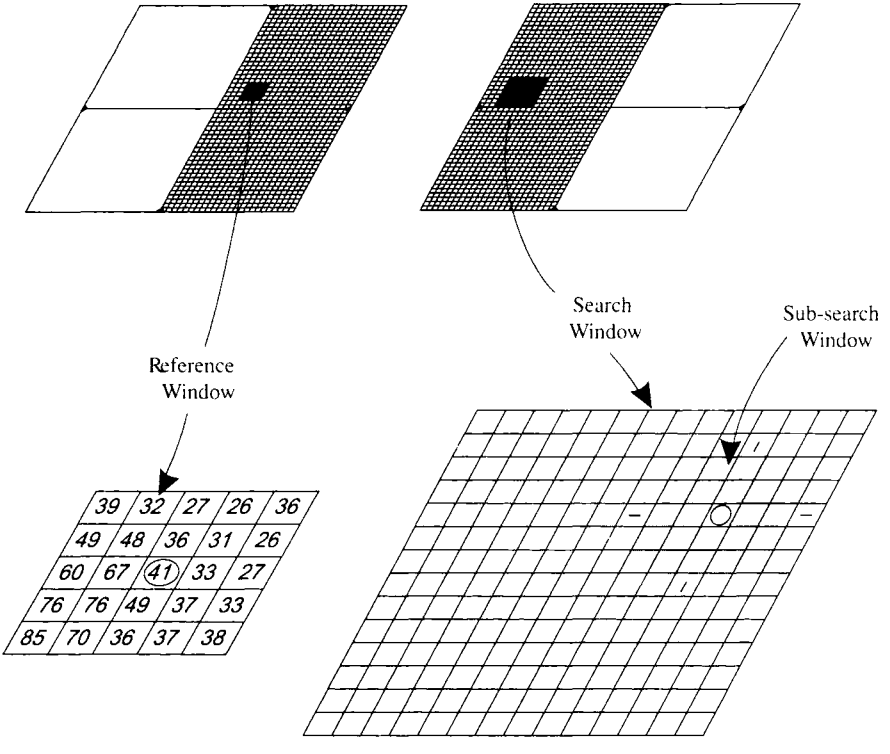

Figure 3.22 Principle of image matching. (After Wolf, 1983.)

illustrates the general concept of digital image matching. Shown is a stereopair of photographs with the pixels contained in the overlap area depicted (greatly exaggerated in size). A *reference window* on the left photograph comprises a local neighborhood of pixels around a fixed location. In this case the reference window is square and 5×5 pixels in size. (Windows vary in size and shape based on the particular matching technique.)

A *search window* is established on the right-hand photo of sufficient size and general location to encompass the conjugate image of the central pixel of the reference window. The initial location of the search window can be determined based on the location of the reference window, the camera focal length, and the size of the area of overlap. A subsearch "moving window" of pixels (Chapter 7) is then systematically moved pixel by pixel about the rows and columns of the search window and the numerical correlation between the digital numbers within the reference and subsearch windows at each location of the moving subsearch window is computed. The conjugate image is assumed to be at the location where the correlation is a maximum.

There are various types of algorithms that can be used to perform image matching. The details of these procedures are not as important as the general concept of locating the conjugate image point for all points on a reference image. The resulting photocoordinates can then be used in the various parallax equations earlier described (Eqs. 3.10 to 3.13). However, the parallax equations assume perfectly vertical photography and equal flying heights for all images. This simplifies the geometry and hence the mathematics of computing ground positions from the photo measurements. However, softcopy systems are not constrained to the above assumptions. Such systems employ mathematical models of the imaging process that readily handle variations in the flying height and attitude of each photograph. As we discuss in Section 3.9, the relationship among image coordinates, ground coordinates, the exposure station position, and angular orientation of each photograph is normally described by a series of *collinearity equations*. They are used in the process of analytical *aerotriangulation*, which involves determining the X, Y, Z, ground coordinates of individual points based on photocoordinate measurements.

3.8 GROUND CONTROL FOR AERIAL PHOTOGRAPHY

As we have indicated throughout, most remote sensing analyses involve some form of ground reference data. Photogrammetric operations are no exception. In fact, for most photogrammetric activities one form of ground reference data is often essential—ground control. *Ground control* refers to physical points on the ground whose ground positions are known with respect to some horizontal coordinate system and/or vertical datum. When mutually identifi-

able on the ground and on a photograph, ground control points can be used to establish the exact spatial position and orientation of a photograph relative to the ground at the instant of exposure.

Ground control points may be *horizontal control points*, *vertical control points*, or both. Horizontal control point positions are known planimetrically in some *XY* coordinate systems (e.g., a state plane coordinate system). Vertical control points have known elevations with respect to a level datum (e.g., mean sea level). A single point with known planimetric position and known elevation can serve as both a horizontal and vertical control point.

Historically, ground control has been established through ground-surveying techniques in the form of triangulation, trilateration, traversing, and leveling. Currently, the establishment of ground control is aided by the use of GPS procedures. The details of these and other more sophisticated surveying techniques used for establishing ground control are not important for the reader of this book to understand. It does warrant reiteration, however, that *accurate ground control is essential to virtually all photogrammetric operations* because photogrammetric measurements can only be as reliable as the ground control on which they are based. Measurements on the photo can be accurately extrapolated to the ground only when we know the location and orientation of the photograph relative to the ground at the instant of exposure. Ground control is required to determine these factors.

As we mentioned, ground control points must be clearly identifiable both on the ground and on the photography being used. Often, control points are selected and surveyed after photography has been taken, thereby ensuring that the points are identifiable on the image. Cultural features, such as road intersections, are often used as control points in such cases. If a ground survey is made prior to a photo mission, control points may be premarked with artificial targets to aid in their identification on the photography. Crosses that contrast with the background land cover make ideal control point markers. Their size is selected in accordance with the scale of the photography to be flown and their material form can be quite variable. In many cases, markers are made by simply painting white crosses on roadways. Alternatively, markers can be painted on contrasting sheets of Masonite, plywood, or heavy cloth.

Research is now extremely active and promising in developing means to minimize the effort needed to establish ground control in photogrammetric operations. One approach uses a pair of interrelated GPS receivers, one stationed at a ground control point, and the other in the aircraft transporting the camera. In this way, the precise location of each photograph, in the ground coordinate system, can be determined. At the same time, an *Inertial Measurement Unit (IMU)* is employed to determine the angular orientation or attitude of each exposure. With the location and attitude of each photograph known, there is no need for ground control (except at the base station).

3.9 MAPPING WITH AERIAL PHOTOGRAPHS

Stereoscopic Plotting Instruments

As we mentioned in the introductory section of this chapter, one of the most widespread uses of photogrammetry is in the preparation of topographic maps. *Stereoplotters* are precision analog instruments designed for this purpose. Two projectors are used that can be adjusted in their position and angular orientation to duplicate the exact relative position and orientation of the aerial camera at the instants the two photos of a stereopair were exposed. That is, camera tilts are precisely re-created in the projection process. Likewise, the base distance between exposures and differences in flying heights are simulated by adjusting the relative positions of the projectors.

Conceptually, the operating principle of a stereoplotter is quite simple. Each photograph in a stereopair is the result of rays projected from the terrain, through a lens, onto an image plane that has a particular position and attitude. In a stereoplotter, the direction of projection is simply reversed. We project rays from the photographs (in the same relative orientation in which they were taken) to form a greatly reduced scale model of the terrain in the overlap area. The model can be viewed and measured in three dimensions and can be projected orthographically to a map sheet. This process eliminates the perspective view distortions present when we attempt to map directly from a single photo. It also eliminates errors introduced by tilts and unequal flying heights when measuring parallax on stereopairs.

There are many different types of stereoplotters, but all of them are made up of three basic components:

1. A projection system (to create the terrain model).
2. A viewing system (to enable the instrument operator to see the model stereoscopically).
3. A measuring and tracing system (for measuring elevations in the model and tracing features onto a map sheet).

Figure 3.23 illustrates a *direct optical projection* plotter. Such systems directly project overlapping images onto a *tracing table* where the terrain model is viewed in stereo. The projectors can be both translated along and rotated about their x, y, and z axes. This permits the instrument operator to perform a *relative orientation* to re-create the position and angular orientation of the two photographs at the time of exposure. This is done by adjusting the projectors until all conjugate image points coincide in the y direction (at this point, only the elevation-caused x parallax remains). The two projectors are then adjusted in tandem to arrive at an *absolute orientation* of the projected model. This is accomplished by scaling and leveling the pair of projectors until the images of ground control points occupy their appropriate preplotted posi-

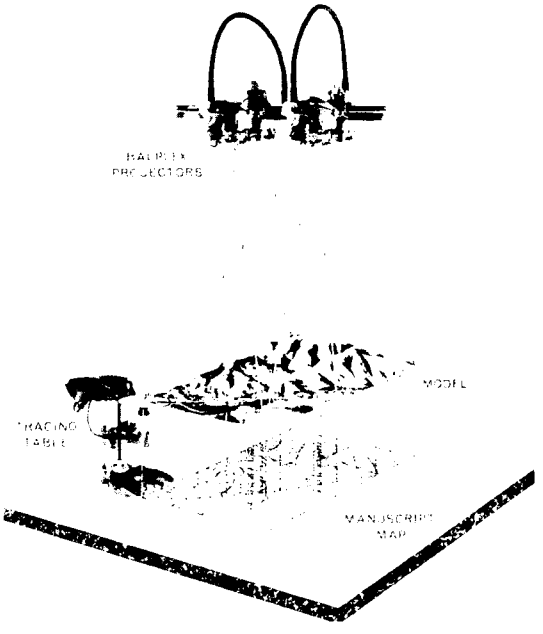

Figure 3.23 Stereomodel projected in a Balplex stereoplotter. (Courtesy TBR Associates, Inc.)

tions on the map manuscript (Figure 3.23). Following these two orientation procedures, a geometrically correct model will be projected and a complete topographic map may be drawn.

In a direct projection plotter, both images in a stereopair are projected onto the same surface. In order to see stereo, the operator's eyes must view each image separately. This can be accomplished by using an *anaglyphic viewing system*, in which one photo is projected through a cyan filter and the other through a red filter. By viewing the model through eyeglasses having corresponding color filters, the operator's left eye will see only the left photo and the right eye will see only the right photo.

Anaglyphic viewing systems cannot be used with color photography. Even in the case of viewing black and white images, these systems reduce the brightness and resolution of the projected images. An alternative projection method employs a *polarized platen viewer (PPV)* system, which uses polarizing filters and eyeglass lenses instead of colored filters. *Stereo image alternator (SIA)* systems use shutters in the projectors to rapidly alternate the projection of the two photos. The operator views the model through a synchronized shutter system, causing the left eye and right eye to see the images from the corresponding projector only.

Portions of the stereomodel are projected onto a *tracing table platen*, which has a small point of light at its center. This point forms a floating mark

whose elevation can be adjusted by raising or lowering the platen. Because the stereomodel has been absolutely oriented to ground control, the platen table height can be equated to terrain elevations. These elevations may be directly read from a height meter on the tracing platen.

Features are mapped planimetrically in the model by tracing them with the floating mark, while continuously raising and lowering the mark to maintain contact with the terrain. Relief displacement of the plotted positions is eliminated by this process. A pencil attached to the platen plots the feature being traced onto the map manuscript, which is located on the plotter table.

Contours are compiled by setting the platen height meter at a desired contour elevation and moving the floating mark along the terrain so that it just maintains contact with the surface of the model. For the novice, these plotting operations seem impossible to perform. It takes considerable training and experience to become proficient at the art of accurate topographic map preparation using a stereoplotter.

To this point, we have discussed direct optical projection plotters only. These were the earliest type of stereoplotter to be developed and were used extensively during the 1950s and 1960s. Another class of stereoplotter instruments receiving substantial use historically is the *mechanical* and *optical-mechanical* projection plotters. These systems simulate the direct projection of rays by mechanical or optical-mechanical means. The operator views the photographs in stereo through a binocular system and the viewing optics are connected to a measuring and tracing system by a precise mechanical linkage. Such a design increases the accuracy of the map production process by minimizing the optical distortions associated with direct project systems.

As digital computers became readily available, *analytical stereoplotters* were developed in order to determine the positions in a stereomodel through mathematical simulation of light ray projection. This was yet another increase in the accuracy and versatility of the stereoplotting process in that such systems have virtually no optical or mechanical limitations. They use hardcopy images and involve linking a comparator-type viewing and measuring system to a computer. The operator simply inputs the camera focal length and data about the calibrated positions of the fiducial marks (and lens distortions) into the computer. Then, under cursor control, the coordinates of the fiducial marks and several ground control points are measured and the computer performs the complete orientation of the stereomodel. Positions in the model can then be mathematically transformed into ground coordinates and elevations. Many systems provide for simultaneous viewing, in color, of the stereomodel and digitized line work (Figure 3.24). Modern softcopy systems employ the same analytical photogrammetric procedures but utilize digital rather than analog images.

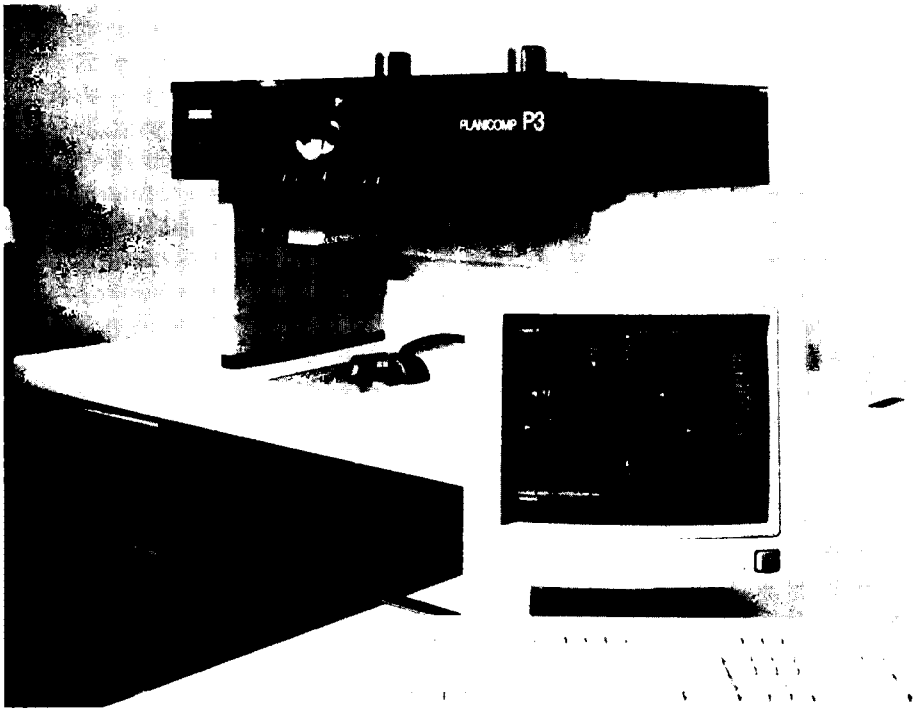

Figure 3.24 Zeiss P3 Planicomp analytical plotter (background) with display terminal (foreground). (Courtesy Z/I Imaging Corporation.)

Orthophotos

As implied by their name, orthophotos are orthographic photographs. They do not contain the scale, tilt, and relief distortions characterizing normal aerial photographs. In essence, orthophotos are "photomaps." Like maps, they have one scale (even in varying terrain), and like photographs, they show the terrain in actual detail (not by lines and symbols). Hence, orthophotos give the resource analyst the "best of both worlds"—a product that can be readily interpreted like a photograph but one on which true distances, angles, and areas may be measured directly. Because of these characteristics, orthophotos make excellent base maps for compiling data to be input to a GIS or overlaying and editing data already incorporated in a GIS. Orthophotos also enhance the communication of spatial data, since data users can often relate better to an orthophoto than a conventional line and symbol map or display.

Analog orthophotos are generated from overlapping conventional photos in a process called *differential rectification*. The result of this process is elimination of photo-scale variation and image displacement resulting from relief

Figure 3.25 Portion of (*a*) a perspective photograph and (*b*) an orthophoto showing a power line clearing traversing hilly terrain. (Note the excessive crookedness of the power line clearing in the perspective photo that is eliminated in the orthophoto.) (Courtesy USGS.)

and tilt. Figure 3.25 illustrates the effect of this process. Figure 3.25*a* is a conventional (perspective) photograph of a power line clearing traversing a hilly forested area. The excessively crooked appearance of the clearing is due to relief displacement. Figure 3.25*b* is a portion of an orthophoto covering the same area. In this image, relief displacement has been removed and the true path of the power line is shown.

Analog orthophotos are prepared in instruments called *orthophotoscopes* in much the same manner as maps are prepared in direct optical projection stereoplotters. However, instead of plotting *selected* features in the stereomodel onto a base map, *all* points of the stereomodel are photographed onto an *orthophoto negative*, which is then used to print the orthophotograph.

The principle of operation of a direct optical projection orthophotoscope is shown in Figure 3.26. In operation, diapositives for a stereopair are relatively and absolutely oriented in the instrument as if normal map compilation were to commence. Unlike that of a normal stereoplotter, however, the floating mark for an orthophotoscope is a very small slit in a film holder containing

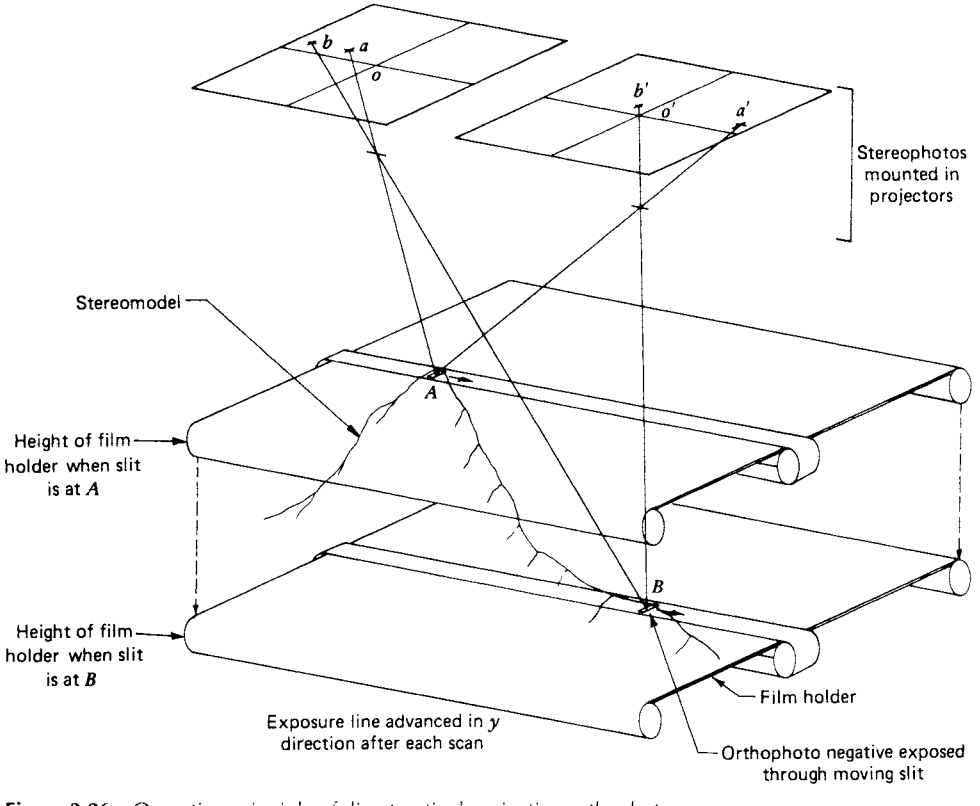

Figure 3.26 Operating principle of direct optical projection orthophotoscope.

the orthophoto negative. A small area of the negative is exposed to light through the slit that is continuously scanned across the film. At the end of each scan, the slit is moved over and scanned in reverse to expose an adjacent strip of film. In this way, the film is eventually exposed to the full stereomodel through the small slit. Along the way, the instrument operator controls the height of the film holder, keeping the slit just in contact with the terrain. Hence, point by point, the scale variation and relief displacement present in the original photography are removed by varying the projection distance. (All tilt distortions are eliminated in the process of orienting the stereomodel.)

Orthophotos alone do not convey topographic information. However, they can be used as base maps for contour line overlays prepared in a separate stereoplotting operation. The result of overprinting contour information on an orthophoto is a *topographic orthophotomap*. Much time is saved in the preparation of such maps because the instrument operator need not map the planimetric data in the map compilation process. Figure 3.27 illustrates a portion of a topographic orthophotomap.

The method of orthophoto preparation illustrated in Figure 3.26 is termed "on line" in that the terrain scanning and film exposure occur simultaneously. In "off-line" systems, the stereomodel is first scanned using a standard floating mark, instead of the film holder slit. During this process, the scan line elevation profiles are stored in digital form. At a later time, the digital profiles are read by instruments that automatically raise and lower the film holder while exposing a negative. An off-line system offers the advantage that the operator can vary the terrain scanning rate, devoting more time to complex topography. Also, the profiles can be rechecked, and mistakes can be corrected.

The digital terrain profiles generated in the orthophoto production process actually comprise a DEM of the terrain covered by the orthophoto. As with any other DEM, the data extracted from these profiles can be used in a broad range of GIS and digital image processing operations (Chapter 7). Also it should be noted that if a DEM already exists for an area, it can be used as the basis for creating an orthophoto. Hence, DEMs created from previous orthophoto production or from digitized maps often form the basis for producing new orthophotos.

Orthophotos may be viewed stereoscopically when they are paired with *stereomates*. These products are photographs made in an orthophoto instrument by *introducing* image parallax as a function of known terrain elevations obtained during the production of their corresponding orthophoto. Figure 3.28 illustrates an orthophoto and a corresponding stereomate that may be viewed stereoscopically. These products were generated as a part of a stereoscopic orthophotomapping program undertaken by the Canadian Forest Management Institute. The advantage of such products is that they combine the attributes of an orthophoto with the benefits of stereo observation. (Note that Figure 3.25 can also be viewed in stereo. This figure consists of an orthophoto and one of the two photos comprising the stereopair from which the orthophoto was produced.)

Photogrammetric Workstations

Photogrammetric workstations (Figure 3.29) involve integrated hardware and software systems for end-to-end spatial data capture, manipulation, analysis, storage, display, and output of softcopy images. Such systems not only incorporate the functionality of analytical stereoplotters but also provide for automated generation of DEMs, computation of digital orthophotos, preparation of perspective views (singly or in a series of fly-throughs), and capture of two-dimensional and three-dimensional data for direct entry into a GIS. Digital orthophotos in particular receive widespread use in modern spatial data systems because they make ideal image bases for image interpretation and feature encoding in a GIS environment. Not only do they greatly facilitate the

Figure 3.28 Stereo orthophotograph showing a portion of Gatineau Park, Canada: (*a*) An orthophoto and (*b*) a stereomate provide for three-dimensional viewing of the terrain. Measurements made from, or plots made on, the orthophoto have map accuracy. Forest-type information is overprinted on this scene along with a Universal Transverse Mercator (UTM) grid. Note that the UTM grid is square on the orthophoto but is distorted by the introduction of parallax on the stereomate. Scale 1 : 38,000. (Courtesy Forest Management Institute, Canadian Forestry Service.)

possible. A major federal source of such data in the United States is the U.S. Geological Survey (USGS) National Digital Orthophoto Program (NDOP), listed in Appendix B.

Figures 3.30 and 3.31 illustrate the visualization capability of sample output products from a photogrammetric workstation. Figure 3.30 shows a perspective view of a rural area located near Madison, Wisconsin. This image was created by draping digital orthophoto data over a DEM of the same area. Figure 3.31 shows a stereopair (*a*) and a perspective view (*b*) of the Clinical Science Center, located on the University of Wisconsin-Madison campus. The images of the various faces of the buildings shown in (*b*) were extracted from the original digitized aerial photograph in which that face was displayed with the greatest relief displacement in accordance with the direction of the perspective view. This process is done automatically from among all of the relevant photographs of the original block of aerial photographs covering the area of interest. Figures 3.30 and 3.31 show only a small sample of the possible output products from a photogrammetric workstation. It should also be noted that most of these systems also provide links to image processing software, making them amenable to the analysis of virtually any source of digital image data (e.g., high resolution satellite data).

Figure 3.30 Perspective view of a rural area generated digitally by draping orthophoto image data over a digital elevation model of the same area. (Courtesy University of Wisconsin-Madison, Environmental Remote Sensing Center, and NASA Affiliated Research Center Program.)

Before leaving the topic of photogrammetric workstations and softcopy photogrammetry in general, it is worth reiterating that the accuracy and flexibility of these systems is rooted in their use of digital data and the mathematical principles of analytical photogrammetry. Among the most important and common principles incorporated in the operation of these systems is the *collinearity condition*. As shown in Figure 3.32, collinearity is the condition in which the exposure station of any photograph, any object point in the ground coordinate system, and its photographic image all lie on a straight line. This condition holds irrespective of the angular tilt of a photograph. The possible angular rotations of the image plane from that of an equivalent vertical photograph are the ω, ϕ, and κ angles shown near the top of Figure 3.32.

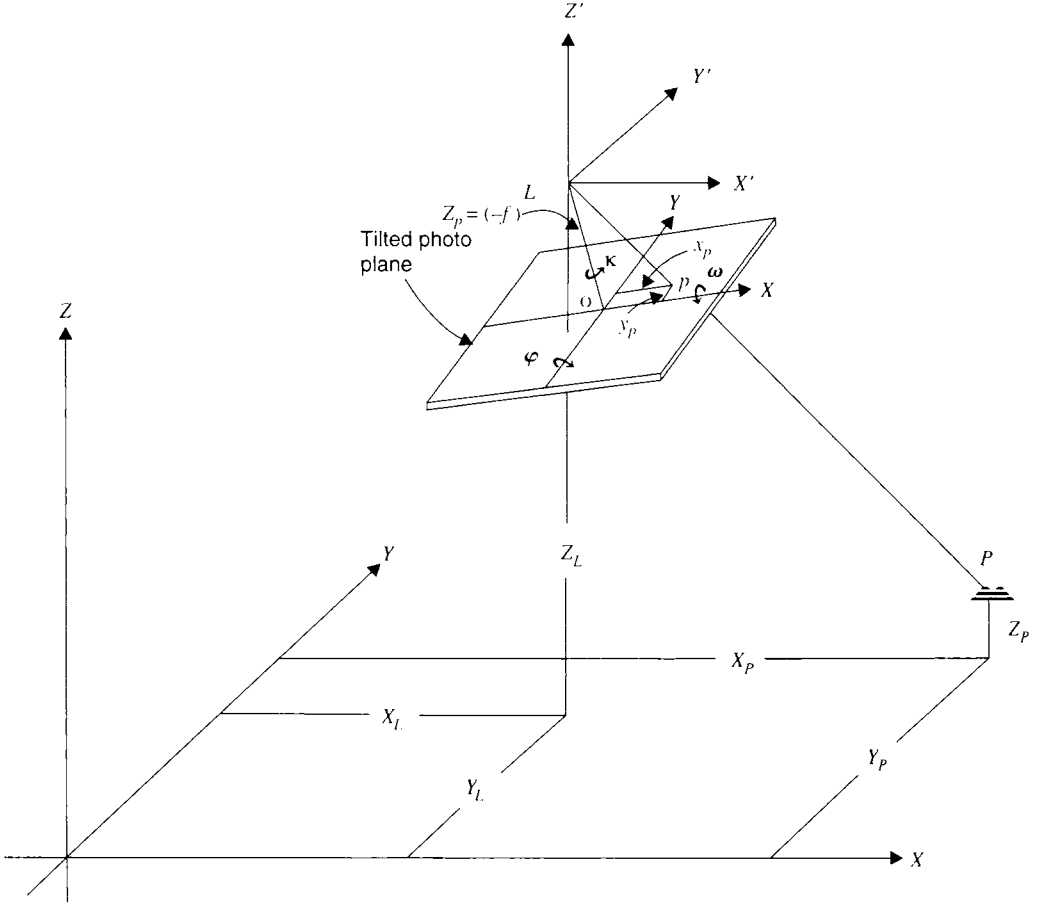

Figure 3.32 The collinearity condition.

The equations that express the collinearity condition are the *collinearity equations*. They describe the relationships among image coordinates, ground coordinates, the exposure station position, and angular orientation of a photograph as follows:

$$x_p = -f\left[\frac{m_{11}(X_P - X_L) + m_{12}(Y_P - Y_L) + m_{13}(Z_P - Z_L)}{m_{31}(X_P - X_L) + m_{32}(Y_P - Y_L) + m_{33}(Z_P - Z_L)}\right] \tag{3.14}$$

$$y_p = -f\left[\frac{m_{21}(X_P - X_L) + m_{22}(Y_P - Y_L) + m_{23}(Z_P - Z_L)}{m_{31}(X_P - X_L) + m_{32}(Y_P - Y_L) + m_{33}(Z_P - Z_L)}\right] \tag{3.15}$$

where

x_p, y_p = image coordinates of any point p
f = focal length
X_P, Y_P, Z_P = ground coordinates of point P
X_L, Y_L, Z_L = ground coordinates of exposure station L
$m_{11}, \ldots, m_{33}$ = coefficients of a 3×3 rotation matrix defined by the angles ω, ϕ, and κ that transforms the ground coordinate system to the image coordinate system

The above equations are nonlinear and contain nine unknowns: the exposure station position (X_L, Y_L, Z_L), the three rotation angles (ω, ϕ, and κ, which are imbedded in the m coefficients), and the three object point coordinates (X_P, Y_P, Z_P). (The equations are linearized using Taylor's theorem.)

The collinearity equations are at the heart of many softcopy photogrammetric operations. For example, if the location of the exposure station is known (X_L, Y_L, Z_L) as well as the rotation angles ω, ϕ, and κ, from which m_{11}, $\ldots$, m_{33} are known, then any position on the ground (X_P, Y_P, Z_P) can be located on the photo (at x_p, y_p). This is how DEMs are used to generate digital orthophotos. That is, at each ground position in the DEM (X_P, Y_P, Z_P) the associated image point can be computed through the collinearity equations as x_p, y_p. The brightness value of the image at that point is then inserted into an output array and the process is repeated for every line and column position in the DEM to form the entire digital orthophoto. A minor complication in this whole process is the fact that rarely will the photocoordinate value (x_p, y_p) computed for a given DEM cell be exactly centered over a pixel in the original digital input image. Accordingly, the process of *resampling* (Chapter 7 and Appendix C) is employed to determine the best brightness value to assign to each pixel in the orthophoto based on a consideration of the brightness values of a neighborhood of pixels surrounding each computed photocoordinate position (x_p, y_p).

The six parameters X_L, Y_L, Z_L and ω, ϕ, and κ comprise the *exterior orientation* of a photograph. A combination of GPS and IMU system observations can be used to determine the exterior orientation of an image if such equipment is

available. If not, the six elements of exterior orientation can be determined through the process of *space resection*. In this process, photocoordinates for at least three ground control points are measured. In that Eqs. 3.14 and 3.15 yield two equations for each control point, three such points yield six equations that can be solved simultaneously for the six unknowns. If more than three control points are available, then more than six equations can be formed and a least squares solution for the unknowns is performed.

Other applications of collinearity include *relative orientation* of a pair of overlapping photographs. This is similar to the relative orientation of projectors in a stereoplotter. *Absolute orientation* is accomplished by performing a coordinate transformation between the relatively oriented model and ground control (again, similar to fitting preplotted ground control in analog stereoplotter map compilation).

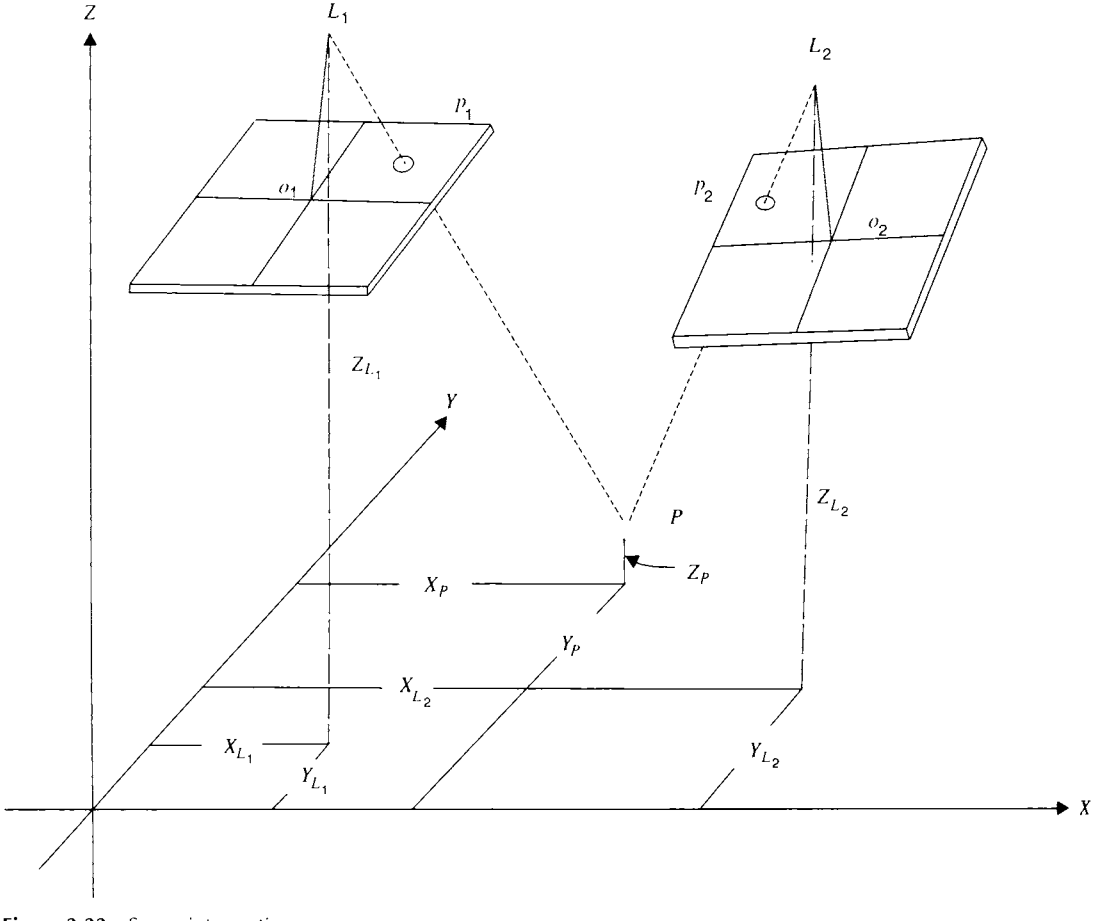

Figure 3.33 Space intersection.

Another important application of the collinearity equations is the process of *space intersection*. This is a procedure by which the X, Y, and Z coordinates of any point in the overlap of a stereopair of tilted photographs can be determined. As shown in Figure 3.33, space intersection makes use of the fact that corresponding rays from overlapping photos intersect at a unique point. Image correlation (Section 3.7) is generally used to match any given point with its conjugate image to determine the point of intersection.

Space intersection makes use of the fact that a total of four collinearity equations can be written for each point in the overlap area. Two of these equations relate to the point's x and y coordinates on the left-hand photo; two result from the x' and y' coordinates measured on the right-hand photo. If the exterior orientation of both photos is known, then the only unknowns in each equation are X, Y, and Z for the point under analysis. Given four equations for three unknowns, a least squares solution for the ground coordinates of each point can be performed. Systematic sampling throughout the overlap area in this manner forms the basis for DEM production with softcopy systems. While this process is highly automated, the image correlation involved is often far from perfect. This normally leads to the need to edit the resulting DEM, but the automated DEM compilation process is still a very useful one.

A final important function performed by photogrammetric workstations is *bundle adjustment*. This process is the extension of the principles described above to an entire block of photos simultaneously. In its most robust form, bundle adjustment provides for simultaneous mathematical treatment of photocoordinate measurements and ground control measurements, as well as treating the exterior orientation parameters of each photo in the block as unknowns. It can be thought of as simultaneous space resection and space intersection of all photos in a block at once. This process both minimizes the need for ground control and increases the precision of the resulting location of points in the ground coordinate system.

3.10 FLIGHT PLANNING

Frequently, the objectives of a photographic remote sensing project can only be met through procurement of new photography of a study area. These occasions can arise for many reasons. For example, photography available for a particular area could be outdated for applications such as land use mapping. In addition, available photography may have been taken in the wrong season. For example, photography acquired for topographic mapping is usually flown in the fall or spring to minimize vegetative cover. This photography will likely be inappropriate for applications involving vegetation analysis. Furthermore, existing photos could be at an inappropriate scale for the application at hand or they could have been taken with an unsuitable

film type. Frequently, analysts who require color infrared coverage of an area will find that only black and white panchromatic photography is available. Highly specialized applications may require unusual film–filter combinations or exposure settings, making it highly unlikely that existing photography will be suitable.

When new photography is required, the interpreter is frequently involved in planning the flight. The interpreter soon learns firsthand that one of the most important parameters in an aerial mission is beyond the control of even the best planner—the weather. In most areas, only a few days of the year are ideal for aerial photography. In order to take advantage of clear weather, commercial aerial photography firms will fly many jobs in a single day, often at widely separated locations. Flights are usually scheduled between 10 a.m. and 2 p.m. for maximum illumination and minimum shadow. Overall, a great deal of time, effort, and expense go into the planning and execution of a photographic mission. In many respects, it is an art as well as a science.

Below, we discuss the geometric aspects of the task of flight planning. The parameters needed for this task are (1) the focal length of the camera to be used; (2) the film format size; (3) the photo scale desired; (4) the size of the area to be photographed; (5) the average elevation of the area to be photographed; (6) the overlap desired; (7) the sidelap desired; and (8) the ground speed of the aircraft to be used.

Based on the above parameters, the mission planner prepares computations and a flight map that indicate to the flight crew (1) the flying height above datum from which the photos are to be taken; (2) the location, direction, and number of flight lines to be made over the area to be photographed; (3) the time interval between exposures; (4) the number of exposures on each flight line; and (5) the total number of exposures necessary for the mission.

Flight plans are normally portrayed on a map for the flight crew. However, old photography, an index mosaic, or even a satellite image may be used for this purpose. The computations prerequisite to preparing a flight plan are given in the following example.

EXAMPLE 3.11

A study area is 10 km wide in the east–west direction and 16 km long in the north–south direction (see Figure 3.34). A camera having a 152.4-mm-focal-length lens and a 230-mm format is to be used. The desired photo scale is 1 : 25,000 and the nominal endlap and sidelap are to be 60 and 30 percent. Beginning and ending flight lines are to be positioned along the boundaries of the study area. The only map available for the area is at a scale of 1 : 62,500. This map indicates that the average terrain

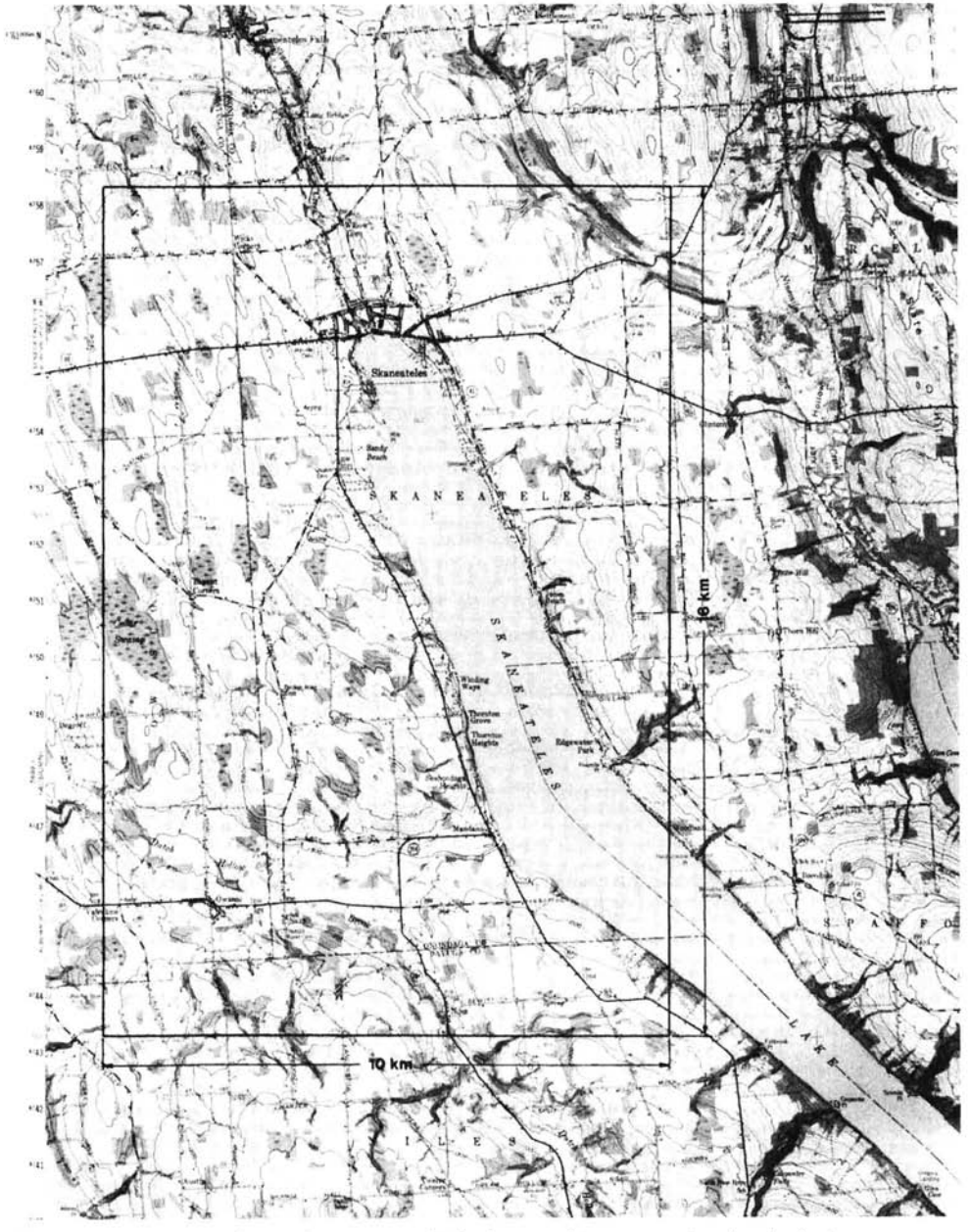

Figure 3.34 A 10 × 16-km study area over which photographic coverage is to be obtained.

elevation is 300 m above datum. Perform the computations necessary to develop a flight plan and draw a flight map.

Solution

(a) Use north–south flight lines. Note that using north–south flight lines minimizes the number of lines required and consequently the number of aircraft turns and realignments necessary. (Also, flying in a cardinal direction often facilitates the identification of roads, section lines, and other features that can be used for aligning the flight lines.)

(b) Find the flying height above terrain ($H' = f/S$) and add the mean site elevation to find flying height above mean sea level:

$$H = \frac{f}{S} + h_{avg} = \frac{0.1524 \text{ m}}{1/25{,}000} + 300 \text{ m} = 4110 \text{ m}$$

(c) Determine ground coverage per image from film format size and photo scale:

$$\text{Coverage per photo} = \frac{0.23 \text{ m}}{1/25{,}000} = 5750 \text{ m on a side}$$

(d) Determine ground separation between photos on a line for 40 percent advance per photo (i.e., 60 percent endlap):

$$0.40 \times 5750 \text{ m} = 2300 \text{ m between photo centers}$$

(e) Assuming an aircraft speed of 160 km/hr, the time between exposures is

$$\frac{2300 \text{ m/photo}}{160 \text{ km/hr}} \times \frac{3600 \text{ sec/hr}}{1000 \text{ m/km}} = 51.75 \text{ sec} \qquad \text{(use 51 sec)}$$

(f) Because the intervalometer can only be set in even seconds (this varies between models), the number is rounded off. By rounding down, at least 60 percent coverage is ensured. Recalculate the distance between photo centers using the reverse of the above equation:

$$51 \text{ sec/photo} \times 160 \text{ km/hr} \times \frac{1000 \text{ m/km}}{3600 \text{ sec/hr}} = 2267 \text{ m}$$

(g) Compute the number of photos per 16-km line by dividing this length by the photo advance. Add one photo to each end and round the number up to ensure coverage:

$$\frac{16{,}000 \text{ m/line}}{2267 \text{ m/photo}} + 1 + 1 = 9.1 \text{ photos/line} \qquad \text{(use 10)}$$

(h) If the flight lines are to have a sidelap of 30 percent of the coverage, they must be separated by 70 percent of the coverage:

$$0.70 \times 5750 \text{ m coverage} = 4025 \text{ m between flight lines}$$

(i) Find the number of flight lines required to cover the 10-km study area width by dividing this width by distance between flight lines (note: this division gives number of spaces between flight lines; add 1 to arrive at the number of lines):

$$\frac{10{,}000 \text{ m width}}{4025 \text{ m/flight line}} + 1 = 3.48 \qquad \text{(use 4)}$$

The adjusted spacing between lines for using four lines is

$$\frac{10{,}000 \text{ m}}{4 - 1 \text{ spaces}} = 3333 \text{ m/space}$$

(j) Find the spacing of flight lines on the map (1 : 62,500 scale):

$$3333 \text{ m} \times \frac{1}{62{,}500} = 53.3 \text{ mm}$$

(k) Find the total number of photos needed:

$$10 \text{ photos/line} \times 4 \text{ lines} = 40 \text{ photos}$$

(Note: The first and last flight lines in this example were positioned coincident with the boundaries of the study area. This provision ensures complete coverage of the area under the "better safe than sorry" philosophy. Often, a savings in film, flight time, and money is realized by experienced flight crews by moving the first and last lines in toward the middle of the study area.)

In computer-supported mission planning, the position of the exposure station for each photo would also be computed for use in the aircraft navigation system.

The above computations would be summarized on a flight map as shown in Figure 3.35. In addition, a set of detailed specifications outlining the material, equipment, and procedures to be used for the mission would be agreed upon prior to the mission. These specifications typically spell out the requirements and tolerances for flying the mission, the form and quality of the products to be delivered, and the ownership rights to the original images. Among other things, mission specifications normally include such details as mission timing, ground control requirements, camera calibration characteristics, film and filter type, exposure conditions, scale tolerance, endlap, sidelap, tilt and crab, photographic quality, GPS encoding, product indexing, and product delivery schedules.

Table 3.1 summarizes the flight planning parameters for various commonly used photo scales. For each scale, the table indicates the required flying height (above ground), the ground spacing between photos and between flight lines, and the lineal and areal coverage of a single photo. The table is based on a 230-mm (9-in.) format camera having a 152.4-mm- (6-in.-) focal-length lens.

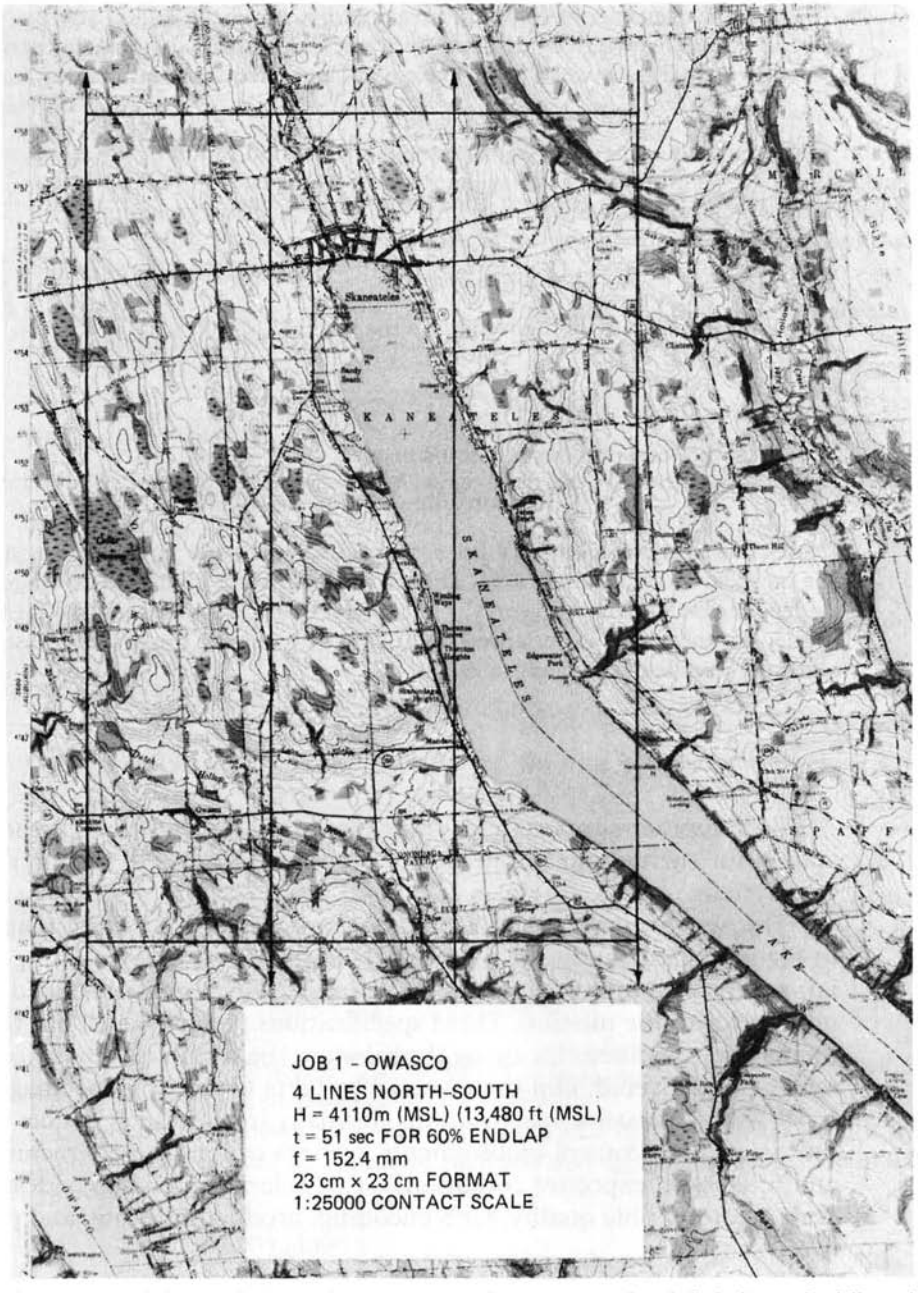

Figure 3.35 Flight map for Example 3.11. (Lines indicate centers of each flight line to be followed.)

TABLE 3.1 Flight Planning Parameters for a 230-mm[a] (9-in.) Format Mapping Camera Equipped with a 152.4-mm- (6-in.-) Focal-Length Lens

	English Units					
Photo Scale (Ratio)	Photo Scale (in./ft)	Flying Height (ft)	Exposure Spacing (ft, 60% endlap)	Flight Line Spacing (ft, 30% sidelap)	Length (ft, one side)	Area (mi^2)
1 : 1800	1″/150′	900	540	945	1,350	0.07
1 : 2400	1″/200′	1,200	720	1,260	1,800	0.12
1 : 3000	1″/250′	1,500	900	1,575	2,250	0.18
1 : 3600	1″/300′	1,800	1,080	1,890	2,700	0.26
1 : 4800	1″/400′	2,400	1,440	2,520	3,600	0.46
1 : 6000	1″/500′	3,000	1,800	3,150	4,500	0.73
1 : 7200	1″/600′	3,600	2,160	3,780	5,400	1.05
1 : 9600	1″/800′	4,800	2,880	5,040	7,200	1.86
1 : 12,000	1″/1000′	6,000	3,600	6,300	9,000	2.91
1 : 15,840	1″/1320′	7,920	4,752	8,316	11,880	5.06
1 : 20,000	1″/1667′	10,000	6,000	10,500	15,000	8.07
1 : 24,000	1″/2000′	12,000	7,200	12,600	18,000	11.6
1 : 40,000	1″/3333′	20,000	12,000	21,000	30,000	32.3
1 : 60,000	1″/5000′	30,000	18,000	31,500	45,000	72.6
1 : 80,000	1″/6667′	40,000	24,000	42,000	60,000	129.1
1 : 100,000	1″/8333′	50,000	30,000	52,500	75,000	201.8
	SI Units					
Photo Scale (Ratio)	Photo Scale (mm/m)	Flying Height (m)	Exposure Spacing (m, 60% endlap)	Flight Line Spacing (m, 30% sidelap)	Length (m, one side)	Area (km^2)
1 : 1800	1 mm/1.8 m	274	165	288	411	0.17
1 : 2400	1 mm/2.4 m	366	219	384	549	0.30
1 : 3000	1 mm/3.0 m	457	274	480	686	0.47
1 : 3600	1 mm/3.6 m	549	329	576	823	0.68
1 : 4800	1 mm/4.8 m	732	439	768	1,097	1.20
1 : 6000	1 mm/6.0 m	914	549	960	1,372	1.88
1 : 7200	1 mm/7.2 m	1,097	658	1,152	1,646	2.71
1 : 9600	1 mm/9.6 m	1,463	878	1,536	2,195	4.82
1 : 12,000	1 mm/12.0 m	1,829	1,097	1,920	2,743	7.52
1 : 15,840	1 mm/15.8 m	2,414	1,448	2,535	3,621	13.1
1 : 20,000	1 mm/20.0 m	3,048	1,829	3,200	4,572	20.9
1 : 24,000	1 mm/24.0 m	3,658	2,195	3,840	5,486	30.1
1 : 40,000	1 mm/40.0 m	6,096	3,658	6,401	9,144	83.6
1 : 60,000	1 mm/60.0 m	9,144	5,486	9,601	13,716	188.1
1 : 80,000	1 mm/80.0 m	12,192	7,315	12,802	18,288	334.5
1 : 100,000	1 mm/100.0 m	15,240	9,144	16,002	22,860	522.6

[a]Calculations based on an actual film format of 228.6 × 228.6 mm.

3.11 CONCLUSION

As we have seen in this chapter, photogrammetry is a very large and rapidly changing subject. Historically, most photogrammetric operations were analog in nature, involving the physical projection and measurement of hardcopy images with the aid of precise optical or mechanical equipment. Today, mathematical models using softcopy data are common. Most softcopy systems are also amenable to the analysis of many different types of digital image data (e.g., airborne digital camera data, satellite data).

With links to various GIS and image processing software, softcopy workstations often represent highly integrated systems for spatial data capture, manipulation, analysis, storage, display, and output.

185–188.

4 INTRODUCTION TO VISUAL IMAGE INTERPRETATION

4.1 INTRODUCTION

When we look at aerial and space images, we see various objects of different sizes and shapes. Some of these objects may be readily identifiable while others may not, depending on our own individual perceptions and experience. When we can identify what we see on the images and communicate this information to others, we are practicing *image interpretation*. The images contain raw image *data*. These data, when processed by a human interpreter's brain, become usable *information*.

As previously mentioned, aerial photography dates to the year 1858 and the balloon photographs of Nadar. Aerial photography did not receive much emphasis during the ensuing decades because the process was cumbersome and risky and the results uncertain. However, some scientists and inventors did recognize the potential value of aerial photographs in presenting a new view of the earth's surface. Military strategists also understood the potential of this medium for the remote acquisition of military information. During World War I, aerial photography was established as an operational military reconnaissance tool.

After World War I, many nonmilitary applications appeared. The experience gained by World War I pilots in taking pictures from the air convinced quite a number of them that they could put their newly acquired skills to

work on such civilian applications as agricultural surveys, timber surveys, and mineral exploration. The U.S. Department of Agriculture's Agricultural Stabilization and Conservation Service (USDA-ASCS) began photographing selected counties of the United States on a repetitive basis in 1937.

Images from space with various levels of detail have been available since the 1960s. Earlier images were of low resolution and were often at oblique angles. Since the advent of the Landsat satellite program in the 1970s and the SPOT satellite program in the 1980s (see Chapter 6), near-vertical images with resolutions useful for earth resources mapping have been available.

In this chapter, we explore the applications of image interpretation to the solution of a variety of problems in different fields. *Aerial photographic image interpretation* is emphasized in this chapter, but it should be noted that most of the principles described here also apply to the interpretation of space images. Space images are often smaller in scale than aerial images and are typically not analyzed stereoscopically.

Because image interpretation is best learned through the experience of viewing hundreds of remotely sensed images according to the requirements of specific fields of application, we cannot hope to train our readers in image interpretation. Here, we will simply present many potential applications of image interpretation and illustrate a few with sample images.

In the next two sections, we present the fundamentals of image interpretation and describe basic image interpretation equipment. In Sections 4.4 through 4.16 we treat the application of image interpretation to a variety of application areas—land use/land cover mapping, geologic and soil mapping, agriculture, forestry, rangeland, water resources, urban and regional planning, wetland mapping, wildlife ecology, archaeology, environmental assessment, disaster assessment, and landform identification and evaluation.

4.2 FUNDAMENTALS OF VISUAL IMAGE INTERPRETATION

Aerial and space images contain a detailed record of features on the ground at the time of data acquisition. An image interpreter systematically examines the images and, frequently, other supporting materials such as maps and reports of field observations. Based on this study, an interpretation is made as to the physical nature of objects and phenomena appearing in the images. Interpretations may take place at a number of levels of complexity, from the simple recognition of objects on the earth's surface to the derivation of detailed information regarding the complex interactions among earth surface and subsurface features. Success in image interpretation varies with the training and experience of the interpreter, the nature of the objects or phenomena being interpreted, and the quality of the images being utilized. Generally, the most capable image interpreters have keen powers of observation coupled with imagination and a great deal of patience. In addition, it is im-

portant that the interpreter have a thorough understanding of the phenomenon being studied as well as knowledge of the geographic region under study.

Elements of Image Interpretation

Although most individuals have had substantial experience in interpreting "conventional" photographs in their daily lives (e.g., newspaper photographs), the interpretation of aerial and space images often departs from everyday image interpretation in three important respects: (1) the portrayal of features from an overhead, often unfamiliar, perspective; (2) the frequent use of wavelengths outside of the visible portion of the spectrum; and (3) the depiction of the earth's surface at unfamiliar scales and resolutions (Campbell, 2002). While these factors may be insignificant to the experienced image interpreter, they can represent a substantial challenge to the novice image analyst! A systematic study of aerial and space images usually involves several basic characteristics of features shown on an image. The exact characteristics useful for any specific task and the manner in which they are considered depend on the field of application. However, most applications consider the following basic characteristics, or variations of them: shape, size, pattern, tone (or hue), texture, shadows, site, association, and resolution (Olson, 1960).

Shape refers to the general form, configuration, or outline of individual objects. In the case of stereoscopic images, the object's *height* also defines its shape. The shape of some objects is so distinctive that their images may be identified solely from this criterion. The Pentagon building near Washington, D.C., is a classic example. All shapes are obviously not this diagnostic, but every shape is of some significance to the image interpreter.

Size of objects on images must be considered in the context of the image scale. A small storage shed, for example, might be misinterpreted as a barn if size were not considered. Relative sizes among objects on images of the same scale must also be considered.

Pattern relates to the spatial arrangement of objects. The repetition of certain general forms or relationships is characteristic of many objects, both natural and constructed, and gives objects a pattern that aids the image interpreter in recognizing them. For example, the ordered spatial arrangement of trees in an orchard is in distinct contrast to that of forest tree stands.

Tone (or *hue*) refers to the relative brightness or color of objects on an image. Figure 1.9 showed how relative photo tones could be used to distinguish between deciduous and coniferous trees on black and white infrared photographs. Figure 4.50c (in Section 4.16) shows a striking pattern of light-toned and dark-toned soils where the tonal patterns vary according to the drainage conditions of the soil (the lighter toned areas are topographically higher and drier; the darker toned areas are lower and wetter). Without tonal differences, the shapes, patterns, and textures of objects could not be discerned.

Texture is the frequency of tonal change on an image. Texture is produced by an aggregation of unit features that may be too small to be discerned individually on the image, such as tree leaves and leaf shadows. It is a product of their individual shape, size, pattern, shadow, and tone. It determines the overall visual "smoothness" or "coarseness" of image features. As the scale of the image is reduced, the texture of any given object or area becomes progressively finer and ultimately disappears. An interpreter can often distinguish between features with similar reflectances based on their texture differences. An example would be the smooth texture of green grass as contrasted with the rough texture of green tree crowns on medium-scale airphotos. Another example can be seen in Figure 4.19, which shows the contrasting textures of two tree species.

Shadows are important to interpreters in two opposing respects: (1) the shape or outline of a shadow affords an impression of the profile view of objects (which aids interpretation) and (2) objects within shadows reflect little light and are difficult to discern on an image (which hinders interpretation). For example, the shadows cast by various tree species or cultural features (bridges, silos, towers, etc.) can definitely aid in their identification on airphotos. Also, the shadows resulting from subtle variations in terrain elevations, especially in the case of low sun angle images, can aid in assessing natural topographic variations that may be diagnostic of various geologic landforms. As a general rule, images are more easily interpreted when shadows fall toward the observer. This is especially true when images are examined monoscopically, where relief cannot be seen directly, as in stereoscopic images. In Figure 4.1*a*, a large ridge with numerous side valleys can be seen in the center of the image. When this image is inverted (i.e., turned such that the shadows fall away from the observer), as in (*b*), the result is a confusing image that almost seems to have a valley of sorts running through the center of the image (from bottom to top). This arises because one "expects" light sources to generally be above objects (ASPRS, 1997b, p. 73).

Site refers to topographic or geographic location and is a particularly important aid in the identification of vegetation types. For example, certain tree species would be expected to occur on well-drained upland sites, whereas other tree species would be expected to occur on poorly drained lowland sites. Also, various tree species occur only in certain geographic areas (e.g., redwoods occur in California, but not in Indiana).

Association refers to the occurrence of certain features in relation to others. For example, a Ferris wheel might be difficult to identify if standing in a field near a barn but would be easy to identify if in an area recognized as an amusement park.

Resolution depends on many factors, but it always places a practical limit on interpretation because some objects are too small or have too little contrast with their surroundings to be clearly seen on the image.

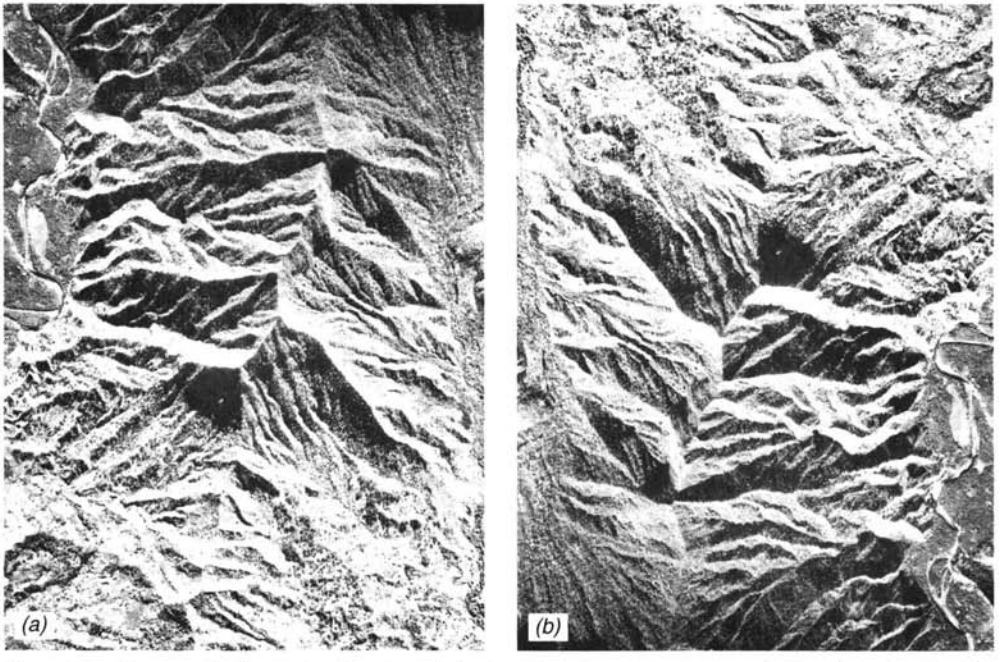

Figure 4.1 Photograph illustrating the effect of shadow direction on the interpretability of terrain. Island of Kauai, Hawaii, mid-January. Scale 1 : 48,000. (*a*) Shadows falling toward observer, (*b*) same image turned such that shadows are falling away from observer. (USDA–ASCS panchromatic photograph.)

Other factors, such as image scale, image color balance, and condition of images (e.g., torn or faded photographic prints) also affect the success of image interpretation activities.

Many of the above elements of airphoto interpretation are illustrated in Figure 4.2. Figure 4.2*a* is a nearly full-scale copy of a 240-mm airphoto that was at an original scale of 1:28,000. Parts (*b*) through (*e*) of Figure 4.2 show four scenes extracted and enlarged from this airphoto. Among the land cover types in Figure 4.2*b* are water, trees, suburban houses, grass, a divided highway, and a drive-in theater. Most of the land cover types are easily identified in this figure. The drive-in theater could be difficult for inexperienced interpreters to identify, but a careful study of the elements of image interpretation leads to its identification. It has a unique *shape* and *pattern*. Its *size* is consistent with a drive-in theater (note the relative size of the cars on the highway and the parking spaces of the theater). In addition to the curved rows of the parking area, the *pattern* also shows the projection building and the screen. The identification of the screen is aided by its *shadow*. It is located in *association* with a divided highway, which is accessed by a short roadway.

Many different land cover types can be seen in Figure 4.2*c*. Immediately noticeable in this photograph, at upper left, is a feature with a superficially

Figure 4.2 *(Continued)*

similar appearance to the drive-in theater. Careful examination of this feature, and the surrounding grassy area, leads to the conclusion that this is a baseball diamond. The trees that can be seen in numerous places in the photograph are casting shadows of their trunks and branches because the mid-October date of this photograph is a time when deciduous trees are in a leaf-off condition. Seen in the right one-third of the photograph is a residential area. Running top to bottom through the center of the image is a commercial area with buildings that have a larger size than the houses in the residential area and large parking areas surrounding these larger buildings.

Figure 4.2 *(Continued)*

Figure 4.2*d* shows two major linear features. Near the top of the photograph is a divided highway. Running diagonally from upper left to lower right is an airport runway 1390 m long (the scale of this figure is 1:15,000, and the length of this linear feature is 9.28 cm at this scale). The terminal area for this airport is near the top center of Figure 4.2*d*.

Figure 4.2*e* illustrates natural versus constructed features. The water body at *a* is a natural feature, with an irregular shoreline and some surrounding wetland areas (especially visible at the narrow end of the lake). The water body at *b* is part of a sewage treatment plant; the shoreline of this feature has unnaturally straight sections in comparison with the water body shown at *a*.

Image Interpretation Strategies

As previously mentioned, the image interpretation process can involve various levels of complexity, from a simple direct recognition of objects in the scene

to the inference of site conditions. An example of direct recognition would be the identification of a highway interchange. Assuming the interpreter has some experience with the vertical perspective of aerial and space images, recognition of a highway interchange should be a straightforward process. On the other hand, it may often be necessary to infer, rather than directly observe, the characteristics of features based on their appearance on images. In the case of a buried gas pipeline, for example, the actual pipeline cannot be seen, but there are often changes at the ground surface caused by the buried pipeline that are visible on aerial and space images. Soils are typically better drained over the pipeline because of the sand and gravel used for backfill, and the presence of a buried pipeline can often be inferred by the appearance of a light-toned linear streak across the image. Also, the interpreter can take into account the probability of certain ground cover types occurring on certain dates at certain places. Knowledge of the crop development stages (*crop calendar*) for an area would determine if a particular crop is likely to be visible on a particular date. For example, corn, peas, and winter wheat would each have a significant vegetative ground cover on different dates. Likewise, in a particular growing region, one crop type may be present over a geographic area many times larger than that of another crop type; therefore, the probability of occurrence of one crop type would be much greater than another.

In a sense, the image interpretation process is like the work of a detective trying to put all the pieces of evidence together to solve a mystery. For the interpreter, the mystery might be presented in terms of trying to understand why certain areas in an agricultural field look different from the rest of that field. At the most general level, the interpreter must recognize the area under study as an agricultural field. Beyond this, consideration might be made as to whether the crop present in the field is a row crop (e.g., corn) or a continuous cover crop (e.g., alfalfa). Based on the crop calendar and regional growing conditions, a decision might be made that the crop is indeed corn, rather than another row crop, such as soybeans. Furthermore, it might be noted that the anomalously appearing areas in the field are associated with areas of slightly higher topographic relief relative to the rest of the field. With knowledge of the recent local weather conditions, the interpreter might infer that the anomalously appearing areas are associated with drier soil conditions and the corn in these areas is likely drought stressed. Hence, the interpreter uses the process of *convergence of evidence* to successively increase the accuracy and detail of the interpretation.

Image Interpretation Keys

The image interpretation process can often be facilitated through the use of *image interpretation keys*. Keys can be valuable training aids for novice interpreters and provide useful reference or refresher materials for more experienced

interpreters. An image interpretation key helps the interpreter evaluate the information presented on aerial and space images in an organized and consistent manner. It provides guidance about the correct identification of features or conditions on the images. Ideally, a key consists of two basic parts: (1) a collection of annotated or captioned images (preferably stereopairs) illustrative of the features or conditions to be identified and (2) a graphic or word description that sets forth in some systematic fashion the image recognition characteristics of those features or conditions. Two general types of image interpretation keys exist, differentiated by the method of presentation of diagnostic features. A *selective key* contains numerous example images with supporting text. The interpreter selects the example that most nearly resembles the feature or condition found on the image under study.

An *elimination key* is arranged so that the interpretation proceeds step by step from the general to the specific and leads to the elimination of all features or conditions except the one being identified. Elimination keys often take the form of *dichotomous keys* where the interpreter makes a series of choices between two alternatives and progressively eliminates all but one possible answer. Figure 4.3 shows a dichotomous key prepared for the identification of fruit and nut crops in the Sacramento Valley, California. The use of elimination keys can lead to more positive answers than selective keys but may result in erroneous answers if the interpreter is forced to make an uncertain choice between two unfamiliar image characteristics.

As a generalization, keys are more easily constructed and more reliably utilized for cultural feature identification (houses, bridges, roads, water towers) than for vegetation or landform identification. However, a number of keys have been successfully employed for agricultural crop identification and tree species identification. *Such keys are normally developed and used on a region-by-region and season-by-season basis in that the appearance of vegetation can vary widely with location and season.*

Wavelengths of Sensing

The band(s) of the electromagnetic energy spectrum selected for aerial and space imaging affects the amount of information that can be interpreted from the images. Numerous examples of this are scattered throughout this book.

Temporal Aspects of Image Interpretation

The temporal aspects of natural phenomena are important for image interpretation because such factors as vegetative growth and soil moisture vary during the year. For crop identification, more positive results can be achieved

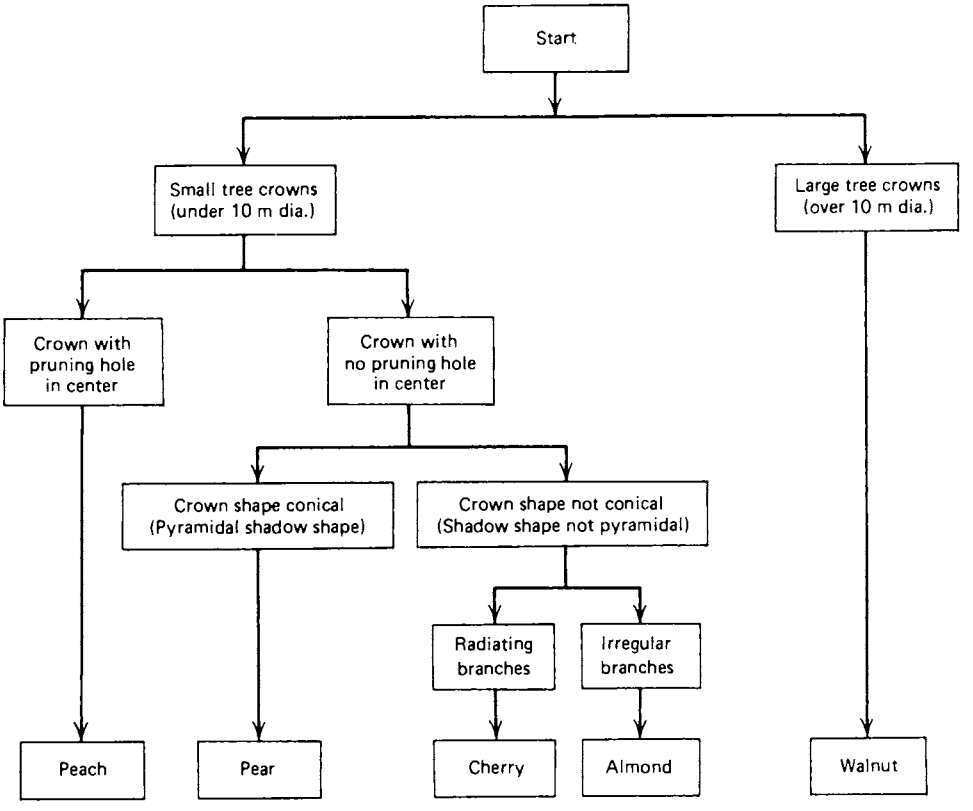

Figure 4.3 Dichotomous airphoto interpretation key to fruit and nut crops in the Sacramento Valley, CA, designed for use with 1 : 6000 scale panchromatic aerial photographs. (Adapted from American Society of Photogrammetry, 1983. Copyright © 1975, American Society of Photogrammetry. Reproduced with permission.)

by obtaining images at several times during the annual growing cycle. Observations of local vegetation emergence and recession can aid in the timing of image acquisition for natural vegetation mapping. In addition to seasonal variations, weather can cause significant short-term changes. Because soil moisture conditions may change dramatically during the day or two immediately following a rainstorm, the timing of image acquisition for soil studies is very critical.

Image Scale

Image scale affects the level of useful information that can be extracted from aerial and space images. Typical scales and areas of coverage are shown in

Table 4.1 for some of the more commonly available sources of aerial photographs. Although terminology with regard to airphoto scale has not been standardized, we can consider that *small-scale* airphotos have a scale of 1:50,000 or smaller, *medium-scale* airphotos have a scale between 1:12,000 and 1:50,000, and *large-scale* airphotos have a scale of 1:12,000 or larger.

In the case of nonphotographic sensors (including digital cameras), images do not have a scale per se; rather, they have a certain ground resolution cell size (e.g., 10 × 10 or 20 × 20 m square per pixel), as illustrated in Figures 1.19 and 1.20, and can be reproduced at various scales.

In the figure captions of this book, we have stated the scale of many images—including photographic, multispectral, and radar images—so that the reader can develop a feel for the degree of detail that can be extracted from images of varying scales.

As generalizations, the following statements can be made about the appropriateness of various image scales for resource studies. Small-scale images are used for reconnaissance mapping, large-area resource assessment, and general resource management planning. Medium-scale images are used for

TABLE 4.1 Typical Aerial Photograph Scales and Areas of Coverage for 240-mm Format Film (230 × 230-mm Image)

Photo Scale	Area per Frame (km)	Comments
1:130,000 or 1:120,000	29.9 × 29.9 or 27.6 × 27.6	NASA high altitude photography, 152-mm-focal-length lens
1:80,000	18.4 × 18.4	National High Altitude Photography (NHAP) program, 152-mm-focal-length lens, panchromatic film
1:65,000 or 1:60,000	14.9 × 14.9 or 13.8 × 13.8	NASA high altitude photography, 305-mm-focal-length lens
1:58,000	13.3 × 13.3	NHAP program, 210-mm-focal-length lens, color infrared film
1:40,000	9.2 × 9.2	National Aerial Photography Program (NAPP); U.S. Geological Survey (USGS) and USDA current mapping photography programs
1:24,000	5.5 × 5.5	Photography flown to match scale of USGS $7\frac{1}{2}'$ quadrangle maps
1:20,000	4.6 × 4.6	Typical scale of older (archival) USGS and USDA mapping photography
1:15,840	3.6 × 3.6	Traditional U.S. Forest Service (USFS) photography (4 in./mile)
1:6000	1.4 × 1.4	Typical EPA photography for emergency response and intensive analysis of hazardous waste sites

the identification, classification, and mapping of such features as tree species, agricultural crop type, vegetation community, and soil type. Large-scale images are used for the intensive monitoring of specific items such as surveys of the damage caused by plant disease, insects, or tree blowdown. Large-scale images are also used by the EPA for emergency response to hazardous waste spills and for the intensive site analysis of hazardous waste sites.

Conducted between 1980 and 1987, the National High-Altitude Photography (NHAP) program was a federal multiagency activity coordinated by the U.S. Geological Survey (USGS). It provided nationwide photographic coverage at a nominal scale of 1 : 58,000 using color infrared film and of 1 : 80,000 using panchromatic film exposed simultaneously. Stereoscopic photographs were typically taken from an aircraft altitude of 12,200 m above mean terrain, with a sun angle of at least 30° to minimize shadows, and on days with no cloud cover and minimal haze. The NHAP flight lines were flown in a north–south direction and were positioned to correspond to the centerline of each map sheet included in the national USGS 7.5′ quadrangle series. NHAP I began in 1980 and provided nationwide coverage under the "leaf-off" conditions of spring and fall. NHAP II began in 1985 with photography under "leaf-on" conditions. The leaf-off conditions are preferable for land cover mapping when it is important to be able to see as much detail as possible underneath trees. Leaf-on conditions are preferred for vegetation mapping. In 1987, the program name was changed to the National Aerial Photography Program (NAPP) in recognition of modifications in the user requirements and flight specifications (the flying height is no longer "high altitude").

The objectives of NAPP are to provide a complete photographic database of the 48 conterminous United States and to provide 5- to 7-year updates to the database. The first three NAPP photo acquisition cycles were 1987 to 1991, 1992 to 1996, and 1997 to 2003. The NAPP specifications call for 1 : 40,000 scale cloud-free black and white or color infrared photography with stereoscopic coverage. Spatial resolution of the NAPP photos is 1 to 2 m. Vegetation status (leaf-on, leaf-off) depends on requirements for the respective state involved.

As with NHAP coverage, NAPP photographs are taken along north–south flight lines positioned with respect to the USGS 7.5′ quadrangle maps covering the United States. Two flight lines (each incorporating five photographs) are included over each map area. Thus, every other NAPP photo is nominally centered on one-quarter of a 7.5′ quadrangle.

The NAPP photos have proven to be an extremely valuable ongoing source of medium-scale images supporting a wide range of applications. NAPP photos are the primary source of aerial photographs used in the production of 1-m resolution digital orthophotos for the National Digital Orthophoto Program (NDOP).

Information on the availability of NHAP and NAPP photographs can be obtained from the USGS EROS Data Center (see Appendix B).

Approaching the Image Interpretation Process

There is no single, "right" way to approach the image interpretation process. The specific image products and interpretation equipment available will, in part, influence how a particular interpretation task is undertaken. Beyond these factors, the specific goals of the task will determine the image interpretation process employed. Many applications simply require the image analyst to identify and count various discrete objects occurring in a study area. For example, counts may be made of such items as motor vehicles, residential dwellings, recreational watercraft, or animals. Other applications of the interpretation process often involve the identification of anomalous conditions. For example, the image analyst might survey large areas looking for such features as failing septic systems, sources of water pollution entering a stream, areas of a forest stressed by an insect or disease problem, or evidence of sites having potential archaeological significance.

Many applications of image interpretation involve the delineation of discrete areal units throughout images. For example, the mapping of land use, soil types, or forest types requires the interpreter to outline the boundaries between areas of one type versus another. Such tasks can be problematic when the boundary is not a discrete edge, but rather a "fuzzy edge" or gradation from one type of area to another, as is common with natural phenomena such as soils and natural vegetation.

Two extremely important issues must be addressed before an interpreter undertakes the task of delineating separate areal units on aerial or space images. The first is the definition of the *classification system* or criteria to be used to separate the various categories of features occurring in the images. For example, in mapping land use the interpreter must fix firmly in mind what specific characteristics determine if an area is "residential," "commercial," or "industrial." Similarly, the forest type mapping process must involve clear definition of what constitutes an area to be delineated in a particular species, height, or crown density class.

The second important issue in delineation of discrete areal units on images is the selection of the *minimum mapping unit* (MMU) to be employed in the process. This refers to the smallest size areal entity to be mapped as a discrete area. Selection of the MMU will determine the extent of detail conveyed by an interpretation. This is illustrated in Figure 4.4. In (*a*), a small MMU results in a much more detailed interpretation than does the use of a large MMU, as illustrated in (*b*).

Once the classification system and MMU have been determined, the interpreter can begin the process of delineating boundaries between feature types.

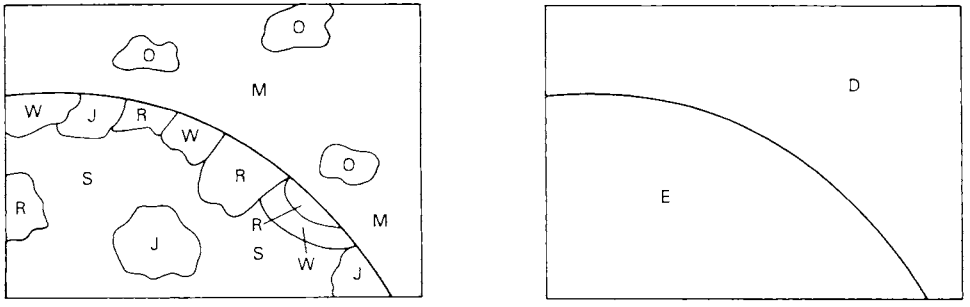

Figure 4.4 Influence of minimum mapping unit size on interpretation detail. (*a*) Forest types mapped using a small MMU: O, oak; M, maple; W, white pine; J, jack pine; R, red pine; S, spruce. (*b*) Forest types mapped using a large MMU: D, deciduous; E, evergreen.

Experience suggests that it is advisable to delineate the most highly contrasting feature types first and to work from the general to the specific. For example, in a land use mapping effort it would be better to separate "urban" from "water" and "agriculture" before separating more detailed categories of each of these feature types based on subtle differences.

In certain applications, the interpreter might choose to delineate *photomorphic regions* as part of the delineation process. These are regions of reasonably uniform tone, texture, and other image characteristics. When initially delineated, the feature type identity of these regions may not be known. Field observations or other ground truth can then be used to verify the identity of each region. Regrettably, there is not always a one-to-one correspondence between the appearance of a photomorphic region and a mapping category of interest. However, the delineation of such regions often serves as a stratification tool in the interpretation process and can be valuable in applications such as vegetation mapping (where photomorphic regions often correspond directly to vegetation classes of interest).

Image Preparation and Viewing

Before undertaking any visual image interpretation task, there are several other factors the image analyst should consider. These range from collecting any relevant collateral sources of information (e.g., maps, field reports, other images) to identifying what viewing equipment is available. Good lighting and access to equipment yielding a range of image magnifications are essential. Beyond this, the interpreter will also want to be sure the images to be viewed are systematically labeled and indexed so cross-referencing to other data sources (e.g., maps) is facilitated. Boundary delineations might be made directly on the images or interpretations might be made directly in a digital

format if the required equipment is available. Often, delineations are made on either a clear acetate or Mylar overlay affixed to the images. In such cases, it is important to mark a number of points (e.g., fiducial marks, road intersections) on the overlay to be used to ensure proper registration of the overlay to the image during interpretation (and if the overlay and image are separated and then need to be reregistered).

When the interpretation involves multiple overlapping photographs along a flight line or series of flight lines, the interpreter should first delineate the *effective areas* for the photo coverage before commencing the interpretation. The effective area is typically defined as the central area on each photograph bounded by lines bisecting the area of overlap with every adjacent photograph. Interpreting only within these areas ensures that the entire ground area included in the photos is covered, but with no duplication of interpretation effort. Likewise, because the effective area of a photograph includes all areas closer to the center of that photograph than to the center of any other, it is the area in which objects can be viewed with the least relief displacement. This minimizes the effect of topographic displacement when data interpreted from the individual photos are transferred to a composite base map.

Effective areas can be established by drawing lines on one photo of a stereopair which approximately bisect the endlap and sidelap and transferring three or four points stereoscopically to the adjacent photo (usually at the high and low points of the terrain) along the original line. The transferred points are then connected with straight lines. In areas of high relief, the transferred line will not be straight (due to relief displacement).

Sometimes, effective areas are delineated on every other photograph, rather than on each photograph. In this case, photos without effective areas are used for stereoscopic viewing but are not used for mapping purposes. The advantage of mapping on every photo is the minimization of relief displacement. The disadvantages include the need to delineate, interpret, and transfer twice as many effective areas. In any case, the interpreter should make certain that interpretations crossing the boundaries between effective areas match both spatially and in terms of the identification of the interpreted unit. That is, interpretation polygons spanning more than one effective area must have one interpretation label and the portions in each photo must "line up" with one another.

4.3 BASIC VISUAL IMAGE INTERPRETATION EQUIPMENT

Visual image interpretation equipment generally serves one of several fundamental purposes: viewing images, making measurements on images, performing image interpretation tasks, and transferring interpreted information to base maps or digital databases. Basic equipment for viewing images and

transferring interpreted information is described here. Equipment involved in performing measuring and mapping tasks was described in Chapter 3.

The airphoto interpretation process typically involves the utilization of stereoscopic viewing to provide a three-dimensional view of the terrain. Some space images are also analyzed stereoscopically. The stereo effect is possible because we have binocular vision. That is, since we have two eyes that are slightly separated, we continually view the world from two slightly different perspectives. Whenever objects lie at different distances in a scene, each eye sees a slightly different view of the objects. The differences between the two views are synthesized by the mind to provide depth perception. Thus, the two views provided by our separated eyes enable us to see in three dimensions.

When aerial photographs overlap, they also provide two views taken from separated positions. By viewing the left photograph of a pair with the left eye and the right photo with the right eye, we obtain a three-dimensional view of the terrain surface. A *stereoscope* facilitates the stereoviewing process. This book contains many *stereopairs*, or *stereograms*, which can be viewed in three dimensions using a lens stereoscope such as shown in Figure 4.5. An average separation of about 58 mm between common points has been used in the stereograms in this book. The exact spacing varies somewhat because of the different elevations of the points. The original vertical aerial photographs with about 60 percent endlap have been cropped and are mounted here with 100 percent overlap.

Figure 4.5 Simple lens stereoscope.

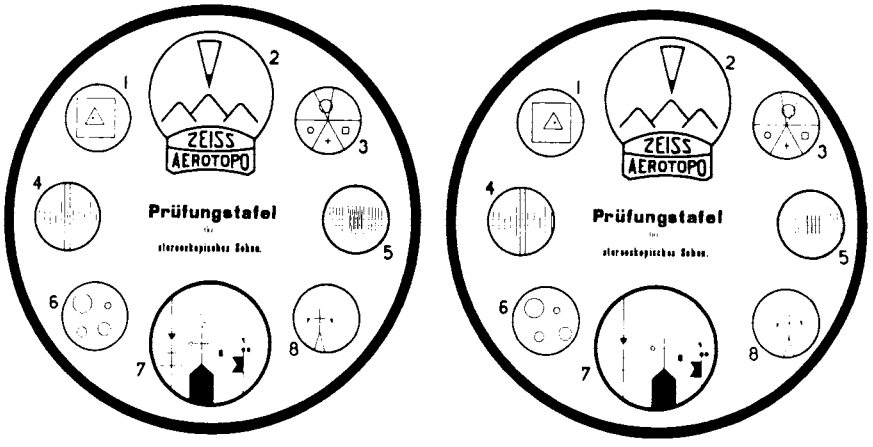

Figure 4.6 Stereoscopic vision test. (Courtesy Carl Zeiss, Inc.)

Figure 4.6 can be used to test stereoscopic vision. When this diagram is viewed through a stereoscope, the rings and other objects should appear to be at varying distances from the observer. Your stereovision ability can be evaluated by filling in Table 4.2 (answers are in the second part of the table). People whose eyesight is very weak in one eye may not have the ability to see in stereo. This will preclude three-dimensional viewing of the stereograms in this book. However, many people with essentially monocular vision have become proficient photo interpreters. In fact, many forms of interpretation involve monocular viewing with such basic equipment as handheld magnifying glasses or tube magnifiers (2 × to 10 × lenses mounted in a transparent stand).

Some people will be able to view the stereograms in this book without a stereoscope. This can be accomplished by holding the book about 25 cm from your eyes and allowing the view of each eye to drift into a straight-ahead viewing position (as when looking at objects at an infinite distance) while still maintaining focus on the stereogram. When the two images have fused into one, the stereogram will be seen in three dimensions. Most persons will find stereoviewing without proper stereoscopes to be a tiring procedure, producing "eyestrain." It is, however, a useful technique to employ when stereoscopes are not available.

Several types of stereoscopes are available, utilizing lenses or a combination of lenses, mirrors, and prisms.

Lens stereoscopes, such as the one shown in Figure 4.5, are portable and comparatively inexpensive. Most are small instruments with folding legs. The lens spacing can usually be adjusted from about 45 to 75 mm to accommodate individual eye spacings. Lens magnification is typically 2 power but may be adjustable. The principal disadvantage of small lens stereoscopes is that

the images must be quite close together to be positioned properly underneath the lenses. Because of this, the interpreter cannot view the entire stereoscopic area of 240-mm aerial photographs without raising the edge of one of the photographs.

Mirror stereoscopes use a combination of prisms and mirrors to separate the lines of sight from each of the viewer's eyes. Such stereoscopes typically have little or no magnification in their normal viewing mode. Binoculars can be fitted to the eyepieces to provide a magnification of 2 to 4 power, with a resulting decrease in field of view. With a mirror stereoscope using little or no

TABLE 4.2 Stereovision Test for Use with Figure 4.6

PART I

Within the rings marked 1 through 8 are designs that appear to be at different elevations. Using "1" to designate the highest elevation, write down the depth order of the designs. It is possible that two or more designs may be at the same elevation. In this case, use the same number for all designs at the same elevation.

Ring 1		**Ring 6**	
Square	(2)	Lower left circle	( )
Marginal ring	(1)	Lower right circle	( )
Triangle	(3)	Upper right circle	( )
Point	(4)	Upper left circle	( )
		Marginal ring	( )
Ring 7		**Ring 3**	
Black flag with ball	( )	Square	( )
Marginal ring	( )	Marginal ring	( )
Black circle	( )	Cross	( )
Arrow	( )	Lower left circle	( )
Tower with cross	( )	Upper center circle	( )
Double cross	( )		
Black triangle	( )		
Black rectangle	( )		

PART II

Indicate the relative elevations of the rings 1 through 8.

( )( )( )( )( )( )( )( )

Highest Lowest

PART III

Draw profiles to indicate the relative elevations of the letters in the words "prufungstafel" and "stereoskopisches sehen."

P R U F U N G S T A F E L S T E R E O S K O P I S C H E S S E H E N

(Answers to Stereovision Test on next page)

TABLE 4.2 *(Continued)*

PART I

Ring 1		**Ring 6**	
Square	(2)	Lower left circle	(4)
Marginal ring	(1)	Lower right circle	(5)
Triangle	(3)	Upper right circle	(1)
Point	(4)	Upper left circle	(3)
		Marginal ring	(2)
Ring 7		**Ring 3**	
Black flag with ball	(5)	Square	(4)
Marginal ring	(1)	Marginal ring	(2)
Black circle	(4)	Cross	(3)
Arrow	(2)	Lower left circle	(1)
Tower with cross	(7)	Upper center circle	(5)
Double cross	(2)		
Black triangle	(3)		
Black rectangle	(6)		

PART II

(7) (6) (5) (1) (4) (2)[a] (3)[a] (8)
Highest Lowest

PART III

PRUFUNGSTAFEL STEREOSKOPISCHES SEHEN

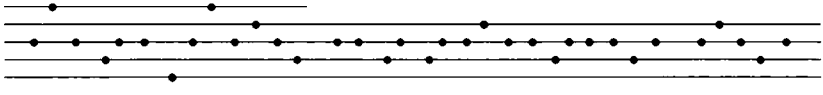

[a]Rings 2 and 3 are at the same elevation.

magnification, the interpreter can view all or most of the stereoscopic portion of a 240-mm stereopair without moving either the photographs or the stereoscope. This type of stereoscope has the disadvantage that it is too large for easy portability and is much more costly than simple lens stereoscopes.

Zoom stereoscopes have a continuously variable magnification, typically 2.5 to 10 power. Zoom stereoscopes are expensive precision instruments, typically with a very high lens resolution.

Either paper prints or transparencies can be viewed using a stereoscope. Paper prints are more convenient to handle, more easily annotated, and better suited to field use; transparencies have better spatial resolution and color fidelity. An interpreter would generally use a simple lens or mirror stereoscope with paper prints and a more elaborate viewer such as the zoom stereoscope with transparencies. Transparencies are placed on a *light table* (Figure 4.7) for viewing because the light source must come from behind the transparency. The spectral characteristics of the transparency and light table

lamps should be balanced for optimum viewing conditions. Light tables typically have bulbs with a "color temperature" around 3500 K, which means that the spectral distribution of their light output is similar to that of a blackbody heated to 3500 K. The color temperature of "noon daylight" is about 5500 K; tungsten bulbs used for indoor lighting have a color temperature of about 3200 K.

Once information has been interpreted from aerial and space images, it is frequently transferred to a base map. When the base map is not at the same scale as the image, special optical devices may be used in the transfer process. Some of these devices use high precision opaque projectors to enlarge or reduce the image data to the scale of the map. Other devices employ viewing systems that optically superimpose a view of an image and a map. By adjusting the magnification of the two views, the image can be matched to the scale of the map.

An example of the latter device was the Bausch & Lomb Stereo Zoom Transfer Scope, which has been replaced by the Thales-Optem *Digital Transfer Scope* (*DTS*) shown in Figure 4.8. The DTS combines interpretation of hardcopy images and superimposition of a map directly with a geographic information system on a personal computer. It allows the operator to simultaneously view both a vector format digital base map, displayed on a

liquid-crystal display (LCD) monitor within the instrument, and a stereopair of hardcopy images (paper or film). The DTS allows interpretation of aerial or satellite images in stereo (or mono) through the eyepieces. Through a combination of the zooming optical system (7:1) and software, this device can accommodate a large disparity of image and map scales. The software also "warps" (reshapes, scales, and transforms) the base map data to match the scale and geographic distortions of the hardcopy image. Image interpretation (map editing, feature delineation, and annotation) is then performed in the transformed image space. After the interpretation, the original map data and the information compiled from interpretation are then transformed back into

the original, geometrically correct map space. The DTS can also superimpose two images (e.g., a raster image displayed on the internal monitor and hardcopy image) for change detection analysis. A digital camera can be attached to the built-in camera port of the DTS (the black cylinder located on the top of the instrument head) for capturing the superimposition of a digital map and hardcopy image for use in publications or further analysis.

4.4 LAND USE/LAND COVER MAPPING

A knowledge of land use and land cover is important for many planning and management activities and is considered an essential element for modeling and understanding the earth as a system. Land cover maps are presently being developed from local to national to global scales. The use of panchromatic, medium-scale aerial photographs to map land use has been an accepted practice since the 1940s. More recently, small-scale aerial photographs and satellite images have been utilized for land use/land cover mapping.

The term *land cover* relates to the type of feature present on the surface of the earth. Corn fields, lakes, maple trees, and concrete highways are all examples of land cover types. The term *land use* relates to the human activity or economic function associated with a specific piece of land. As an example, a tract of land on the fringe of an urban area may be used for single-family housing. Depending on the level of mapping detail, its *land use* could be described as urban use, residential use, or single-family residential use. The same tract of land would have a *land cover* consisting of roofs, pavement, grass, and trees. For a study of the socioeconomic aspects of land use planning (school requirements, municipal services, tax income, etc.), it would be important to know that the use of this land is for single-family dwellings. For a hydrologic study of rainfall-runoff characteristics, it would be important to know the amount and distribution of roofs, pavement, grass, and trees in this tract. Thus, a knowledge of both land use and land cover can be important for land planning and land management activities.

The USGS devised a land use and land cover classification system for use with remote sensor data in the mid-1970s (Anderson et al., 1976). The basic concepts and structure of this system are still valid today. A number of more recent land use/land cover mapping efforts follow these basic concepts and, although their mapping units may be more detailed or more specialized, and they may use more recent remote sensing systems as data sources, they still follow the basic structure originally set forth by the USGS. In the remainder of this section, we first explain the USGS land use and land cover classification system, then describe some ongoing land use/land cover mapping efforts in the United States and elsewhere.

Ideally, land use and land cover information should be presented on separate maps and not intermixed as in the USGS classification system. From a

practical standpoint, however, it is often most efficient to mix the two systems when remote sensing data form the principal data source for such mapping activities. While land cover information can be directly interpreted from appropriate remote sensing images, information about human activity on the land (land use) cannot always be inferred directly from land cover. As an example, extensive recreational activities covering large tracts of land are not particularly amenable to interpretation from aerial photographs or satellite images. For instance, hunting is a common and pervasive recreational use occurring on land that would be classified as some type of forest, range, wetland, or agricultural land during either a ground survey or image interpretation. Thus, additional information sources are needed to supplement the land cover data. Supplemental information is also necessary for determining the use of such lands as parks, game refuges, or water conservation districts that may have land uses coincident with administrative boundaries not usually identifiable on remote sensor images. Recognizing that some information cannot be derived from remote sensing data, the USGS system is based on categories that can be reasonably interpreted from aerial or space imagery.

The USGS land use and land cover classification system was designed according to the following criteria: (1) the minimum level of interpretation accuracy using remotely sensed data should be at least 85 percent, (2) the accuracy of interpretation for the several categories should be about equal, (3) repeatable results should be obtainable from one interpreter to another and from one time of sensing to another, (4) the classification system should be applicable over extensive areas, (5) the categorization should permit land use to be inferred from the land cover types, (6) the classification system should be suitable for use with remote sensor data obtained at different times of the year, (7) categories should be divisible into more detailed subcategories that can be obtained from large-scale imagery or ground surveys, (8) aggregation of categories must be possible, (9) comparison with future land use and land cover data should be possible, and (10) multiple uses of land should be recognized when possible.

It is important to note that these criteria were developed prior to the widespread use of satellite imagery and computer-assisted classification techniques. While most of the 10 criteria have withstood the test of time, experience has shown that the first two criteria regarding overall and per class consistency and accuracy are not always attainable when mapping land use and land cover over large, complex geographic areas. In particular, when using computer-assisted classification methods, it is frequently not possible to map consistently at a single level of the USGS hierarchy. This is typically due to the occasionally ambiguous relationship between land cover and spectral response and the implications of land use on land cover.

The basic USGS land use and land cover classification system for use with remote sensor data is shown in Table 4.3. The system is designed to use four

TABLE 4.3 USGS Land Use/Land Cover Classification System for Use with Remote Sensor Data

Level I	Level II
1 Urban or built-up land	11 Residential
	12 Commercial and service
	13 Industrial
	14 Transportation, communications, and utilities
	15 Industrial and commercial complexes
	16 Mixed urban or built-up land
	17 Other urban or built-up land
2 Agricultural land	21 Cropland and pasture
	22 Orchards, groves, vineyards, nurseries, and ornamental horticultural areas
	23 Confined feeding operations
	24 Other agricultural land
3 Rangeland	31 Herbaceous rangeland
	32 Shrub and brush rangeland
	33 Mixed rangeland
4 Forest land	41 Deciduous forest land
	42 Evergreen forest land
	43 Mixed forest land
5 Water	51 Streams and canals
	52 Lakes
	53 Reservoirs
	54 Bays and estuaries
6 Wetland	61 Forested wetland
	62 Nonforested wetland
7 Barren land	71 Dry salt flats
	72 Beaches
	73 Sandy areas other than beaches
	74 Bare exposed rock
	75 Strip mines, quarries, and gravel pits
	76 Transitional areas
	77 Mixed barren land
8 Tundra	81 Shrub and brush tundra
	82 Herbaceous tundra
	83 Bare ground tundra
	84 Wet tundra
	85 Mixed tundra
9 Perennial snow or ice	91 Perennial snowfields
	92 Glaciers

"levels" of information, two of which are detailed in Table 4.3. A multilevel system has been devised because different degrees of detail can be obtained from different aerial and space images, depending on the sensor system and image resolution.

The USGS classification system also provides for the inclusion of more detailed land use/land cover categories in Levels III and IV. Levels I and II, with classifications specified by the USGS (Table 4.3), are principally of inter-

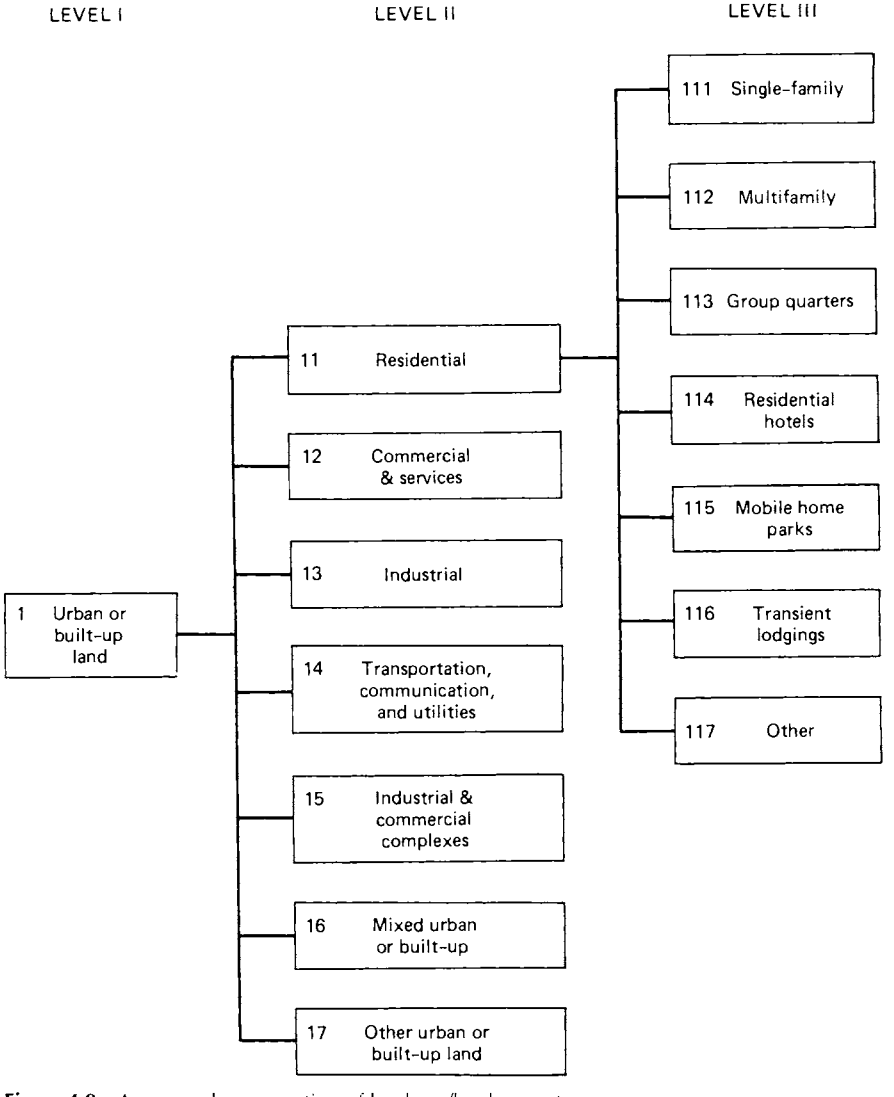

Figure 4.9 An example aggregation of land use/land cover types.

est to users who desire information on a nationwide, interstate, or statewide basis. Levels III and IV can be utilized to provide information at a resolution appropriate for regional (multicounty), county, or local planning and management activities. Again, as shown in Table 4.3, Level I and II categories are specified by the USGS. It is intended that Levels III and IV be designed by the local users of the USGS system, keeping in mind that the categories in each level must aggregate into the categories in the next higher level. Figure 4.9 illustrates a sample aggregation of classifications for Levels III, II, and I.

Table 4.4 lists representative image interpretation formats for the four USGS land use and land cover classification levels (Jensen, 2000). Level I was originally designed for use with low to moderate resolution satellite data such as Landsat Multispectral Scanner (MSS) images. (See Chapter 6 for a description of the Landsat satellites and the other satellite systems mentioned below.) Image resolutions of 20 to 100 m are appropriate for this level of mapping.

Level II was designed for use with small-scale aerial photographs. Image resolutions of 5 to 20 m are appropriate for this level of mapping. The most widely used image type for this level has been high altitude color infrared photographs. However, small-scale panchromatic aerial photographs (Figure 4.10), Landsat Thematic Mapper (TM) and Enhanced Thematic Mapper Plus (ETM+) data, SPOT satellite data, and Indian Remote Sensing Satellite (IRS) data are also representative data sources for many Level II mapping categories.

The general relationships shown in Table 4.4 are not intended to restrict users to particular data sources or scales, either in the original imagery or in the final map products. For example, Level I land use/land cover information, while efficiently and economically gathered over large areas by the Landsat MSS, could also be interpreted from conventional medium-scale photographs or compiled from a ground survey. Conversely, some of the Level II categories have been accurately interpreted from Landsat MSS data.

TABLE 4.4 Representative Image Interpretation Formats for Various Land Use/Land Cover Classification Levels

Land Use/Land Cover Classification Level	Representative Format for Image Interpretation
I	Low to moderate resolution satellite data (e.g., Landsat MSS data)
II	Small-scale aerial photographs; moderate resolution satellite data (e.g., Landsat TM data)
III	Medium-scale aerial photographs; high resolution satellite data (e.g., IKONOS data)
IV	Large-scale aerial photographs

For mapping at Level III, substantial amounts of supplemental information, in addition to that obtained from medium-scale images, may need to be acquired. At this level, a resolution of 1 to 5 m is appropriate. Both aerial photographs and high resolution satellite data can be used as data sources at this level.

Mapping at Level IV also requires substantial amounts of supplemental information, in addition to that obtained from aerial images. At this level, a resolution of 0.25 to 1.0 m is appropriate. Large-scale aerial photographs are often the most appropriate form of remotely sensed data for this level of mapping.

The USGS definitions for Level I classes are set forth in the following paragraphs. This system is intended to account for 100 percent of the earth's land surface (including inland water bodies). Each Level II subcategory is explained in Anderson et al. (1976) but is not detailed here.

Urban or *built-up land* is composed of areas of intensive use with much of the land covered by structures. Included in this category are cities; towns; villages; strip developments along highways; transportation, power, and communication facilities; and areas such as those occupied by mills, shopping centers, industrial and commercial complexes, and institutions that may, in some instances, be isolated from urban areas. This category takes precedence over others when the criteria for more than one category are met. For example, residential areas that have sufficient tree cover to meet *forest land* criteria should be placed in the urban or built-up land category.

Agricultural land may be broadly defined as land used primarily for production of food and fiber. The category includes the following uses: cropland and pasture, orchards, groves and vineyards, nurseries and ornamental horticultural areas, and confined feeding operations. Where farming activities are limited by soil wetness, the exact boundary may be difficult to locate and *agricultural land* may grade into *wetland*. When wetlands are drained for agricultural purposes, they are included in the *agricultural land* category. When such drainage enterprises fall into disuse and if wetland vegetation is reestablished, the land reverts to the *wetland* category.

Rangeland historically has been defined as land where the potential natural vegetation is predominantly grasses, grasslike plants, forbs, or shrubs and where natural grazing was an important influence in its precivilization state. Under this traditional definition, most of the rangelands in the United States are in the western range, the area to the west of an irregular north–south line that cuts through the Dakotas, Nebraska, Kansas, Oklahoma, and Texas. Rangelands also are found in additional regions, such as the Flint Hills (eastern Kansas), the southeastern states, and Alaska. The historical connotation of rangeland is expanded in the USGS classification to include those areas in the eastern states called brushlands.

Forest land represents areas that have a tree-crown areal density (crown closure percentage) of 10 percent or more, are stocked with trees capable of

producing timber or other wood products, and exert an influence on the climate or water regime. Lands from which trees have been removed to less than 10 percent crown closure but that have not been developed for other uses are also included. For example, lands on which there are rotation cycles of clearcutting and blockplanting are part of the forest land category. Forest land that is extensively grazed, as in the southeastern United States, would also be included in this category because the dominant cover is forest and the dominant activities are forest related. Areas that meet the criteria for forest land and also urban and built-up land are placed in the latter category. Forested areas that have wetland characteristics are placed in the *wetland* class.

The *water* category includes streams, canals, lakes, reservoirs, bays, and estuaries.

The *wetland* category designates those areas where the water table is at, near, or above the land surface for a significant part of most years. The hydrologic regime is such that aquatic or hydrophytic vegetation is usually established, although alluvial and tidal flats may be nonvegetated. Examples of wetlands include marshes, mudflats, and swamps situated on the shallow margins of bays, lakes, ponds, streams, and artificial impoundments such as reservoirs. Included are wet meadows or perched bogs in high mountain valleys and seasonally wet or flooded basins, playas, or potholes with no surface water outflow. Shallow water areas where aquatic vegetation is submerged are classified as *water* and are not included in the *wetland* category. Areas in which soil wetness or flooding is so short-lived that no typical wetland vegetation is developed belong in other categories. Cultivated wetlands such as the flooded fields associated with rice production and developed cranberry bogs are classified as *agricultural land*. Uncultivated wetlands from which wild rice, cattails, and so forth are harvested are retained in the *wetland* category, as are wetlands grazed by livestock. Wetland areas drained for any purpose belong to the other land use/land cover categories such as urban or built-up land, agricultural land, rangeland, or forest land. If the drainage is discontinued and wetland conditions resume, the classification will revert to *wetland*. Wetlands managed for wildlife purposes are properly classified as *wetland*.

Barren land is land of limited ability to support life and in which less than one-third of the area has vegetation or other cover. This category includes such areas as dry salt flats, beaches, bare exposed rock, strip mines, quarries, and gravel pits. Wet, nonvegetated barren lands are included in the wetland category. Agricultural land temporarily without vegetative cover because of cropping season or tillage practices is considered *agricultural land*. Areas of intensively managed forest land that have clear-cut blocks evident are classified as *forest land*.

Tundra is the term applied to the treeless regions beyond the geographic limit of the boreal forest and above the altitudinal limit of trees in high mountain ranges. In North America, tundra occurs primarily in Alaska and northern Canada and in isolated areas of the high mountain ranges.

Perennial snow or *ice* areas occur because of a combination of environmental factors that cause these features to survive the summer melting season. In so doing, they persist as relatively permanent features on the landscape.

As noted above, some parcels of land could be placed into more than one category, and specific definitions are necessary to explain the classification priorities. This comes about because the USGS land use/land cover classification system contains a mixture of land activity, land cover, and land condition attributes.

Several land use/land cover mapping efforts that have been undertaken in the United States and elsewhere use the USGS land use/land cover classification system, or variations thereof. A representative subset of these efforts is summarized below (new initiatives continue to develop given the importance of such data).

The USGS land use/land cover classification system was used to prepare Level I and II land use/land cover maps for most of the conterminous United States and Hawaii at a scale of 1:250,000. For most categories, a minimum mapping unit of 16 ha was used. A limited number of maps are available at a scale of 1:100,000. Digital land use/land cover data have been compiled from these maps by the USGS in vector format and are available for the conterminous United States and Hawaii. Polygons delineating "natural" areas have a minimum size of 4 ha with a minimum feature width of 400 m. The minimum size of polygons representing cultural features (e.g., urban areas, highways) is also 4 ha, with a minimum feature width of 200 m. The data are also available in raster (grid-cell) format. The digital data use the Universal Transverse Mercator (UTM) coordinate system and can be transformed into other map projections. In digital form, the land use/land cover data can be combined with other data types in a GIS. These data are available from the USGS EROS Data Center (see Appendix B) at no cost when downloaded over the Internet.

Traditionally, land cover mapping activities in the United States, as well as a variety of natural resource mapping activities, have used topographic base maps produced by the USGS, at scales generally ranging from 1:24,000 to 1:250,000, for their base maps. Over time, mapping activities have become increasingly digitally based. In response to this, the USGS will be providing, on the Internet, current, accurate, and nationally consistent digital data and topographic maps derived from those data. The resulting product, *The National Map*, will be a seamless, continuously maintained set of geographic base data that will serve as a foundation for integrating, sharing, and using other data easily and consistently. The National Map will include the following: (1) high resolution digital orthorectified imagery that will provide some of the feature information now symbolized on topographic maps; (2) high resolution surface elevation data, including bathymetry, to derive contours for primary series topographic maps and to support production of accurate orthorectified imagery; (3) vector feature data for hydrography, transportation (roads, railways, and waterways), structures, government unit boundaries,

and publicly owned land boundaries; (4) geographic names for physical and cultural features to support the U.S. Board on Geographic Names, and other names, such as those for highways and streets; and, (5) extensive land cover data. Data will be seamlessly and consistently classified, enabling users to extract data and information for irregular geographic areas, such as counties or drainage basins. For further information, see http://nationalmap.usgs.gov.

The USGS and the EPA are cooperating on a North American Landscape Characterization Project (NALC) that has completed production of a standardized digital data set for the contiguous 48 states and Mexico that contains Landsat MSS satellite data (Chapter 6) from the 1970s, 1980s, and 1990s. This data set allows researchers to inventory land use and land cover and to conduct land cover change analysis using a standardized data set.

The U.S. Department of Agriculture's Natural Resources Conservation Service (NRCS) conducts a statistically based National Resources Inventory (NRI) at 5-year intervals. The NRI is an inventory of land use and land cover, soil erosion, prime farmland, wetlands, and other natural resource characteristics of nonfederal rural land in the United States. It provides a record of the nation's conservation accomplishments and future program needs. Specifically, it provides valuable information concerning the effect of legislative actions on protecting land from erosion and slowing the rate of loss of wetlands, wildlife habitat diversity, and prime agricultural land. The NRI data are also used by federal and state agencies in regional and state environmental planning to determine the magnitude and location of soil and water resource problems. With each 5-year cycle of data gathering, the NRI places increasing emphasis on remote sensing data acquisition and computer-based data analysis.

As part of NASA's Earth Observing System (EOS) Pathfinder Program, the USGS, the University of Nebraska-Lincoln, and the European Commission's Joint Research Centre are involved with a Global Land Cover Characterization study that has generated a 1-km resolution global land cover database for use in a wide range of environmental research and modeling applications. The global land cover characteristics database was developed on a continent-by-continent basis and each continental database contains unique elements based on the geographical aspects of the specific continent. The initial remote sensing data source for this study was Advanced Very High Resolution Radiometer (AVHRR) data (Chapter 6) spanning April 1992 through March 1993. These global land cover data are available from the USGS EROS Data Center (see Appendix B) at no cost when downloaded over the Internet.

The USGS National Gap Analysis Program (GAP) is a state-, regional-, and national-level program established to provide map data, and other information, about natural vegetation, distribution of native vertebrate species, and land ownership. Gap analysis is a scientific method for identifying the degree to which native animal species and natural communities are represented in our present-day mix of conservation lands. Those species and communities not adequately represented in the existing network of conservation lands con-

stitute conservation "gaps." The GAP data sets are produced at a nominal scale of 1:100,000. A minimum mapping unit (MMU) of 30 × 30 m (the resolution of the Landsat TM data typically used for data acquisition and analysis) is generally used. (Some GAP data sets use a larger MMU.)

The Multi-Resolution Land Characteristics (MRLC) Consortium was established as an interagency initiative to provide a consistent national Landsat TM data set and, ultimately, a 30-m national land cover classification for the conterminous United States. The original members of the MLRC were the USGS, the EPA, the National Oceanic and Atmospheric Administration (NOAA), and the U.S. Forest Service (USFS). Later joining the MLRC were the National Aeronautics and Space Administration (NASA) and the Bureau of Land Management (BLM). This consortium of agencies developed a common set of requirements and specifications for Landsat TM data acquisition and data processing. The initial result of MRLC was a multitemporal geocoded Landsat TM data set for the 48 conterminous states, with dates of data acquisition centered on 1992. The ultimate purpose of this data set was the development of the land cover database needed by each of the participating projects and programs. Several complementary land cover databases are being developed from the MRLC coverage. For additional information, see the MRLC website at http://www.epa.gov/mlrc.

Land use and land cover mapping is also being addressed by various groups outside of the United States. For example, the Land Cover Working Group of the Asian Association on Remote Sensing is involved with the preparation of a 1-km-resolution land cover database of Asia based on AVHRR satellite data.

The Coordination of Information on the Environment (CORINE) land cover initiative is led by the European Environment Agency. The CORINE land cover database provides a pan-European inventory of biophysical land cover, using a 44-class nomenclature. It is made available on a 250 by 250 m grid database. CORINE land cover is a key database for integrated environmental assessment across Europe. For additional information, see http://www.eea.eu.int.

The Africover project of the United Nations Food and Agriculture Organization has as its goal the establishment, for the whole of Africa, of a digital geo-referenced database on land cover, the *Multipurpose Africover Database for Environmental Resources*, at a 1:200,000 scale (1:100,000 for small countries and specific areas). This project has been prepared in response to a number of national requests for assistance on the implementation of reliable and geo-referenced information on natural resources (e.g., "early warning" of potential agricultural problems, forest and rangeland monitoring, watershed management, wildlife monitoring, natural resource planning, production statistics, biodiversity and climate change assessment) at subnational, national, and regional levels. The land cover information is mainly derived from visual interpretation of recent high resolution satellite images that have been

enhanced digitally. Additional information about the Africover database is available at http://www.africover.org.

4.5 GEOLOGIC AND SOIL MAPPING

The earth has a highly complex and variable surface whose topographic relief and material composition reflect the bedrock and unconsolidated materials that underlie each part of the surface as well as the agents of change that have acted on them. Each type of rock, each fracture or other effect of internal movement, and each erosional and depositional feature bear the imprint of the processes that produced them. Persons who seek to describe and explain earth materials and structures must understand geomorphological principles and be able to recognize the surface expressions of the various materials and structures. Through the processes of visual image interpretation and geologic and soil mapping, these materials and structures can be identified and evaluated. Geologic and soil mapping will always require a considerable amount of field exploration, but the mapping process can be greatly facilitated through the use of visual image interpretation. Here, we briefly describe the application of visual image interpretation to geologic and soil mapping. Section 4.16 provides a more detailed coverage of this application and contains stereoscopic aerial photographs illustrating visual image interpretation for landform identification and evaluation.

Geologic Mapping

The first aerial photographs taken from an airplane for geologic mapping purposes were used to construct a mosaic covering Bengasi, Libya, in 1913. In general, the earliest uses of airphotos were simply as base maps for geologic data compilation, especially as applied to petroleum exploration. Some interpretive use of aerial photographs began in the 1920s. Since the 1940s, the interpretive use of airphotos for geologic mapping and evaluation has been widespread.

Geologic mapping involves the identification of landforms, rock types, and rock structures (folds, faults, fractures) and the portrayal of geologic units and structures on a map or other display in their correct spatial relationship with one another. Mineral resource exploration is an important type of geologic mapping activity. Because most of the surface and near-surface mineral deposits in accessible regions of the earth have been found, current emphasis is on the location of deposits far below the earth's surface or in inaccessible regions. Geophysical methods that provide deep penetration into the earth are generally needed to locate potential deposits and drill holes are required to confirm their existence. However, much information about potential areas for mineral exploration can be provided by interpretation of surface features on aerial photographs and satellite images.

Interpretation of satellite images and aerial photographs is a critical preliminary step for most field-based geologic mapping projects, especially in remote regions. Such imagery provides an efficient, comparatively low-cost means of targeting key areas for the much more expensive ground-based field surveys. Images are used to locate areas where rocks are exposed at the surface and are thus accessible to the geologist for study, and to trace key geologic units across the landscape. Images also allow the geologist to make important distinctions between landforms, relate them to the geologic processes that formed them, and thus interpret the geologic history of the area. At the most utilitarian level, images can be indispensable to the geologist in navigation and in determining how to access an area of interest, whether by road or trail, by river, or by air. (The terrain and vegetation characteristics will dictate how a geologist will be able to reach the rocks and features that must be evaluated and mapped.)

Satellite images provide geologists several advantages over aerial photographs: (1) they provide the advantage of large-area or synoptic coverage, which allows an analyst to examine in single scenes (or in mosaics) the geological portrayal of the earth on a regional basis; (2) they provide the ability to analyze multispectral bands quantitatively in terms of numbers (DNs), which permits the application of computer processing routines to discern and enhance certain compositional properties of earth materials; and, (3) they provide the capability of merging different types of remote sensing data products (e.g., reflectance images with radar or thermal imagery) or combining them with topographic elevation data and other kinds of information bases (e.g., thematic maps, geophysical measurements, chemical sampling surveys), which enables new solutions to determining interrelations among various natural properties of earth phenomena. These new space-driven approaches are beginning to revolutionize the ways in which geologists conduct their field studies, and they have proven to be indispensable techniques for improving the geologic mapping process and carrying out practical exploration for mineral and energy resources on an extensive scale.

Multistage image interpretation is typically utilized in geologic studies. The interpreter may begin by making interpretations of satellite images at scales of 1:250,000 to 1:1,000,000, then examining high altitude stereoscopic aerial photographs at scales from 1:58,000 to 1:130,000. For detailed mapping, stereoscopic aerial photographs at scales as large as 1:20,000 may be utilized.

Small-scale mapping often involves the mapping of *lineaments*, regional linear features that are caused by the linear alignment of morphological features, such as streams, escarpments, and mountain ranges, and tonal features that in many areas are the surface expressions of fractures or fault zones. Increased moisture retention within the fractured material of a fracture or fault zone is often manifested as distinctive vegetation or small impounded bodies known as "sag ponds." Major lineaments can range from a few to hundreds of kilometers in length. Note the clear expression of the linear Garlock and San Andreas faults in Figure 4.11*a*, a small-scale satellite image that covers an

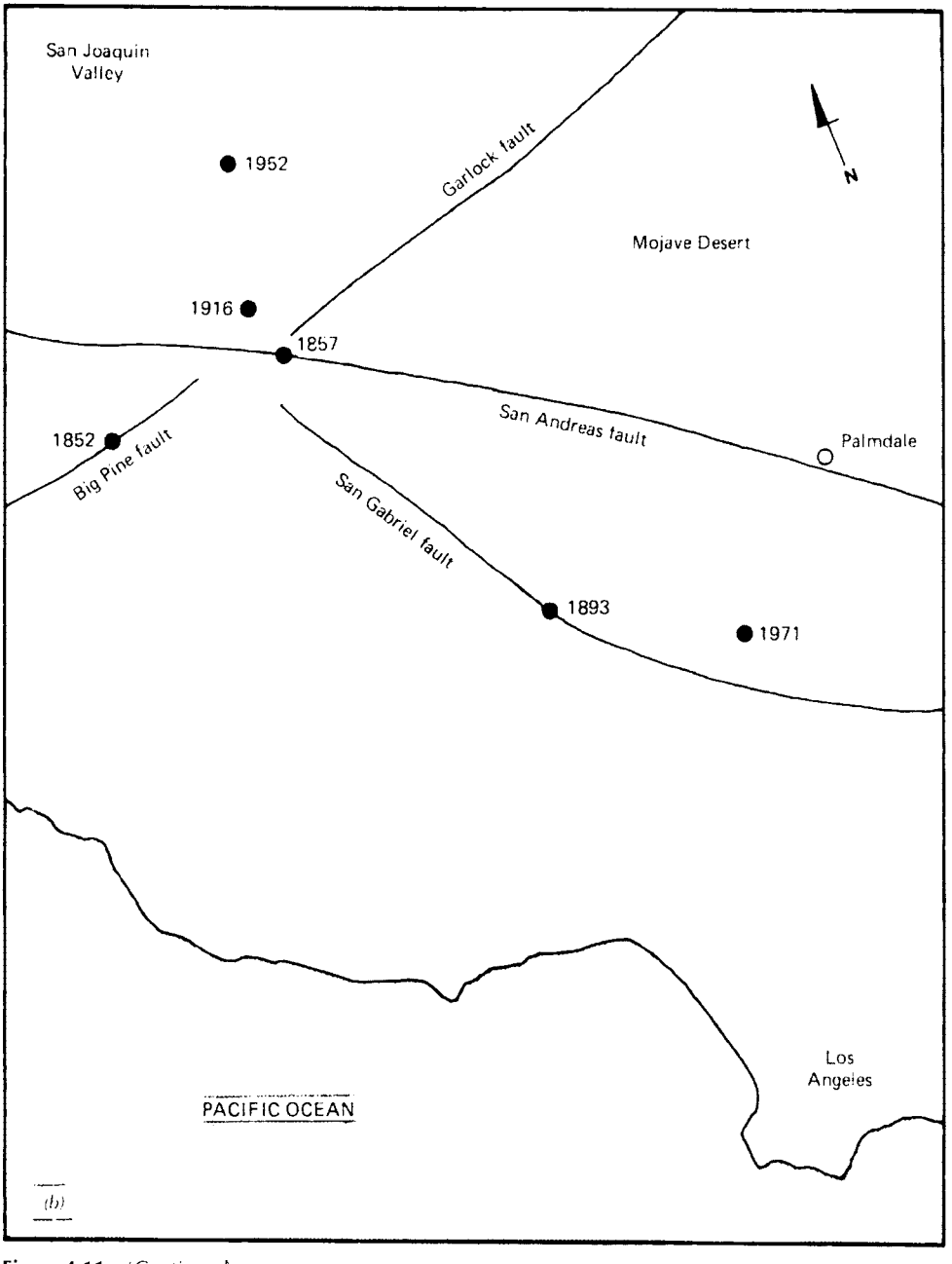

Figure 4.11 *(Continued)*

area 127 by 165 km in size. The mapping of lineaments is also important in mineral resource studies because many ore deposits are located along fracture zones.

Several factors influence the detection of lineaments and other topographic features of geologic significance. One of the most important is the angular relationship between the feature and the illumination source. In general, features that trend parallel to the illumination source are not detected as readily as those that are oriented perpendicularly. Moderately low illumination angles are preferred for the detection of subtle topographic linear features. An example of low sun angle photography, taken under wintertime conditions with snow-covered ground, is shown in Figure 4.12. This figure shows an early space station (Skylab) photograph of northwestern Wyoming and eastern Idaho. The light-toned area at the upper left is the Snake River Plain of Idaho, an extensive area of volcanic flood basalt. The dark, tree-covered area at the

Figure 4.12 Low oblique photograph (from Skylab), eastern Idaho and northwestern Wyoming (including Yellowstone and Grand Teton National Parks), late afternoon, midwinter, scale approximately 1 : 5,000,000 at photo center, black and white reproduction of color original. (NASA image.)

upper right is Yellowstone National Park. Below and to the left of Yellowstone Park are the Grand Teton mountains and "Jackson Hole." The tilted sedimentary rocks of the Wyoming Range and Salt River Range can be seen in the lower left quadrant, and the glaciated Wind River Range at lower right. Side-looking radar images (see Chapter 8) often provide a relatively low angle illumination that accentuates such topographic features.

Many interpreters use a *Ronchi grid* for lineament mapping. The Ronchi grid is a diffraction grating commonly ruled with 78 lines/cm that enhances or suppresses linear features on an image. When an image is viewed through the grid, with the grid held near the eye, linear features parallel to the grid appear diffused and suppressed, and linear features perpendicular to the grid are enhanced.

Many geologists believe that reflection in spectral bands around 1.6 and 2.2 μm is particularly important for mineral exploration and lithologic mapping. These bands cannot be photographed, but they can be sensed with various multispectral and hyperspectral scanners (see Chapters 5 and 6). Also, the examination of multiple narrow bands in the thermal infrared spectral region shows great promise in discriminating rock and mineral types.

Although monoscopic viewing is often suitable for lineament mapping, *lithologic mapping*, the mapping of rock units, is greatly enhanced by the use of stereoscopic viewing. As outlined in Section 4.16, the process of rock unit identification and mapping involves the stereoscopic examination of images to determine the topographic form (including drainage pattern and texture), image tone, and natural vegetative cover of the area under study. In unvegetated areas, many lithologic units are distinguishable on the basis of their topographic form and spectral properties. In vegetated areas, identification is much more difficult because the rock surface is obscured, and some of the more subtle aspects of changes in vegetative cover must be considered.

Because some 70 percent of the earth's land surface is covered with vegetation, a geobotanical approach to geologic unit discrimination is important. The basis of *geobotany* is the relationship between a plant's nutrient requirements and two interrelated factors—the availability of nutrients in the soil and the physical properties of the soil, including the availability of soil moisture. The distribution of vegetation often is used as an indirect indicator of the composition of the underlying soil and rock materials. A geobotanical approach to geologic mapping using remotely sensed images suggests a cooperative effort among geologists, soil scientists, and field-oriented botanists, each of whom should be familiar with remote sensing. An especially important aspect of this approach is the identification of vegetation anomalies related to mineralized areas. Geobotanical anomalies may be expressed in a number of ways: (1) anomalous distribution of species and/or plant communities, (2) stunted or enhanced growth and/or anomalously sparse or dense ground cover, (3) alteration of leaf pigment and/or physiographic processes that produce leaf color changes, and (4) anomalous changes in the phenologic cycle,

such as early foliage change or senescence in the fall, alteration of flowering periods, and/or late leaf flush in the spring. Such vegetation anomalies are best identified by analyzing images acquired several times during the year, with emphasis placed on the growing period, from leaf flush in the spring to fall senescence. Using this approach, "normal" vegetation conditions can be established, and anomalous conditions can be more readily identified.

Soil Mapping

Detailed soil surveys form a primary source of resource information about an area. Hence, they are used heavily in such activities as comprehensive land use planning. Understanding soil suitability for various land use activities is essential to preventing environmental deterioration associated with misuse of land. In short, if planning is to be an effective tool for guiding land use, it must be premised on a thorough inventory of the natural resource base; soil data are an essential facet of such inventories.

Detailed soil surveys are the product of an intensive study of soil resources by trained scientists. The delineation of soil units has traditionally utilized airphoto interpretation coupled with extensive field work. Soil scientists traverse the landscape on foot, identify soils, and delineate soil boundaries. This process involves the field examination of numerous soil profiles (cross sections) and the identification and classification of soil units. The soil scientist's experience and training are relied on to evaluate the relationship of soils to vegetation, geologic parent material, landform, and landscape position. Airphoto interpretation has been utilized since the early 1930s to facilitate the soil mapping process. Typically, panchromatic aerial photographs at scales ranging from 1:15,840 to 1:40,000 have been used as mapping bases.

Agricultural soil survey maps have been prepared for portions of the United States by the USDA since about the year 1900. Most of the soil surveys published since 1957 contain soil maps printed on a photomosaic base at a scale of 1:24,000, 1:20,000, or 1:15,840. Beginning in the mid-1980s, soil survey map information for many counties has been made available both as line maps and as digital files that can be incorporated into geographic information systems. The original purpose of these surveys was to provide technical assistance to farmers and ranchers for cropland and grazing operations. Soil surveys published since 1957 contain information about the suitability of each mapped soil unit for a variety of uses. They contain information for such purposes as estimating yields of common agricultural crops; evaluating rangeland suitability; determining woodland productivity; assessing wildlife habitat conditions; judging suitability for various recreational uses; and determining suitability for various developmental uses, such as highways, local streets and roads, building foundations, and septic tank absorption fields.

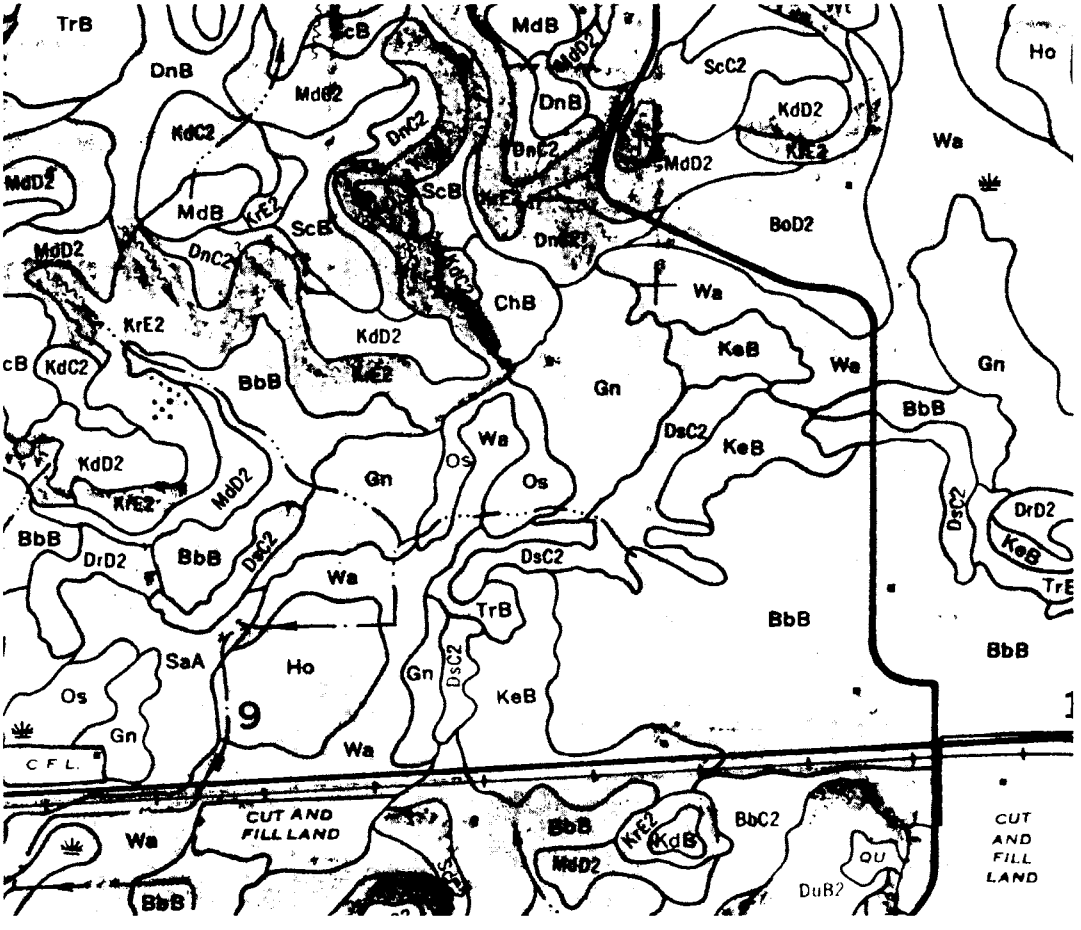

Figure 4.13 Portion of a USDA–ASCS soil map, Dane County, WI. Original scale 1:15,840 (4 in. = 1 mile). (From U.S. Department of Agriculture, 1977.)

The USDA Natural Resources Conservation Service (formerly the Soil Conservation Service) provides soil survey maps in digital form for many areas of the United States. Since 1994 it has provided nationwide detailed soil information by means of the *National Soil Information System*, an online soil attribute database system, available at http://nasis.nrcs.usda.gov.

A portion of a 1:15,840 scale USDA soil map printed on a photomosaic base is shown as Figure 4.13. Table 4.5 shows a sampling of the kind of soil information and interpretations contained in USDA soil survey reports. This map and table show that the nature of soil conditions and, therefore, the appropriateness of land areas for various uses can vary greatly over short distances. As with soil map data, much of the interpretive soil information (such as shown in Table 4.5) is available as computer-based files.

TABLE 4.5 Soil Information and Interpretation for Five Soils Shown in Figure 4.13

Map Unit (Figure 4.13)	Soil Name	Soil Description	Depth to Groundwater Table (cm)	Predicted Corn Yield (kg/ha)	Predicted Degree of Limitations for Use As		
					Septic Tank Absorption Fields	Dwellings with Basements	Sites for Golf Course Fairways
BbB	Batavia silt loam, gravelly substratum, 2–6% slope	100–200 cm silt over stratified sand and gravel	>150	8700	Moderate	Slight	Slight
Ho	Houghton muck, 0–2% slope	Muck at least 150 cm deep	0–30	8100 (when drained)	Very severe	Very severe	Severe
KrE2	Kidder soils, 20–35% slope	About 60 cm silt over sandy loam glacial till	>150	Not suited	Severe	Severe	Severe
MdB	McHenry silty loam, 2–6% slope	25–40 cm silt over sandy loam glacial till	>150	7000	Slight	Slight	Slight
Wa	Wacousta silty clay loam, 0–2% slope	Silty clay loam and silt loam glacial lakebed materials	0–30	7000	Very severe	Very severe	Severe

Source: From U.S. Department of Agriculture, 1977.

As described in Section 1.4, the reflection of sunlight from bare (unvegetated) soil surfaces depends on many interrelated factors, including soil moisture content, soil texture, surface roughness, the presence of iron oxide, and the organic matter content. A unit of bare soil may manifest significantly different image tones on different days, depending especially on its moisture content. Also, as the area of vegetated surfaces (e.g., leaves) increases during the growing season, the reflectance from the scene is more the result of vegetative characteristics than the soil type.

Plate 9 illustrates the dramatically different appearance of one agricultural field, approximately 15 ha in size, during one growing season. Except for a small area at the upper right, the entire field is mapped as one soil type by the USDA (map unit BbB, as shown in Figure 4.13 and described in Table 4.5). The soil parent materials in this field consist of glacial meltwater deposits of stratified sand and gravel overlain by 45 to 150 cm of loess (wind-deposited silt). Maximum relief is about 2 m and slope ranges from 0 to 6 percent. This field was planted to corn (*Zea mays* L.) in May and harvested in November.

Plates 9*a*, *b*, and *c* illustrate the change in surface moisture patterns visible on the cultivated soil over a span of 48 hours in early summer. During this period, the corn plants were only about 10 cm tall, and consequently most of the field surface was bare soil. The area received about 2.5 cm of rain on June 29. On June 30, when the photo in Plate 9*a* was exposed, the moist soil had a nearly uniform surface tone. By July 2 (9*c*), distinct patterns of dry soil surface (light image tone) could be differentiated from areas of wet soil surface (darker image tones). The dry areas have relatively high infiltration capacity and are slight mounds of 1 to 2 m relief. These topographic highs have very gentle slopes. Rainfall that does not infiltrate into the soil on these areas runs off onto lower portions of the landscape. These lower areas remain wet longer because they have relatively low infiltration capacity and receive runoff from the higher areas in addition to their original increment of rainfall.

Plates 9*d*, *e*, and *f* illustrate changes in the appearance of the corn crop during the growing season. By August 11 (9*d*), the corn had grown to a height of 2 m. Vegetation completely covered the soil surface and the field had a very uniform appearance. However, by September 17 (9*e*), distinct tonal patterns were again evident. Very little rain fell on this field during July, August, and early September, and growth of the corn during this period was dependent on moisture stored in the soil. In the dry areas, shown in light tan-yellow, the leaves and stalks of the corn were drying out and turning brown. In the wetter areas of pink and red photo colors, the corn plants were still green and continuing to grow. Note the striking similarity of the pattern of wet and dry soils in (9*c*) versus the "green" and brown areas of corn in (9*e*). The pattern seen in the September photograph (9*e*) persists in the October photograph (9*f*); however, there are larger areas of dry corn in October.

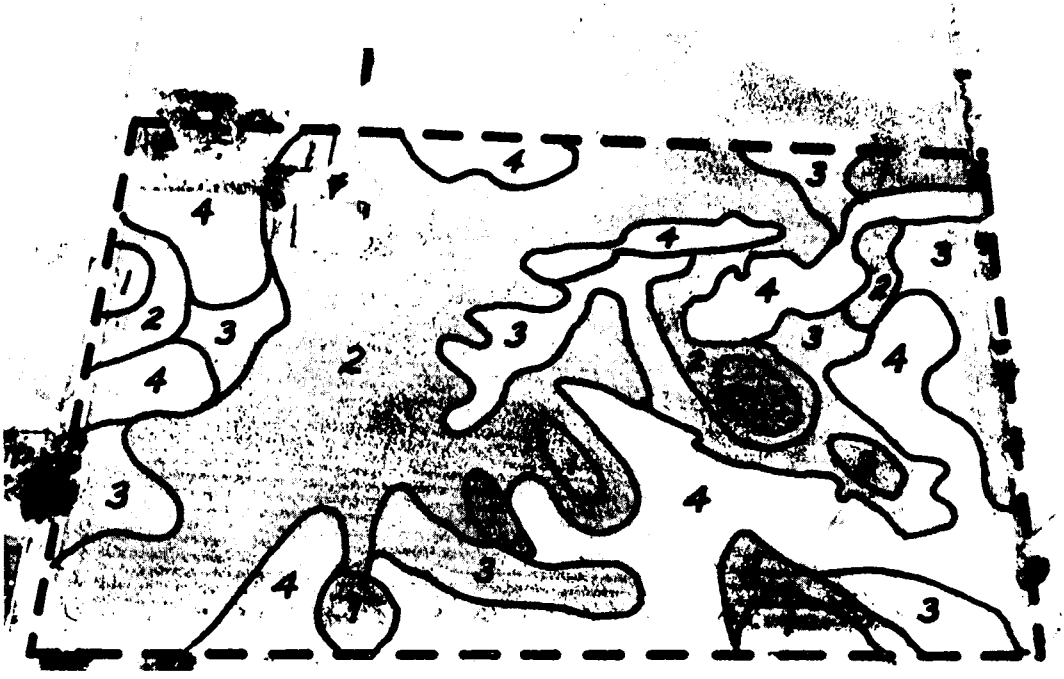

Figure 4.14 Oblique aerial photograph, September 17, with overlay showing four levels of soil moisture (see also Plate 9e), Dane County, WI. Scale approximately 1 : 3300 at photo center.

Based on these photographs, a soil scientist was able to divide the soil moisture conditions in this field into four classes, as shown in Figure 4.14. Field inspection of selected sites in each of the four units produced the information in Table 4.6. Note that the corn yield is more than 50 percent greater in unit 2 than in unit 4.

This sequence of photographs taken during one growing season illustrates that certain times of the year are better suited to image acquisition for soil mapping (and crop management) purposes than others. In any given region and season, the most appropriate dates will vary widely, depending on

TABLE 4.6 Selected Characteristics of the Four Soil Units Shown in Figure 4.14

Characteristic	Unit 1	Unit 2	Unit 3	Unit 4
Thickness of silt over sand and gravel	At least 150 cm	105–135 cm	90–120 cm	45–105 cm
Soil drainage class (see Section 4.16)	Somewhat poorly drained	Moderately well drained	Moderately well to well drained	Well drained
Average corn yield, kg/ha)	Not sampled	9100	8250	5850

many factors, including temperature, rainfall, elevation, vegetative cover, and soil infiltration characteristics.

4.6 AGRICULTURAL APPLICATIONS

When one considers the components involved in studying the worldwide supply and demand for agricultural products, the applications of remote sensing in general are indeed many and varied. The scope of the physical, biological, and technological problems facing modern agriculture is an extremely broad one that is intimately related with worldwide problems of population, energy, environmental quality, climate, and weather. These factors are in turn influenced by human values and traditions and economic, political, and social systems. We make no attempt here to look at the "big picture" of how remote sensing is used in agriculture. Instead, we consider the direct application of visual image interpretation in three selected areas: crop-type classification, "precision farming," and crop management in general.

Crop-type classification (and area inventory) through visual image interpretation is based on the premise that specific crop types can be identified by their spectral response patterns and image texture. Successful identification of crops requires a knowledge of the developmental stages of each crop in the area to be inventoried. This information is typically summarized in the form of a *crop calendar* that lists the expected developmental status and appearance of each crop in an area throughout the year. Because of changes in crop characteristics during the growing season, it is often desirable to use images acquired on several dates during the growing cycle for crop identification. Often, crops that appear very similar on one date will look quite different on another date, and several dates of image acquisition may be necessary to obtain unique spectral response patterns from each crop type. When photographic methods are employed, the use of color and color infrared films provides advantages over the use of panchromatic film because of the increased spectral information of the color materials. Also, stereoscopic coverage provides the advantage of being able to use plant height in the discrimination process.

When only broad classes of crops are to be inventoried, single-date panchromatic photography may be sufficient. Table 4.7 shows a dichotomous airphoto interpretation key developed for the identification of major crop and land cover types in agricultural areas of California using medium-scale panchromatic aerial photographs. This tabular style of dichotomous key is an alternative format to the style shown in Figure 4.3. This generalized classification scheme does not attempt to distinguish among various types of vine and bush crops, row crops, or continuous cover crops. When specific crop types are to be inventoried, a more detailed interpretation key employing multidate aerial imaging, using color and/or color infrared film, or multispectral imagery may be required.

TABLE 4.7 Dichotomous Airphoto Interpretation Key for Identification of Major Crop and Land Cover Types in Agricultural Areas of California for Use with Summertime Panchromatic Aerial Photographs at a Scale of 1:15,000

1. Vegetation or soil clearly discernible on photographs	See 2
1. Vegetation and soil either absent or largely obscured by artificial structures, bare rock, or water	Nonproductive lands
2. Cultivation pattern absent; field boundaries irregularly shaped	See 3
2. Cultivation pattern present; field boundaries regularly shaped	See 5
3. Trees present, covering most of ground surface	Timberland
3. Trees absent or widely scattered; ground surface covered by low-lying vegetation	See 4
4. Crowns of individual plants discernible; texture coarse and mottled	Brushland
4. Crowns of individual plants not discernible; texture fine	Grassland
5. Crop vegetation absent	Fallow
5. Crop vegetation present	See 6
6. Crowns of individual plants clearly discernible	See 7
6. Crowns of individual plants not clearly discernible	See 8
7. Alignment and spacing of individual trees at intervals of 6 m or more	Orchards
7. Alignment and spacing of individual plants at intervals of 3 m or more	Vine and bush crops
8. Rows of vegetation clearly discernible, usually at intervals of 0.5–1.5 m	Row crops
8. Rows of vegetation not clearly discernible; crops forming a continuous cover before reaching maturity	See 9
9. Evidence of use by livestock present; evidence of irrigation from sprinklers or ditches usually conspicuous	Irrigated pasture crops
9. Evidence of use by livestock absent; evidence of irrigation from sprinklers or ditches usually inconspicuous or absent; bundles of straw or hay and harvesting marks frequently discernible	Continuous cover crops (small grains, hay, etc.)

Source: From National Research Council, 1970.

Figure 4.15 illustrates some of the factors important to visual image interpretation for crop identification. The photographs shown in this figure are black and white reproductions of color infrared originals covering the same area on two different dates during the same growing season. The area shown is part of an experimental farm located in southern Minnesota. The crops present are alfalfa, corn, sunflowers, soybeans, and wheat. The photograph

shown in (*a*) was taken during the early summer; the stereopair shown in (*b*) was taken in the late summer. Collectively, these images demonstrate the importance of date of image acquisition, photo tone and texture, and stereoscopic coverage in the crop discrimination process.

Precision farming or "precision crop management (PCM)," has been defined as an *information- and technology-based agricultural management system to identify, analyze, and manage site-soil spatial and temporal variability within fields for optimum profitability, sustainability, and protection of the environment* (Robert, 1997). An essential component of precision farming, or PCM, is the use of *variable rate technology* (*VRT*). This refers to the application of various crop production inputs on a location-specific basis. Variable rate equipment has been developed for a range of materials, including herbicide, fertilizer, water, insecticide, and seeds. The within-field position of such equipment is typically determined through the use of GPS technology. In turn, the GPS guidance system is often linked to a GIS, which provides the "intelligence" necessary to determine the rate at which a given material should be applied at a given location within a field. The data used to determine application rates for various materials usually come from a range of sources (e.g., remote sensing images, detailed soil mapping, historical yield records, equipment-mounted sensors).

Historically, agricultural fields have been managed as if they were homogeneous units. That is, one set of management practices would be used for the entire field. For example, one fertilizer rate or one herbicide rate would be used across the entire field. These rates would tend to be chosen for the most productive soil occurring in the field, meaning many portions of the field would be overtreated or undertreated. The goal of PCM is to target application rates to the location-specific conditions occurring within a field and thereby maximize profitability and minimize energy waste and surface and ground water pollution.

Plate 9 illustrated how variable the soil-site conditions can be within a single field in terms of the surface moisture patterns observable prior to corn crop development (9*a-c*) and following an extended period with little rainfall as the corn crop matured (9*e*).

Figure 4.16 illustrates another cornfield that manifests a great deal of spatial variability in terms of crop development. Multiple factors contribute to the anomalous tones occurring across this field. Among these are planter skips (small bright rectangles), drought stress (irregular bright areas), weeds (difficult to see in this black and white reproduction), and water erosion (narrow dark ditch trending from lower center toward upper right).

Whereas PCM is a relatively recent development, the utility of image interpretation in *crop management* in general has been documented for many years. For example, large-scale images have proven useful for documenting deleterious conditions due to crop disease, insect damage, plant stress from other causes, and disaster damage. The most successful applications have uti-

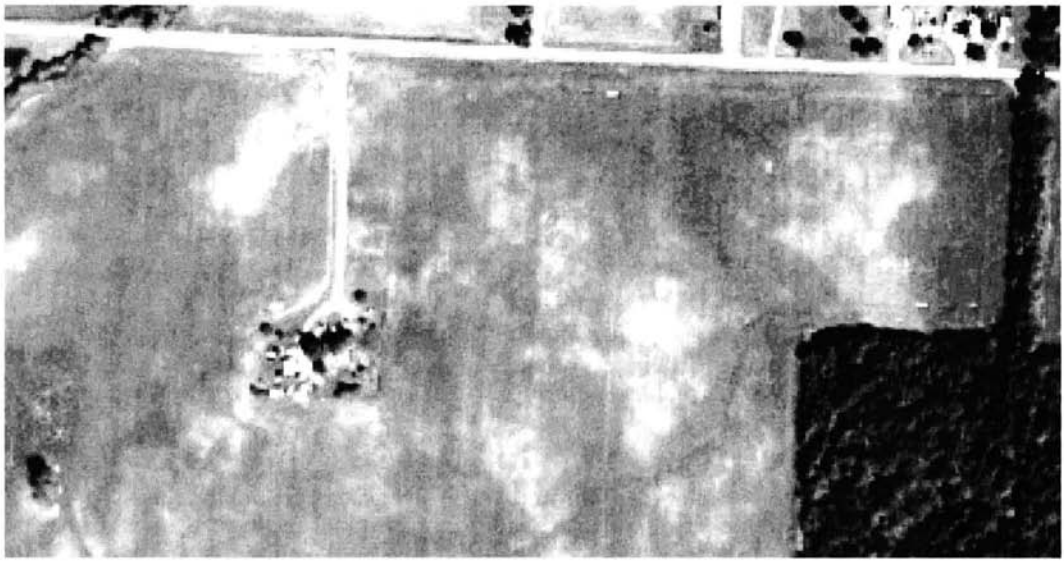

Figure 4.16 Anomalous growth conditions within a cornfield. Black and white rendering of a color composite acquired with 1 m ground resolution cell size per pixel, east-central Indiana, early August. (Courtesy Purdue University Laboratory for Applications of Remote Sensing and Emerge. Copyright © 1998.)

lized large-scale color infrared aerial photographs taken on various dates. In addition to "stress detection," such photographs can provide many other forms of information important to crop management. Table 4.8 lists the kinds of information potentially available from large-scale color infrared aerial photographs obtained at different times in the growing season.

Some of the plant diseases that have been detected using visual image interpretation are southern corn leaf blight, bacterial blight of field beans, potato wilt, sugar beet leaf spot, stem rust of wheat and oats, late blight fungus of potatoes, fusarium wilt and downy mildew in tomato and watermelon, powdery mildew on lettuce and cucumber, powdery mildew in barley, root rotting fungus in cotton, vineyard *Armillaria mellea* soil fungus, pecan root rot, and coconut wilt. Some types of insect damage that have been detected are aphid infestation in corn fields, phylloxera root feeding damage to vineyards, red mite damage to peach tree foliage, and plant damage due to fire ants, harvester ants, leaf cutting ants, army worms, and grasshoppers. Other types of plant damage that have been detected include those from moisture stress, iron deficiency, nitrogen deficiency, excessive soil salinity, wind and water erosion, rodent activity, road salts, air pollution, and cultivator damage.

Visual image interpretation for crop condition assessment is a much more difficult task than visual image interpretation for crop type and area inventory. Ground reference data are essential, and in most studies to date,

TABLE 4.8 Typical Crop Management Information Potentially Obtainable from Large-Scale Color Infrared Aerial Photographs

Preplanting	Study variations in soil surface moisture, texture, and organic content in bare fields. Monitor residue and check conditions of terraces, grass waterways, and other surface features.
Plowing/Planting	Determine plowing and planting progress, poorly or excessively drained areas, runoff and erosion problems, and tile line locations.
Emergence	Detect delayed emergence and low plant density, looking for insect, disease, or weather problems, planting failure due to malfunctioning equipment, human error in planting, and effectiveness of preemergent herbicides. Determine necessary remedial measures (such as replanting).
Mid-growing Season	Check on stand growth and development through the growing season, looking for evidence of plant loss or damage due to adverse moisture conditions, misapplication of chemicals, insects, diseases, eroded topsoil, nitrogen deficiencies, and problems in irrigation distribution. Monitor effectiveness of herbicide treatment and drainage.
Preharvest	Check stand condition and acreage to be harvested, looking for lodging, significant weed infestations, or other potential problems for harvesting operations. Check for uniformity of ripening.
Postharvest	Determine total area harvested. Check field cover in harvested areas for weed and volunteer regrowth, erosion, and soil moisture problems.
As Required	Document special situations such as flooding, drought, frost, fire, hail storms, tornadoes, hurricanes, or other problems.

Source: Adapted from Baber and Flowerday, 1979.

comparisons have been made between healthy and stressed vegetation growing in adjacent fields or plots. Under these conditions, interpreters might discriminate between finer differences in spectral response than would be possible in a noncomparative analysis—that is, the level of success would be lower if they did not know a stress existed in an area. It would also be more difficult to differentiate among the effects of disease, insect damage, nutrient deficiencies, or drought, from variations caused by plant variety, plant maturity, planting rate, or background soil color differences. Because many stress effects are most apparent during dry spells, images should not be acquired too soon after rainy weather. (Note that Plate 6 shows color infrared aerial photographs and multiband video images of cotton fields with harvester ant damage and poor growth in areas with saline soils.)

In addition to crop damage due to disease, insects, and various other stresses, crop damage resulting from such disasters as flooding, drought, frost, fire, hailstorms, tornados, and hurricanes can be assessed by visual image interpretation.

Until the early 2000s, the overwhelming majority of applications of image interpretation to precision crop management involved airborne remote sensing as opposed to the use of satellite images. The reason for this is that the satellite systems available to that point lacked the spatial resolution, frequency of coverage, and data delivery timeliness required for crop management. With the increased availability of high resolution satellite data collected by pointable systems with very rapid data supply rates (such systems are covered in Chapter 6), the use of satellite data has greatly increased.

4.7 FORESTRY APPLICATIONS

Forestry is concerned with the management of forests for wood, forage, water, wildlife, and recreation. Because the principal raw product from forests is wood, forestry is especially concerned with timber management, maintenance and improvement of existing forest stands, and fire control. Forests of one type or another cover nearly a third of the world's land area. They are distributed unevenly and their resource value varies widely.

Visual image interpretation provides a feasible means of monitoring many of the world's forest conditions. We will be concerned principally with the application of visual image interpretation to tree species identification, studying harvested areas, timber cruising, and the assessment of disease and insect infestations.

The visual image interpretation process for *tree species identification* is generally more complex than for agricultural crop identification. A given area of forest land is often occupied by a complex mixture of many tree species, as contrasted with agricultural land where large, relatively uniform fields typically are encountered. Also, foresters may be interested in the species composition of the "forest understory," which is often blocked from view on aerial and satellite images by the crowns of the large trees.

Tree species can be identified on aerial and satellite images through the process of elimination. The first step is to eliminate those species whose presence in an area is impossible or improbable because of location, physiography, or climate. The second step is to establish which groups of species do occur in the area, based on a knowledge of the common species associations and their requirements. The final stage is the identification of individual tree species using basic image interpretation principles.

The image characteristics of shape, size, pattern, shadow, tone, and texture, as described in Section 4.2, are used by interpreters in tree species identification. Individual tree species have their own characteristic crown *shape* and *size*. As illustrated in Figures 4.17 and 4.18, some species have rounded crowns,

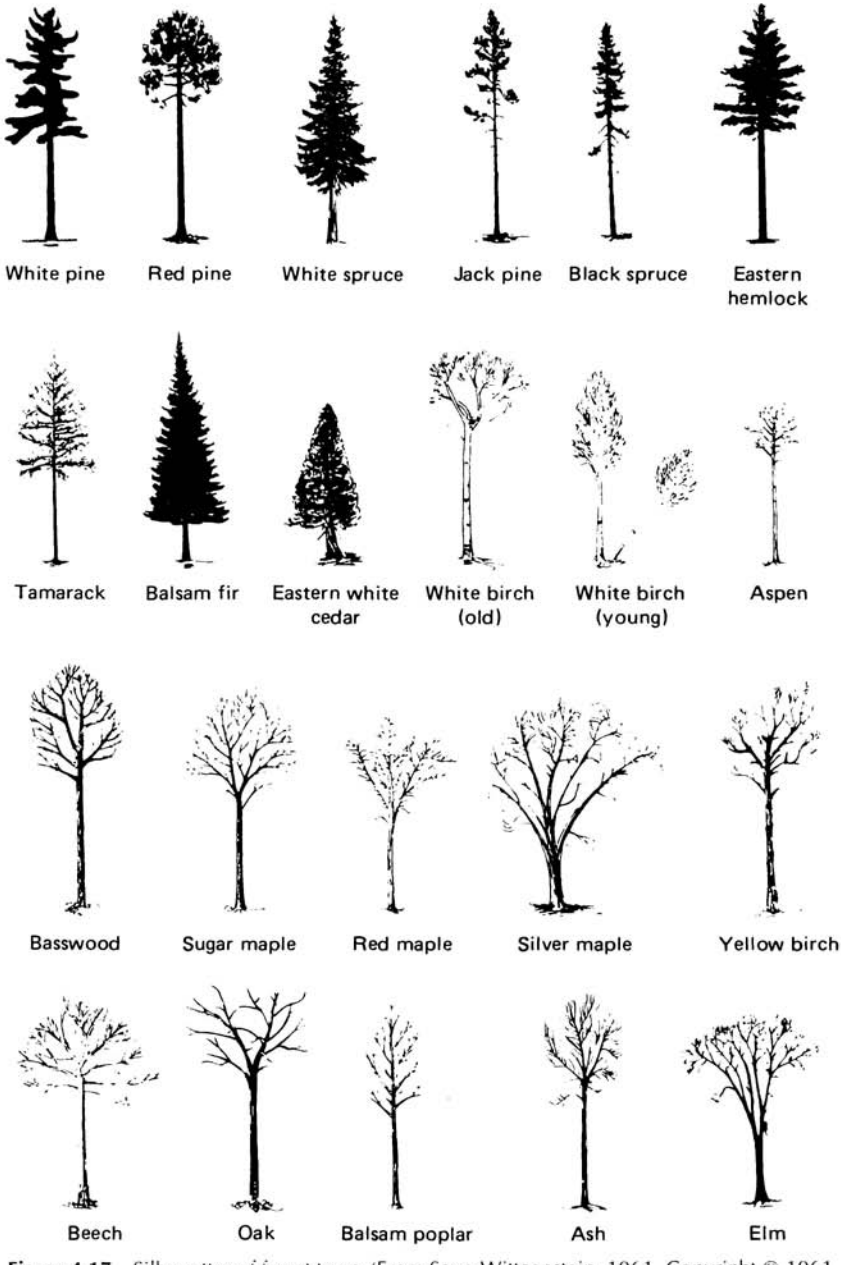

Figure 4.17 Silhouettes of forest trees. (From Sayn-Wittgenstein, 1961. Copyright © 1961, American Society of Photogrammetry. Reproduced with permission.)

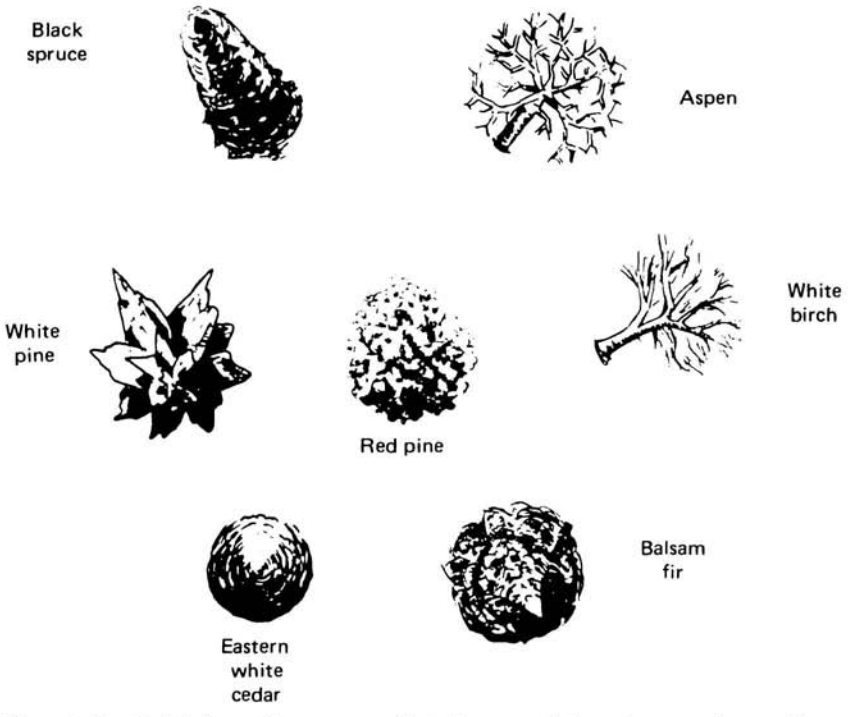

Figure 4.18 Aerial views of tree crowns. Note that most of these trees are shown with radial displacement. (From Sayn-Wittgenstein, 1961. Copyright © 1961, American Society of Photogrammetry. Reproduced with permission.)

some have cone-shaped crowns, and some have star-shaped crowns. Variations of these basic crown shapes also occur. In dense stands, the arrangement of tree crowns produces a *pattern* that is distinct for many species. When trees are isolated, *shadows* often provide a profile image of trees that is useful in species identification. Toward the edges of aerial images, relief displacement can afford somewhat of a profile view of trees. *Image tone* depends on many factors, and it is not generally possible to correlate absolute tonal values with individual tree species. Relative tones on a single image, or a group of images, may be of great value in delineating adjacent stands of different species. Variations in crown *texture* are important in species identification. Some species have a tufted appearance, others appear smooth, and still others look billowy. As mentioned in Section 4.2, image texture is very scale dependent.

Figure 4.19 illustrates how the above-described image characteristics can be used to identify tree species. A pure stand of black spruce (outlined area) surrounded by aspen is shown in Figure 4.19. Black spruce are coniferous trees with very slender crowns and pointed tops. In pure stands, the canopy is regular in pattern and the tree height is even or changes gradually with the quality of the site. The crown texture of dense black spruce stands is carpetlike

in appearance. In contrast, aspen are deciduous trees with rounded crowns that are more widely spaced and more variable in size and density than the spruce trees. The striking difference in image texture between black spruce and aspen is apparent in Figure 4.19.

The process of tree species identification using visual image interpretation is not as simple as might be implied by the straightforward examples shown in these figures. Naturally, the process is easiest to accomplish when dealing with pure, even-aged stands. Under other conditions, species identification can be as much of an art as a science. Identification of tree species has, however, been very successful when practiced by skilled, experienced interpreters. Field visitation is virtually always used to aid the interpreter in the type map compilation process.

The extent to which tree species can be recognized on aerial photographs is largely determined by the scale and quality of the images, as well as the variety and arrangement of species on the image. The characteristics of tree form, such as crown shape and branching habit, are heavily used for identification on large-scale images. The interpretability of these characteristics becomes progressively less as the scale is decreased. Eventually, the characteristics of individual trees become so indistinct that they are replaced by overall stand characteristics in terms of image tone, texture, and shadow pattern. On images at extremely large scales (such as 1 : 600), most species can be recognized almost entirely by their morphological characteristics. At this scale, twig structure, leaf arrangement, and crown shape are important clues to species recognition. At scales of 1 : 2400 to 1 : 3000, small and medium branches are still visible and individual crowns can be clearly distinguished. At 1 : 8000, in-

dividual trees can still be separated, except when growing in dense stands, but it is not always possible to describe crown shape. At 1:15,840 (Figure 4.19), crown shape can still be determined from tree shadows for large trees growing in the open. At scales smaller than 1:20,000, individual trees generally cannot be recognized when growing in stands, and stand tone and texture become the important identifying criteria (Sayn-Wittgenstein, 1961). This is particularly true when satellite data sources are employed.

Historically, the format most widely used for tree species identification has been black and white photographic paper prints at a scale of 1:15,840 to 1:24,000. Black and white infrared paper prints are especially valuable in separating evergreen from deciduous types. However, color and color infrared films, as well as digital frame cameras and video cameras and also high resolution multiband satellite images, are being used with increasing frequency.

It is difficult to develop visual image interpretation keys for tree species identification because individual stands vary considerably in appearance depending on age, site conditions, geographic location, geomorphic setting, and other factors. However, a number of elimination keys have been developed for use with aerial photographs that have proven to be valuable interpretive tools when utilized by experienced image interpreters. Tables 4.9 and 4.10 are examples of such keys.

Phenological correlations are useful in tree species identification. Changes in the appearance of trees in the different seasons of the year sometimes enable discrimination of species that are indistinguishable on single dates. The most obvious example is the separation of deciduous and evergreen trees that is easily made on images acquired when the deciduous foliage has fallen. This distinction can also be discerned on spring images acquired shortly after the flushing of leaves or on fall images acquired after the trees have turned color. For example, in the summer, panchromatic and color photographs show little difference in tone between deciduous and evergreen trees (Figure 1.9*a*). Differences in tones are generally quite striking, however, on summer color infrared and black and white infrared photographs (Figure 1.9*b*).

In spring images, differences in the time at which species leaf out can provide valuable clues for species recognition. For example, trembling aspen and white birch consistently are among the first trees to leaf out, while the oaks, ashes, and large-tooth aspen are among the last. These two groups could be distinguished on images acquired shortly after trembling aspen and white birch have leafed out. Tone differences between hardwoods, which are small during the summer, become definite during the fall, when some species turn yellow and others red or brown. The best species distinctions in the fall are obtained on images acquired when fall coloring is at its peak, rather than when some trees have lost their leaves (Sayn-Wittgenstein, 1961).

TABLE 4.9 Airphoto Interpretation Key for the Identification of Hardwoods in Summer

1. Crowns compact, dense, large	
2. Crowns very symmetrical and very smooth, oblong or oval; trees form small portion of stand	Basswood
2. Crowns irregularly rounded (sometimes symmetrical), billowy, or tufted	
3. Surface of crown not smooth, but billowy	Oak
3. Crowns rounded, sometimes symmetrical, smooth surfaced	Sugar maple,[a] beech[a]
3. Crowns irregularly rounded or tufted	Yellow birch[a]
1. Crowns small or, if large, open or multiple	
6. Crowns small or, if large, open and irregular, revealing light-colored trunk	
7. Trunk chalk white, often forked; trees tend to grow in clumps	White birch
7. Trunk light, but not white, undivided trunk reaching high into crown, generally not in clumps	Aspen
6. Crown medium sized or large; trunk dark	
8. Crown tufted or narrow and pointed	
9. Trunk often divided, crown tufted	Red maple
9. Undivided trunk, crown narrow	Balsam poplar
8. Crowns flat topped or rounded	
10. Crowns medium sized, rounded; undivided trunk; branches ascending	Ash
10. Crowns large, wide; trunk divided into big spreading branches	
11. Top of crown appears pitted	Elm
11. Top of crown closed	Silver maple

Source: From Sayn-Wittgenstein, 1961. Copyright © 1961, American Society of Photogrammetry. Reproduced with permission.

[a]A local tone-key showing levels 4 and 5 is usually necessary to distinguish these species.

Harvested areas are clearly visible on many aerial and satellite images. Figure 4.20 shows a satellite image illustrating timber harvesting in the northwestern United States. Here the darker toned areas are dense stands of Douglas fir and the lighter toned areas are recently cleared areas consisting of tree stumps, shrubs, and various grasses, in areas where essentially all trees have been removed during the harvesting operations. Mottled, intermediate toned areas have been replanted with Douglas fir trees and are at an intermediate growth stage. (For other examples of satellite images showing timber harvesting, see Chapters 6 and 8.)

Visual image interpretation is used extensively for "timber cruising." The primary objective of such operations is to determine the volume of timber that might be harvested from an individual tree or (more commonly) a stand

TABLE 4.10 Airphoto Interpretation Key for the Identification of Conifers

1. Crowns small; if large, then definitely cone shaped	
Crowns broadly conical, usually rounded tip; branches not prominent	Cedar
Crowns narrow, often cylindrical; trees frequently grow in swamps	Swamp-type black spruce
Crowns conical, deciduous, very light toned in fall, usually associated with black spruce	Tamarack
Crowns narrowly conical, very symmetrical, top pointed; branches less prominent than in white spruce	Balsam fir
Crowns narrowly conical; top often appears obtuse on photograph (except northern white spruce); branches more prominent than in balsam fir	White spruce, black spruce (except swamp type)
Crowns irregular, sometimes with pointed top; have thinner foliage and smoother texture than spruce and balsam fir	Jack pine
1. Crowns large and spreading, not narrowly conical; top often not well defined	
2. Crowns very dense, irregular or broadly conical	
Individual branches very prominent; crown usually irregular	White pine
Individual branches rarely very prominent; crown usually conical	Eastern hemlock
2. Crowns open, oval (circular in plain view)	Red pine

Source: From Sayn-Wittgenstein, 1961. Copyright © 1961, American Society of Photogrammetry. Reproduced with permission.

of trees. To be successful, image-based timber cruising requires a highly skilled interpreter working with both aerial or satellite and ground data. Image measurements on individual trees or stands are statistically related to ground measurements of tree volume in selected plots. The results are then extrapolated to large areas. The image measurements most often used are (1) tree height or stand height, (2) tree-crown diameter, (3) density of stocking, and (4) stand area.

The height of an individual tree, or the mean height of a stand of trees, is normally determined by measuring relief displacement or image parallax. The task of measuring tree-crown diameters is no different from obtaining other distance measurements on images. Ground distances are obtained from image distances via the scale relationship. The process is expedited by the use of special-purpose overlays similar to dot grids. Overlays are also used to measure the density of stocking in an area in terms of the crown closure or percentage of the ground area covered by tree crowns. Alternatively, some measure of the number of individual crowns per unit area may be made. The accuracy of these measurements is influenced by such factors as the band(s)

in which the image is sensed, the season of image acquisition, and the amount of shadow in the images.

Once data on individual trees or stands are extracted from images, they are statistically related (using multiple regression) with ground data on timber volume to prepare *volume tables*. The volume of *individual* trees is normally determined as a function of species, crown diameter, and height. This method of timber volume estimation is practical only on large-scale images and is normally used to measure the volume of scattered trees in open areas. More frequently, *stand volumes* are of interest. Stand volume tables are normally based on combinations of species, height, crown diameter, and crown closure (Table 4.11).

Visual image interpretation has been used in many instances to survey forest and urban shade tree damage from disease and insect infestations as well as from other causes. A variety of image bands and scales have been utilized for damage surveys. Although panchromatic photographs have often been used, the most successful surveys have typically used medium- or large-scale color and color infrared photographs (digital frame cameras and video cameras can also be used, as well as high resolution multiband satellite images). Some types of tree disease damage due to bacteria, fungus, virus, and other

TABLE 4.11 Estimated Volume of Kentucky Hardwood Stands

Average Stand Height (m)	Average Crown Diameter (m)	Estimated Volume (m^3/ha) at Selected Crown Closures								
		15%	25%	35%	45%	55%	65%	75%	85%	95%
9	3–4	21	26	30	33	36	40	44	49	54
12	3–4	25	30	35	39	42	46	49	53	56
15	3–4	28	33	39	44	49	54	58	63	68
18	3–4	39	47	55	61	67	72	78	84	90
21	3–4	63	75	85	93	98	103	107	112	117
9	5–6	24	28	31	35	38	43	48	52	57
12	5–6	28	31	35	40	45	50	55	59	64
15	5–6	31	37	42	47	52	58	64	70	76
18	5–6	42	51	59	66	73	77	80	84	87
21	5–6	70	80	91	98	105	108	112	115	119
24	5–6	105	114	122	128	133	138	142	147	152
12	7–8	35	44	52	59	66	72	78	84	90
15	7–8	42	52	63	70	77	83	89	94	100
18	7–8	63	73	84	89	94	99	104	108	113
21	7–8	94	103	112	117	122	127	132	136	141
24	7–8	122	133	143	149	154	159	163	168	173
27	7–8	155	165	175	180	185	190	195	199	204
30	7–8	190	200	210	215	220	224	227	231	234
12	9+	59	72	84	89	94	99	104	108	113
15	9+	73	84	94	100	105	110	114	119	124
18	9+	91	101	110	115	120	125	130	135	140
21	9+	119	129	138	145	150	155	160	165	170
24	9+	150	159	168	175	182	186	190	195	200
27	9+	182	190	200	205	210	215	220	225	230
30	9+	213	222	231	236	241	245	248	252	255
33	9+	252	259	266	271	276	281	286	290	295

Source: Adapted from U.S. Department of Agriculture, 1978.

agents that have been detected using visual image interpretation are ash dieback, beech bark disease, Douglas fir root rot, Dutch elm disease, maple dieback, oak wilt, and white pine blister rust. Some types of insect damage that have been detected are those caused by the balsam wooly aphid, black-headed budworm, Black Hills bark beetle, Douglas fir beetle, gypsy moth larva, pine butterfly, mountain pine beetle, southern pine beetle, spruce budworm, western hemlock looper, western pine beetle, and white pine weevil. Other types of forest damage that have been detected include those resulting from air pollution (e.g., ozone, sulfur dioxide, "smog"), animals (e.g., beaver, deer, porcupine), fire, frost, moisture stress, soil salinity, nutrient imbalance, and storms.

In this discussion we have highlighted the application of visual image interpretation to tree species identification, studying harvested areas, timber cruising, and forest damage assessment. However, the forest management applications of visual image interpretation extend far beyond the scope of these four activities. Additional applications include such tasks as forest land appraisal, timber harvest planning, monitoring logging and reforestation, planning and assessing applications of herbicides and fertilizer in forest stands, assessing plant vigor and health in forest nurseries, mapping "forest fuels" to assess fire potential, planning fire suppression activities, assessing potential slope failures and soil erosion, planning forest roads, inventorying forest recreation resources, censusing wildlife and assessing wildlife habitat, and monitoring vegetation regrowth in fire lanes and power line rights-of-way.

Again, the success of virtually all of the above applications is premised on the existence of high quality reference data to aid in the interpretation. The use of aerial and satellite images and "conventional" ground methods of observation and measurement are typically closely intertwined. For example, timber volume inventories are basically premised on extensive ground measurement in sample plots (of tree volumes), but images are used to stratify the area to be inventoried and establish the location of these plots (typically based on interpreted tree type, stand area, and stocking density information). Thus, the image interpretation process complements, rather than replaces, the field activities.

4.8 RANGELAND APPLICATIONS

Rangeland has historically been defined as land where the potential natural vegetation is predominantly grasses, grasslike plants, forbs, or shrubs and where animal grazing was an important influence in its precivilization state. Rangelands not only provide forage for domestic and wild animals, they also represent areas potentially supporting land uses as varied as intensive agriculture, recreation, and housing.

Rangeland management utilizes rangeland science and practical experience for the purpose of the protection, improvement, and continued welfare of the basic rangeland resources, including soils, vegetation, endangered plants and animals, wilderness, water, and historical sites.

Rangeland management places emphasis on the following: (1) determining the suitability of vegetation for multiple uses, (2) designing and implementing vegetation improvements, (3) understanding the social and economic effects of alternative land uses, (4) controlling range pests and undesirable vegetation, (5) determining multiple-use carrying capacities, (6) reducing or eliminating soil erosion and protecting soil stability, (7) reclaiming soil and vegetation on disturbed areas, (8) designing and controlling livestock grazing systems, (9) coordinating rangeland management activities with other resource managers, (10) protecting and maintaining environmental

quality, (11) mediating land use conflicts, and (12) furnishing information to policymakers (Heady and Child, 1994).

Given the expanse and remoteness of rangelands and the diversity and intensity of pressures upon them, visual image interpretation has been shown to be a valuable range management tool. A physical-measurement-oriented list of range management activities that have some potential for being accomplished by image interpretation techniques includes: (1) inventory and classification of rangeland vegetation, (2) determination of carrying capacity of rangeland plant communities, (3) determination of the productivity of rangeland plant communities, (4) condition classification and trend monitoring, (5) determination of forage and browse utilization, (6) determination of range readiness for grazing, (7) kind, class, and breed of livestock using a range area, (8) measurement of watershed values, including measurements of erosion, (9) making wildlife censuses and evaluations of rangelands for wildlife habitat, (10) evaluating the recreational use of rangelands, (11) judging and measuring the improvement potential of various range sites, and (12) implementing intensive grazing management systems (Tueller, 1996). Table 4.12 outlines the appropriate rangeland management uses of imagery of various scales.

TABLE 4.12 Appropriate Rangeland Management Uses of Aerial and Satellite Imagery of Various Scales

Imagery Scale	Rangeland Management Uses
1:100 to 1:500	Species identification, including grasses and seedlings, identification and measurement of erosion features, forage production estimates, rodent activities in the surface soil, assessment of the amounts of other surface features such as litter, and wildlife habitat assessment.
1:600 to 1:2000	Species measurements, erosion estimates over larger land areas, condition and trend assessment, production and utilization estimates, and wildlife habitat assessment.
1:5000 to 1:10,000	Detailed vegetation mapping, condition and trend assessment, production and utilization estimates, and wildlife habitat assessment.
1:15,000 to 1:30,000	Vegetation mapping at the habitat-type or ecological site level, allotment management planning, and planning for multiple use, including wildlife habitat assessment.
1:30,000 to 1:80,000	Planning for range management, vegetation and soil unit mapping on a pasture or allotment basis, and multiple-use planning, including wildlife habitat mapping.
1:100,000 to 1:2,500,000	Synoptic views for planning rangeland use and mapping large vegetation zones covering large areas such as entire mountain ranges.

Source: Adapted from Tueller, 1996.

4.9 WATER RESOURCE APPLICATIONS

Whether for irrigation, power generation, drinking, manufacturing, or recreation, water is one of our most critical resources. Visual image interpretation can be used in a variety of ways to help monitor the quality, quantity, and geographic distribution of this resource. In this section, we are concerned principally with the use of visual image interpretation in water pollution detection, lake eutrophication assessment, and flood damage estimation. Before describing each of these applications, let us review some of the basic properties of the interaction of sunlight with clear water.

In general, most of the sunlight that enters a clear water body is absorbed within about 2 m of the surface. The degree of absorption is highly dependent on wavelength. Near-infrared wavelengths are absorbed in only a few tenths of a meter of water, resulting in very dark image tones of even shallow water bodies on near-infrared images. Absorption in the visible portion of the spectrum varies quite dramatically with the characteristics of the water body under study. From the standpoint of the imaging of bottom details through clear water, the best light penetration is achieved between the wavelengths of 0.48 and 0.60 μm. Penetration of up to about 20 m in clear, calm ocean water has been reported in this wavelength band (Jupp et al., 1984; Smith and Jensen, 1998). Although blue wavelengths penetrate well, they are extensively scattered and an "underwater haze" results. Red wavelengths penetrate only a few meters.

The analysis of underwater features is often permitted by using imaging systems sensitive to at least the wavelengths of 0.48 to 0.60 μm. For example, excellent photographs of bottom details in clear ocean water have been obtained using both normal color and color infrared photography. White sand bottoms under clear ocean water will appear blue-green using normal color film and blue using color infrared film (with a yellow filter). Bottom details are somewhat sharper using color infrared film because the blue wavelengths are filtered out and, thus, the effects of "underwater haze" are minimized. With such photography, the color infrared film becomes essentially a two-layer film because there is almost no near-infrared reflection from the water and, therefore, virtually no image on the infrared-sensitive film layer.

Figure 4.21 illustrates the penetration of different wavelengths of sunlight into clear ocean water. The upper part of the photographs shows an exposed coral reef (varying amounts are exposed in the different frames due to wave action). The high infrared reflectance from the exposed coral results from the presence of algae that live in a symbiotic relationship with the coral. Most of the underwater reef consists of coral whose uppermost surfaces come to within about 0.3 m of the water surface. The keyhole-shaped area in the photo center has water depths ranging from very shallow near the dry white

sand beach at lower right to a maximum of about 2 m near the center of the round part of the keyhole (upper left part of the photos).

Water Pollution Detection

All naturally occurring water contains some impurities. Water is considered polluted when the presence of impurities is sufficient to limit its use for a given domestic and/or industrial purpose. Not all pollutants are the result of human activity. Natural sources of pollution include such things as minerals leached from soil and decaying vegetation. When dealing with water pollution, it is appropriate to consider two types of sources: point and nonpoint. *Point sources* are highly localized, such as industrial outfalls. *Nonpoint sources*, such as fertilizer and sediment runoff from agricultural fields, have large and dispersed source areas.

Each of the following categories of materials, when present in excessive amounts, can result in water pollution: (1) organic wastes contributed by domestic sewage and industrial wastes of plant and animal origin that remove oxygen from the water through decomposition; (2) infectious agents contributed by domestic sewage and by certain kinds of industrial wastes that may transmit disease; (3) plant nutrients that promote nuisance growths of aquatic plant life such as algae and water weeds; (4) synthetic-organic chemicals such as detergents and pesticides resulting from chemical technology that are toxic to aquatic life and potentially toxic to humans; (5) inorganic chemical and mineral substances resulting from mining, manufacturing processes, oil plant operations, and agricultural practices that interfere with natural stream purification, destroy fish and aquatic life, cause excessive hardness of water supplies, produce corrosive effects, and in general add to the cost of water treatment; (6) sediments that fill streams, channels, harbors, and reservoirs, cause abrasion of hydroelectric power and pumping equipment, affect the fish and shellfish population by blanketing fish nests, spawn, and food supplies, and increase the cost of water treatment; (7) radioactive pollution resulting from the mining and processing of radioactive ores, the use of refined radioactive materials, and fallout following nuclear testing; and (8) temperature increases that result from the use of water for cooling purposes by steam electric power plants and industries and from impoundment of water in reservoirs, have harmful effects on fish and aquatic life, and reduce the capacity of the receiving water to assimilate wastes.

It is rarely possible to make a positive identification of the type and concentration of a pollutant by visual image interpretation alone. However, it is possible to use visual image interpretation to identify the point at which a discharge reaches a body of water and to determine the general dispersion characteristics of its plume. In some instances, such as the case of sediment

Figure 4.21 *(Continued)*

suspended in water, it is possible to make valid observations about sediment concentrations using quantitative radiometry coupled with the laboratory analysis of selective water samples.

Sediment pollution is often clearly depicted on aerial and space images. Figure 4.22 is a space photograph showing the silt-laden waters of the Po River discharging into the Adriatic Sea. The seawater has a low reflectance of sunlight, similar to that for "Water (Clear)" shown in Figure 1.10. The spectral response pattern of the suspended solids resembles that of "Dry Bare Soil (Gray-Brown)" shown in Figure 1.10. Because the spectral response pattern of the suspended materials is distinct from that of the natural seawater, these two materials can be readily distinguished on the photograph.

When point-source pollutants—such as domestic and industrial wastes—enter natural water bodies, there is typically a dispersed plume similar to that shown in Figure 4.22. If pollutants have reflectance characteristics different from the water bodies, their mixing and dispersal can be traced on aerial photographs. Aerial photographs have been successfully used in the enforcement of antipollution laws. In such cases, it is normally mandatory that reference water samples be collected from within the plume and outside the plume coincident with the time of aerial photography. The aerial photographs can be used as evidence in court cases to establish the source of the pollutant samples collected. However, extreme care must be taken to follow the legal rules of evidence pertaining to photographic exhibits.

Materials that form films on the water surface, such as oil films, can also be detected through the use of aerial and satellite images. Oil enters the world's water bodies from a variety of sources, including natural seeps, municipal and industrial waste discharges, urban runoff, and refinery and shipping losses and accidents. Thick *oil slicks* have a distinct brown or black color. Thinner *oil sheens* and *oil rainbows* have a characteristic silvery sheen or iridescent color banding but do not have a distinct brown or black color. The principal reflectance differences between water bodies and oil films in the photographic part of the spectrum occur between 0.30 and 0.45 μm. Therefore, the best results are obtained when the imaging systems are sensitive to these wavelengths.

Normal color or ultraviolet aerial photography is often employed for the detection of oil films on water. Oil slicks on seawater can also be detected using imaging radar because of the dampening effect of oil slicks on waves (Chapter 8).

Lake Eutrophication Assessment

Water quality in inland lakes is often described in terms of *trophic state* (nutritional state). A lake choked with aquatic weeds or a lake with extreme-nuisance algal blooms is called a *eutrophic* (nutrient-rich) lake. A lake with

very clear water is called an *oligotrophic* (low nutrient, high oxygen) lake. The general process by which lakes age is referred to as *eutrophication*. Eutrophication is a natural process expressed in terms of geologic time. However, when influenced by human activity, the process is greatly accelerated and may result in "polluted" water conditions. Such processes are termed *cultural eutrophication* and are intimately related to land use/land cover.

What constitutes an unacceptable degree of eutrophication is a function of who is making the judgment. Most recreational users of water bodies prefer clear water free of excessive *macrophytes* (large aquatic plants) and *algae*. Swimmers, boaters, and water skiers prefer lakes relatively free of submersed macrophytes, while persons fishing for bass and similar fish generally prefer some macrophytes. Large concentrations of blue-green algae have an unpleasant odor that is offensive to most people, especially during "blooms," or periods following active algal growth. Green algae tend to be less bothersome, unless present in large quantities.

The use of visual image interpretation coupled with selective field observations is an effective technique for mapping aquatic macrophytes. Macrophyte community mapping can be aided by the use of image interpretation keys. More detailed information regarding total plant biomass or plant density can often be achieved by utilizing quantitative technique (Chapter 7). Airphoto interpretation has been used to economically plan and monitor operations such as mechanical harvesting or chemical treatment of weeds.

Concentrations of free-floating algae are a good indicator of a lake's trophic status. Excessive concentrations of blue-green algae are especially prevalent under eutrophic conditions. Seasonally, blooms of blue-green algae occur during warm water conditions in late summer, whereas diatoms are more common in the cold water of spring and fall. Green algae are typically present at any point in the seasonal cycle of lakes. Because the different broad classes of algae have somewhat different spectral response patterns, they can be distinguished by aerial and space imaging. However, the wavelengths corresponding to peak reflectance of blue-green and green algae are often close together, and the most positive results can be obtained using narrow band multiband photography with filters selected to maximize the differences between the spectral response of the two algae types or by using multispectral or hyperspectral scanners (Chapter 5) with at least several bands in the 0.45- to 0.60-μm wavelength range. Algae blooms floating on or very near the water surface also reflect highly in the near infrared, as illustrated in Figure 4.23. (See Plate 31*b* for an additional example of algae blooms.)

Flood Assessment

The use of aerial and satellite images for *flood assessment* is illustrated in Figures 4.24 to 4.27. Such images can help determine the extent of flooding and

Figure 4.24 *(Continued)*

was taken 6 weeks after the flooding. Although the soil moisture conditions have returned to normal, the widespread crop damage is still very evident on this photograph. The streaked pattern of light-toned lines in the right-hand part clearly shows the direction of river flow at the time of flooding. Note that each light-toned streak is just downstream from a tree or group of trees and aligned with the direction of flow (the direction of flood water flow was from left to right in the right-hand part of this photograph).

Figure 4.25 illustrates the appearance of a flooding river from a satellite perspective. Here we see composite images of the near- and mid-infrared bands of Landsat TM data (Chapter 6), bands in which water appears very dark as contrasted with the surrounding vegetation. In (*a*) we see the Missouri River under low flow conditions, with a river width of about 500 m. In (*b*) we see a major flood in progress, with a river width of about 3000 m. This is the well-known 1993 flood, a flood with a severity expected only once every 100 years, that occurred on the Missouri and Mississippi Rivers.

Figures 4.26 and 4.27 illustrate new lakes formed by the overflow of the Nile River. First spotted in 1998 by astronauts aboard the Space Shuttle *Discovery*, the Toshka Lakes have fluctuated in size and shape through alternating dry spells and monsoons. Together, the lakes hold about one-quarter of the Nile's total water supply. The future existence of these lakes is unknown. Figure 4.26 illustrates the location of these lakes relative to Lake Nasser, the lake formed by the Aswan High Dam on the Nile River. Figure 4.27 illustrates how these lakes grew in size and number during the 2-year period beginning November 1999.

Other Selected Applications

A knowledge of *groundwater location* is important for both water supply and pollution control analysis. The identification of topographic and vegetation indicators of groundwater and the determination of the location of *groundwater discharge areas* (springs and seeps) can assist in the location of potential well sites. Also, it is important to be able to identify *groundwater recharge zones* in order to protect these areas (via zoning restrictions) from activities that would pollute the groundwater supply. Available image interpretation techniques cannot be used directly to map the depth to water in a groundwater system. However, vegetation types have been successfully used as indicators of approximate depth to groundwater. Estimates of *groundwater use* have also been made based on the interpretation of crop type, area, and irrigation method.

Additional water resource applications of visual image interpretation include hydrologic watershed assessment, riparian vegetation mapping, reservoir site selection, shoreline erosion studies, fish habitat surveys, snow cover mapping, floodplain and shoreland zoning compliance, and survey of recreational use of lakes and rivers.

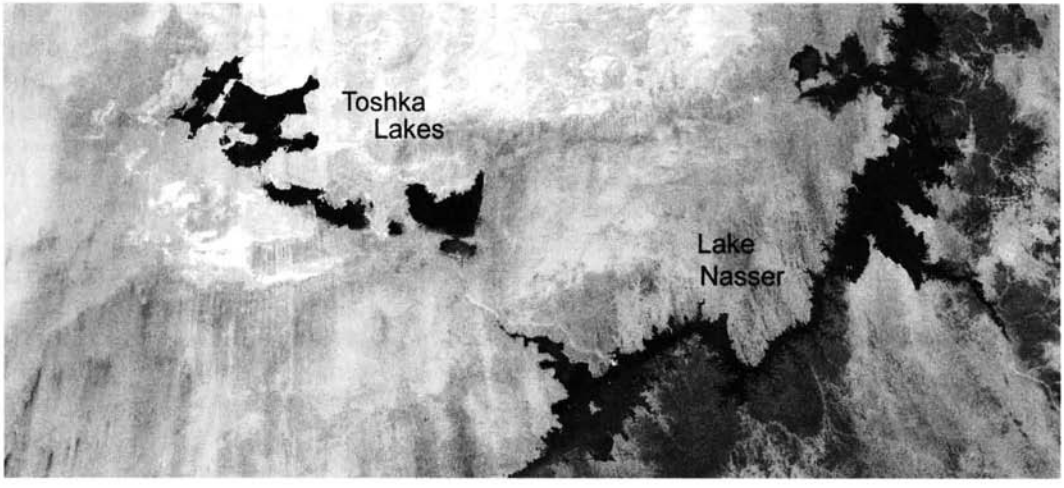

Figure 4.26 MODIS image of newly formed Toshka Lakes in southern Egypt. Approximate scale 1:3,000,000. September 14, 2002. (Courtesy NASA.)

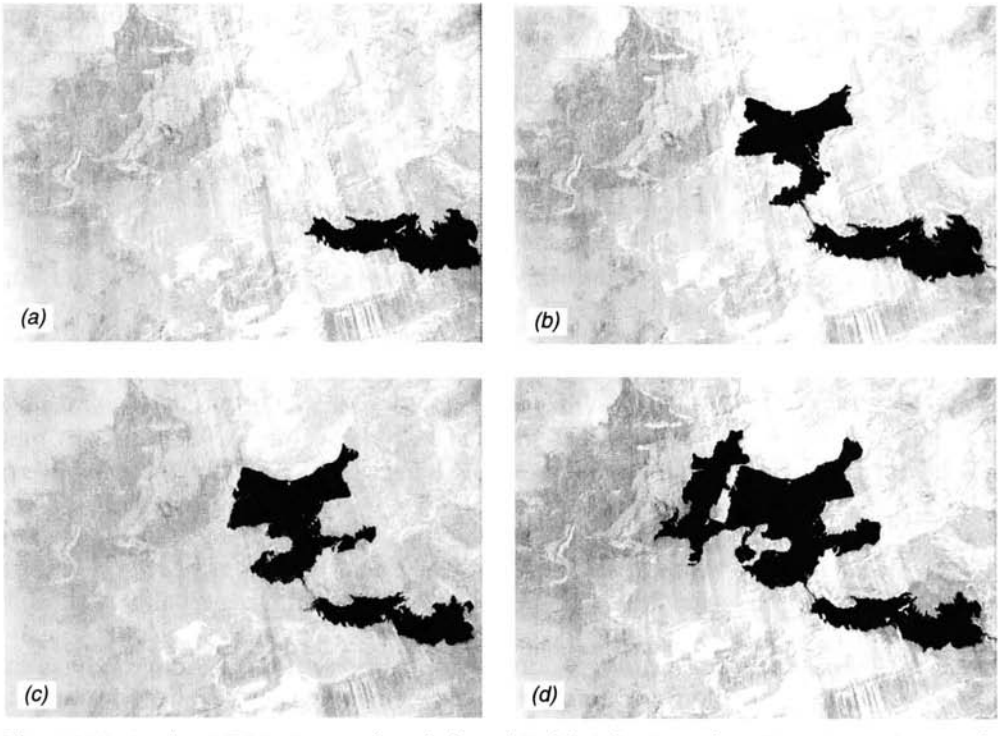

Figure 4.27 Landsat-7 ETM+ images of newly formed Toshka Lakes in southern Egypt. Approximate scale 1:2,000,000. (*a*) November 9, 1999, (*b*) January 12, 2000, (*c*) August 23, 2000, and (*d*) December 16, 2001. (Courtesy NASA.)

4.10 URBAN AND REGIONAL PLANNING APPLICATIONS

Urban and regional planners require nearly continuous acquisition of data to formulate governmental policies and programs. These policies and programs might range from the social, economic, and cultural domain to the context of environmental and natural resource planning. The role of planning agencies is becoming increasingly more complex and is extending to a wider range of activities. Consequently, there is an increased need for these agencies to have timely, accurate, and cost-effective sources of data of various forms. Several of these data needs are well served by visual image interpretation. A key example is land use/land cover mapping, as discussed in Section 4.4. Another example is the use of image interpretation to contribute data for land use suitability evaluation purposes, as outlined in Section 4.16. Here we discuss the utility of visual image interpretation in population estimation, housing quality studies, traffic and parking studies, site selection processes, and urban change detection.

Population estimates can be indirectly obtained through visual image interpretation. Traditionally, the procedure has been to use medium- to large-scale aerial photographs to estimate the number of dwelling units of each housing type in an area (single-family, two-family, multiple-family) and then multiply the number of dwelling units by the average family size per dwelling unit for each housing type. The identification of housing types is based on such criteria as size and shape of buildings, yards, courts, and driveways.

Images from the *Defense Meteorological Satellite Program (DMSP)* (Chapter 6) have been used to examine the earth's urban development from space. One of the DMSP's scanners, the *Operational Linescan System* (*OLS*), is sensitive enough to detect low levels of visible and near-IR energy at night. With this sensor, it is possible to detect clouds illuminated by moonlight, plus lights from cities, towns, industrial sites, gas flares, and ephemeral events such as fires and lightning-illuminated clouds (Elvidge et al., 1997). Figure 4.28 is a global example of DMSP nighttime image data (a composite of hundreds of individual scenes). Figure 4.29 shows DMSP data of the eastern United States. The brightness of the light patterns in Figure 4.29 corresponds closely with the population distribution of the eastern United States, as seen in Figure 4.30. Care must be taken when attempting to compare data from different parts of the world. The brightest areas of the earth are the most urbanized, but not necessarily the most populated (compare western Europe with India and China). Nevertheless, DMSP data provide a valuable data source for tracking the growth of the earth's urbanization over time.

Visual image interpretation can also assist in *housing quality studies*. Many environmental factors affecting housing quality can be readily interpreted from aerial and satellite images, whereas others (such as the interior condition of buildings) cannot be directly interpreted. A reasonable estimate of housing quality can usually be obtained through statistical analysis of a limited, carefully selected set of environmental quality factors. Environmental factors that are

interpretable from aerial photographs and that have been found to be useful in housing quality studies include house size, lot size, building density, building setback, street width and condition, curb and sidewalk condition, driveway presence/absence, garage presence/absence, vegetation quality, yard and open space maintenance, proximity to parkland, and proximity to industrial land use. Large-scale panchromatic photography has typically been used for housing quality studies. However, large- to medium-scale color infrared film has been shown to be superior in evaluating vegetation condition (lawns, shrubs, and trees).

Visual image interpretation can assist in *traffic and parking studies*. Traditional on-the-ground vehicle counts show the number of vehicles passing a few selected points over a period of time. An aerial image shows the distribution of vehicles over space at an instant of time. Vehicle spacings—and thus areas of congestion—can be evaluated by viewing such photographs. Average vehicle speeds can be determined when the image scale and time interval between exposures of overlapping photographs are known. The number and spatial distribution of vehicles parked in open-air lots and streets can be inventoried from aerial images. Not all vehicles in urban areas are visible on aerial images, however. Vehicles in tunnels and enclosed parking will obviously not be visible. In an area of tall buildings, streets near the edges of photographs may be hidden from view because of the radial relief displacement of the buildings. In addition, it may be difficult to discern vehicles in shadow areas on films of high contrast.

Visual image interpretation can assist in various location and siting problems, such as transportation route location, sanitary landfill site selection, power plant siting, commercial site selection, and transmission line location. The same general decision-making process is followed in each of these selection processes. First the factors to be assessed in the route/site selection process are determined. Natural and cultural features plus various economic, social, and political factors are considered. Then data files containing information on these factors are assembled and alternative routes/sites are analyzed and the final route/site is selected. Visual image interpretation has been used to collect much of the natural and cultural data dealing with topography, geology, soils, potential construction materials, vegetation, land use, wetland location, historical/archaeological sites, and natural hazards (earthquakes, landslides, floods, volcanoes, and tsunami). Various methods for obtaining such natural and cultural data through visual image interpretation are described elsewhere in this chapter. The task of analyzing the data is greatly facilitated by the use of a GIS.

Urban change detection mapping and analysis can be facilitated through the interpretation of multidate aerial and satellite images, such as the photographs shown in Figure 4.31, which illustrate the changes in an urban fringe area over a period of 53 years. The 1937 photograph (*a*) shows the area to be entirely agricultural land. The 1955 photograph (*b*) shows that a "beltline" highway has been constructed across the top of the area and that a gravel pit has begun operation in a glacial outwash plain at lower left. The 1968 photograph (*c*) shows that commercial development has begun at upper left and that extensive single-family housing development has begun at lower right. A

Figure 4.31 Multidate aerial photographs illustrating urban change, southwest Madison, WI (scale 1:20,000): (*a*) 1937; (*b*) 1955; (*c*) 1968; (*d*) 1990. [(*a*–*c*) USDA–ASCS photos. (*d*) Courtesy Dane County Regional Planning Commission.]

school has been constructed at lower center and the gravel pit continues operation. The 1990 photograph (*d*) shows that the commercial and single-family development has continued. Multiple-family housing units have been constructed at left. The gravel pit site is now a city park that was a sanitary landfill site for a number of years between the dates of photographs (*c*) and (*d*).

Plate 10 illustrates the use of satellite data for urban change detection. These Landsat images (Chapter 6) dramatically illustrate population growth in the Las Vegas metropolitan area (the fastest growing metropolitan area in the United States) over a 28-year period. The estimated population in the area shown was 300,000 in 1972 (*a*), and 1,425,000 in 2000 (*b*).

Visual image interpretation for urban change detection and analysis can be facilitated through the use of a Digital Transfer Scope (Section 4.3) as an aid in comparing images of two different dates or an image with a map.

4.11 WETLAND MAPPING

The value of the world's wetland systems has gained increased recognition. Wetlands contribute to a healthy environment in many ways. They act to retain water during dry periods, thus keeping the water table high and relatively stable. During periods of flooding, they act to reduce flood levels and to trap suspended solids and attached nutrients. Thus, streams flowing into lakes by way of wetland areas will transport fewer suspended solids and nutrients to the lakes than if they flow directly into the lakes. The removal of such wetland systems because of urbanization or other factors typically causes lake water quality to worsen. In addition, wetlands are important feeding, breeding, and drinking areas for wildlife and provide a stopping place and refuge for waterfowl. As with any natural habitat, wetlands are important in supporting species diversity and have a complex and important food web. Scientific values of wetlands include a record of biological and botanical events of the past, a place to study biological relationships, and a place for teaching. It is especially easy to obtain a feel for the biological world by studying a wetland. Other human uses include low intensity recreation and esthetic enjoyment.

Accompanying the increased interest in wetlands has been an increased emphasis on inventorying. The design of any particular wetland inventory is dependent on the objectives to be met by that inventory. Thus, a clearly defined purpose must be established before the inventory is even contemplated. Wetland inventories may be designed to meet the general needs of a broad range of users or to fulfill a very specific purpose for a particular application. Multipurpose and single-purpose inventories are both valid ways of obtaining wetland information, but the former minimizes duplication of effort. To perform a wetlands inventory, a classification system must be devised that will provide the information necessary to the inventory users. The system should be based primarily on enduring wetland characteristics so that the inventory does not become outdated too quickly, but the classification should also accommodate user

information requirements for ephemeral wetland characteristics. In addition, the inventory system must provide a detailed description of specifically what is considered to be a wetland. If the wetland definition used for various "wetland maps" is not c learly stated, then it is not possible to tell if apparent wetland changes noted between maps of different ages result from actual wetland changes or are due to differences in concepts of what is considered a wetland.

At the federal level in the United States, four principal agencies are involved with wetland identification and delineation: (1) the Environmental Protection Agency, (2) the Army Corps of Engineers, (3) the Natural Resources Conservation Service, and (4) the Fish and Wildlife Service. The Environmental Protection Agency is concerned principally with water quality, the Army Corps of Engineers is concerned principally with navigable water issues that may be related to wetlands, the Natural Resources Conservation Service is concerned principally with identifying and mapping wetlands, and the Fish and Wildlife Service is principally interested in the use of wetlands for wildlife habitat. In 1989, these four agencies produced a *Federal Manual for Identifying and Delineating Jurisdictional Wetlands* (Federal Interagency Committee for Wetland Delineation, 1989), which provides a common basis for identifying and delineating wetlands. There is general agreement on the three basic elements for identifying wetlands: (1) hydrophytic vegetation, (2) hydric soils, and (3) wetland hydrology. *Hydrophytic vegetation* is defined as macrophytic plant life growing in water, soil, or substrate that is at least periodically deficient in oxygen as a result of excessive water content. *Hydric soils* are defined as soils that are saturated, flooded, or ponded long enough during the growing season to develop anaerobic (lacking free oxygen) conditions in the upper part. In general, hydric soils are flooded, ponded, or saturated for 1 week or more during the period when soil temperatures are above biologic zero (5°C) and usually support hydrophytic vegetation. *Wetland hydrology* refers to conditions of permanent or periodic inundation, or soil saturation to the surface, at least seasonally, hydrologic conditions that are the driving forces behind wetland formation. Numerous factors influence the wetness of an area, including precipitation, stratigraphy, topography, soil permeability, and plant cover. All wetlands typically have at least a seasonal abundance of water that may come from direct precipitation, overbank flooding, surface water runoff resulting from precipitation or snow melt, groundwater discharge, or tidal flooding.

Color infrared photography has been the preferred film type for wetlands image interpretation. It provides interpreters with a high level of contrast in image tone and color between wetland and nonwetland environments, and moist soil spectral reflectance patterns contrast more distinctively with less moist soils on color infrared film than on panchromatic or normal color films. Other multiband image types (e.g., multispectral scanners, hyperspectral scanners) can also be used, but should include at least one visible band and one near-infrared band.

An example of wetland mapping is shown in Figures 4.32 and 4.33. Figure 4.32 is a 6.7× enlargement of a color infrared airphoto that was used for

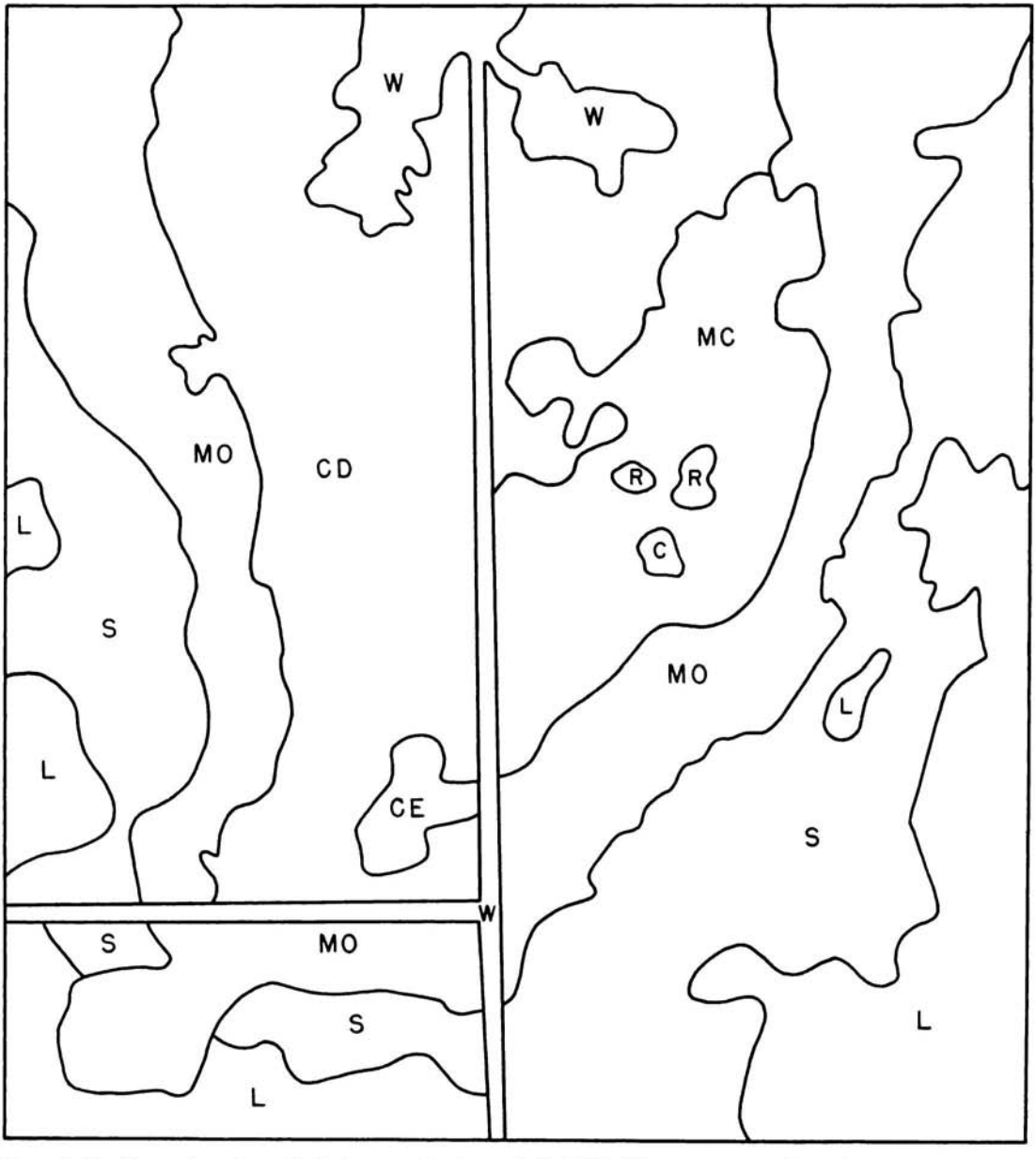

Figure 4.33 Vegetation classes in Sheboygan Marsh (scale 1:9000): W = open water, D = deep water emergents, E = shallow water emergents, C = cattail (solid stand), O = sedges and grasses, R = reed canary grass (solid stand), M = mixed wetland vegetation, S = shrubs, L = lowland conifer forest.

TABLE 4.13 Airphoto Interpretation Key to Vegetation Classes in Sheboygan Marsh for Use with Late-Spring 1:60,000 Color Infrared Film

Map Symbol (Figure 4.33)	Class Definition and Airphoto Interpretation Key
W	*Open water:* Areas of open water produce a dark blue image. The dark color and uniform smooth texture of the open water are in distinct contrast with the lighter tones of the surrounding vegetation.
D	*Deep water emergents:* These exist in water depths of 0.15–0.45 m or more and consist predominantly of cattail (*Typha latifolia*, *T. augustifolia*), burreed (*Sparganium eurycarpum*), and sometimes reedgrass (*Phragmites communis*). These species, when interspersed with water, form an image made up of a dull bluish color with soft texture, a tone produced by background reflectance of water blending with the vegetation reflectance. This subcommunity is sometimes interspersed with shallow water emergents.
E	*Shallow water emergents:* These consist of a mixture of such wetland species as cattail (*T. latifolia*, *T. augustifolia*), arrowhead (*Saggitaria latifolia*), water plantain (*Alisma plantago-aquatica*), burreed (*S. eurycarpum*), and several sedge species (*Carex lacustris*, *C. rostrata*, *C. stricta*, *C. aquatilis*) in water depths of 0.15 m or less. A medium bluish tone is produced that is lighter than the deep water areas.
C	*Cattail-solid stand:* This consists of solid stands of cattail (*T. latifolia*, *T. augustifolia*) that appear as mottled white patches in water ranging in depth from 0.10 to 0.75 m.
O	*Sedges and grasses:* The main components of a sedge meadow, sedges (*C. lacustris*, *C. rostrata*, *C. stricta*, *C. aquatilis*) and grasses (*Spartina* sp, *Phragmites* sp, *Calamagrostis* sp) are generally interspersed with small depressions of shallow water that together produce a continuous pattern of bluish water color intermixed with small white blotches.
R	*Reed canary grass-solid stand:* Reed canary grass appears as a uniform vegetation type that produces a bright white tone on the image. Reed canary grass occurs in small irregular patches and as linear features along stream banks. It is often difficult to differentiate from sedges and grasses because of the almost identical tones produced. Large areas of the species that were planted for marsh hay often retain their unnatural rectangular boundaries.
M	*Mixed wetland vegetation:* This consists primarily of sedges (*C. rostrata*, *C. stricta*, *C. lacustris*), forbs (marsh dock, *Rumex brittanica*; marsh bellflower, *Campanula aparinoides*; and marsh bedstraw, *Galium trifidum*), grasses (bluejoint, *Calamagrostis canadensis*), and cord grass (*Sparganium* sp). This community produces an interlacing pattern of magenta tones, light blues, and white colors, indicating the mixture of the component species.
S	*Shrubs:* This consists of buttonbush (*Cephalanthus occidentalis* L.), alder (*Alnus rugosa*), willow (*Salix interior*, *S. petiolaris*, *S. bebbiana*), and red osier dogwood (*Cornus stolonifera*). Shrubby areas have an intense magenta tone with coarse texture.
L	*Lowland conifer forest:* This consists, at this site, primarily of tamarack (*Larix laricina*) and white cedar (*Thuja occidentalis*) that display a deep mauve tone with considerable texture.

wetland vegetation mapping at an original scale of 1 : 60,000. The vegetation classification system and airphoto interpretation key are shown in Table 4.13. The wetland vegetation map (Figure 4.33) shows the vegetation in this scene grouped into nine classes. The smallest units mapped at the original scale of 1 : 60,000 are a few distinctive stands of reed canary grass and cattails about $\frac{1}{3}$ ha in size. Most of the units mapped are much larger.

Another example of wetland mapping can be seen in Plate 28, which illustrates multitemporal data merging as an aid in mapping invasive plant species, in this case reed canary grass.

At the federal level, the U.S. Fish and Wildlife Service is responsible for a National Wetlands Inventory that produces information on the characteristics, extent, and status of the nation's wetlands and deep water habitats. This information is used by federal, state, and local agencies, academic institutions, the U.S. Congress, and the private sector. As of 2002, the National Wetlands Inventory had mapped 90 percent of the lower 48 states, and 34 percent of Alaska. About 44 percent of the lower 48 states, and 13 percent of Alaska had been digitized. Congressional mandates require the production of status and trends reports at 10-year intervals. Updates to map and digital coverage are available on the Internet at: http//www.nwi.fws.gov.

4.12 WILDLIFE ECOLOGY APPLICATIONS

The term *wildlife* refers to animals that live in a wild, undomesticated state. *Wildlife ecology* is concerned with the interactions between wildlife and their environment. Related activities are *wildlife conservation* and *wildlife management*. Two aspects of wildlife ecology for which visual image interpretation can most readily provide useful information are wildlife habitat mapping and wildlife censusing.

A *wildlife habitat* provides the necessary combination of climate, substrate, and vegetation that each animal species requires. Within a habitat, the functional area that an animal occupies is referred to as its *niche*. Throughout evolution, various species of animals have adapted to various combinations of physical factors and vegetation. The adaptations of each species suit it to a particular habitat and rule out its use of other places. The number and type of animals that can be supported in a habitat are determined by the amount and distribution of food, shelter, and water in relation to the mobility of the animal. By determining the food, shelter, and water characteristics of a particular area, general inferences can be drawn about the ability of that area to meet the habitat requirements of different wildlife species. Because these requirements involve many natural factors, the image interpretation techniques described elsewhere in this chapter for mapping land cover, soil, forests, wetlands, and water resources are applicable to

wildlife habitat analysis. Also, delineation of the "edges" between various landscape features is an important aspect of habitat analysis. Often, the interpreted habitat characteristics are incorporated in GIS-based modeling of the relationship between the habitat and the number and behavior of various species.

Figure 4.34 illustrates wildlife habitat mapping. This figure shows the Sheboygan Marsh, which was also shown in Figure 4.32 for the purpose of illustrating wetland vegetation mapping. In Figure 4.34, the nine vegetation classes shown in Figure 4.33 have been grouped into five wildlife habitat types, as follows: (1) *open water*, (2) *aquatic vegetation* (cattail, burreed, and reed grass), (3) *sedge meadow* (sedges and grasses), (4) *shrubs* (alder, willow, and dogwood), and (5) *lowland conifer forest* (tamarack and white cedar). Each of these five habitat types supports a significantly different population of mammals, birds, and fish. For example, a careful examination of the "aquatic vegetation" habitat area of Figure 4.34 on the original color infrared transparency (1 : 60,000) reveals that there are more than 100 white spots on the photograph, each surrounded by a dark area. Each of these white spots is a muskrat hut. Within the area of this photograph, muskrat huts can be found only in the area identified as aquatic vegetation habitat.

Wildlife censusing can be accomplished by ground surveys, aerial visual observations, or aerial imaging. Ground surveys rely on statistical sampling techniques and are often tedious, time consuming, and inaccurate. Many of the wildlife areas to be sampled are often nearly inaccessible on the ground. Aerial visual observations involve attempting to count the number of individuals of a species while flying over a survey area. Although this can be a low cost and relatively rapid type of survey, there are many problems involved. Aerial visual observations require quick decisions on the part of the observer regarding numbers, species composition, and percentages of various age and sex classes. Aggregations of mammals or birds may be too large for accurate counting in the brief time period available. In addition, low-flying aircraft almost invariably disturb wildlife, with much of the population taking cover before being counted.

Vertical aerial photography has been the best method of accurately censusing many wildlife populations. If the mammals or birds are not disturbed by the aircraft, the airphotos will permit very accurate counts to be undertaken. In addition, normal patterns of spatial distributions of individuals within groups will be apparent. Aerial photographs provide a permanent record that can be examined any number of times. Prolonged study of the photographs may reveal information that could not have been otherwise understood.

A variety of mammals and birds have been successfully censused using vertical aerial photography, including moose, elephants, whales, elk, sheep,

deer, antelope, sea lions, caribou, beavers, seals, geese, ducks, flamingos, gulls, oyster catchers, and penguins. Vertical aerial photography obviously cannot be used to census all wildlife populations. Only those that frequent relatively open areas during daylight hours can be counted. (Thermal scanning can be used to detect large animals in open areas.)

Wildlife censusing also requires that individual animals be large enough to be resolved on the photographs. A scale not smaller than 1 : 8000 is recommended for large mammals such as elk, whereas scales as large as 1 : 3000 should be used for smaller mammals such as sheep, deer, and antelope. A critical factor is the tonal contrast between the animal and its surroundings. For example, flocks of snow geese (large white birds) can be identified at a scale of 1 : 12,000 against a dark background. Individual birds are identifiable at scales of 1 : 6000 and larger.

In Figure 4.35, snow geese appear as white dots against a darker water background in the Bosque del Apache National Wildlife Refuge in New Mexico, where as many as 45,000 snow geese visit during their migrations.

Dark-colored wildlife species often can be discerned better in the winter against a snow or ice background than in the summer with a soil, vegetation, or water background. This is also the time of year when many species tend to band together and leaves have fallen from deciduous trees, making censusing possible even in certain kinds of forests. Special film–filter combinations can be selected to maximize the contrast.

The counting of individual animals on aerial images may present a problem when large numbers are present. Transparent grid overlays are often used as an aid in estimating numbers. Aerial images can also be used to stratify population densities (individuals per unit area) for use in stratified sampling techniques. Alternatively, aerial images not already in digital form can be digitized (via image scanning) and digital image processing techniques used to automatically "count" individuals.

Figure 4.36 shows a prairie dog colony on a plateau in South Dakota. Prairie dogs feed upon grasses and broad-leaved plants and construct burrows with mounded entrances. They disturb the ground in the vicinity of the colony, making the area susceptible to invasion by plants that exist in disturbed areas. The lighter toned area on the plateau in the center of the photograph is covered by such vegetation (mostly forbs) and the surrounding darker toned area is covered by native prairie grass. Each white spot in this lighter toned area is the bare soil associated with one prairie dog mound.

Figure 4.37 shows a large group of beluga whales (small white whales) that have congregated in an arctic estuarine environment principally for the purpose of calving. At the image scales shown here, it is possible to determine the number and characteristics of individual whales and to measure their lengths. On the full 230 × 230-mm aerial photograph from which Figure 4.37 was rephotographed, a total of about 1600 individual whales were counted. At

Figure 4.37 Large group of beluga whales, Cunningham Inlet, Somerset Island, northern Canada (black and white copy of photograph taken with Kodak Water Penetration Color Film, SO-224): (*a*) 1 : 2,400; (*b*) 1 : 800. (*b*) is a 3 times enlargement of the lower left portion of (*a*). (Courtesy J. D. Heyland, Metcalfe, Ontario.)

the original film scale of 1:2000, the average adult length was measured as 4 m and the average calf length was measured as 2 m. Numerous adults with calves can be seen, especially in the enlargement (Figure 4.37*b*). "Bachelor groups" of eight and six males can be seen at the lower left and lower right of Figure 4.37*b*.

4.13 ARCHAEOLOGICAL APPLICATIONS

Archaeology is concerned with the scientific study of historic or prehistoric peoples by analysis of the remains of their existence, especially those remains that have been discovered through earth excavation.

The earliest archaeological investigations dealt with obvious monuments of earlier societies. The existence of these sites was often known from histori-

cal accounts. Visual image interpretation has proven particularly useful in locating sites whose existence has been lost to history. Both surface and subsurface features of interest to archaeologists have been detected using visual image interpretation.

Surface features include visible ruins, mounds, rock piles, and various other surface markings. Examples of visible ruins are rock structures such as Stonehenge (England), castles (throughout Europe), and Indian dwellings in the southwestern United States. Examples of mounds are the bird-shaped and serpent-shaped Indian mounds of the Midwestern United States. Examples of rock structures are the various medicine wheels such as the Bighorn Medicine Wheel in Wyoming and the Moose Mountain Medicine Wheel in Saskatchewan. Other surface markings include Indian pictographs and the ancient Nazca Lines in Peru.

Figure 4.38 shows the Nazca Lines. They are estimated to have been made between 1300 and 2200 years ago and cover an area of about 500 km^2. Many geometric shapes have been found, as well as narrow straight lines that extend for as long as 8 km. They were made by clearing away literally millions of rocks to expose the lighter toned ground beneath. The cleared rocks were piled around the outer boundaries of the "lines." These markings were first noticed from the air during the 1920s. At that time, it was hypothesized that they formed a gigantic astronomical calendar, a belief still held by some scientists. The definite reason for their construction remains unknown.

Subsurface archaeological features include buried ruins of buildings, ditches, canals, and roads. When such features are covered by agricultural fields or native vegetation, they may be revealed on aerial or satellite images by tonal anomalies resulting from subtle differences in soil moisture or crop growth. On occasion, such features have been revealed by ephemeral differences in frost patterns.

Figure 4.39 shows the site of the ancient city of Spina on the Po River delta in Italy. Spina flourished during the fifth century B.C. and later became a "lost" city whose very existence was doubted by many. An extensive search for Spina ended in 1956 when it was identified on aerial photographs by an Italian archaeologist. Ancient Spina was a city of canals and waterways. The dark-toned linear features in Figure 4.39 are areas of dense vegetation growing in wet soils at the former location of the canals. The lighter toned rectangular areas are sparse vegetation over sand and the rubble of brick foundations. The light-toned linear features that run diagonally across this photograph are present-day drainage ditches.

The sites of more than a thousand Roman villas have been discovered in northern France through the use of 35-mm aerial photography. The buildings were destroyed in the third century A.D., but their foundation materials remain in the soil. In Figure 4.40, we see the villa foundation because of

differences in crop vigor. The area shown in this figure has recently been converted from pasture to cropland. In the early years following such conversion, farmers apply little or no fertilizer to the fields. The cereal crops over the foundation materials are light toned owing to both the lack of fertilizer and a period of drought prior to the date of photography. The crops are darker toned over the remainder of the field. The main building (in the foreground) was 95 × 60 m.

Figure 4.41, an IKONOS image (Chapter 6) of the pyramids and sphinx at Giza, Egypt, shows the level of detail that can be seen in high resolution space images of archaeological sites. Shown at *a* is the Great Pyramid of Khufu. At

b is the Pyramid of Khafre; at *c* is the Pyramid of Menkaure, and just left of *d* is the Great Sphinx. The numerous small rectangular features left and right of the Great Pyramid are flat-topped funerary structures called "mastabas." The pyramids and sphinx were built about 4500 years ago. The length of each side of the Great Pyramid averages 230 m at its base, and the four sides are accurately oriented in the four cardinal directions (north, east, south, and west). The Great Sphinx is 73 m long, is carved out of limestone bedrock, and faces the rising sun.

4.14 ENVIRONMENTAL ASSESSMENT

Many human activities produce potentially adverse environmental effects. Examples include the construction and operation of highways, railroads, pipelines, airports, industrial sites, power plants, and transmission lines; subdivision and commercial developments; sanitary landfill and hazardous waste disposal operations; and timber harvesting and strip mining operations.

Dating as far back as 1969, the *National Environmental Policy Act* (NEPA) established as national policy the creation and maintenance of conditions that encourage harmony between people and their environment and minimize environmental degradation. This act requires that *environmental impact statements* be prepared for any federal action having significant impact on the environment. The key items to be evaluated in an environmental impact statement are (1) the environmental impact of the proposed action; (2) any adverse environmental effects that cannot be avoided should the action be implemented; (3) alternatives to the proposed action; (4) the relationship between local short term uses of the environment and the maintenance and enhancement of long term productivity; and (5) any irreversible and irretrievable commitments of resources that would be involved in the proposed action should it be implemented. Since the passage of NEPA, many other federal and state laws have been passed with environmental assessment as a primary component.

Environmental assessments involve, at a minimum, comprehensive inventory of physiographic, geologic, soil, cultural, vegetative, wildlife, watershed, and airshed conditions. Such assessments will typically draw on expertise of persons from many areas such as civil engineering, forestry, landscape architecture, land planning, geography, geology, archaeology, environmental economics, rural sociology, ecology, seismology, soils engineering, pedology, botany, biology, zoology, hydrology, water chemistry, aquatic biology, environmental engineering, meteorology, air chemistry, and air pollution engineering. Many of the remote sensing and image interpretation techniques set forth in this book can be utilized to assist in the conduct of such assessments. Overall, the applications of remote sensing in environmental monitoring and assessment are virtually limitless, ranging from environmental impact assessment to emergency response planning, landfill monitoring, permitting and enforcement, and natural disaster mitigation, to name but a few.

Effectively "real-time" imaging is used in such applications as responding to the spillage of hazardous materials. Such images are used to determine the extent and location of visible spillage and release, vegetation damage, and threats to natural drainage and human welfare. On the other hand, historical images are often used to conduct intensive site analyses of waste sites, augmenting these with current images when necessary. These analyses may include characterizing changes in surface drainage conditions through time; identifying the location of landfills, waste treatment ponds, and lagoons and their subsequent burial and abandonment; and detecting and identifying drums containing waste materials. Also, image interpretation may be used to help locate potential sites for drilling and sampling of hazardous wastes.

Figure 4.42 shows a plume of chlorine gas resulting from a train derailment. When such incidents occur, there is immediate need to assess downwind susceptibility of human exposure and the other potential impacts of the event. When available, remote sensing imagery and numerous forms of GIS

Figure 4.42 Low altitude, oblique aerial photograph of chlorine spill resulting from train derailment near Alberton, MT. (Courtesy RMP Systems.)

data are used in conjunction with ancillary ground information (such as wind speed and direction) to develop emergency evacuation and response plans in the general vicinity of the incident. In the specific case of Figure 4.42, the GIS and remote sensing initiated for immediate response was also very useful and important for the longer term monitoring of the spill site. Thus, the GIS established for the response was also useful in monitoring and change detection, as would be the case with many similar applications.

Figure 4.43 shows an oil spill in Bull Run, near Manassas, Virginia. Several thousand barrels of oil entered a nearby creek and then flowed into the connecting river and a reservoir. Several oil containment booms, clearly visible in Figure 4.43, were placed across the run to entrap the oil and facilitate cleanup efforts. Aerial photographs taken over the next few days followed the path of the oil spill movement. The photographs guided the on-scene coordinator in selecting locations for containment booms and pinpointing areas of oil accumulation. Subsequent photographs verified the success of the containment and cleanup of the spill. An example of a radar image showing an oil slick in the Mediterranean Sea can be seen in Figure 8.44.

Large-scale airphotos have been used in such applications as the identification of failing septic systems. The principal manifestations of septic system

Figure 4.43 Aerial photograph of an oil spill on Bull Run, near Manassas, Virginia. Note the series of booms placed across the river to entrap the oil (the flow of water is from right to left in this photograph). (Courtesy EPA Environmental Photographic Interpretation Center.)

failure are typically the upward or lateral movement of partially treated or untreated wastewater toward the soil surface. As the effluent moves upward and approaches the ground surface, the large amount of nutrients in the effluent causes enhanced growth in the vegetation directly above it. When the effluent reaches the surface, the overabundance of nutrients, coupled with an imbalance in the soil's air–water ratio, causes the vegetation to become stressed and eventually die. Finally, the effluent surfaces and either stands on the ground surface or flows downslope, often manifesting the same growth–stress–death pattern as it moves. Both normal color and color infrared photographs at a scale of around 1 : 8000 have been used for the detection of such situations (Evans, 1982). Open areas can be photographed

throughout much of the year. Areas with sparse tree cover should be photographed during early spring (after grasses have emerged but before tree leaves have appeared) or late fall (after tree leaves have dropped). Areas of dense tree cover may be impossible to analyze using airphoto interpretation at any time.

An analysis of the photo characteristics of color, texture, site, and association, along with collateral soil information, is important for the identification of failing septic systems. Stereoscopic viewing is also important because it allows for the identification of slope, relief, and direction of surface drainage.

4.15 NATURAL DISASTER ASSESSMENT

Many forms of natural and human-induced disasters have caused loss of life, property damage, and damage to natural features. A variety of remote sensing systems can be used to detect, monitor, and respond to natural disasters, as well as assess disaster vulnerability. Here, we discuss wildfires, severe storms, floods, volcanic eruptions, dust and smoke, earthquakes, shoreline erosion, and landslides. NASA, NOAA, and the USGS maintain websites devoted to natural hazards (Appendix B).

Wildfires

Wildfires are a serious and growing hazard over much of the world. They pose a great threat to life and property, especially when they move into populated areas. Wildfires are a natural process, and their suppression is now recognized to have created greater fire hazards than in the past. Wildfire suppression has also disrupted natural plant succession and wildlife habitat in many areas.

Plate 11 shows a wildfire burning near the city of Los Alamos, New Mexico, as imaged by Landsat-7 (Chapter 6). Los Alamos is located on a series of mesas in the upper-right quadrant of the image. Plate 11*a* is a composite of bands 1, 2, and 3 (displayed as blue, green, and red, respectively), resulting in a "normal color" image. Plate 11*b* is a composite of bands 2, 4, and 7 (again displayed as blue, green, and red) and is a "false color image." The normal color image shows the smoke plumes well but does not reveal much specific information about the areas that are burning at the time of image acquisition. In the false color image (*b*), the hottest actively burning areas appear bright red-orange in color, visible because of the large amount of energy emitted from the fires in the 2.08- to 2.35-μm wavelength sensitivity range of band 7 (Figure 2.22). The darker red and near-black-toned areas

are recently burned areas. The nearby darker green areas are unburned forest lands.

Severe Storms

Severe storms can take many forms, including tornados and cyclones. Tornadoes are rotating columns of air, usually with a funnel-shaped vortex several hundred meters in diameter, whirling destructively at speeds up to about 500 km/hr. Tornadoes occur most often in association with thunderstorms during the spring and summer in the midlatitudes of both the Northern and Southern Hemispheres. Cyclones are atmospheric systems characterized by the rapid, inward circulation of air masses about a low-pressure center, accompanied by stormy, often destructive, weather. Cyclones circulate counterclockwise in the Northern Hemisphere, and clockwise in the Southern Hemisphere. Hurricanes are severe tropical cyclones originating in the equatorial regions of the Atlantic Ocean or Caribbean Sea. Typhoons are tropical cyclones occurring in the western Pacific or Indian Oceans.

Tornado intensity is commonly estimated by analyzing damage to structures and then correlating it with the wind speeds required to produce such destruction. Tornado intensity is most often determined using the *Fujita Scale*, or *F-Scale* (Table 4.14). Although very few (about 2 percent) of all tornadoes reach F4 and F5 intensities, they account for about 65 percent of all deaths.

TABLE 4.14 Fujita Scale (F-Scale) of Tornado Intensity

F-Scale Value	Wind Speed (km/hr)	Tornado Intensity	Description of Damage	Examples
F0	64–116	Weak	Light	Branches broken, shallow-rooted trees pushed over
F1	117–181	Weak	Moderate	Surfaces peeled off roofs, mobile homes pushed off foundations or overturned
F2	182–253	Strong	Considerable	Roofs torn off frame houses, large trees snapped or uprooted
F3	254–332	Strong	Severe	Roofs and some walls torn off well-constructed houses, trains overturned, heavy cars lifted off ground and thrown
F4	333–418	Violent	Devastating	Well-constructed houses leveled, cars thrown.
F5	419–512	Violent	Incredible	Strong frame houses lifted off foundations and carried a considerable distance to disintegration, automobile-sized missiles flung through the air more than 100 m

Source: 2002 Encyclopedia Britannica online (http://www.britannica.com).

Plate 12 is a large-scale digital camera image showing a portion of the aftermath of an F4 tornado that struck Hayesville, Kansas. This tornado was responsible for 6 deaths, 150 injuries, and over $140 million in property damage.

Plate 32 contains "before" and "after" Landsat-7 satellite (Chapter 6) images of the damage caused by an F3 tornado that struck Burnett County, Wisconsin. This storm resulted in 3 deaths, 8 serious injuries, complete destruction of 180 homes and businesses, and damage to 200 others. Figure 4.44 is a large-scale aerial photograph showing the "blowdown" of trees by this tornado. Tornado damage is also shown in Figure 8.31, a radar image of a forested area in northern Wisconsin.

Hurricane intensity is most often determined using the Saffir–Simpson Hurricane Scale, which rates hurricane intensity on a scale from 1 to 5, and is used to give an estimate of potential property damage and flooding along the coast from a hurricane landfall. The strongest hurricanes are "Category 5" hurricanes, with winds greater than 249 km/hr. Category 5 hurricanes typically have a storm surge 5.5 m above normal sea level (this value varies widely with ocean bottom topography) and result in complete roof failure on many residences, and some complete building failures. Many shrubs, trees, and signs are blown down. Severe and extensive window and door damage can occur, as can complete destruction of mobile homes. Also, there is typically major damage to the lower floors of all structures located less than 5 m above sea level and within 500 m of the shoreline. Before the 1940s, many hurricanes went undetected. At present every hurricane is detected and tracked by satellite imaging. Figure 4.45 is a MODIS satellite (Chapter 6) image of an offshore hurricane that peaked as a Category 5 hurricane. A typical hurricane structure can be seen, with a counterclockwise flow of air, and a center "eye," with reduced wind speed and rainfall. Side-looking radar satellite images from Radarsat (Chapter 8) have also been used to monitor hurricanes.

Floods

Over-the-bank river flooding delivers valuable topsoil and nutrients to farmland and brings life to otherwise infertile regions of the world, such as the Nile River Valley. On the other hand, flash floods and large "100-year" floods are responsible for more deaths than tornadoes or hurricanes and cause great amounts of property damage.

Various examples of flooding can be found elsewhere in this book. Figure 4.24 is a multidate sequence of low altitude aerial photographs showing river flooding and its aftereffects. Figure 4.25 illustrates the appearance of a flooding river from a satellite perspective. Figures 4.26 and 4.27 illustrate new lakes formed by the overflow of the Nile River, again from a satellite perspective. And, Figure 8.48 shows flooding of Canada's Red River as imaged by the Radarsat satellite.

Figure 4.44 Aerial photograph showing the destruction of hundreds of trees by an F3 tornado that struck Burnett County, WI, on June 18, 2001. Scale 1:8100. (Courtesy Burnett County Land Information Office, University of Wisconsin-Madison Environmental Remote Sensing Center, and NASA Regional Earth Science Applications Center Program.)

Figure 4.45 Hurricane Herman off Baja California, September 2, 2002, as imaged by MODIS. (Courtesy NASA.)

Volcanic Eruptions

Volcanic eruptions are one of earth's most dramatic and violent agents of change. Eruptions often force people living near volcanoes to abandon their land and homes, sometimes forever. Volcanic activity in the last 300 years has killed more than 250,000 people, destroyed entire cities and forests, and severely disrupted local economies. Volcanoes can present a major hazard to those who live near them, for a variety of reasons: (1) pyroclastic eruptions can smother large areas of the landscape with hot ash, dust, and smoke within a span of minutes to hours; (2) red hot rocks spewed from the mouth of a volcano can ignite fires in nearby forests and towns, while rivers of molten lava can consume almost anything in their paths as they reshape the landscape; (3) heavy rains or rapidly melting summit snowpacks can trigger lahars, sluices of mud that can flow for miles, overrunning roads and villages; and, (4) large plumes of ash and gas ejected high into the atmosphere can influence climate, sometimes on a global scale (from USGS and NASA Natural Hazards websites—see Appendix B).

Plate 38 shows an extensive volcanic terrain in central Africa. Numerous lava flows can be seen on the slopes of Nyamuragiro volcano, which dominates the lower portion of the image. To the upper right of Nyamuragiro volcano is Nyiragongo volcano, which erupted in 2002 with loss of life and great property damage in and around the city of Goma, located on the shore of Lake Kivu, which can be seen at the right edge of Plate 38.

Plate 13 is a Landsat-5 (Chapter 6) image showing the eruption of 3350-m-high Mt. Etna, Italy, Europe's most active volcano. The bright red-orange areas on the volcano's flanks are flowing lava and fissures containing molten lava. This image is a composite of Landsat bands 2 (sensitive to green energy), 5 (mid-IR), and 7 (mid-IR). In this color composite, band 2 is displayed as blue, band 5 as green, and band 7 as red. Because the molten lava emits very little energy in green wavelengths, and a great deal of energy in the mid-IR (Figure 2.22), it appears in Plate 13 with a red-orange color. (Note that Plate 4*b* showed flowing lava as photographed with color infrared film.) The bright, puffy clouds near the volcano were formed from water vapor released during the eruption. A thick plume of airborne ash can be seen blowing from the volcano, to the southeast (north is to the top of Plate 13).

Dust and Smoke

Aerosols are small particles suspended in the air. Some occur naturally, originating from volcanoes, dust storms, and forest and grassland fires. Human activities, such as the burning of fossil fuels, prescribed fires, and the alteration of natural land surface cover (e.g., slash-and-burn activities), also generate aerosols. Many human-produced aerosols are small enough to be inhaled,

so they can present a serious health hazard around industrial centers, or even hundreds of miles downwind. Additionally, thick dust or smoke plumes severely limit visibility and can make it hazardous to travel by air or road. Examples of smoke and volcanic ash can be seen in Plates 11 and 13, previously discussed.

Dust plumes have been observed in many arid regions around the globe. They can be extensive and travel great distances. For example, using satellite images, dust plumes originating near the west coast of Africa have been observed reaching the east coast of South America. Figure 4.46 shows an example of dust plumes over Baja California, blowing in a southwesterly direction, as imaged by the SeaWiFS satellite (Chapter 6).

Earthquakes

Earthquakes occur in many parts of the world and can cause considerable loss of life and property damage. Figure 4.11 illustrates extensive geologic features visible on satellite imagery that can be correlated with major geologic faults and major earthquake sites. Figure 6.29 shows the trace of ground cracks created during an earthquake that are clearly evident on a postearthquake satellite image. For information on earthquake hazards, see the USGS Earthquake Hazards Program website (Appendix B).

Shoreline Erosion

Driven by rising sea and lake levels, large storms, flooding, and powerful ocean waves, erosion wears away the beaches and bluffs along the world's shorelines. Bluff erosion rates vary widely, depending on geologic setting, waves, and weather. The erosion rate for a bluff can be regular over the years, or it can change from near zero for decades to several meters in a matter of seconds. Remote sensing studies of shoreline erosion have used a variety of platforms, from cameras in microlite aircraft to satellite data. Historical data using aerial photographs dating back to the 1930s, as well as more recent satellite data, can be used to document shoreline erosion over time. Also, recent studies of shoreline erosion have used Lidar data (Chapter 8).

Landslides

Landslides are mass movements of soil or rock down slopes and a major natural hazard because they are widespread. Globally, landslides cause an estimated 1000 deaths per year and great property damage. They commonly occur in conjunction with other major natural disasters, such as earthquakes,

Figure 4.46 Dust plumes over Baja California as imaged by the SeaWiFS satellite, February 2002. Scale 1:8,600,000. (Courtesy NASA.)

floods, and volcanic eruptions. Landslides can also be caused by excessive precipitation or human activities, such as deforestation or developments that disturb natural slope stability. They do considerable damage to infrastructure, especially highways, railways, waterways, and pipelines.

Historically, aerial photographs have been used extensively to characterize landslides and to produce landslide inventory maps, particularly because of their stereo-viewing capability and high spatial resolution. High resolution satellite data (Chapter 6), such as IKONOS, and the stereo data from SPOT-4, have proven useful for mapping large landslides, and the multi-incidence, stereo, and high resolution capabilities of Radarsat (Chapter 8) are also proving useful for landslide studies. Radar interferometry techniques (Chapter 8) have also been used in landslide studies in mountainous areas (Singhroy et al., 1998).

For additional information on landslide hazards, see the USGS Geologic Hazards—Landslides website (Appendix B).

4.16 PRINCIPLES OF LANDFORM IDENTIFICATION AND EVALUATION

Various terrain characteristics are important to soil scientists, geologists, geographers, civil engineers, urban and regional planners, landscape architects, real estate developers, and others who wish to evaluate the suitability of the terrain for various land uses. Because terrain conditions strongly influence the capability of the land to support various species of vegetation, an understanding of image interpretation for terrain evaluation is also important for botanists, conservation biologists, foresters, wildlife ecologists, and others concerned with vegetation mapping and evaluation.

The principal terrain characteristics that can be estimated by means of visual image interpretation are bedrock type, landform, soil texture, site drainage conditions, susceptibility to flooding, and depth of unconsolidated materials over bedrock. In addition, the slope of the land surface can be estimated by stereo image viewing and measured by photogrammetric methods.

Space limits the image interpretation process described to the assessment of terrain characteristics that are visible on medium-scale stereoscopic aerial photographs. Similar principles apply to nonphotographic and spaceborne sources.

Soil Characteristics

The term *soil* has specific scientific connotations to different groups involved with soil surveying and mapping. For example, engineers and agricultural soil scientists each have a different concept of soils and use a different terminology in describing soils. Most engineers consider all unconsolidated earth ma-

terial lying above bedrock to be "soil." Agricultural soil scientists regard soil as a material that develops from a geologic parent material through the natural process of weathering and contains a certain amount of organic material and other constituents that support plant life. For example, a 10-m-thick deposit of glacial till over bedrock might be extensively weathered and altered to a depth of 1 m. The remaining 9 m would be relatively unaltered. An engineer would consider this a soil deposit 10 m thick lying over bedrock. A soil scientist would consider this a soil layer 1 m thick lying over glacial till parent material. We use the soil science (pedological) concept of soil in this chapter.

Through the processes of weathering, including the effects of climate and plant and animal activity, unconsolidated earth materials develop distinct layers that soil scientists call *soil horizons*. The top layer is designated the *A horizon* and called the *surface soil*, or *topsoil*. It can range from about 0 to 60 cm in thickness and is typically 15 to 30 cm. The A horizon is the most extensively weathered horizon. It contains the most organic matter of any horizon and has had some of its fine-textured particles washed down into lower horizons. The second layer is designated the *B horizon* and called the *subsoil*. It can range from 0 to 250 cm in thickness and usually is 45 to 60 cm. The B horizon contains some organic matter and is the layer of accumulation for the fine-textured particles washed down from the A horizon. The portion of the soil profile occupied by the A and B horizons is called the *soil* (or *solum*) by soil scientists. The *C horizon* is the underlying geologic material from which the A and B horizons have developed and is called the *parent material* (or *initial material*). The concept of soil profile development into distinct horizons is vitally important for agricultural soils mapping and productivity estimation as well as for many developmental uses of the landscape.

There are three principal origins of soil materials. *Residual soils* are formed in place from bedrock by the natural process of weathering. *Transported soils* are formed from parent materials that have been transported to their present location by wind, water, and/or glacial ice. *Organic soils* (muck and peat) are formed from decomposed plant materials in a very wet environment, typically in shallow lakes or areas with a very high groundwater table.

Soils consist of combinations of solid particles, water, and air. Particles are given size names, such as gravel, sand, silt, and clay, based on particle size. Particle size terminology is not standardized for all disciplines and several classification systems exist. Typical particle size definitions for engineers and agricultural soil scientists are shown in Table 4.15. For our purposes, the differences in particle size definitions between engineers and soil scientists for gravel, sand, silt, and clay are relatively unimportant. We use the soil science definition because it has a convenient system for naming combinations of particle sizes.

We consider materials containing more than 50 percent silt and clay to be *fine textured* and materials containing more than 50 percent sand and gravel to be *coarse textured*.

TABLE 4.15 Soil Particle Size Designations

	Soil Particle Size (mm)	
Soil Particle Size Name	Engineering Definition	Agricultural Soil Science Definition
Gravel	2.0–76.2	2.0–76.2
Sand	0.074–2.0	0.05–2.0
Silt	0.005–0.074	0.002–0.05
Clay	Below 0.005	Below 0.002

Soils have characteristic drainage conditions that depend on surface runoff, soil permeability, and internal soil drainage. We use the USDA soil drainage classification system (U.S. Department of Agriculture, 1997) for soils in their natural condition, with the seven soil drainage classes described as follows. (1) *Very poorly drained.* Natural removal of water from the soil is so slow that the water table remains at or near the surface most of the time. Soils of this drainage class usually occupy level or depressed sites and are frequently ponded. (2) *Poorly drained.* Natural removal of water from the soil is so slow that it remains wet for a large part of the time. The water table is commonly at or near the ground surface during a considerable part of the year. (3) *Somewhat poorly drained.* Natural removal of water from the soil is slow enough to keep it wet for significant periods, but not all the time. (4) *Moderately well drained.* Natural removal of water from the soil is somewhat slow so that the soil is wet for a small but significant part of the time. (5) *Well drained.* Natural removal of water from the soil is at a moderate rate without notable impedance. (6) *Somewhat excessively drained.* Natural removal of water from the soil is rapid. Many soils of this drainage class are sandy and very porous. (7) *Excessively drained.* Natural removal of water from the soil is very rapid. Excessively drained soils may be on steep slopes, very porous, or both.

Land Use Suitability Evaluation

Terrain information can be used to evaluate the suitability of land areas for a variety of land uses. Our emphasis is on suitability for developmental purposes, principally urban and suburban land uses.

The topographic characteristics of an area are one of the most important determinants of the suitability of an area for development. For subdivision development, slopes in the 2 to 6 percent range are steep enough to provide for good surface drainage and interesting siting and yet flat enough so that

few significant site development problems will be encountered provided the soil is well drained. Some drainage problems may be encountered in the 0 to 2 percent range, but these can be readily overcome unless there is a large expanse of absolutely flat land with insufficient internal drainage. The site plan in the 6 to 12 percent range may be more interesting than in the 2 to 6 percent range but will be more costly to develop. Slopes over 12 percent present problems in street development and lot design and also pose serious problems when septic tanks are used for domestic sewage disposal. Severe limitations to subdivision development occur on slopes over 20 percent. For industrial park and commercial sites, slopes of not more than 5 percent are preferred.

The soil texture and drainage conditions also affect land use suitability. Well-drained, coarse-textured soils present few limitations to development. Poorly drained or very poorly drained, fine-textured soils can present severe limitations. Shallow groundwater tables and poor soil drainage conditions cause problems in septic tank installation and operation, in basement and foundation excavation, and in keeping basements water free after construction. In general, depths to the water table of at least 2 m are preferred. Depths of 1 to 2 m may be satisfactory where public sewage disposal is provided and buildings are constructed without basements.

Shallow depths to bedrock cause problems in septic tank installation and maintenance, in utility line construction, in basement and foundation excavation, and in street location and construction, especially when present in combination with steep slopes. Depths to bedrock over 2 m are preferred. Sites with a depth to bedrock of 1 to 2 m are generally unsatisfactory, but the development of these areas may be feasible in some cases. These sites are generally unsatisfactory where septic tank sewage disposal is to be provided. Also, additional excavation costs are involved where basements and public sewage disposal facilities are to be constructed. A depth to bedrock of less than 1 m presents serious limitations to development and is an unsatisfactory condition in almost all cases of land development.

Slope stability problems occur with certain soil-slope conditions. Although we will not discuss techniques for slope stability analysis using image interpretation, it should be mentioned that numerous areas of incipient landslide failure have been detected by image interpretation.

Despite the emphasis here on land development, it must be recognized that many land areas are worthy of preservation in their natural state because of outstanding topographic or geologic characteristics or because rare or endangered plant or animal species occupy those areas. The potential alteration of the hydrology of an area must also be kept in mind. In addition, the maintenance of prime agricultural land for agricultural rather than developmental use must be an important consideration in all land use planning decisions. Similar concerns also apply to the preservation of wetland systems.

Elements of Image Interpretation for Landform Identification and Evaluation

Image interpretation for landform identification and evaluation is based on a systematic observation and evaluation of key elements that are studied stereoscopically. These are topography, drainage pattern and texture, erosion, image tone, and vegetation and land use.

Topography

Each landform and bedrock type described here has its own characteristic topographic form, including a typical size and shape. In fact, there is often a distinct topographic change at the boundary between two different landforms.

With vertical photographs having a normal 60 percent overlap, most individuals see the terrain exaggerated in height about three or four times. Consequently, slopes appear steeper than they actually are. The specific amount of vertical exaggeration observed in any given stereopair is a function of the geometric conditions under which the photographs are viewed and taken.

Drainage Pattern and Texture

The drainage pattern and texture seen on aerial and space images are indicators of landform and bedrock type and also suggest soil characteristics and site drainage conditions.

Six of the most common drainage patterns are illustrated in Figure 4.47. The *dendritic drainage pattern* is a well-integrated pattern formed by a main stream with its tributaries branching and rebranching freely in all directions and occurs on relatively homogeneous materials such as horizontally bedded sedimentary rock and granite. The *rectangular drainage pattern* is basically a dendritic pattern modified by structural bedrock control such that the tributaries meet at right angles and is typical of flat-lying massive sandstone formations with a well-developed joint system. The *trellis drainage pattern* consists of streams having one dominant direction, with subsidiary directions of drainage at right angles, and occurs in areas of folded sedimentary rocks. The *radial drainage pattern* is formed by streams that radiate outward from a central area as is typical of volcanoes and domes. The *centripetal drainage pattern* is the reverse of the radial drainage pattern (drainage is directed toward a central point) and occurs in areas of limestone sinkholes, glacial kettle holes, volcanic craters, and other depressions. The *deranged drainage pattern* is a disordered pattern of aimlessly directed short streams, ponds, and wetland areas typical of ablation glacial till areas.

The previously described drainage patterns are all "erosional" drainage patterns resulting from the erosion of the land surface; they should not be confused with "depositional" drainage features that are remnants of the mode of origin of landforms such as alluvial fans and glacial outwash plains.

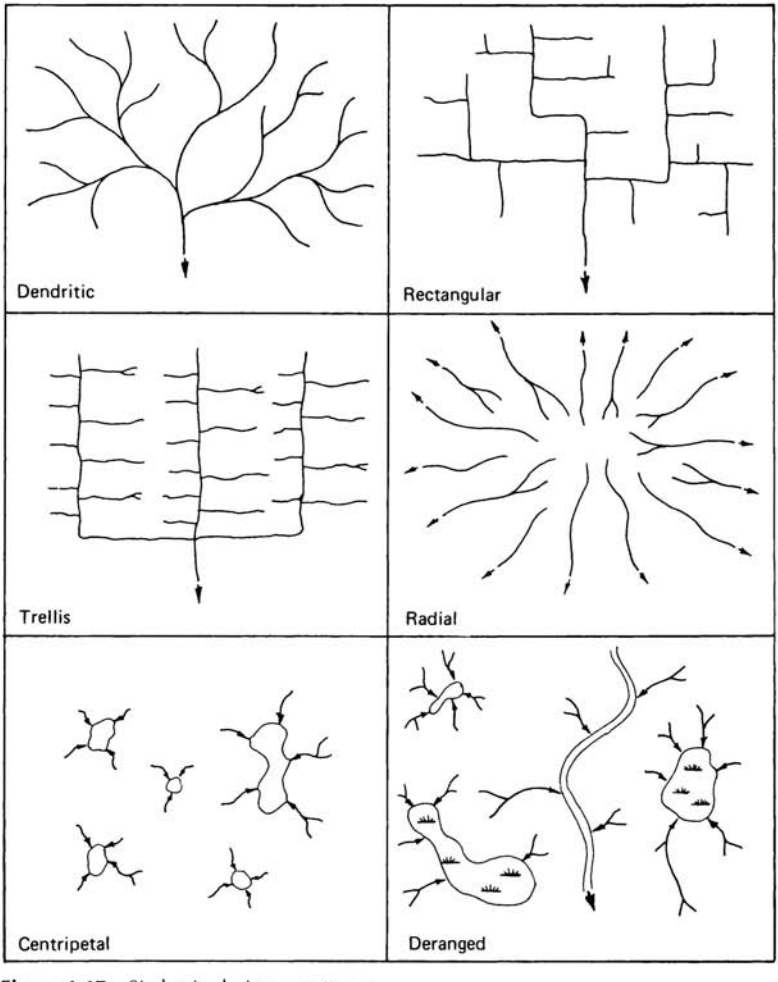

Figure 4.47 Six basic drainage patterns.

Coupled with drainage pattern is drainage texture. Figure 4.48 shows *coarse-textured* and *fine-textured* drainage patterns. Coarse-textured patterns develop where the soils and rocks have good internal drainage with little surface runoff. Fine-textured patterns develop where the soils and rocks have poor internal drainage and high surface runoff. Also, fine-textured drainage patterns develop on soft, easily eroded rocks, such as shale, whereas coarse-textured patterns develop on hard, massive rocks, such as granite.

Erosion

Gullies are small drainage features that may be as small as a meter wide and a hundred meters long. Gullies result from the erosion of unconsolidated material

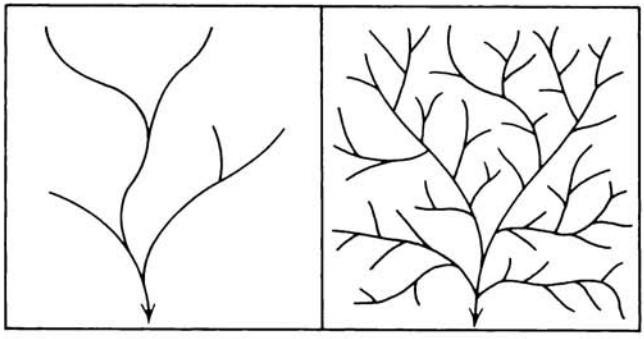

Figure 4.48 Illustrative drainage patterns: (*a*) coarse-textured dendritic pattern; (*b*) fine-textured dendritic pattern.

by runoff and develop where rainfall cannot adequately percolate into the ground but instead collects and flows across the surface in small rivulets. These initial rivulets enlarge and take on a particular shape characteristic of the material in which they are formed. As illustrated in Figures 4.49 and 4.50, short gullies with V-shaped cross sections tend to develop in sand and gravel; gullies with U-shaped cross sections tend to develop in silty soils; and long gullies with gently rounded cross sections tend to develop in silty clay and clay soils.

Image Tone

The term *image tone* refers to the "brightness" at any point on an aerial or space image. The absolute value of the image tone depends not only on certain terrain characteristics but also on image acquisition factors such as film–filter combination (or the bands used for multispectral or hyperspectral scanning), exposure, and photographic/data processing. Image tone also depends on meteorological and climatological factors such as atmospheric haze, sun angle, and cloud shadows. Because of the effect of these non-terrain-related factors, image interpretation for terrain evaluation must rely on an analysis of *relative* tone values, rather than absolute tone values. Relative

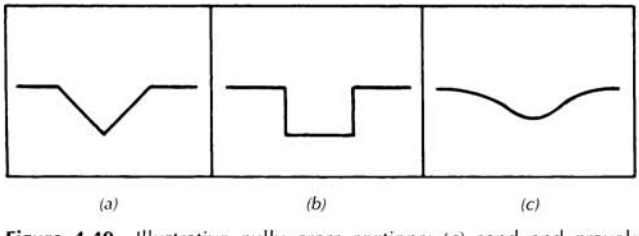

Figure 4.49 Illustrative gully cross sections: (*a*) sand and gravel; (*b*) silt; (*c*) silty clay or clay.

Figure 4.50 Stereopairs illustrating basic gully shapes: (*a*) sand and gravel terrace, Dunn County, WI; (*b*) loess (wind-deposited silt), Buffalo County, NE; (*c*) silty clay loam glacial till, Madison County, IN. Scale 1 : 20,000. (USDA–ASCS panchromatic photos.)

tone values are important because they often form distinct image patterns that may be of great significance in image interpretation.

The effect of terrain conditions on relative image tone can be seen in Figure 4.50*c*. In the case of bare soils (nonvegetated soils), the lighter toned areas tend to have a topographically higher position, a coarser soil texture, a lower soil moisture content, and a lower organic content. Figure 4.50*c* shows a striking tonal pattern often seen on fine-textured glacial till soils. The tonal differences are caused by differences in sunlight reflection due principally to the varying moisture content of the soil. The lighter toned areas are somewhat poorly drained silt loam soils on rises to 1 m above the surrounding darker toned areas of very poorly drained silty clay loam soils. The degree of contrast between lighter and darker toned bare soils varies depending on the overall moisture conditions of the soil, as illustrated in Plate 9.

The sharpness of the boundary between lighter and darker toned areas is often related to the soil texture. Coarser textured soils will generally have sharper gradations between light and dark tones while finer textured soils will generally have more gradual gradations. These variations in tonal gradients result from differences in capillary action occurring in soils of different textures.

Our discussion of image interpretation for terrain evaluation relates primarily to the use of panchromatic film because this film type has historically received the most use for this purpose. Subtle differences in soil and rock colors can be detected using multiple bands in the visible part of the spectrum (e.g., using color film rather than using panchromatic film), and subtle differences in soil moisture and vegetation vigor can be detected using at least one near-infrared band (e.g., color infrared film). Because there is a wide variety of soil and vegetation colors possible on color and color infrared films, it is not possible to consider them all here. Therefore, our discussion of image tone will describe tone as the shades of gray seen on panchromatic photographs. Persons working with color or color infrared photographs (or other sensors such as multispectral or hyperspectral scanners or side-looking radar) of specific geographic regions at specific times of the year can work out their own criteria for image tone evaluation following the principles outlined in this section.

Vegetation and Land Use

Differences in natural or cultivated vegetation often indicate differences in terrain conditions. For example, orchards and vineyards are generally located on well-drained soils, whereas truck farming activities often take place on highly organic soils such as muck and peat deposits. In many cases, however, vegetation and land use obscure differences in terrain conditions and the interpreter must be careful to draw inferences only from meaningful differences in vegetation and land use.

The Image Interpretation Process

Through an analysis of the elements of image interpretation (topography, drainage pattern and texture, erosion, image tone, vegetation, and land use), the image interpreter can identify different terrain conditions and can determine the boundaries between them. Initially, image interpreters will need to consider carefully each of the above elements individually and in combination in order to estimate terrain conditions. After some experience, these elements are often applied subconsciously as the interpreter develops the facility to recognize certain recurring image patterns almost instantaneously. In complex areas, the interpreter should not make snap decisions about terrain conditions but should carefully consider the topography, drainage pattern and texture, erosion, image tone, vegetation, and land use characteristics exhibited on the aerial and space images.

In the remainder of this section, we examine several of the principal bedrock types common on the earth's surface. For each of these, we consider geologic origin and formation, soil and/or bedrock characteristics, implications for land use planning, and image identification using the elements of image interpretation for terrain evaluation. Our illustrations are limited to occurrences in the United States. We emphasize the recognition of clear-cut examples of various bedrock types. In nature, there are many variations to each type. Interpreters working in specific localities can use the principles set forth here to develop their own image interpretation keys.

In cases where distinctions in image appearance must be made for different climatic situations, we will speak of "humid" and "arid" climates. We will consider *humid climates* to occur in areas that receive 50 cm or more rainfall per year and *arid climates* to occur in areas that receive less than 50 cm/year rainfall. In the United States, farming without irrigation is generally feasible in areas with a rainfall of about 50 cm/year or more. Areas receiving less than 50 cm/year rainfall typically require irrigation for farming.

Even the most searching and capable image analysis can benefit from field verification as the image interpretation process is seldom expected to stand alone. The image interpreter should consult existing topographic, geologic, and soil maps and should conduct a selective field check. The principal benefits of image interpretation for terrain evaluation should be a savings in time, money, and effort. The use of image interpretation techniques can allow for terrain mapping during periods of unsuitable weather for field mapping and can provide for more efficient field operations.

In order to illustrate the process of image interpretation for landform identification and evaluation, we will consider the terrain characteristics and image identification of several common bedrock types. Specifically, we treat the analysis of selected sedimentary and igneous rocks. The first three editions of this book treated the subject of landform identification and evaluation in

greater detail by including discussions of aeolian landforms, glacial landforms, fluvial landforms, and organic soils (the first and second editions contain the most detailed coverage).

Sedimentary Rocks

The principal sedimentary rock types to be considered are sandstone, shale, and limestone. Sedimentary rocks are by far the most common rock type exposed at the earth's surface and extend over approximately 75 percent of the earth's land surface (igneous rocks extend over approximately 20 percent and metamorphic rocks over about 5 percent).

Sedimentary rocks are formed by the consolidation of layers of sediments that have settled out of water or air. Sediments are converted into coherent rock masses by lithification, a process that involves cementation and compaction by the weight of overlying sediments.

Clastic sedimentary rocks are rocks containing discrete particles derived from the erosion, transportation, and deposition of preexisting rocks and soils. The nature of the constituent particles and the way in which they are bound together determine the texture, permeability, and strength of the rocks. Clastic sedimentary rocks containing primarily sand-sized particles are called *sandstone*, those containing primarily silt-sized particles are called *siltstone*, and those containing primarily clay-sized particles are called *shale*.

Limestone has a high calcium carbonate content and is formed from chemical or biochemical action. The distinction between the two methods of formation is as follows. Chemically formed limestone results from the precipitation of calcium carbonate from water. Biochemically formed limestone results from chemical processes acting on shells, shell fragments, and plant materials.

The principal sedimentary rock characteristics that affect the appearance of the terrain on aerial and space images are *bedding*, *jointing*, and *resistance to erosion*.

Sedimentary rocks are typically stratified or layered as the result of variations in the depositional process. The individual strata or layers are called *beds*. The top and bottom of each bed have more or less distinct surfaces, called bedding planes, that delineate the termination of one bed and the beginning of another with somewhat different characteristics. Individual beds may range in thickness from a few millimeters to many meters. Beds in their initial condition usually are nearly horizontal but may be tilted to any angle by subsequent movements of the earth's crust.

Joints are cracks through solid bodies of rock with little or no movement parallel to joint surfaces. Joints in sedimentary rocks are primarily perpendicular to bedding planes and form plane surfaces that may intersect other

joint planes. Several systematic joints constitute a joint set, and when two or more sets are recognized in an area, the overall pattern is called a joint system. Because joints are planes of weakness in rocks, they often form surfaces clearly visible on aerial and space images, especially in the case of sandstone. Streams often follow joint lines and may zig-zag from one joint line to another.

The *resistance to erosion* of sedimentary rocks depends on rock strength, permeability, and solubility. Rock strength depends principally on the strength of the bonding agent holding the individual sediment particles together and on the thickness of the beds. Thick beds of sandstone cemented by quartz are very strong and may be used as building materials. Thin beds of shale are often so weak that they can be shattered by hand into flakes and plates. Rock permeability refers to the ability of the rock mass to transmit water and depends on the size of the pore spaces between sediment particles and on the continuity of their connections. Sandstone is generally a very permeable rock. Shale is usually quite impermeable and water moves principally along joint planes rather than in sediment void spaces. Limestones high in calcium carbonate are soluble in water and may dissolve under the action of rainfall and ground water movement.

Here, we describe the characteristics of sandstone, shale, and limestone with a horizontally bedded attitude. The first and second editions of this book include a discussion of interbedded sedimentary rocks (both horizontally bedded and tilted).

Sandstone

Sandstone deposits commonly occur in beds a few meters thick interbedded with shale and/or limestone. Here we are concerned primarily with sandstone formations about 10 m or more in thickness.

Sandstone *bedding* is often prominent on images, especially when the sandstone beds occur over softer, more easily eroded formations such as shale. *Jointing* is prominent, with a joint system consisting of two or three dominant directions. The *resistance to erosion* varies, depending on the strength of the cementing agent. Sandstone cemented with iron compounds and silica is typically very strong, whereas sandstone cemented with carbonates is generally quite weak. Since sandstone is very permeable, most rainfall percolates downward through the rock rather than becoming erosion-producing surface runoff. Sandstone cemented with carbonates may weaken as percolating water dissolves the cementing agent.

In arid areas, there is seldom a residual soil cover over sandstone because any weathered sand particles are removed by wind erosion. In humid areas, the depth of residual soil cover depends on the strength of the cementing agent but is commonly less than 1 m and seldom more than 2 m. The residual soil texture in humid areas depends on the particle size of the sandstone and on the strength of the cementing agent. Weakly cemented sandstone weathers

to sand while residual soils formed from strongly cemented sandstone may contain some silt and clay. Residual soils are typically well drained to excessively drained sand, loamy sand, and sandy loam.

Areas of massive sandstone beds with a residual soil cover are commonly undeveloped because of a combination of their typically rugged topography and shallow depths to bedrock. Buried sandstone strata are often an excellent source of groundwater for both individual homeowners and municipalities. Well-cemented sandstone rock is often used as building stone for residential construction.

Image Identification of Horizontally Bedded Sandstone

Topography: Bold, massive, relatively flat-topped hills with nearly vertical or very steep hillsides. *Drainage:* Coarse-textured, joint-controlled, modified dendritic pattern; often a rectangular pattern caused by perpendicular directions of joint sets. *Erosion:* Few gullies; V-shaped if present in residual soil. *Photographic image tone:* Generally light toned due to light rock color and excellent internal drainage of both residual soil and sandstone rock. Reddish sandstone in arid areas may photograph with a somewhat dark tone on panchromatic film. A dense tree cover over sandstone in humid areas generally appears dark, but in this case the interpreter is looking at the tree canopy rather than the soil or rock surface. *Vegetation and land use:* Sparse vegetation in arid areas. Commonly forested in humid areas as residual soil is too well drained to support crops. In a humid climate, flat-topped sandstone ridges with a loess cover are often farmed. *Other:* Sandstone is sometimes mistakenly identified as granite.

Figure 4.51 shows horizontally bedded sandstone in an arid climate interbedded with a few thin shale beds. The bedding can best be seen by inspecting the valley walls where the deeply incised stream cuts across the terrain. The direction of the major joint set is nearly vertical on the page; a secondary direction is perpendicular to the major joint set. These joint sets only partially control the direction of flow of the major stream but strongly influence the direction of secondary drainage.

Shale

Deposits of shale are common throughout the world as both thick deposits and thin deposits interbedded with sandstone and limestone. Shale *bedding* is very extensive with beds typically 1 to 20 cm in thickness. Bedding is not al-

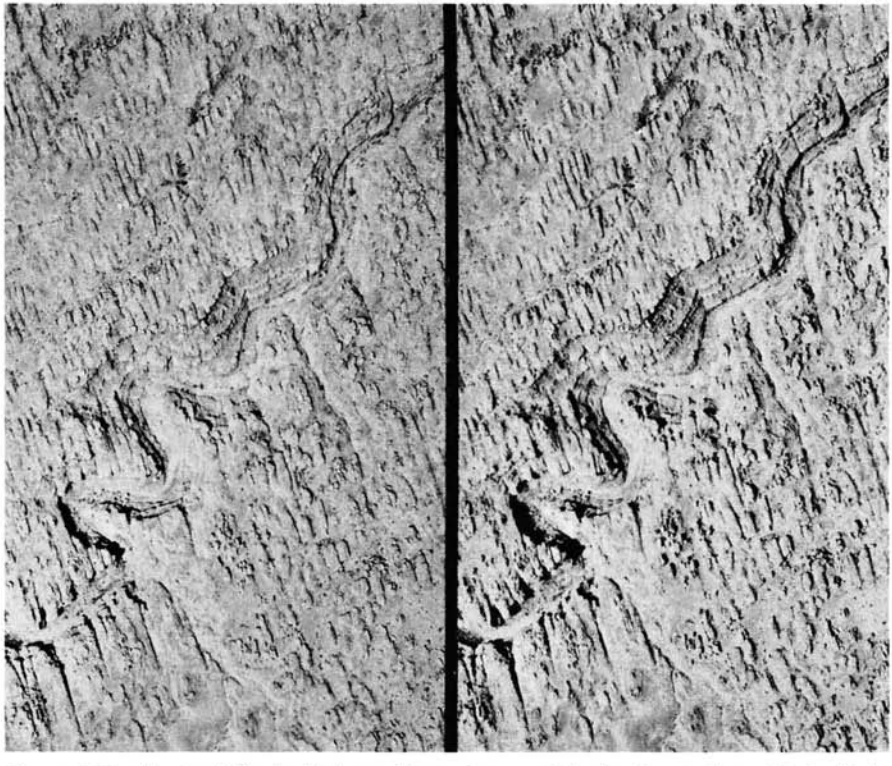

Figure 4.51 Horizontally bedded sandstone in an arid climate, southern Utah. Scale 1 : 20,000. (USGS panchromatic photos.)

ways visible on aerial and space images. However, if beds with a distinct difference in color or resistance to erosion are present or if shale is interbedded with sandstone or limestone, bedding may be seen. The effect of *jointing* is not always strong enough to alter the surface drainage system into a significantly joint-controlled pattern. The *resistance to erosion* is low, compared with other sedimentary rock types. Since shale is relatively impermeable, most rainfall runs off the ground surface, causing extensive erosion.

The depth of residual soil cover is generally less than 1 m and seldom more than 2 m. The residual soil is high in silt and clay, with textures typically silty loam, silty clay loam, silty clay, and clay. Internal soil drainage is typically moderately well drained or poorer, depending on soil texture and on soil and rock structure.

Although the topography in shale areas is generally favorable to urban development, the soil drainage and depth to bedrock conditions may limit residential development by causing problems in basement excavation and in septic tank installation and maintenance. The groundwater supply is extremely variable in shale bedrock. If the shale is strongly jointed, groundwater

may be available. In many cases, however, it will be necessary to drill through the shale into an underlying water-bearing stratum.

Image Identification of Horizontally Bedded Shale

Topography: In an arid climate, minutely dissected terrain with steep stream/gully side slopes resulting from rapid surface runoff associated with short duration heavy rainfall. In a humid climate, gently to moderately sloping, softly rounded hills. *Drainage:* A dendritic pattern with gently curving streams; fine textured in arid climates and medium to fine textured in humid climates. *Erosion:* Gullies in residual soil have gently rounded cross sections. *Photographic image tone:* Varies widely, generally dark toned compared with sandstone and limestone. Differences in image tone may outline bedding. *Vegetation and land use:* Arid areas usually barren, except for desert vegetation. Humid areas intensively cultivated or heavily forested. *Other:* Shale is sometimes mistakenly identified as loess.

Figure 4.52 shows horizontally bedded shale in an arid climate. A comparison with Figure 4.51 illustrates the contrast in bedding, jointing, and resistance to erosion between shale and sandstone.

Limestone

Limestone consists mainly of calcium carbonate, which is soluble in water. Limestone that contains a significant amount of calcium carbonate and magnesium carbonate (or calcium magnesium carbonate) is called dolomitic limestone, or dolomite, and is less soluble in water. Limestone occurs throughout the world. For example, an area of very soluble limestone occurs in the United States in a region spanning portions of Indiana, Kentucky, and Tennessee.

Limestone *bedding* is generally not prominent on images unless the limestone is interbedded with sandstone or shale. *Jointing* is strong and determines the location of many of the pathways for subsurface drainage. However, jointing is generally not prominent on images of limestone in a humid climate. The *resistance to erosion* varies, depending on the solubility and jointing of the rock. Since calcium carbonate is soluble in water, many limestone areas have been severely eroded by rainfall and groundwater action.

The ground surface in areas of soluble limestone in humid climates is typically dotted with literally thousands of roughly circular depressions called *sinkholes*. They form when surface runoff drains vertically through the rock

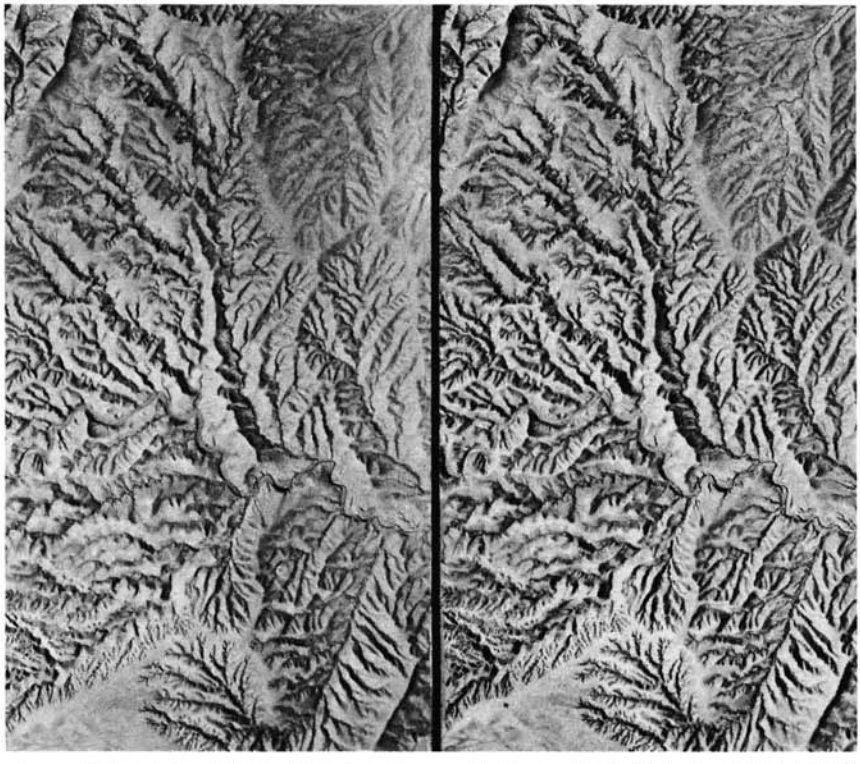

Figure 4.52 Horizontally bedded shale in an arid climate, Utah. Scale 1:26,700. (USGS panchromatic photos.)

along joint planes and the intersections of joint planes, gradually enlarging the underground drainageways by solution and causing the ground surface to collapse and form sinkholes.

There is generally only a shallow residual soil cover over limestone in arid areas where limestone often caps ridges and plateaus. In humid areas, the depth of residual soil cover is extremely variable and depends on the amount of solution weathering. Generally, residual soil depth ranges from 2 to 4 m for soluble limestone (which typically occurs as valleys or plains) and is somewhat less for dolomite (which may cap ridges and plateaus). The residual soil in humid areas contains a great deal of clay. Soil textures of clay, silty clay, clay loam, and silty clay loam are common. Soils are often well drained, except in sinkhole bottoms, due to soil structure and solution openings in the underlying rock. If these soils are extensively disturbed by human activity—such as subdivision development—soil drainage can become very poor.

Although limestone areas may be generally satisfactory for urban development, there are limiting characteristics that must be carefully considered. Because the residual soils contain a great deal of clay, they are relatively poor

foundation soils. Often, it will be necessary to locate foundations directly on bedrock for proper building support. Although the soils are well drained in a natural condition, there may be problems with septic tank operation because of a low percolation rate in the disturbed soil. Groundwater may be difficult to locate and may be very "hard." In addition, effluent from septic tanks can often contaminate the groundwater. There is usually considerable variation in topography, depth to bedrock, and soil drainage conditions, requiring careful soil exploration and mapping before development proceeds. Sinkhole collapse under heavy loads such as construction equipment, highways, and airport runways is a serious problem in some limestone areas.

Image Identification of Horizontally Bedded Limestone

This discussion refers to soluble limestone in humid climates. *Topography:* A gently rolling surface broken by numerous roughly circular sinkholes that are typically 3 to 15 m in depth and 5 to 50 m in diameter. *Drainage:* Centripetal drainage into individual sinkholes. Very few surface streams. Surface streams from adjacent landforms or rock types may disappear underground via sinkholes when streams reach the limestone. *Erosion:* Gullies with gently rounded cross sections develop in the fine-textured residual soil. *Photographic image tone:* Mottled tone due to extensive sinkhole development. *Vegetation and land use:* Typically farmed, except for sinkhole bottoms that are often wet or contain standing water a portion of the year. *Other:* Limestone with extensive sinkhole development might be mistakenly identified as ablation till. Dolomitic limestone is more difficult to identify than soluble limestone. It is generally well drained and has subtle sinkholes.

Figure 4.53 shows horizontally bedded soluble limestone in a humid climate. Note the extensive sinkhole development (up to 40 sinkholes per square kilometer are present) and the complete lack of surface streams. The residual soils here are well-drained silty clay loam and silty clay 1.5 to 3 m deep over limestone bedrock.

Igneous Rocks

Igneous rocks are formed by the cooling and consequent solidification of magma, a molten mass of rock material. Igneous rocks are divided into two groups: intrusive and extrusive. *Intrusive igneous rocks* are formed when

Figure 4.53 Horizontally bedded soluble limestone in a humid climate, Harrison County, IN. Scale 1 : 20,000. (USDA–ASCS panchromatic photos.)

magma does not reach the earth's surface but solidifies in cavities or cracks it has made by pushing the surrounding rock apart or by melting or dissolving it. *Extrusive igneous rocks* are formed when magma reaches the ground surface.

Intrusive igneous rocks commonly occur in large masses in which the molten magma has cooled very slowly and solidified into large crystals. The crystal grains interlock closely to produce a dense, strong rock that is free of cavities. Erosion of overlying materials exposes intrusive igneous rocks.

Extrusive igneous rocks occur as various volcanic forms, including various types of lava flows, cones, and ash deposits. These rocks have cooled more rapidly than intrusive rocks and consequently have smaller crystals.

Intrusive Igneous Rocks

Intrusive igneous rocks range from granite, a light-colored, coarse-grained rock consisting principally of quartz and feldspar, to gabbro, a dark-colored, coarse-grained rock consisting principally of ferromagnesian minerals and feldspar. There are many intrusive igneous rocks intermediate between granite and gabbro in composition, such as granodiorite and diorite. We consider

only the broad class of intrusive igneous rocks called *granitic rocks*, a term used to describe any coarse-grained, light-colored, intrusive igneous rock.

Granitic rocks occur as massive, *unbedded* formations such as the Sierra Nevada Mountains and the Black Hills of South Dakota. They are often strongly fractured into a series of irregularly oriented *joints* as a result of cooling from a molten state and/or pressure relief as overburden is eroded. Granitic rocks have a high *resistance to erosion*. As they weather, they tend to break or peel in concentric sheets through a process called exfoliation.

In arid areas, the depth of residual soil cover over granitic bedrock is typically very thin (less than $\frac{1}{2}$ m), except in fracture zones where it may be thicker. In humid areas, the depths to bedrock is typically 1 to 2 m. The residual soil texture in humid areas is typically loamy sand, sand loam, or sandy clay loam. Granitic rocks yield essentially no water, except in fracture zones. Limited water may be available from the sandy soil above the solid rock.

Areas of massive granitic rocks with residual soil cover are typically not well suited to urban development because of a combination of rugged topography, shallow depth to bedrock, and poor groundwater supply.

Image Identification of Granite Rocks

Topography: Massive, rounded, unbedded, domelike hills with variable summit elevations and steep side slopes. Often strongly jointed with an irregular and sometimes gently curving pattern. Joints may form topographic depressions in which soil and vegetation accumulate and along which water tends to flow. *Drainage and erosion:* Coarse-textured dendritic pattern with a tendency for streams to curve around the bases of domelike hills. Secondary drainage channels form along joints. Few gullies, except in areas of deeper residual soil. *Photographic image tone:* Light toned due to light rock color. Darker toned in depressions that form along joints. *Vegetation and land use:* Sparse vegetation in an arid climate. Often forested with some bare rock outcrops in a humid climate. Vegetation may be concentrated in depressions that form along some joints. *Other:* Granitic rocks are sometimes mistakenly identified as horizontally bedded sandstone. The principal difference in image identification of granitic rocks versus sandstone can be summarized as follows. (1) *Evidences of bedding:* Granitic rocks are unbedded; sandstone is bedded. (2) *Topography:* Granitic outcrops have variable summit elevations, sandstone caprocks form plateaus; granitic rocks have rounded cliffs, sandstone has vertical cliffs; granitic microfeatures are rounded, sandstone microfeatures are blocky. (3) *Joint pattern:* Granitic rocks have an irregular joint pattern with some distinct linear depressions; sandstone has a joint system consisting of two or three principal directions.

Figure 4.54 shows granitic rocks in an arid climate with very little soil or vegetative cover. Note the massive, unbedded formation with rounded cliffs. Note also that a number of joints are enlarged and form depressions with some soil and vegetative cover.

Extrusive Igneous Rocks

Extrusive igneous rocks consist principally of lava flows and pyroclastic materials. Lava flows are the rock bodies formed from the solidification of molten rock that issued from volcanic cones or fissures with little or no explosive activity. In contrast, pyroclastic materials, such as cinders and ash, were ejected from volcanic vents.

The form of lava flows depends principally on the viscosity of the flowing lava. The viscosity of lava increases with the proportion of silica (SiO_2) and alumina (Al_2O_3) in the lava. The least viscous (most fluid) lavas are the basaltic lavas, which contain about 65 percent silica and alumina. Andesitic lavas are intermediate in viscosity and contain about 75 percent silica and alumina. Rhyolitic lavas are very viscous and contain about 85 percent silica and alumina. Several basic volcanic forms are recognized.

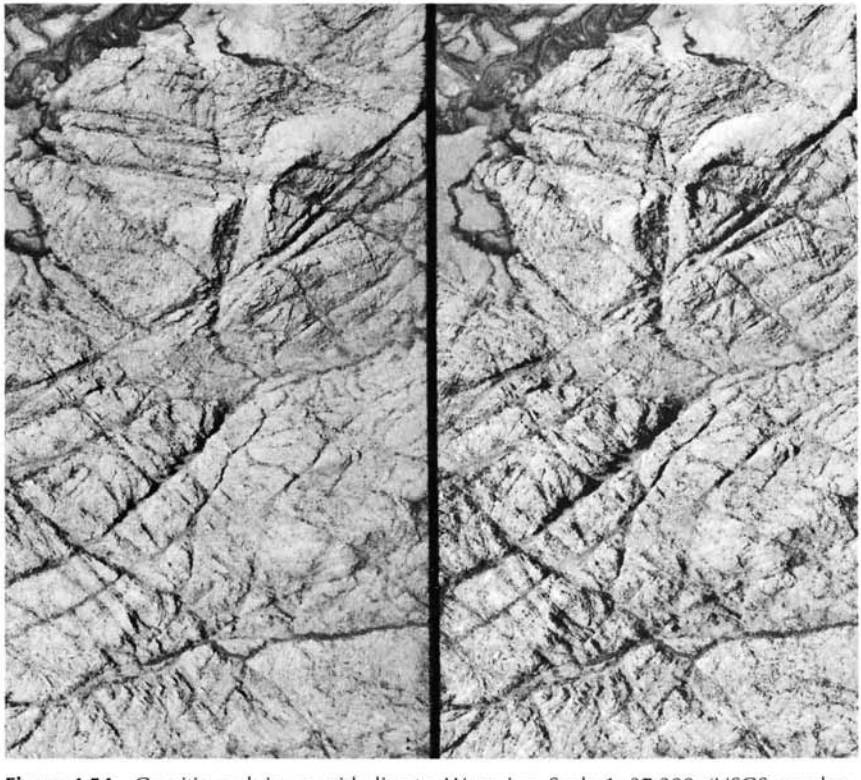

Figure 4.54 Granitic rock in an arid climate, Wyoming. Scale 1 : 37,300. (USGS panchromatic photos.)

Strato volcanoes (also called composite volcanoes) are steep-sided, cone-shaped volcanoes composed of alternating layers of lava and pyroclastic materials. The lava is typically andesitic or rhyolitic and side slopes can be 30° or more. Many strato volcanoes are graceful cones of striking beauty and grandeur. Each of the following mountains is a strato volcano: Shasta (California), Hood (Oregon), Ranier (Washington), St. Helens (Washington), Fuji (Japan), Vesuvius (Italy), and Kilimanjaro (Tanzania).

Shield volcanoes (also called Hawaiian-type volcanoes) are broad, gently sloping volcanic cones of flat domical shape built chiefly of overlapping basaltic lava flows. Side slopes generally range from about 4° to 10°. The Hawaiian volcanoes Haleakala, Mauna Kea, Mauna Loa, and Kilauea are shield volcanoes.

Flood basalt (also called plateau basalt) consists of large-scale eruptions of very fluid basalt that build broad, nearly level plains, some of which are at high elevation. Extensive flood basalt flows form the Columbia River and Snake River plains of the northwest United States.

Image Identification of Lava Flows

Topography: A series of tonguelike flows that may overlap and interbed, often with associated cinder and spatter cones. Viscous lavas (andesite and rhyolite) form thick flows with prominent, steep edges. Fluid lavas (basalt) form thin flows, seldom exceeding 15 m in thickness. *Drainage and erosion:* Lava is well drained internally and there is seldom a well-developed drainage pattern. *Photographic image tone and vegetation:* The color of unweathered, unvegetated, lava is dark toned in the case of basalt, medium toned for andesite, and light toned for rhyolite. In general, recent unvegetated flows are darker toned than weathered, vegetated flows. *Land use:* Recent flows are seldom farmed or developed.

Here, we illustrate only one example of a lava flow issuing from a volcano. Figure 4.55 shows a viscous lava flow that emanated from Mt. Shasta, California, a strato volcano. This flow is 60 m thick and has a 307 slope on its front face.

Metamorphic Rocks

Common metamorphic rocks are quartzite, slate, marble, gneiss, and schist. They are formed from preexisting sedimentary or igneous rocks due princi-

Figure 4.55 Viscous lava flow in an arid climate, Siskiyou County, CA. Scale 1:33,000. (USDA–ASCS panchromatic photos.)

pally to the action of heat and pressure. Occasionally, chemical action or shearing stresses are also involved.

Most metamorphic rocks have a distinct banding that can be seen via field observations and that sets them apart from sedimentary and igneous rocks.

Metamorphic rocks can be found throughout the world. However, since their extent is limited, the identification of metamorphic rocks is not covered here. In addition, the image identification of metamorphic rocks is more difficult than for sedimentary and igneous rocks, and interpretive techniques for metamorphic rocks are not well established.